Experimental and Theoretical Studies of Phase Transitions and Micellar Size Distributions in Ternary Surfactant Systems

by

Henry George Thomas

B.S.(Physics) University of Lowell (1990)

Submitted to the Department of Physics
in partial fulfillment of the requirements for the degree of

Doctor of Philosophy

at the

MASSACHUSETTS INSTITUTE OF TECHNOLOGY

February 1995

Author .....
Department of Physics
December 27, 1994

Certified by .....
George B. Benedek
Alfred H. Caspary Professor of Physics and Biological Physics
Thesis Supervisor

Accepted by .....
George F. Koster
Chairman, Departmental Committee
Science

Experimental and Theoretical Studies of Phase Transitions and Micellar Size Distributions in Ternary Surfactant Systems

by

Henry George Thomas

Submitted to the Department of Physics
on December 23, 1994, in partial fulfillment of the
requirements for the degree of
Doctor of Philosophy

Abstract

We have used static and quasielastic light scattering to investigate the mixed micellar system composed of dodecyl hexaoxyethylene glycol monoether ($C_{12}E_6$), dodecyl octaoxyethylene glycol monoether ($C_{12}E_8$) and water. Using light scattering determinations of the molecular weight and diffusion coefficient, we show that the mixed micelles are rodlike. We determined the average diffusion coefficient, D, of the micelles for several isotherms in the range $10°C \leq T \leq 55°C$ for aqueous solutions of pure $C_{12}E_6$ pure $C_{12}E_8$ and three different mixtures of $C_{12}E_6$ and $C_{12}E_8$. The concentrations studied ranged from approximately 30 to 1000 times the critical micellar concentration (cmc). In addition, we determined the intensity of light scattered from micelles of pure $C_{12}E_6$ and of pure $C_{12}E_8$ in the close vicinity of the cmc for these solutions. These results were used to estimate the cmc for $C_{12}E_6$ and for $C_{12}E_8$ as a function of temperature.

We present a "two-dimensional" generalization of the ladder model to quantitatively describe the linear growth of mixed, rodlike micelles. Both the diffusion measurements and the intensity measurements were compared to the two-dimensional ladder model. Excellent agreement was found between theory and experiment in the regions of the phase diagram where intermicellar interactions could be neglected. We have also been successful in explaining the concentration dependence of D in domains where intermicellar interactions become important by including the interactions into a mean-field model for the Gibbs free energy of the solution.

The parameters found for the two-dimensional ladder model for the $C_{12}E_6$, $C_{12}E_8$ and water system were compared with the molecular model of Puvvada and Blankschtein (*J. Phys. Chem.*, 96:5567-5579, 1992; 96:5579-5592, 1992).

Thesis Supervisor: George B. Benedek
Title: Alfred H. Caspary Professor of Physics and Biological Physics

Contents

List of Figures

List of Tables

Chapter 1

Introduction

1.1 Amphiphiles and Micelles

Amphiphilic molecules consist of two distinct regions. One region is exclusively non-polar, consisting of, for example, one or more long hydrocarbon chains. Because of its non-polar nature, this region would be relatively insoluble in aqueous solution on its own, and is therefore called hydrophobic, meaning "water fearing." This region is covalently bonded to the second region, which is charged, zwitterionic, or simply polar. This second region, on its own, is readily soluble in water and so is called hydrophilic, or "water loving." Because these two regions are covalently bonded together, the amphiphilic molecule is possessed of a dual nature: partly hydrophobic and partly hydrophilic.

Amphiphiles are surfactants. When a small number of amphiphiles are placed in contact with water, they are preferentially adsorbed onto the surface, reducing the surface tension. This preferential adsorption occurs because there is a free energy cost, known as the hydrophobic effect, associated with immersing the hydrophobic regions of the amphiphiles in the solvent. It is believed [1] that the water in the vicinity of the nonpolar region maintains its hydrogen bonded structure, but that in order to do so, the water molecules must reorient themselves into a more ordered structure than in the bulk solvent. Thus, it is believed that the free energy cost of the hydrophobic effect is mostly entropic in nature.

As the concentration of amphiphiles is increased, the available area on the surface for additional amphiphiles decreases, and the proportion of surfactant dissolved in the bulk solvent increases. When the concentration of dissolved solvent reaches a sufficiently high value, it becomes thermodynamically advantageous for the amphiphiles in solution to spontaneously aggregate and rearrange themselves into various specific geometries in which the hydrophobic "tails" are all somehow shielded from the surrounding water by the attached hydrophilic "head groups." Examples of these structures include micelles, bilayers, and vesicles. The tendency of certain amphiphiles to form certain structures is related to the molecular geometry. In a micelle, the hydrophobic tails are all collected together in a single, continuous volume that is completely enclosed by the attached hydrophilic heads. Micelles can exist spheroids, rods of varying length and flexibility, and discs.

It is important to emphasize that micelles are quite different from other forms of aggregates. Micelles are not held together because the amphiphiles attract one another. Rather, the micelle is stable because of the great attraction of water for itself. Micelles are in thermodynamic equilibrium with the surrounding solution of water and dissolved amphiphiles. Thus, the aggregation number of the micelle is subject to thermodynamic fluctuations, as individual amphiphiles are constantly entering and leaving the micellar environment. More importantly, the process of micellization is fully reversible. If the solution is sufficiently diluted by the addition of water, micelles will once again become thermodynamically unstable, and they will vanish from the solution. Subsequently increase the amphiphile concentration, and micelles will reappear. The concentration at which the micelles first begin to appear is called the critical micellar concentration.

A second important distinction between micelles and other aggregates is that micelles have a minimum aggregation number, which is often quite large, below which they are no longer stable. This large minimum size is due to the fact that in order for the micelle to be stable, the hydrophobic tails in the micelle must be sufficiently shielded from the water in all directions. Because of the large minimum size of micelles, the transition in the region near the critical micellar concentration

is very sharp. Above the critical micellar concentration nearly all additional surfactant added to the solution results in the creation of additional micelles or the enlargement of existing micelles. This sharpness is also reflected strongly in many of the measurable properties of the system. For example, the surface tension and the intensity of scattered light both show sharp transitions near the critical micellar concentration.

The properties of surfactant systems are exploited in a wide variety of industrial and commercial applications. They are used for their detergency, their solubilization and surface wetting capabilities in such diverse areas as from the mining and petroleum industries to the pharmaceutical industry, and in biochemical and medical research. They can be found in commercial products ranging from laundry detergents to gasoline, motor oil, and salad dressing. Each of these specific applications and products exploit specific properties of the surfactant solution. It is of extreme importance to be able to tailor these solutions by the proper choice of surfactant and solution conditions such that the solution properties best suit the desired application. Mixtures of surfactants offer the best hope of optimizing the solution properties, since by changing solution composition one can precisely tune any desired property to the range needed, even though it may not be possible to find a single surfactant with all of the required properties. Therefore a thorough understanding of the physics and chemistry of such mixed systems is invaluable. It is the goal of this thesis to contribute to this much needed understanding.

1.2 Historical Review

Early studies of micellar systems were concentrated on the critical micellar concentration and the process of self-assembly and micellization. The name micelle, as we use it here to refer to a colloidal aggregate of amphiphiles, was first used by J. W. McBain [2] in 1913. It was not until 1936, however, that the first model of the spherical micelle and discussions of the aggregation mechanism were developed by Hartley [3]. Since that time, many authors have contributed to our understanding

of the physics of micellization, both theoretically and experimentally.

In the early 1960's, the development of the laser opened the possibility of measuring very small frequency shifts through "optical mixing" techniques. In 1964, Pecora [4] showed that the broadening of the spectrum of scattered light from a solution of macromolecules could give information about the diffusion of those macromolecules. The first such measurements were carried out on solutions of polystyrene latex spheres by Cummins, Knable, and Yeh [5] in 1964, using what is known now as the heterodyne technique. Shortly thereafter, Ford and Benedek [6] used the technique of "self-beating", now referred to as the homodyne technique, to study the decay of the entropy fluctuations in SF_6 in the region near its liquid-vapor critical point. The rapid development of the technique of quasielastic light scattering took place in the years following, and it was inevitable that this new and powerful technique should be applied to the study of micellar systems.

From 1976-1978, Mazer et. al. [7, 8, 9] performed a series of experiments in which the size and polydispersity of micelles of Sodium Dodecyl Sulfate in salt solution were investigated by quasielastic light scattering spectroscopy [7, 8] and by total intensity and angular dissymmetry [9] measurements. It was observed that in regions well above the critical micellar concentration, the micellar solution underwent a continuous transition from a monodisperse solution containing small, spherical micelles to a solution containing a polydisperse distribution of long, cylindrical micelles. In 1980, Missel et. al. [10] reported a new set of measurements of the size and polydispersity of the SDS micelles in salt solution. They presented and applied a model of micellar growth, known as the "ladder model," to describe their findings. The ladder model describes the free energy advantage to form a locally cylindrical micelle with two ends in terms of two energetic parameters. The first parameter is the free energy advantage to form a micelle of minimal size, which is assumed to be the same as the free energy advantage of the two ends of an elongated micelle. The second parameter is the free energy advantage per monomer associated with the surfactant in the cylindrical portion of the elongated micelle. The spectrum of energy levels corresponding to micelles of increasing total aggregation number can

therefore be described as an infinite ladder with a gap between the base and the initial rung, hence the name "ladder model."

Although the ladder model can be used to successfully describe the growth of individual micelles, it does not include the effects of interactions between micelles. On the other hand, it is well known that many systems of ionic, zwitterionic, and nonionic micelles exhibit the phenomenon of phase separation, indicating that interactions between micelles can become quite important. By changing temperature, pressure, and concentration appropriately, the micellar solution, which normally exists as a single, isotropic liquid phase, spontaneously separates into two isotropic liquid phases that differ in total surfactant concentration. The phase separation is caused by two opposing contributions to the total free energy of the system. The first contribution arises from the net attraction of like molecules for one another. The other contribution is an entropic factor, the magnitude of which is determined by the number of possible configurations of the molecules in the system.

Water molecules can attract each other quite strongly because of their highly polar nature. If this self-attraction of water is stronger than the interaction between water and micelles, then the water will want to segregate itself from the micelles. The effect of this segregation will be to form a region in the solution with a high concentration of water and another region with a high concentration of micelles. If this kind of energetic consideration were the only relevant consideration, then we would expect the system to segregate as far as possible. That is, the solution would separate into two phases with as small an interface as possible existing between them: one phase containing pure water, and the other phase containing pure surfactant.

Of course, since at equilibrium it is the total free energy which must be minimized, the entropy of the system must also be considered. The larger the number of geometric configurations that are available to the molecules in the system, the higher the entropy, and the lower the free energy. The full segregation we have mentioned above is a state of the system with very low entropy. Only a very small portion of the total possible arrangements of all of the molecules in the system correspond to the case where the two phases are pure. At a small cost in energy, the entropy can

be increased tremendously by allowing a small amount of water to mix in with the pure micelles and a small number of micelles to mix in with the pure water. Thus at equilibrium, if the solution phase separates, we will have two coexisting phases: one phase rich in micelles, and the other phase poor in micelles. The amount of segregation that occurs will depend on the balance between the net attraction between like molecules and the entropic cost associated with the segregation. Of course, if the entropic cost is too strong as compared to the net attraction between like molecules, or, alternatively, if there is no net attraction between like molecules, then the system will not phase separate at all.

In 1985-1986, Blankschtein, Thurston, and Benedek [11, 12, 13] proposed a new theory which is capable of explaining both the thermodynamic properties and the phase separation of micellar solutions. A model Gibbs free energy was proposed, including the effects of intermicellar interactions at the level of a mean-field model, considering the pairwise interaction between monomers. For micellar systems exhibiting one-dimensional growth, the ladder model was also incorporated into this model Gibbs free energy. The resulting framework has been successfully used to describe both the C8-Lecithin and water system and the dodecyl hexaoxyethylene glycol monoether ($C_{12}E_6$) and water system [14].

In an effort to understand the molecular basis for the magnitudes of the parameters in the Blankschtein, Thurston, and Benedek free energy, Puvvada and Blankschtein [15] have constructed a model of micellization that utilizes readily available or easily estimated molecular information to calculate the free energy advantage to form a micelle. This information includes the size and nature of the hydrophilic and hydrophobic regions of the surfactant molecule, the magnitude of the interfacial tension between hydrocarbon and water as a function of curvature, and the magnitude of the free energy of transfer associated with transferring hydrocarbon from a pure hydrocarbon environment to water. A detailed thought process is introduced that is helpful to clearly identify the essential physical factors responsible for micellization, including: the free energy contribution associated with transferring the hydrophobic tails from water into the micellar core, the creation and partial

screening of an interface between the micellar core and the surrounding water, the loss of entropy in the core associated with the restriction that one end of each hydrophobic tail must reside at the interface, steric repulsions between the hydrophilic head groups on the micellar core-water interface, and the electrostatic interactions between head groups if they are charged. These contributions are modeled, and their magnitudes are estimated utilizing the molecular information described above. When incorporated into the thermodynamic framework of Blankschtein, Thurston, and Benedek [11, 12, 13], this approach is capable of predicting numerically the critical micellar concentration, the distribution of micellar sizes, the shape and location of the coexistence curve for phase separation, and the osmotic compressibility. In addition, we can use this molecular approach to understand the molecular basis for the phenomenological parameters of the ladder model.

1.3 Overview

In this work, we shall approach the problem of understanding the properties of mixtures of similar surfactants using an approach that parallels the historical development discussed in the previous section. Toward this end, we have performed light scattering experiments on the mixed nonionic system consisting of water and the two surfactants dodecyl hexaoxyethylene glycol monoether ($C_{12}E_6$) and dodecyl octaoxyethylene glycol monoether ($C_{12}E_8$). Further rationale for the choice of these particular surfactants will be given in Chapter 3. A generalization of the ladder model, appropriate to the case of the linear growth of micelles composed of two different surfactants has been developed, and will be applied to the results of the light scattering measurements. In its simplest form, this generalization of the ladder model contains four energetic parameters rather than the two of the original ladder model. The gap and rung spacings for micelles of a fixed relative composition of surfactant are interpolated between the gap and rung spacings for the two pure components. For this reason, we shall call this generalization of the ladder model the "two-dimensional ladder model."

Recently, Puvvada and Blankschtein have generalized the thermodynamic framework of Blankschtein, Thurston, and Benedek to the case of mixtures of two similar surfactants [16]. In addition, they have generalized their molecular model for calculating the magnitudes of the parameters of this framework [17]. We shall use this work in two different, but related ways. First, as the approach of Puvvada and Blankschtein has been proven useful previously for single component micellar solutions in estimating the magnitudes of the parameters of the original ladder model, we shall examine their generalization of these calculations in the light of our two-dimensional ladder model. By clearly identifying the means by which the calculations of Puvvada and Blankschtein can be used to compute the physically meaningful parameters of the two-dimensional ladder model, we will gain physical insight into the process of micellar growth. Second, we note that it will become clear, when the experimental data are presented, that there will be regions where intermicellar interactions are clearly important. We shall incorporate our two-dimensional ladder model into the generalization of the Gibbs free energy model of Blankschtein, Thurston and Benedek [16] and investigate the consequences of adopting this model in the regions where micellar interactions become important.

The remainder of this thesis is divided into three main sections. Chapters 2 and 3 together comprise the experimental section. In Chapter 2 the basics of light scattering theory are discussed. The derivation of an expression for the scattered electric field, $\boldsymbol{E}(\boldsymbol{R},t)$, from an isotropic, continuous medium in the limit of large distances from the scattering source is outlined. This expression is used to compute the correlation function $\langle E_i^*(\boldsymbol{R}_1,t_1)E_i(\boldsymbol{R}_2,t_2)\rangle$, from which can be obtained expressions for both the total intensity of scattered light and the homodyne time autocorrelation function measured in our experiments.

In Chapter 3, our light scattering measurements of the $C_{12}E_6$, $C_{12}E_8$ and water system are presented, and discussed. We begin by describing the methods used to prepare the samples and the techniques used to obtain and analyze the experimental data. The data are then presented, and their interpretation is discussed. In the region of the phase diagram for concentrations below the critical concentration for

liquid-liquid phase separation and for temperatures far from the phase boundary, where it is reasonable that intermicellar interactions are small, we have represented the temperature and concentration dependence of the measured diffusivity in terms of an effective hydrodynamic radius. In this same region of the phase boundary, we also represent measurements of the osmotic compressibility in terms of the weight-averaged molecular weight of the micelles in solution. We find that our data are consistent with a hydrodynamic model of elongated prolate ellipsoidal micelles.

Chapters 4 and 5 constitute the second main section of this thesis. In Chapter 4, starting from a general expression for the partition function, we review the ladder model for the linear growth of micelles composed of a single surfactant, and propose a simple generalization to the case of multicomponent mixtures. Our treatment is appropriate to the case where the different surfactant species are not too dissimilar. For the case of two different surfactant species and water, we present the two-dimensional ladder model in detail. The subsequent generalization of the two-dimensional ladder model to a system containing k different kinds of similar amphiphiles is clear. As was true for the original ladder model, our proposed generalization does not account for the interactions between micelles.

In Chapter 5, the thermodynamics of mixed micellar systems is reexamined from the basis of a model for the total Gibbs free energy of the system. This model Gibbs free energy is based on the work of Blankschtein, Thurston, and Benedek [11, 12, 13] for single-component micellar systems, and was generalized to the case of a mixture of two similar surfactants and water by Puvvada and Blankschtein [16]. The model incorporates a specific model for the entropy of mixing among the various micellar species, the free monomers in solution and water and it considers the interactions between micelles at the level of a mean-field approximation for the pairwise attraction of surfactant monomers. Expressions for the equilibrium micellar distribution of sizes and compositions, the osmotic pressure and the osmotic compressibility of the system are derived using the model Gibbs free energy and our two-dimensional ladder model. Finally, we discuss the molecular approach of Puvvada and Blankschtein and how it may be used to compute the physically meaningful parameters of the

two-dimensional ladder model.

In Chapter 6 we investigate the extent to which the theoretical approaches explored in Chapters 4 and 5 are capable of describing our experimental data on the $C_{12}E_6$, $C_{12}E_8$ and water system. The two-dimensional ladder model is applied in the regions of the phase diagram where the interpretation of our light scattering data is clear, and the four parameters of the model are extracted. The calculations of Puvvada and Blankschtein are performed, using the information appropriate for the $C_{12}E_6$, $C_{12}E_8$ and water system. We find that the four physically meaningful two-dimensional ladder model parameters computed using the numerical procedure of Puvvada and Blankschtein compare well with their experimentally determined values.

Also in Chapter 6, we examine the consequences of adopting the Gibbs free energy model presented in Chapter 5 in the regions of the phase diagram where intermicellar interactions become important. We find that by incorporating the two-dimensional ladder model into the model Gibbs free energy we are capable of correctly describing the observed trends in both our own dynamic light scattering data, and in static light scattering data for the pure $C_{12}E_6$ and water system obtained by Wilcoxon and Kaler [18]. The physical implications of these trends are then discussed in terms of the model Gibbs free energy. Our results are summarized and the prospects for future research are discussed in Chapter 7.

Chapter 2

Light Scattering

In this chapter we provide a review of the basic theory of light scattering as it is specifically applied to the case of an isotopic, continuous medium. Our treatment follows most closely the treatments of Landau, Lifshitz, and Pitaevskiĭ [19] and Berne and Pecora [20]. In Section 2.1 we discuss the basics of light scattering. In Sections 2.2 and 2.3 we discuss those elements of static and dynamic light scattering which are of particular interest to our measurements.

2.1 Basic Light Scattering Theory

The propagation of light is governed by Maxwell's equations. In a continuous, isotropic medium and in the absence of free charges and currents, the following wave equation for the total electric field can be derived from Maxwell's equations

$$\nabla \times (\nabla \times \boldsymbol{E}) = -\frac{1}{c^2}\frac{\partial^2 \boldsymbol{D}}{\partial t^2} \tag{2.1}$$

where $\boldsymbol{E}$ is the electric field, c is the speed of light in a vacuum, and $\boldsymbol{D}$ is the electric displacement vector. In general the electric displacement is related to the electric field through the dielectric tensor ϵ where $\boldsymbol{D} = \epsilon \cdot \boldsymbol{E}$. In a continuous, isotropic medium, the dielectric tensor can be replaced with a scalar. However, if we allow

for small fluctuations in the medium, then we may write

$$\boldsymbol{\epsilon} = \epsilon \boldsymbol{I} + \boldsymbol{\alpha} \tag{2.2}$$

where ϵ is the (scalar) dielectric constant of the (isotropic) medium, $\boldsymbol{I}$ is the identity tensor, and $\boldsymbol{\alpha}$ is a small, local fluctuation in the dielectric tensor of the medium.

Consider now a plane wave incident on the medium with electric field

$$\boldsymbol{E}^{(i)} = \boldsymbol{e} E_0 e^{i(\boldsymbol{k}\cdot\boldsymbol{x} - \omega_i t)}. \tag{2.3}$$

where $\boldsymbol{e}$ is a unit vector indicating the polarization of the incident field. The local fluctuations in the medium will give rise to a scattered field, $\boldsymbol{E}^{(s)}$, that we wish to find. Thus, the total field and total electric displacement may both be written as a sum of incident, (i), and scattered, (s), fields:

$$\boldsymbol{E} = \boldsymbol{E}^{(i)} + \boldsymbol{E}^{(s)} \tag{2.4}$$

$$\boldsymbol{D} = \boldsymbol{D}^{(i)} + \boldsymbol{D}^{(s)}. \tag{2.5}$$

The relationship between the total electric field and the total electric displacement may therefore be written

$$\boldsymbol{D}^{(i)} + \boldsymbol{D}^{(s)} = \epsilon \boldsymbol{E}^{(i)} + \boldsymbol{\alpha}\cdot\boldsymbol{E}^{(i)} + \epsilon \boldsymbol{E}^{(s)} + \boldsymbol{\alpha}\cdot\boldsymbol{E}^{(s)}. \tag{2.6}$$

Noting that $\boldsymbol{D}^{(i)} = \epsilon \boldsymbol{E}^{(i)}$ is a solution to the wave equation (Equation 2.1) for the incident plane wave alone, we have that

$$\boldsymbol{D}^{(s)} = \epsilon \boldsymbol{E}^{(s)} + \boldsymbol{\alpha}\cdot\boldsymbol{E}^{(i)}, \tag{2.7}$$

where the fourth term in Equation 2.6 has been neglected. From Equation 2.7, we see that the last term, $\boldsymbol{\alpha}\cdot\boldsymbol{E}^{(i)}$, is the term responsible for scattering, since it relates the scattered electric displacement to the incident field. The term we have neglected, $\boldsymbol{\alpha}\cdot\boldsymbol{E}^{(s)}$ couples the scattered field to itself through the dielectric fluctuation and is

responsible for multiple scattering effects. Since $\boldsymbol{E}^{(s)}$ is coupled to $\boldsymbol{E}^{(i)}$ through the fluctuation $\boldsymbol{\alpha}$ which is assumed to be small, $\boldsymbol{\alpha} \cdot \boldsymbol{E}^{(s)}$ is second-order in $\boldsymbol{\alpha}$, so that under normal circumstances its neglect causes no problems.

Substituting Equation 2.7 into the wave equation and simplifying, we obtain the relation

$$\nabla^2 \boldsymbol{D}^{(s)} - \frac{\epsilon}{c^2} \frac{\partial^2 \boldsymbol{D}^{(s)}}{\partial t^2} = -\boldsymbol{\nabla} \times \left(\boldsymbol{\nabla} \times (\boldsymbol{\alpha} \cdot \boldsymbol{E}^{(i)}) \right) \tag{2.8}$$

where we have used the fact that $\boldsymbol{\nabla} \cdot \boldsymbol{D}^{(s)} = 0$ in the absence of free charges. This equation is an inhomogeneous wave equation of the form

$$\nabla^2 \psi - \frac{1}{v^2} \frac{\partial^2 \psi}{\partial t^2} = -4\pi f(\boldsymbol{x}, t). \tag{2.9}$$

The formal solution of this problem is given in terms of the Green's function

$$\psi(\boldsymbol{x}, t) = \int d^3x' dt' G(\boldsymbol{x}, t, \boldsymbol{x}', t') f(\boldsymbol{x}', t') \tag{2.10}$$

with the Green's function, $G(\boldsymbol{x}, t, \boldsymbol{x}', t')$, satisfying

$$\nabla^2 G - \frac{1}{v^2} \frac{\partial^2 G}{\partial t^2} = -4\pi \delta(\boldsymbol{x} - \boldsymbol{x}') \delta(t - t'). \tag{2.11}$$

For the special case of no boundary surfaces, the Green's function for this problem is given by [21]

$$G(\boldsymbol{x}, t, \boldsymbol{x}', t') = \frac{\delta\left(t' - \left[t \mp \frac{|\boldsymbol{x} - \boldsymbol{x}'|}{v}\right]\right)}{|\boldsymbol{x} - \boldsymbol{x}'|} \tag{2.12}$$

where we will consider only the minus sign, in order that the electric displacement at time t only depends on the configuration of distant charges at previous times, as is required by the principle of causality. For our problem, $v = c/\sqrt{\epsilon}$, and the formal solution for the component $D_i^{(s)}$ is

$$D_i^{(s)} = \frac{1}{4\pi} \int d^3x' dt' G(\boldsymbol{x}, t, \boldsymbol{x}', t') \epsilon_{ikl} \frac{\partial}{\partial x_k'} \epsilon_{lmn} \frac{\partial}{\partial x_m'} \alpha_{nj}(\boldsymbol{x}', t') E_j^{(i)}, \tag{2.13}$$

where the integration is to be taken over the scattering volume. In the previous

equation, we have used the standard conventions that repeated indices are to be summed over and that ϵ_{ikl} is a third rank totally antisymmetric tensor with the properties that $\epsilon_{ikl}\epsilon_{imn} = \delta_{km}\delta_{ln} - \delta_{kn}\delta_{lm}$ and $\epsilon_{ikl} = -\epsilon_{ilk}$. Integrating Equation 2.13 by parts twice yields

$$D_i^{(s)} = \frac{1}{4\pi}\int d^3x'dt'\epsilon_{ikl}\epsilon_{lmn}\alpha_{nj}(\boldsymbol{x}',t')E_j^{(i)}\frac{\partial}{\partial x_k'}\frac{\partial}{\partial x_m'}G(\boldsymbol{x},t,\boldsymbol{x}',t') \tag{2.14}$$

so that the derivatives now act on the Green's function, $G(\boldsymbol{x},t,\boldsymbol{x}',t')$. Since the Green's function is a function only of $|\boldsymbol{x}-\boldsymbol{x}'|$, the derivatives act identically on the primed or unprimed variables. Thus, we take them to act on the unprimed variables and write

$$D_i^{(s)} = \epsilon_{ikl}\epsilon_{lmn}\frac{\partial}{\partial x_k}\frac{\partial}{\partial x_m}\frac{1}{4\pi}\int d^3x'dt'\frac{1}{|\boldsymbol{x}-\boldsymbol{x}'|}\alpha_{nj}(\boldsymbol{x}',t')E_j^{(i)}\delta\left(t'+\frac{|\boldsymbol{x}-\boldsymbol{x}'|}{c/\sqrt{\epsilon}}-t\right). \tag{2.15}$$

Inserting the incident plane wave (Equation 2.3 and integrating over t', we get

$$D_i^{(s)} = \epsilon_{ikl}\epsilon_{lmn}\frac{\partial}{\partial x_k}\frac{\partial}{\partial x_m}\frac{E_0}{4\pi}\int d^3x'\frac{e^{i(\boldsymbol{k}\cdot\boldsymbol{x}'-\omega t)}}{|\boldsymbol{x}-\boldsymbol{x}'|}\alpha_{nj}(\boldsymbol{x}',t_r)e_j e^{i\omega\sqrt{\epsilon}|\boldsymbol{x}-\boldsymbol{x}'|/c} \tag{2.16}$$

where t_r is the retarded time $t_r = t - \sqrt{\epsilon}\,|\boldsymbol{x}-\boldsymbol{x}'|/c$. We proceed by performing a fourier analysis of the dielectric fluctuation over some time interval T:

$$\alpha_{nj}(\boldsymbol{x}',t_r) = \sum_u \alpha_{nj}^u(\boldsymbol{x}')e^{i\Omega_u t_r} \tag{2.17}$$

with $\Omega_u = 2\pi u/T$. Defining

$$\omega_u = \omega - \Omega_u, \tag{2.18}$$

$$k_u = \frac{\sqrt{\epsilon}}{c}\omega_u, \tag{2.19}$$

we write

$$D_i^{(s)} = \epsilon_{ikl}\epsilon_{lmn}\frac{\partial}{\partial x_k}\frac{\partial}{\partial x_m}\frac{E_0}{4\pi}\int d^3x'\frac{e^{i(\boldsymbol{k}\cdot\boldsymbol{x}'-\omega t)}}{|\boldsymbol{x}-\boldsymbol{x}'|}\sum_u \alpha_{nj}^u(\boldsymbol{x}')e_j e^{i\Omega_u t}e^{ik_u|\boldsymbol{x}-\boldsymbol{x}'|}. \tag{2.20}$$

The terms that contribute significantly to the fourier decomposition of $\boldsymbol{\alpha}(t_r)$ are those terms with frequencies comparable to the frequencies that characterize the rotation and translation of the molecules that constitute the medium. In general these frequencies are much lower than characteristic optical frequencies ($\sim 10^{15}$ sec^{-1}). That is, it is an excellent approximation that $\Omega_u \ll \omega$ for all Ω_u contributing to Equation 2.20. Therefore, we expect $\omega_u \approx \omega$ and thus $k_u \approx k$. That is, the only strong dependencies on u left in Equation 2.20 are the dependence of α^u_{nj} and Ω_u. Using the definition of our fourier analysis, we write

$$D_i^{(s)} = \epsilon_{ikl}\epsilon_{lmn}\frac{\partial}{\partial x_k}\frac{\partial}{\partial x_m}\frac{E_0}{4\pi}\int d^3x' \frac{e^{i(\boldsymbol{k}\cdot\boldsymbol{x}'-\omega t)}}{|\boldsymbol{x}-\boldsymbol{x}'|}\alpha_{nj}(\boldsymbol{x}',t)e_j e^{ik|\boldsymbol{x}-\boldsymbol{x}'|}. \tag{2.21}$$

We are interested in the behavior of the scattered field at a large distance from the scattering volume. Let us consider the field at a point $\boldsymbol{x} = \boldsymbol{R} = R\boldsymbol{n}'$, where $\boldsymbol{n}'$ is the unit vector in the direction of $\boldsymbol{R}$, and $R \gg x'$ for all points in the scattering volume. In this case, we can make the approximation

$$k\,|\boldsymbol{x}-\boldsymbol{x}'| \approx kR - \boldsymbol{k}'\cdot\boldsymbol{x}'. \tag{2.22}$$

where we have defined $\boldsymbol{k}' = k\boldsymbol{n}'$. Making this replacement, we carry out the derivatives, keeping only terms to leading order in $1/R$, since we are interested in the far-field behavior of the scattered field. We obtain

$$E_i^{(s)} = \frac{E_0 k^2}{4\pi\epsilon}\epsilon_{ikl}\epsilon_{lmn}n'_k n'_m \frac{e^{i(kR-\omega t)}}{R}\int d^3x' \alpha_{nj}(\boldsymbol{x}',t)e_j e^{-i\boldsymbol{q}\cdot\boldsymbol{x}'} \tag{2.23}$$

with the scattering vector $\boldsymbol{q} = \boldsymbol{k}' - \boldsymbol{k}$ and where we have used the fact that $\boldsymbol{E}^{(s)} = \boldsymbol{D}^{(s)}/\epsilon$ at the detector. We note that the scattered field is simply the Fourier transform of the dielectric fluctuation:

$$E_i^{(s)} = \frac{E_0 k^2 V e^{i(kR-\omega t)}}{4\pi R\epsilon}(\delta_{kn}\delta_{im} - \delta_{km}\delta_{in})n'_k n'_m \alpha_{nj}(\boldsymbol{q},t)e_j \tag{2.24}$$

with

$$\boldsymbol{\alpha}(\boldsymbol{q},t) = \frac{1}{V}\int d^3x' e^{-i\boldsymbol{q}\cdot\boldsymbol{x}'}\boldsymbol{\alpha}(\boldsymbol{x}',t), \tag{2.25}$$

where V is the scattering volume. Note that we have also carried out the sum over the index l. Simplifying yields:

$$E_i^{(s)} = \frac{E_0 k^2 V e^{i(kR-\omega t)}}{4\pi R\epsilon}\left(n_i' n_k' \alpha_{kj}(\boldsymbol{q},t)e_j - \alpha_{ij}(\boldsymbol{q},t)e_j\right). \tag{2.26}$$

Having obtained an expression for the scattered field at a point far from the scattering volume, we can use our result to calculate the correlation function $\langle \boldsymbol{E}^*(\boldsymbol{R}_1,t_1)\cdot \boldsymbol{E}(\boldsymbol{R}_2,t_2)\rangle$. The brackets denote averaging with respect to the motions of the particles in the medium. We shall assume that the two points $\boldsymbol{R}_1$ and $\boldsymbol{R}_2$ are close together as compared to the distance from the scattering volume, so that $\boldsymbol{k}_1' \approx \boldsymbol{k}_2'$. Using Equation 2.26 for the scattered field,

$$\langle E_i^*(\boldsymbol{R}_1,t_1)E_i(\boldsymbol{R}_2,t_2)\rangle = A^*A\langle(n_i'n_k'\alpha_{kj}^* e_j - \alpha_{ij}^* e_j)(n_i'n_m'\alpha_{ml}e_l - \alpha_{il}e_l)\rangle \tag{2.27}$$

$$= A^*A\left[\langle(\boldsymbol{\alpha}^*\cdot\boldsymbol{e})\cdot(\boldsymbol{\alpha}\cdot\boldsymbol{e})\rangle - \langle(\boldsymbol{n}'\cdot\boldsymbol{\alpha}^*\cdot\boldsymbol{e})(\boldsymbol{n}'\cdot\boldsymbol{\alpha}\cdot\boldsymbol{e})\rangle\right] \tag{2.28}$$

where the conjugated A and $\boldsymbol{\alpha}(\boldsymbol{q},t)$ depend on R_1 and t_1, and the unconjugated quantities depend on R_2 and t_2. Also, we have defined

$$A^*A = \frac{k^4 E_0^2 V^2}{16\pi^2\epsilon^2 R_1 R_2} e^{i[k(R_2-R_1)-\omega(t_2-t_1)]}. \tag{2.29}$$

In general, the dielectric fluctuation tensor $\boldsymbol{\alpha}(\boldsymbol{q},t)$ can be decomposed into three parts, a scalar part, a symmetric part, and an antisymmetric part. For our purposes, it will suffice to only consider scalar scattering, that is, $\alpha_{ik}(\boldsymbol{q},t) = \delta\epsilon(\boldsymbol{q},t)\delta_{ik}$. In this simple case, we obtain

$$\begin{aligned}\langle E_i^*(\boldsymbol{R}_1,t_1)E_i(\boldsymbol{R}_2,t_2)\rangle &= A^*A\langle\delta\epsilon^*(\boldsymbol{q},t_1)\delta\epsilon(\boldsymbol{q},t_2)\rangle\left(1-(\boldsymbol{n}'\cdot\boldsymbol{e})^2\right)\\ &= A^*A\langle\delta\epsilon^*(\boldsymbol{q},t_1)\delta\epsilon(\boldsymbol{q},t_2)\rangle\sin^2\psi\end{aligned} \tag{2.30}$$

where ψ is the angle between the incident field and the scattering direction.

Let us now consider the case of solute particles suspended in a solvent where the dielectric constant fluctuations are caused by concentration fluctuations in the solution. That is, we shall neglect dielectric constant fluctuations that may be induced thermally in the pure solvent, which is the same as assuming that the light scattered from the pure solvent is negligible compared to the light scattered from the suspended particles. If the total concentration of solute particles is not too high, the index of refraction of the solution can be written

$$n = n_0 + \frac{\partial n}{\partial c} c \tag{2.31}$$

where c is the concentration of solute particles and n_0 is the index of refraction of the solvent. In the range of frequencies associated with visible light, the dielectric constant, $\epsilon = n^2$. The fluctuations in dielectric constant can then be related to the concentration fluctuations as follows

$$\delta\epsilon = 2n_0 \frac{\partial n}{\partial c} \delta c, \tag{2.32}$$

giving for the correlation function

$$\langle E_i^*(\boldsymbol{R}_1, t_1) E_i(\boldsymbol{R}_2, t_2) \rangle = K \langle \delta c(\boldsymbol{q}, t_1) \delta c(\boldsymbol{q}, t_2) \rangle \tag{2.33}$$

with

$$K = \frac{k^4 E_0^2 V^2}{4\pi^2 n_0^2 R_1 R_2} \left(\frac{\partial n}{\partial c} \right)^2 \sin^2 \psi e^{i[k(R_2 - R_1) - \omega(t_2 - t_1)]} \tag{2.34}$$

and

$$\delta c(\boldsymbol{q}, t) = \frac{1}{V} \int d^3x' e^{-i\boldsymbol{q}\cdot\boldsymbol{x}'} c(\boldsymbol{x}', t). \tag{2.35}$$

2.2 Static Light Scattering

In a static light scattering experiment, one measures the time-averaged total intensity of the scattered light. We shall assume that our system is ergodic. If this is the case, we can then replace the time averaging by ensemble averaging and thus

use the results derived in the previous section. The intensity at any point in space is proportional to the squared magnitude of the electric field at that point, and can therefore be obtained from Equation 2.33 by setting $\boldsymbol{R}_1 = \boldsymbol{R}_2 = \boldsymbol{R}$ and $t_1 = t_2 = t$. We get

$$\begin{aligned} I &= \langle E_i^*(\boldsymbol{R},t) E_i(\boldsymbol{R},t)\rangle \\ &= \frac{k^4 E_0^2 V^2}{4\pi^2 n_0^2 R^2}\left(\frac{\partial n}{\partial c}\right)^2 \sin^2\psi \langle |\delta c(\boldsymbol{q})|^2\rangle \end{aligned} \tag{2.36}$$

We will show that in the appropriate limit, we can express the total intensity as a function of the osmotic compressibility of the solution. We shall first concentrate our attention on $\langle |\delta c(\boldsymbol{q})|^2\rangle$.

From the definition of $\delta c(\boldsymbol{q})$,

$$\langle |\delta c(\boldsymbol{q})|^2\rangle = \frac{1}{V^2}\langle \int d^3x d^3x' e^{-i\boldsymbol{q}\cdot(\boldsymbol{x}-\boldsymbol{x}')}\delta c(\boldsymbol{x}')\delta c(\boldsymbol{x})\rangle. \tag{2.37}$$

We assume that the fluctuations are homogeneous, that they depend only on the difference $\boldsymbol{r} = \boldsymbol{x} - \boldsymbol{x}'$. This requires that the size of the system be much larger than the characteristic length scale of the fluctuations. In this case, we can perform one integration, obtaining

$$\langle |\delta c(\boldsymbol{q})|^2\rangle = \frac{1}{V}\int d^3r e^{-i\boldsymbol{q}\cdot\boldsymbol{r}}\langle \delta c(0)\delta c(r)\rangle \tag{2.38}$$

with $r = |\boldsymbol{r}|$.

In general, as we noted above, there exists some length scale, R_0 associated with the decay of $\langle \delta c(0)\delta c(r)\rangle$. For a dilute system of macromolecules, R_0 is the characteristic size of the particles. For a strongly interacting system, R_0 would be more appropriately taken to be several interaction radii. The important consideration is that the value of $\langle \delta c(0)\delta c(r)\rangle$ decays to essentially zero over a length scale of the order of R_0.

Let us now consider the limit where q becomes small such that $q^{-1} \gg R_0$, that is, we consider the case where q^{-1} is large compared to any characteristic distance

in the solution. In this case, we can replace the exponential factor in the integrals for $\langle|\delta c(\boldsymbol{q})|^2\rangle$with 1. We note that $\boldsymbol{q}\cdot\boldsymbol{r} \ll 1$ for all $r < R_0$ because of our choice of q. That is, in this region, the exponential factor is always about 1. For $r > R_0$ of course, the exponential factor begins to change appreciably, but this does not matter, since in this region $\langle\delta c(0)\delta c(r)\rangle$ has already decayed to zero. Therefore,

$$\begin{aligned}\langle|\delta c(\boldsymbol{q})|^2\rangle &= \frac{1}{V^2}\langle\left(\int d^3x\delta c(x)\right)^2\rangle \\ &= \langle c^2\rangle - \langle c\rangle^2 \end{aligned} \tag{2.39}$$

and we see that in the limit of small q, that the light scattering intensity is proportional to the mean squared fluctuation in density. These fluctuations, are related to a corresponding thermodynamic susceptibility, χ, through the following simple argument. Let us consider the Gibbs free energy of a small portion of the total system as a function of the local concentration c. The local concentration c has an equilibrium value $\bar{c}$ around which it fluctuates. At any given instant, we can expand the Gibbs free energy around $c = \bar{c}$, giving to lowest nonvanishing order in δc

$$\begin{aligned}G(c) &= G(\bar{c}) + \frac{1}{2}\frac{\partial^2 G}{\partial c^2}(\delta c)^2 \\ &= G(\bar{c}) + \frac{1}{2}\chi(\delta c)^2, \end{aligned} \tag{2.40}$$

where we have identified the thermodynamic susceptibility

$$\chi = \frac{\partial^2 G}{\partial c^2}. \tag{2.41}$$

In Equation 2.40, a term linear in δc does not appear, since at equilibrium,

$$\frac{\partial G}{\partial c} = 0. \tag{2.42}$$

The probability to observe a given value of the local density is proportional to the usual Boltzmann factor. Thus, the mean square density fluctuation may be

expressed

$$\langle(\delta c)^2\rangle = \frac{\int_{-\infty}^{\infty} d(\delta c)(\delta c)^2 e^{-G(c)/k_B T}}{\int_{-\infty}^{\infty} dc e^{-G(c)kbT}}. \tag{2.43}$$

Using Equation 2.40 in Equation 2.43, we obtain

$$\langle(\delta c)^2\rangle = \frac{\int_{-\infty}^{\infty} d(\delta c)(\delta c)^2 e^{-\frac{\chi(\delta c)^2}{2k_B T}}}{\int_{-\infty}^{\infty} d(\delta c) e^{-\frac{\chi(\delta c)^2}{2k_B T}}} = \frac{k_B T}{\chi}. \tag{2.44}$$

The thermodynamic susceptibility χ, is related to the osmotic compressibility of the solution through the relation

$$\chi = \frac{V}{c}\frac{\partial \pi}{\partial c}, \tag{2.45}$$

the derivation of which is discussed in Appendix A. Using Equation 2.45 in Equation 2.44, we can express the mean squared concentration fluctuations

$$\langle(\delta c)^2\rangle = \frac{k_B T c}{V}\left(\frac{\partial \pi}{\partial c}\right)^{-1}, \tag{2.46}$$

which, in turn, allows us to write the total scattered intensity, using Equations 2.39 and 2.36,

$$I = \frac{k^4 E_0^2 V c k_B T}{4\pi^2 n_0^2 R^2}\left(\frac{\partial n}{\partial c}\right)^2\left(\frac{\partial \pi}{\partial c}\right)^{-1}\sin^2\psi. \tag{2.47}$$

Thus we have shown that in the limit of small q, that the total intensity of scattered light is proportional to the osmotic compressibility of the scattering solution.

2.3 Dynamic Light Scattering

In a homodyne dynamic light scattering experiment, one measures the time auto-correlation function of the intensity of the scattered light,

$$\langle I(0)I(\tau)\rangle = \frac{1}{T}\int_{t_0}^{t_0+T} dt I(t)I(t+\tau) \tag{2.48}$$

where T is the total time over which the measurement is collected. For sufficiently large T, if we assume the system is ergodic, the integral is independent of t_0, and

furthermore, we can replace the time averaging with an ensemble average. The total intensity is, of course, proportional to the square of the scattered electric field, so that our measured quantity can be written

$$\langle I(q,0)I(q,t)\rangle = B\langle |E(q,0)|^2 \, |E(q,t)|^2\rangle, \tag{2.49}$$

where B is a proportionality constant that includes such factors as the quantum efficiency of the photomultiplier.

If the scattering volume is large compared to the volume over which particle motions are correlated, then the total scattered electric field can be considered to be made up of contributions from a large number, N, of independent random scatterers. In this case the central limit theorem can be applied, implying that the scattered electric field $E(q,t)$ is a zero-mean Gaussian stochastic variable. This being the case, it is possible to show that

$$\langle I(0)I(t)\rangle = B\langle I\rangle^2 \left(1 + f(A_c)[g(t)]^2\right) \tag{2.50}$$

with

$$g(t) = \frac{|\langle E^*(0)E(t)\rangle|}{\langle I\rangle}. \tag{2.51}$$

The quantity $f(A_c)$ is an instrumental factor with a value between 0 and 1 that takes into consideration the number of coherence areas covered by the finite area of the collection optics.

From Equation 2.33 we see that the normalized electric field correlation function $g(t)$ is related to the time autocorrelation function of the density fluctuations in the solution. We get

$$g(t) = \frac{1}{V\langle |\delta c(\boldsymbol{q})|^2\rangle} \int d^3r e^{-1\boldsymbol{q}\cdot\boldsymbol{r}} \langle \delta c(0,0)\delta c(r,t)\rangle, \tag{2.52}$$

where we have also used the definition of $\delta c(\boldsymbol{q},t)$ and performed one integration over the volume, assuming as we did in Section 2.2 (in arriving at Equation 2.38) that the fluctuations in concentration are homogeneous. In order to evaluate $g(t)$, we

need to understand the properties of $\langle \delta c(0,0)\delta c(r,t)\rangle$.

It is possible to obtain an expression for $g(t)$ in a few special cases. In particular, let us consider the case of particles suspended in solution undergoing Brownian motion. Such particles obey the diffusion equation (Fick's second law), and so also does $\langle \delta c(0,0)\delta c(r,t)\rangle$. That is, we have

$$\frac{\partial}{\partial t}\langle \delta c(0,0)\delta c(r,t)\rangle = D\nabla^2\langle \delta c(0,0)\delta c(r,t)\rangle, \tag{2.53}$$

with D as the particle diffusion coefficient, from which it is easy to see that

$$g(t) = e^{-Dq^2t}. \tag{2.54}$$

A measurement of the time autocorrelation function of the scattered intensity from a solution of Brownian particles can therefore be used to obtain the diffusion coefficient of those particles. In many cases of practical interest, however, the solution contains more than one kind of particles. In this case, the electric field time autocorrelation function $g(t)$ is a superposition of exponentials resulting from the diffusion of different particle species, weighted according to the scattering amplitude of each species. In general we write

$$g(t) = \int_0^\infty d\Gamma A(\Gamma)e^{-\Gamma t}, \tag{2.55}$$

where $A(\Gamma)$ is the scattering intensity associated with the particles of decay rate $\Gamma = Dq^2$. Obtaining information about the $A(\Gamma)$ is a difficult task due to the noise in the experimental measurement of $\langle I(0)I(t)\rangle$. We shall address these issues and discuss various techniques of obtaining information about $A(\Gamma)$ in Chapter 3, where we detail the experimental methods used to obtain and analyze quasielastic light scattering data on our experimental system.

Chapter 3

The $C_{12}E_6$, $C_{12}E_8$, and Water System

Dodecyl hexaoxyethylene glycol monoether ($C_{12}E_6$) and dodecyl octaoxyethylene glycol monoether ($C_{12}E_8$) are both nonionic surfactants consisting of a hydrophobic hydrocarbon chain connected to a hydrophilic chain of ethylene oxide units. The two molecules are shown structurally in Figure 3-1. Because of the similarity between the molecules (the only difference is two ethylene oxide units), solutions of $C_{12}E_6$ and water and solutions of $C_{12}E_8$ and water share many qualitatively similar properties. For example, both solutions are known to form micelles that are generally believed to exhibit linear growth with increasing concentration and temperature [22, 23, 24]. Both also exhibit a lower consolute temperature phase transformation from a single isotropic micellar phase into two isotropic micellar phases differing in total surfactant concentration. The small difference in the molecules, however, is enough to see quantitatively significant differences in the micellar properties of the two solutions, thus illustrating that the process of micellization depends sensitively on the structural balance between the hydrophilic and hydrophobic regions of the surfactant.

The critical micellar concentration at 25°C for the $C_{12}E_8$ and water system is $7.1 \times 10^{-5} M (0.004\%)$ and for the $C_{12}E_6$ and water system is $6.8 \times 10^{-5} M$ [25]. On the other hand the difference of two ethylene oxide groups makes a change of about

n-dodecyl hexaoxyethylene glycol monoether

$$\underbrace{CH_3(CH_2)_{11}}_{\text{hydrophobic}}\text{-}\underbrace{(O(CH_2)_2)_6OH}_{\text{hydrophilic}}$$

n-dodecyl octaoxyethylene glycol monoether

$$\underbrace{CH_3(CH_2)_{11}}_{\text{hydrophobic}}\text{-}\underbrace{(O(CH_2)_2)_8OH}_{\text{hydrophilic}}$$

Figure 3-1: Structure of dodecyl hexaoxyethylene glycol monoether ($C_{12}E_6$) and dodecyl octaoxyethylene glycol monoether ($C_{12}E_8$)

25°C in the phase separation temperature. Reported values for T_C for the $C_{12}E_6$ and water system range from 50.35°C [26] to 51.3°C [18] and for the $C_{12}E_8$ and water system they range from 74.0°C [23] to 78.4°C [17]. Furthermore, we will see that at a given temperature and concentration, the observed extent of micellar growth is much greater in $C_{12}E_6$solutions than in $C_{12}E_8$ solutions.

In this chapter we will experimentally examine, by means of quasielastic light scattering, solutions containing three different relative compositions of $C_{12}E_6$ and $C_{12}E_8$ over a broad range of temperature and total surfactant concentration in the single-phase region of the phase diagram. We shall also examine the behavior of aqueous solutions containing pure $C_{12}E_6$ and solutions containing pure $C_{12}E_8$. Using a combination of total intensity light scattering measurements and quasielastic light scattering measurements, we will also examine the hypothesis that micellar growth in the mixed system is also one-dimensional.

It should be noted here that there still exists a controversy in the literature concerning the interpretation of scattering data from micellar systems that exhibit liquid-liquid phase separation. There are two schools of thought on the subject. Both sides agree that at temperatures far away from the critical temperature for phase separation and for concentrations far below the critical concentra-

tion for phase separation, that interactions between micelles are weak, and that light scattering measurements therefore probe the actual size and mass of the micelles. One school of thought claims that the observed increase in scattered light intensity and the decrease in diffusivity that occur as the concentration is increased towards the critical concentration and the temperature is changed towards the critical temperature is due primarily to changes in the average micellar size [23, 27, 28, 22, 15, 12, 24, 29, 13, 30, 31, 32, 33, 34]. Only when the system is close to the critical point ($|T - T_C| < 5°\mathrm{C}$ is a reasonable consensus value) are the light scattering data completely dominated by critical effects. When the solution concentration is increased to the vicinity of the critical concentration and beyond, the increasing importance of excluded volume effects makes itself felt as an observed minimum in the diffusivity [35]. Thus, the picture is micellar growth with critical effects superimposed in the close vicinity of the critical point, and with increasing solution nonideality as the concentration is increased from the dilute regime to the "semi-dilute" regime.

The other school of thought claims that the observed increase in scattered light intensity and the decrease in diffusivity as concentration is increased from the very dilute regime and temperature is changed towards the phase boundary are due solely to critical effects [26, 36, 37, 38, 39, 18]. They assume that the average micellar size remains constant (or that it changes insignificantly) over the entire phase diagram. The minimum in the diffusivity they attribute to critical slowing-down, and thus they indicate that the critical region extends as far as $|T - T_C| \leq 30°\mathrm{C}$ [18].

In an attempt to shed more light on the subject, workers in the field have performed a series of measurements other than light scattering, notably neutron scattering experiments [32, 36, 39, 31] and nuclear magnetic resonance measurements [22, 29, 30, 24]. The results, however, are still unclear. Some of the authors report findings consistent with the first viewpoint, while others support the second. More recent developments in the technique of cryo-transmission electron microscopy has allowed the direct imaging of micelles in vitrified solutions. By this method, Vinson et. al. [40] and Edwards et. al. [41] have obtained evidence of elongated wormlike

micelles and disclike micelles in several different systems.

Considering the wide selection of experiments that can be interpreted (although not perhaps unambiguously) in terms of micellar growth, and the direct evidence provided by cryo-transmission electron microscopy, we favor the first school of thought. Therefore, we shall interpret our light scattering data assuming that micellar growth does indeed occur in our solutions. In light of the still active controversy, however, we must be careful in our interpretations at temperatures close to T_C and at concentrations close to and above the critical concentration. It should remain clear that an alternative explanation of the light scattering results including only interactions may be possible, although unlikely. In this work we examine the internal self consistency of the first view as compared with our experimental results.

Section 3.1 is dedicated to a discussion of the materials and methods used in our experimental work. Solution preparation is discussed in Section 3.1.1, and the dynamic and static light scattering apparatus and methods are described in Sections 3.1.2 and 3.1.3. In Section 3.2 we present the results of out measurements on the $C_{12}E_6$, $C_{12}E_8$, and water system.

3.1 Materials and Methods

3.1.1 Sample Preparation

High purity crystalline dodecyl hexaoxyethylene glycol monoether ($C_{12}E_6$) and dodecyl octaoxyethylene glycol monoether ($C_{12}E_8$) were obtained from Nikko Chemicals, Tokyo, and used without further purification. Aqueous solutions were prepared by weight, using reagent grade water from a Millipore Milli-Q filtration system (Millipore, Bedford, MA) which was first de-gassed, and then saturated with filtered Argon. Two methods of dust-removal were used in further preparing the samples for light scattering.

Initially, dust-removal was accomplished by circulating the sample through a 0.22 micron filter (Millex-GV, Millipore, Bedford, MA) continuously for approximately

20 minutes, until observed to be free of dust with a 20x telescope attached to our light scattering instrument. It was found, however, that when this method of dust removal was used, that the measured time autocorrelation function of solutions at concentrations within an order of magnitude of the critical micellar concentration did not exhibit a narrow, single modal distribution of relaxation times as expected. Rather, it was found that the distribution of relaxation times in such a sample was bimodal, with one peak centered about the expected relaxation time for micelles, and the other peak an order of magnitude slower. Samples prepared without this continuous filtration did not exhibit the second, slow decay.

In order to avoid the difficulties presented by this bimodal distribution of decay rates, a second method of dust-removal was used. In this method, samples were passed just once through a rinsed 0.22 micron filter (Millex-GV, Millipore, Bedford, MA) into a scattering cell, which was then sealed and centrifuged at $4600 \times g$ for at least 30 minutes.

3.1.2 Dynamic Light Scattering Measurements

Dynamic light scattering measurements were performed using two different instruments. Details of these instruments are to be found elsewhere [7, 10, 42], but the essential features of each will be summarized below.

The light source of the first instrument consists of a vertically polarized argon-ion laser (Spectra-Physics model 164, Mountain View CA) emitting at 488.0 nm. Light from the laser illuminates the sample, which is held at a fixed temperature to within 0.1°C by a Peltier device. Scattered light is collected by a photomultiplier (Pacific Instruments, Concord CA), mounted with the detection optics at the end of a long swinging arm. The signal from the photomultiplier is passed through an amplifier/discriminator (Pacific Instruments, Concord CA) to a Langley-Ford (Amherst, MA) model 1096 autocorrelator with 144 channels for processing.

The second instrument is based on the design of Haller, Destor, and Cannell [43] and was built by Richard Chamberlin. It is described in great detail elsewhere [42]. Light from a vertically polarized argon-ion laser (Coherent Innova 90-5, Santa Clara

CA) emitting at 488.0 nm was used to illuminate the sample, which is held at fixed temperature to within $\pm 0.002K$ within a large water reservoir. Light scattered from the sample is collected by a fiber-optic cable at one of twelve fixed angles ($11.5° \leq \theta \leq 162.6°$) and directed to the photomultiplier (Pacific Instruments, Concord CA). The signal was then passed through an amplifier/discriminator (Langley-Ford PAD-1) and to a Langley-Ford model 1096 autocorrelator similar to the first instrument.

In both instruments the Langley-Ford autocorrelator is used to measure the time autocorrelation function $\langle I(q,0)I(q,t)\rangle$ of the incoming photocounts. Photocounts are accumulated by the correlator over a short time interval, t_s, called the sample time. At the end of each sample time, the accumulated number of photocounts is loaded onto the first position of a shift register after shifting all existing numbers on the register up one position. Thus, if n_k is the number of photocounts received during the k^{th} sample time, then after i sample times, the first element contains n_i, the second element contains n_{i-1}, the third, n_{i-2}, etc.

Furthermore, as each photocount is received by the correlator, each value on 144 of the elements of the shift register is added to its own running total. If the first element is chosen to keep a running total, then after N sample times of operation we will have accumulated

$$\sum_{i=1}^{N} n_i n_{i-1}. \tag{3.1}$$

Likewise, if the k^{th} element is chosen, we will have accumulated

$$\sum_{i=1}^{N} n_i n_{i-k}. \tag{3.2}$$

Since the correlator can accumulate data in the shift register before the measurement is started (that is, before the running totals are cleared and started) values for which $i - k < 1$ are defined. In any case, values for which $i - k < 1$ are few in number if the total number of sample times of the measurement, N, is large.

The 144 running totals, or channels, are chosen in the following way. The first 128 are taken sequentially, following an initial delay, t_d, of up to 1024 sample times. Between channel 128 and 129, there is a further delay of 1024 sample times. The last

16 channels are then taken sequentially. Thus, each of the 144 correlator channels provides an estimate of the average value of $\langle I(q,0)I(q,t)\rangle$ over the time interval from t to $t+t_s$. The first 128 channels record the time correlation function from t_d+t_s to t_d+128t_s. The last 16 channels measure the correlation function from $t_d+1153t_s$ to $t_d+1168t_s$, and thus provide an estimate of $\langle I(q,0)I(q,t)\rangle$ for t much longer than t_s, and can be used to check for the presence of very slow decays, such as those caused by dust. For our measurements, we will always choose t_d equal to either 0 or 1 sample time.

Choice of the sample time is important, as it will dictate the range of decay rates that will be probed by the measurement. For all of our measurements we attempt to choose a sample in a consistent way, coupled to the properties of the sample. The average decay rate was obtained from a trial measurement using the method of cumulants (described below), truncating the series at the second cumulant. The sample time was then adjusted so that the next measurement should span typically either 3 or 6 decay times. A new trial measurement was taken, and the process of adjusting the sample time was repeated until the results were self-consistent, that is, until no further adjustment was necessary. At this point two or three measurements were performed for each choice of the number of decay rates, collecting light for from 3 to 5 minutes for each measurement. An additional measurement with a fixed sample time of $10\mu s$ was sometimes performed to check for the presence of additional, slow decays.

In order to extract from the measured photocount time autocorrelation function useful physical information about our system (like, for example the collective diffusion coefficient of the particles in our solution) we must first obtain the normalized first-order correlation function $g(t)$ which is discussed in Chapter 2. The relation between $\langle I(q,0)I(q,t)\rangle$ and $g(t)$ is given by Equation 2.50. From this equation we see that it is necessary to know $\langle I(q)\rangle^2$. This number can be calculated, since in addition to recording the time autocorrelation function, the correlator also records the total number of sample times during the measurement n_{st}, the total number of photocounts accumulated and loaded onto the shift register during the entire

measurement, n_s, and the total number of add commands during the measurement n_a. In principle n_s should equal n_a, but in practice they are slightly different due to dead-time in the correlator electronics. The best estimate of $\langle I(q)\rangle^2$ is therefore given by

$$\langle I(q)\rangle^2 = \frac{n_s n_a}{n_{st}}, \tag{3.3}$$

which we call the monitor baseline. This baseline was used to calculate $\sqrt{f(A_c)}g(t)$.

As mentioned in Chapter 2, in the regime where interparticle interactions are small, the fluctuations in the scattered light from the sample are caused by the Brownian motion of the particles suspended in solution. The contribution of a particle to the normalized first-order correlation function has an exponential form

$$e^{-\Gamma t} \tag{3.4}$$

with a characteristic decay time of

$$\Gamma = Dq^2, \tag{3.5}$$

where D is the translational diffusion coefficient, of the particle, and q is the scattering vector. If all of the particles in the system are of the same size, then

$$g(t) = e^{-\Gamma t} \tag{3.6}$$

and it is a simple task to extract their diffusion coefficient from the measured correlation function. However, in the case of polydisperse systems, the analysis of the measured correlation function is not so straightforward. For a polydisperse system we may write the normalized first-order correlation function

$$g(t) = \int_0^\infty d\Gamma\, A(\Gamma) e^{-\Gamma t}, \tag{3.7}$$

where $A(\Gamma)$ is the normalized amplitude of scattered light associated with decays having a characteristic decay time Γ^{-1}. Thus, $A(\Gamma)$ will be proportional to the

concentration and the mass of the scattering particles. Determination of $A(\Gamma)$ by a direct inverse-Laplace transform would, in principle, allow us to determine the concentration distribution of particle sizes in the solution. Unfortunately, the inversion of Equation 3.7 is an ill-posed problem [44]. For any reasonable measurement, there exist infinitely many solutions for $A(\Gamma)$ that will fit to within the experimental uncertainties. Furthermore, as a result of arbitrarily small changes in the measured $g(t)$, we obtain large amplitude, fast-oscillating fluctuations in $A(\Gamma)$. Physically, this is unreasonable, since we expect our actual distribution to be a smooth function of Γ. Thus, other alternatives need to be sought.

The most popular method of obtaining information about $A(\Gamma)$ is the method of cumulant analysis [45, 46]. In cumulant analysis, we fit $\ln g(t)$ to a polynomial of the form

$$\ln g(t) = \sum_{i=1}^{N} K_i \frac{(-t)^i}{i!}. \tag{3.8}$$

In the limit of $N \to \infty$ or $t \to 0$, the cumulants, K_i, are related to the moments of $A(\Gamma)$. For example,

$$K_1 = \int_0^\infty d\Gamma\, \Gamma A(\Gamma) = \langle \Gamma \rangle_{av}, \tag{3.9}$$

$$K_2 = \int_0^\infty d\Gamma\, \left(\Gamma^2 - \langle \Gamma \rangle_{av}^2\right) A(\Gamma) = \langle \Gamma^2 \rangle_{av} - \langle \Gamma \rangle_{av}^2, \tag{3.10}$$

and so forth. In practice, this method usually permits the reliable determination of the first cumulant, and with less accuracy, the second cumulant.

Recently, powerful alternatives to the cumulant method have been developed. These methods [44, 47, 48] permit the reconstruction of the distribution of diffusing particles by incorporating *a-priori* information about the system. The method we have used to analyze our data is based on Reference [47], and was implemented by Dr. Aleksey Lomakin [49]. This regularization algorithm is similar to the method of Provencher [44, 50] and the method of Skilling and Bryan [48].

The normalized first-order correlation function given by Equation 3.7 is approx-

imated by a histogram of the form

$$g(t) = \sum_{i=1}^{n_c} A_i e^{-\Gamma_i t}, \tag{3.11}$$

where n_c is the total number of channels taken in the solution, Γ_i is the characteristic decay rate associated with the i^{th} solution channel, and A_i is the amplitude of the i^{th} solution channel. The Γ_i must be chosen consistently with the measured data points. That is, since the data contain no information about time scales shorter than one sample time, it would be senseless to consider solutions with $\Gamma > t_s^{-1}$. Furthermore, we cannot distinguish from each other, decays slower than about twice the range of the first 128 channels taken together. Thus, the Γ_i for $2 \leq i \leq n_c$ are chosen logarithmically between $(256t_s)^{-1}$ and ${t_s}^{-1}$, with $\Gamma_1 = 0$. This choice of the Γ_i constrains the solution points to within the limits allowed by the measurement. All decays slower than twice the range of the first 128 channels are considered together in the first, background channel.

The value of n_c should be chosen larger than the number of independent parameters contained in the data. For example, a measurement from which we can reliably extract a first and second cumulant but not the third, can be said to contain between 2 and 3 independent parameters. The number of independent parameters in a given set of data will depend on the noise level of the data. For our homodyne dynamic light scattering measurements this number is typically around 2 or 3. Thus, we arbitrarily choose the value $n_c = 60$, which provides a reasonably smooth characterization of the solution. Solutions with $n_c > 60$ will provide a smoother approximation to Equation 3.7, but will of course become progressively more computationally expensive. Furthermore, such solutions contain no additional information, since 60 is already well above the number of independent parameters contained in the data.

Experimentally, we determine the quantity

$$G(t_j) = \langle I(q,0)I(q,t_j)\rangle - \langle I(q)\rangle^2, \tag{3.12}$$

where we have used the index on t to indicate that our measurements are at the 144 discrete points chosen by the correlator, as discussed previously. By Equation 2.50, we see that our measurement is proportional to $g(t)^2$. Our task is to calculate the n_c values $\{A_i\}$. Toward this end, we must minimize the fourth order functional in A_i

$$\Omega_0(\{A_i\}) = \sum_{j=1}^{144} \left[G(t_j) - (g(t_j))^2\right]^2 \tag{3.13}$$

subject to the physical restriction that all $A_i \geq 0$.

Unfortunately, that is not all, since the problem is still ill-conditioned. There are still a large number of solutions that will fit equally well to within the experimental uncertainties. Also, small changes in the experimentally measured quantities can still result in fast oscillating fluctuations in the $\{A_i\}$. These fluctuations are physically unreasonable, since in most cases, we expect that our distribution of $\{A_i\}$ should be reasonably smooth. By smooth, we mean that differences between A_i and A_{i+1} should be small. In this way, we also reduce the sensitivity of the solution to noise in the experimental data.

There are a variety of different methods of choosing a solution that is smooth in $\{A_i\}$ [44, 47, 48]. In the algorithm implemented by Dr. Lomakin, we add a stabilization term to the minimization integral that punishes nonzero solution channels. The result of this term is to smooth the resulting distribution. Instead of minimizing Ω_0, we choose to minimize the functional

$$\Omega(\{A_i\}, \delta) = \Omega_0(\{A_i\}) + \delta \sum_{i=1}^{n_c} {A_i}^2, \tag{3.14}$$

where the non-negative regularization parameter δ regulates the amount of smoothing of the solution. Larger values of δ result in smoother solutions, but at the expense of some systematic distortion. This distortion can be felt as a slight increase in $\Omega_0(\{A_i\}_\delta^{min})$ from its absolute minimum at $\delta = 0$, $\Omega_0(\{A_i\}_{\delta=0}^{min})$, where $\{A_i\}_\delta^{min}$ refers to the set of A_i that minimizes Equation 3.14 at the specified value of δ. The regularization parameter must therefore be chosen as small as possible, but yet still large enough to make the solution insensitive to the random errors in the

experimental measurement. We therefore choose the regularization parameter by increasing δ from zero until the value of $\Omega_0(\{A_i\}_\delta^{min})$ has increased from its minimum by some threshold amount, σ, defined relative to $\Omega_0(\{A_i\}_{\delta=0}^{min})$,

$$\Omega_0(\{A_i\}_\delta^{min}) = (1+\sigma)\Omega_0(\{A_i\}_{\delta=0}^{min}). \tag{3.15}$$

In the analysis of our data, we have used $\sigma = 0.01$. This criterion provides an objective way of choosing δ consistent with the measurement accuracy and the shape of the distribution.

To compare measurements from a set of data with the same measurement accuracy, we should choose the same regularization parameter. In this case, we first analyze all of the data, choosing the regularization parameter as described above. From the results of this analysis, we choose a single value of δ that best represents all of the data, and analyze all of the data again using this single value.

3.1.3 Static Light Scattering Measurements

Static light scattering measurements were performed using the light scattering instrument constructed by Richard Chamberlin, described in the previous section and in great detail elsewhere [42]. The angular dependence of the light scattered from a sample was measured in a cylindrical cell. Measurements were obtained by cycling through the 13 fixed angles ($\theta = 0°$ and twelve angles for which $11.5° \leq \theta \leq 162.6°$) by means of computer controlled shutters, collecting the scattered light for ~ 1.5 seconds at each angle. This cycling procedure was repeated until at least 30 such measurements were accumulated from each angle. The intensity measured at each angle in a cycle was normalized to the measured transmitted intensity for that cycle in order to correct for laser power drift and sample turbidity. Since a cylindrical scattering cell was used, no further correction for turbidity was required. In order to reduce the effects of dust (particularly at the smaller angles), the average and standard deviation of the normalized measurements at each angle were calculated, and any measurement falling more than five standard deviations above the

mean intensity was discarded. A new average was computed from the remaining measurements.

The formula we obtained in Chapter 2 for the total intensity of light scattered from a sample (Equation 2.36 with Equation 2.38) depends on quantities that will vary from experiment to experiment. These quantities include the scattering volume, V, the distance from the scattering volume to the detector, R, and the intensity of the illuminating light source, E_0^2. From a practical standpoint, it is useful to define a quantity that depends only on the intrinsic scattering properties of the scattering solution. This quantity is named the Rayleigh ratio, and it is defined

$$\mathcal{R}(\theta) = \frac{I(q)R^2}{E_0^2 V}. \tag{3.16}$$

Comparison with Equation 2.36 and Equation 2.38 shows that the Rayleigh ratio, as defined above, is independent of R, E_0^2, and V.

In our instrument, each angle has its own fixed collection optics. Differences in alignment at the various angles cause the efficiency of light collection to be significantly different at each angle. In order to remove these instrumental factors from the measurements, it is necessary to to perform a comparative measurement. In addition to our sample, a measurement of the same kind as described above was performed on a reference solvent with known scattering properties (Toluene, HPLC grade, Aldrich) contained in a cylindrical scattering cell similar to that containing the sample. The angle dependent Rayleigh ratio of the sample was determined from the relation

$$\mathcal{R}(\theta) = \left(\frac{n_{samp}}{n_{ref}}\right)^2 \left(\frac{I_{samp}(\theta)/I_{samp}(0)}{I_{ref}(\theta)/I_{ref}(0)}\right) \mathcal{R}_{ref} \tag{3.17}$$

which includes the factor $(n_{samp}/n_{ref})^2$ to correct for the change in scattering volume and solid acceptance angle due to the different indices of refraction of the sample and reference solvent. The Rayleigh ratio of toluene is independent of angle, but has some dependency on temperature and wavelength. Values of n and R for toluene at the temperatures and wavelength of interest are given in Table 3.1.

By extrapolating $\mathcal{R}(\theta)$ to $\theta = 0°$, corresponding to $q = 0$, we can determine

Table 3.1: Toluene refractive index and Rayleigh ratio at λ=488 nm as a function of temperature

T (°C)	n[a]	$\mathcal{R}$[b]	T (°C)	n	$\mathcal{R}$
5	1.516	38.4	35	1.500	40.2
10	1.513	38.7	40	1.487	40.5
15	1.511	39.0	45	1.494	40.8
20	1.50781	39.3	50	1.492	41.2
25	1.505	39.6	55	1.489	41.5
30	1.502	39.9			

[a]The temperature dependent values of n were computed in Reference [42].

[b]Taken from Reference [42]. The temperature dependence at λ=488 nm was determined by extrapolating the $I(T)/I(20°C)$ measurements of Ehl [51] for λ=548 nm to the desired temperature, applying the correction $(n_T/n_{20°C})^2$ to correct for temperature dependent index changes, and applying this as a temperature correction to the reported value for $\mathcal{R}$ at 25°C and λ=488 nm by Bender et. al. [52]

the osmotic compressibility as shown in Chapter 2. Using Equation 2.47 for the scattered intensity and Equation 3.16, the definition of the Rayleigh ratio, $\mathcal{R}(\theta)$, we have

$$\frac{1}{k_B T}\frac{\partial \pi}{\partial c} = \frac{4\pi^2 n_0^2 c}{\lambda^4}\left(\frac{\partial n}{\partial c}\right)^2 \frac{1}{\mathcal{R}(0)}. \tag{3.18}$$

An experimental estimate of the refractive index increment is determined by using a refractometer (Bausch and Lomb Abbe-3L) to measure the refractive index of the sample as a function of total concentration.

For a system of particles with interactions that can be approximated by a second virial coefficient suspended in a weakly scattering solvent, Debye [53] has shown that

$$\frac{1}{k_B T}\frac{\partial \pi}{\partial c} = \frac{1}{M} + 2Bc, \tag{3.19}$$

relating the inverse osmotic compressibility to the molecular weight, M, of the particles and their second virial coefficient, B. If the system is polydisperse, then M is actually the weight-averaged molecular weight. In systems such as protein solutions or polymer solutions where the particle size is not expected to change appreciably with concentration, the molecular weight of the particles is properly determined by extrapolating the measured osmotic incompressibility to zero concentration. The concentration dependence of the osmotic incompressibility then provides informa-

tion about the second virial coefficient of the system. If the interactions are weak, the concentration dependence of the osmotic incompressibility will be small, and neglecting the second virial coefficient without performing the extrapolation to zero concentration will not cause too great an error.

In a micellar system, however, the average particle size is determined by a detailed equilibrium between a distribution of micelles of various sizes and shapes, and the free monomers in solution. When the total concentration of surfactant is changed, this equilibrium can shift, and can cause a change in the average particle size. By extrapolating the osmotic incompressibility to zero concentration assuming that all of the actual measurements are for concentrations above the critical micellar concentration, we will obtain an estimate of the average molecular weight of the minimum sized micelle. The meaning of the concentration dependence of the osmotic incompressibility is less clear now, since M is expected to change appreciably with concentration, but also interactions are bound to become important at some point. We have assumed that in the region where our total intensity measurements have been taken (well below the phase boundary and for concentrations well below the critical concentration for phase separation, see Section 3.2.3) that the interactions between micelles are weak and that the concentration dependence of the osmotic incompressibility can be interpreted as a change in the weight-averaged micellar mass. Keeping in mind, however, that other explanations are possible, we call the resulting mass the apparent molecular weight, M_{app}.

3.2 Experimental Results

Having discussed our experimental system and the methods used to prepare samples and accumulate, analyze, and interpret light scattering data on that system, we now present and discuss our experimental results. This section is divided into four subsections. The first two subsections comprise the majority of our results. In Section 3.2.1 we discuss and present quasielastic light scattering measurements over a broad range of temperature and concentration for concentrations well above the

critical micellar concentration for the pure $C_{12}E_6$ and water system and the pure $C_{12}E_8$ and water system. This section serves as background for the next section, Section 3.2.2, in which quasielastic light scattering data on mixtures of $C_{12}E_6$ and $C_{12}E_8$ is presented.

It was stated in the introduction to this chapter that it is generally believed that $C_{12}E_6$ micelles and $C_{12}E_8$ micelles exhibit rodlike growth in aqueous solution at sufficiently high temperature and concentration. It is reasonable, therefore, to propose that mixed micelles composed of the two surfactants should also exhibit linear growth. This hypothesis is investigated by means of combined static and dynamic light scattering measurements in Section 3.2.3. Finally, in Section 3.2.4, we present light scattering measurements in the very dilute regime that allow a determination of the critical micellar concentration at different temperatures for pure $C_{12}E_6$ micelles and for pure $C_{12}E_8$ micelles. We will see in Chapter 4 that these measurements are necessary in order to determine all of the parameters of the generalized ladder model presented there.

3.2.1 Dynamic Light Scattering Measurements on Pure $C_{12}E_6$ and Water and Pure $C_{12}E_8$ and Water

We are primarily interested in the behavior of surfactant mixtures, specifically aqueous solutions containing mixtures of $C_{12}E_6$ and $C_{12}E_8$. However, we first begin with an examination of the behavior of solutions containing pure $C_{12}E_6$ and solutions containing pure $C_{12}E_8$, in order to establish the properties of the two individual micellar systems. Aqueous solutions of pure $C_{12}E_6$ and aqueous solutions of pure $C_{12}E_8$ were prepared as described in Section 3.1.1 and measured using dynamic light scattering as described in Section 3.1.2. All measurements were made at a scattering angle of 90°. The resulting correlation functions were analyzed using the regularization procedure discussed in Section 3.1.2.

Figure 3-2 shows the results of our measurements on the pure $C_{12}E_6$ and water system (3-2a) and the pure $C_{12}E_8$ and water system (3-2b) on the same scale. We

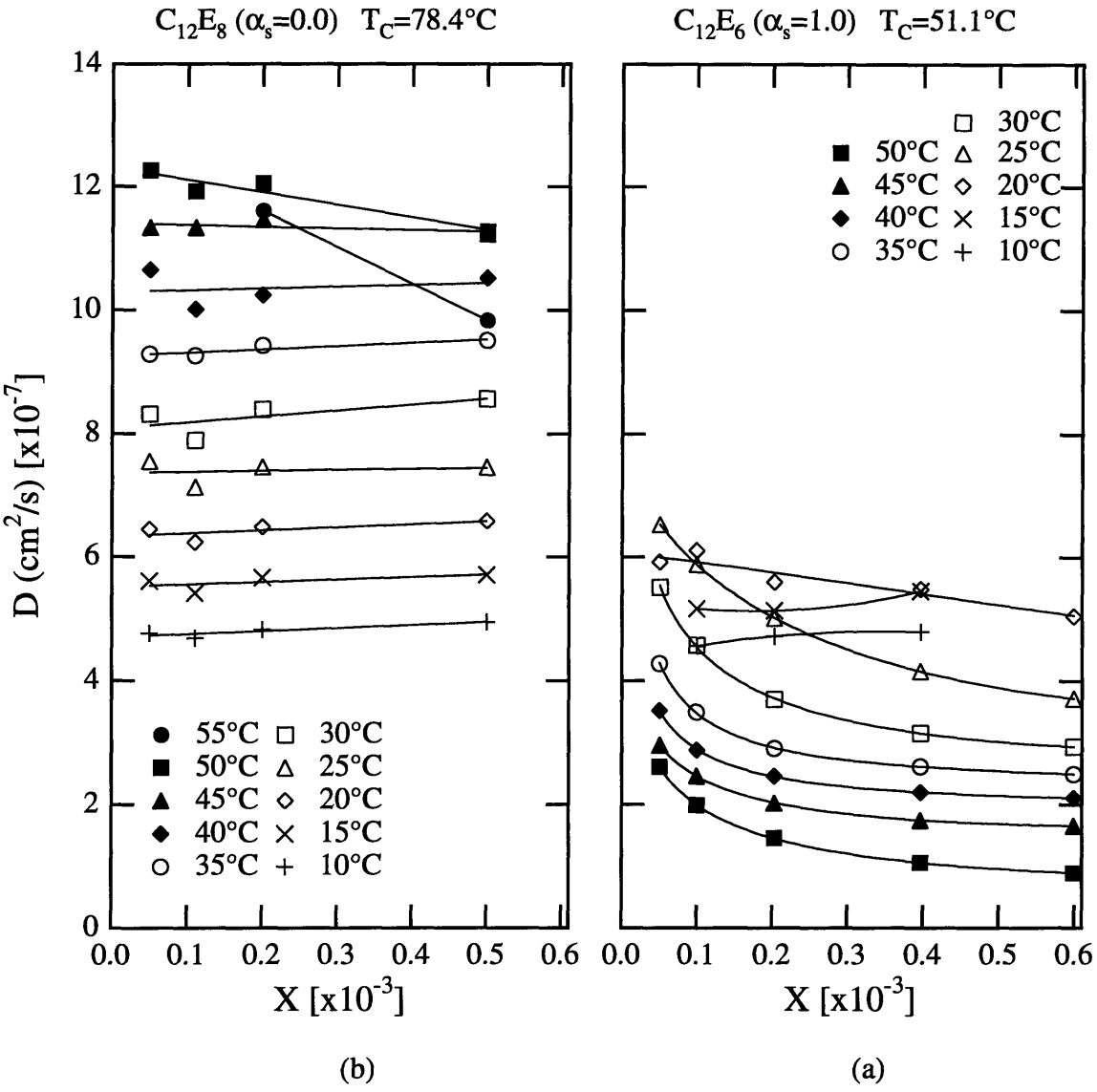

Figure 3-2: The average diffusivity, D, measured as a function of total surfactant mole fraction, X, for aqueous solutions of pure $C_{12}E_6$ (a) and pure $C_{12}E_8$ (b). The different symbols represent measurements at different temperatures. The solid lines through the data points are intended as guides to the eye, to indicate the trends present in the data. The critical temperature for phase separation is indicated at the top of each plot.

have plotted the average diffusivity, D, versus the total surfactant concentration, X, in mole fraction units, over the temperature range $10°C \leq T \leq 50°C$ for $C_{12}E_6$ and $10°C \leq T \leq 55°C$ for $C_{12}E_8$. If N_S is the total number of surfactant molecules in the solution and N_W is the total number of water molecules in the solution, then the total mole fraction, X, of surfactant is given by

$$X = \frac{N_S}{N_S + N_W}. \tag{3.20}$$

Data for $C_{12}E_6$ at 55°C is not available because for $C_{12}E_6$, $T_C = 51.1°C$. The data are plotted on the same scale to illustrate the difference in behavior at any given temperature.

We turn our attention first to the plot for $C_{12}E_8$. We notice first of all that the data show no systematic concentration dependence except at $T = 50°C$ and $T = 55°C$. This indicates that the diffusing micelles are weakly interacting and remain more or less of constant size over this concentration range. The systematic decrease of D with X at $T = 50°C$ and $T = 55°C$ can be understood as either an increase in particle size (larger particles diffuse more slowly), or as an increase in attraction between micelles. We notice also that D increases quite regularly with temperature until, once again, $T = 50 - 55°C$ is reached. The steady increase with temperature does not necessarily mean that the micellar size is changing with T, as we know that the solvent viscosity (the viscosity of water) decreases significantly with temperature. A smaller solvent viscosity clearly allows the particles suspended therein to diffuse more quickly. In fact, when we interpret these data in terms of a particle size, properly accounting for the changes in the solvent viscosity, we will see that there is no systematic change of particle size with temperature, except at $T = 50°C$ and $T = 55°C$. The decrease in D from $T = 50°C$ to $T = 55°C$ in Figure 3-2 clearly indicates either an increase in micellar size or attraction.

At $T = 10°C$ and $T = 15°C$, the data for $C_{12}E_6$ look the same as those data for the pure $C_{12}E_8$ solutions. We see weak concentration dependence, and the magnitude of D at $T = 10°C$ and $T = 15°C$ are nearly the same as the corresponding

curves for $C_{12}E_8$. However, we begin to see a decrease in D with concentration for temperatures as low as $T = 20°C$. At $T = 25°C$ and higher, the concentration dependence becomes quite strong, and between $T = 25°C$ and $T = 30°C$, D begins to decrease with increasing temperature. It is interesting to note that in both the $C_{12}E_6$ data ($T_C = 51.1°C$) and in the $C_{12}E_8$ data ($T_C = 78.4°C$), the concentration dependence of D is first seen at about the same distance in temperature from the phase boundary: about $T_C - 30°C$.

We should also note that all of the data shown so far is in the region below X_C, the critical concentration for phase separation (for $C_{12}E_6$, $X_C = 8.0 \times 10^{-4}$ [18], for $C_{12}E_8$, $X_C = 1.1 \times 10^{-3}$ [54]). In the introduction to this chapter, we mentioned that as X is increased, beyond X_C, a minimum in the observed diffusion coefficient is observed. Figure 3-3 shows such a minimum. In the figure, we have compared our measurements on $C_{12}E_6$ for the $T = 25°C$ isotherm with the measurements of Wilcoxon and Kaler also at $T = 25°C$ [18]. We have also shown their data for $T = 27°C$, which extends to much greater total concentration, and clearly shows the minimum in the diffusion coefficient. Comparison of the $T = 25°C$ isotherm indicates that our measurements are consistent with theirs. As was discussed previously, it is clear that for concentrations near X_C and higher, that intermicellar interactions are important, and the measured diffusivity should not be interpreted in terms of an actual particle size.

On the other hand, as we also discussed previously, we wish to interpret the changes in D occurring below X_C and T_C in terms of a change in the average particle size. The standard way to accomplish this is to use the Stokes-Einstein relation [20], relating the diffusion coefficient to the particle radius in a solution of ideal (noninteracting) spherical particles:

$$D = \frac{k_B T}{6\pi\eta R_H}, \tag{3.21}$$

where D is the diffusivity, R_H is the radius of the spheres, and η is the (solvent) viscosity. If the particles are not spheres, then R_H, called the hydrodynamic radius,

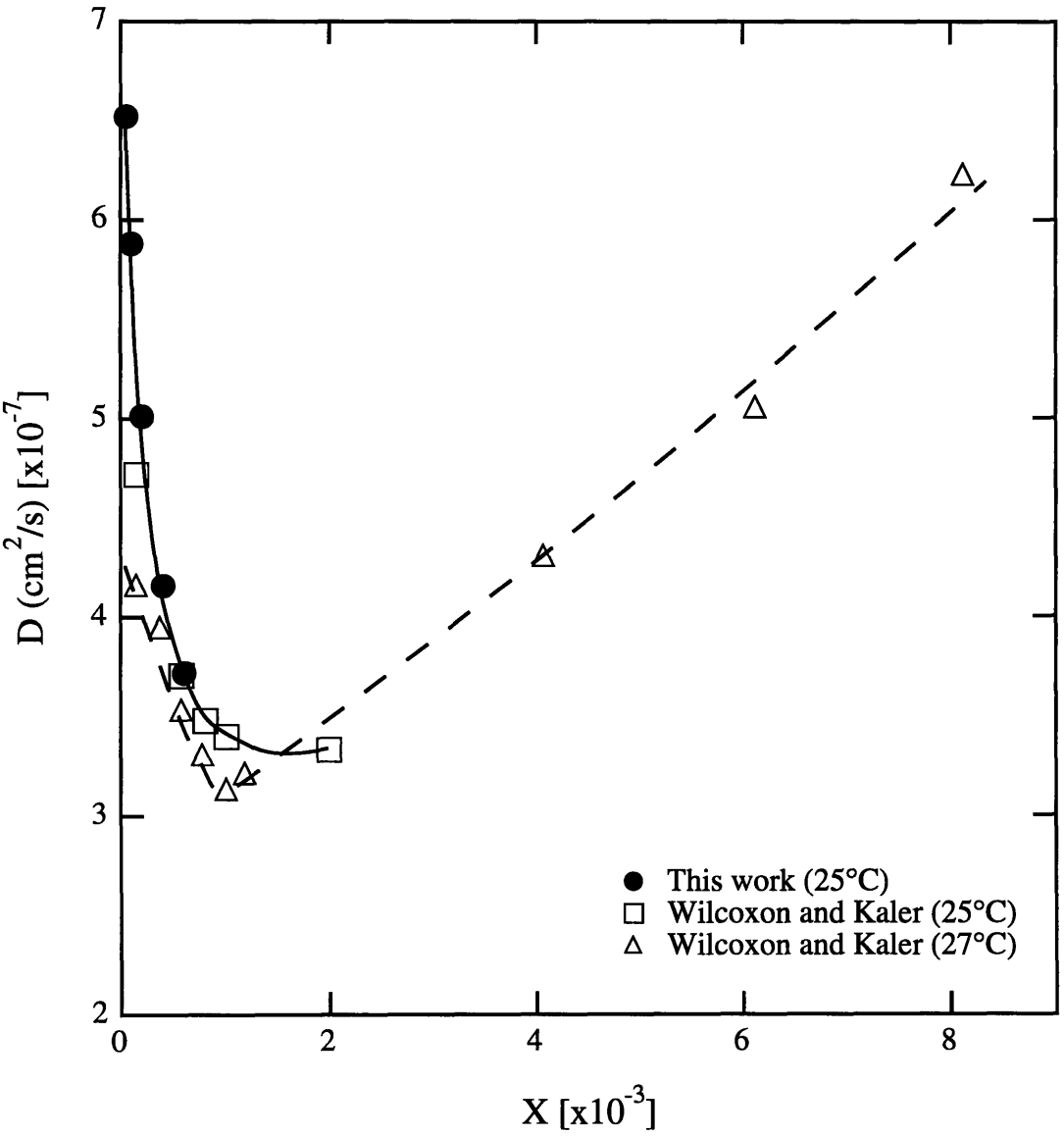

Figure 3-3: The measured diffusivity, D, for pure $C_{12}E_6$ and water along the $T = 25°C$ isotherm from this work (closed circles) is compared to the data of Wilcoxon and Kaler [18] for the $T = 25°C$ isotherm (open squares) and the $T = 27°C$ isotherm (open triangles). The data of Wilcoxon and Kaler clearly show the presence of a minimum in the measured diffusivity as concentration is increased. The lines through the data points are guides to the eye. The solid line indicates that the two sets of data for the $T = 25°C$ isotherm are consistent. The dashed line indicates the trend of the data of Wilcoxon and Kaler for the $T = 27°C$ isotherm.

represents the size of an effective spherical particle with the same diffusive properties as the actual particle. A hydrodynamic model must be constructed to obtain R_H in terms of the structural parameters of the actual particle. Exact solutions exist only for ellipsoids (both prolate and oblate). Many approximate calculations have been performed for other shapes [55]. If there is a distribution of particle sizes (*i. e.* polydispersity), then the hydrodynamic radius we obtain is the z-average over the distribution of sizes (since each particle contributes according to the intensity of light it scatters).

Using the Stokes-Einstein relation, we report our measurements for $C_{12}E_6$ and $C_{12}E_8$ in terms of the hydrodynamic radius versus concentration. Both plots are shown on the same scale in Figure 3-4. We clearly see the difference in the extent of micellar growth over the temperature range studied. All of the data for $C_{12}E_8$ is shown on the plot, it just so happens that all of the points (except for the highest temperatures) fall on top of each other. Thus, we see that over the range $10°C \leq T \leq 50°C$, $C_{12}E_8$ exhibits practically no growth, while $C_{12}E_6$ shows a marked increase in average size with both temperature and concentration. The data for $C_{12}E_8$ are plotted separately on a more appropriate scale in Figure 3-5.

3.2.2 Mixtures of $C_{12}E_6$ and $C_{12}E_8$

Having examined the behavior of aqueous solutions of pure $C_{12}E_6$ and pure $C_{12}E_8$ we are now in a position to consider mixtures of the two surfactants and water. Before presenting the data on the mixtures, however, we will first indicate graphically the regions of the phase diagram studied. This will help to provide a clear understanding of what has been studied, and how the various data should be viewed with respect to each other.

The regions of the phase diagram that we have studied are indicated schematically in Figure 3-6. Since we are examining a mixture including two surfactants, the phase diagram is three-dimensional. The relative proportions of the two surfactants and water are determined by two independent variables. We have chosen these variables to be: X, the total surfactant mole fraction, and α_s, the relative compo-

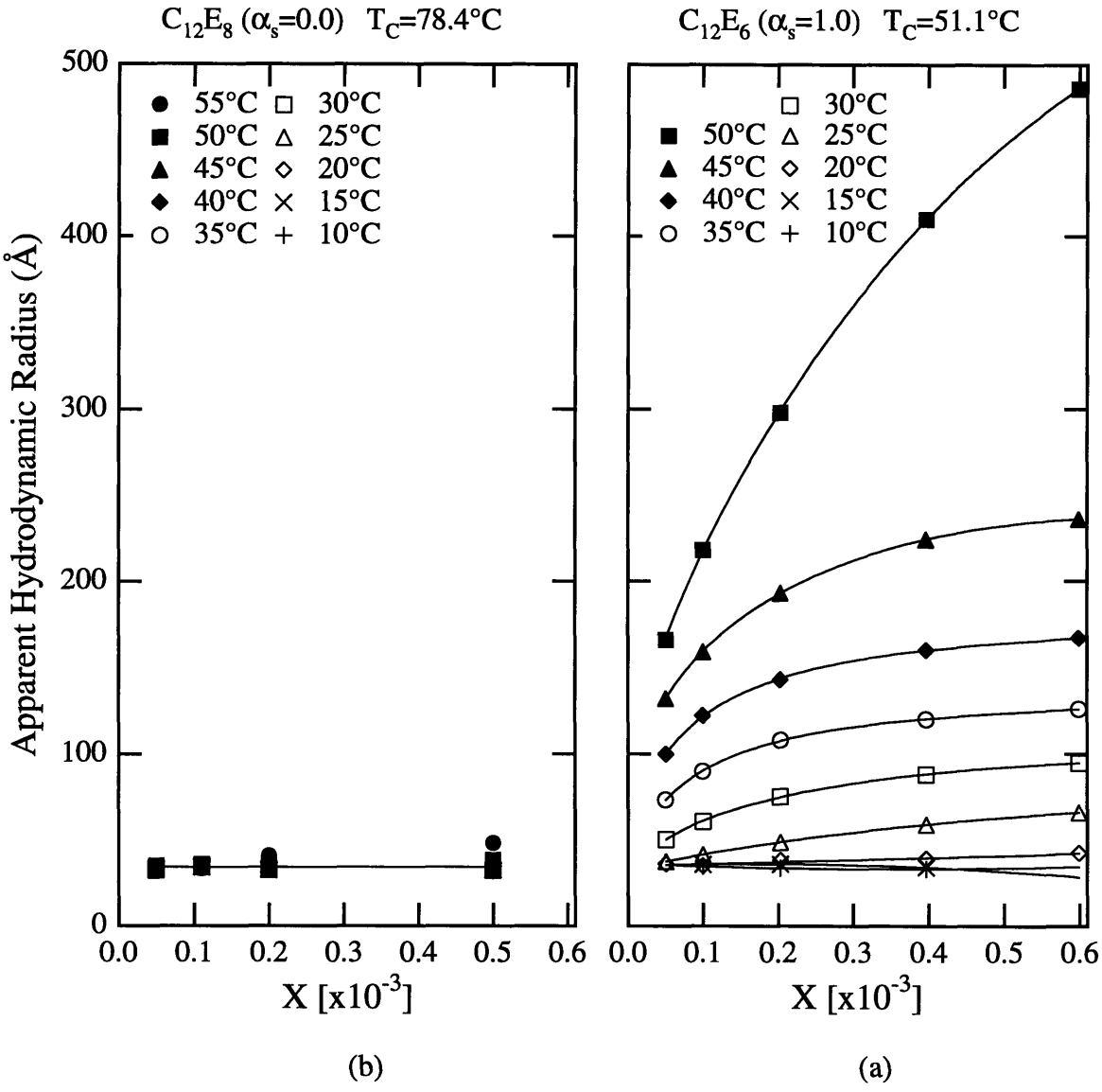

Figure 3-4: The apparent hydrodynamic radius computed from the data of Figure 3-2 for aqueous solutions of pure $C_{12}E_6$ (a) and pure $C_{12}E_8$ (b) using Equation 3.21. The different symbols represent measurements at different temperatures. The solid lines through the data points are intended as guides to the eye, to indicate the trends present in the data.

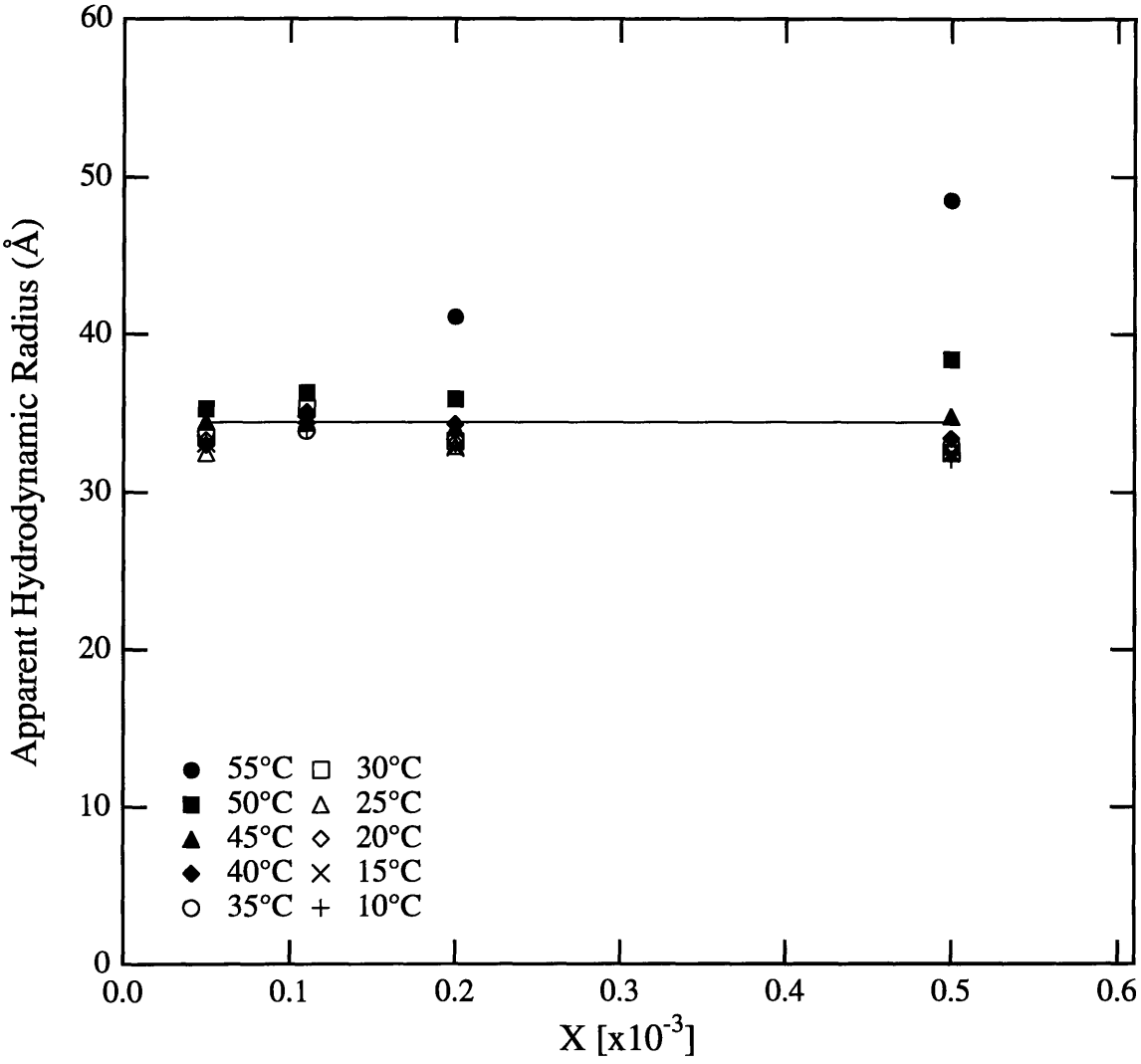

Figure 3-5: The apparent hydrodynamic radius for pure $C_{12}E_8$ from Figure 3-4b plotted on a smaller scale. The solid lines are guides to the eye.

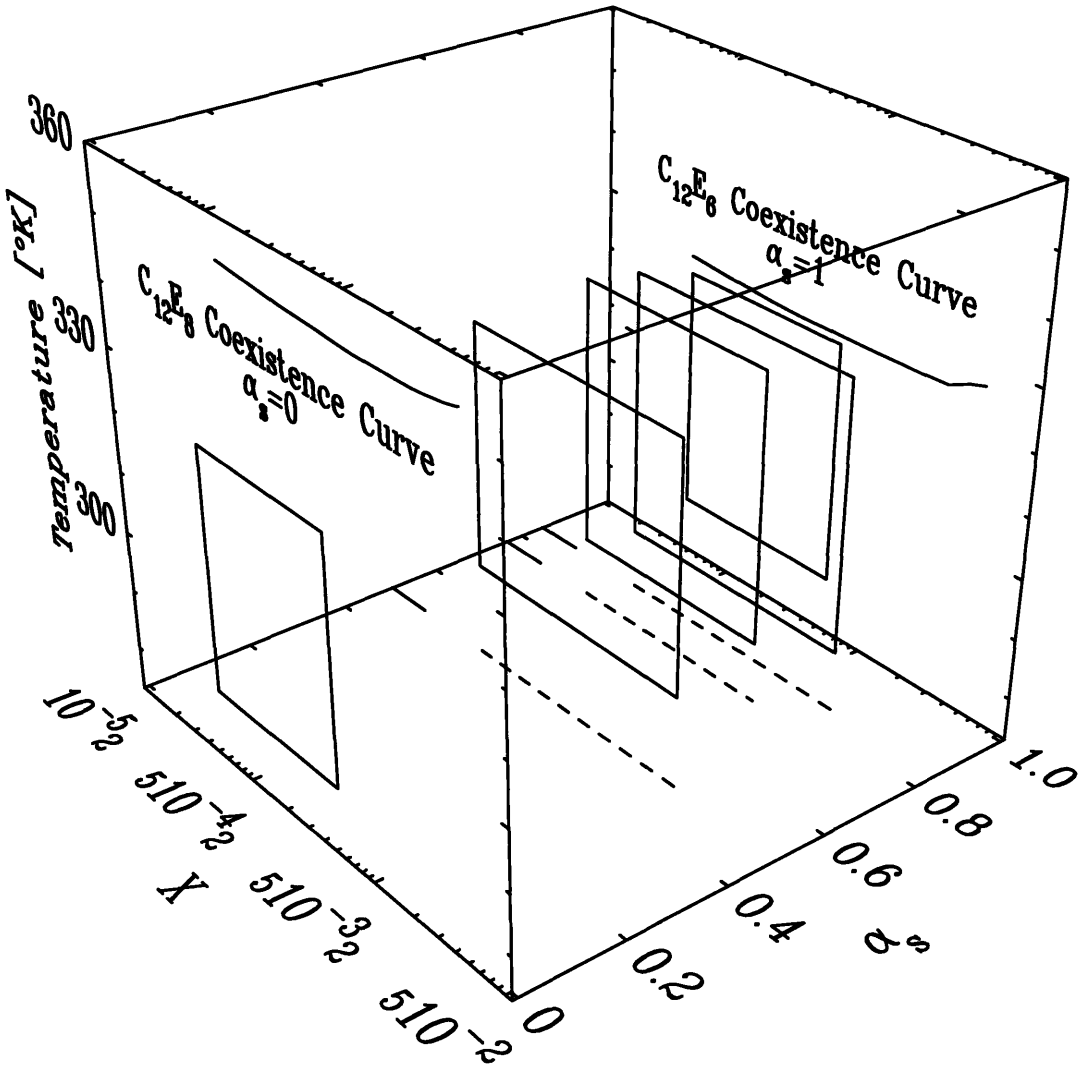

Figure 3-6: The regions of the $C_{12}E_6$, $C_{12}E_8$ and water phase diagram studied using quasielastic light scattering. The absolute temperature, T, is plotted on the vertical axis, while on the x and y axes are plotted the total surfactant mole fraction, X, and the relative composition of surfactant, α_s. The large rectangles indicate the regions studied. The curves at the top of the figure indicate the coexistence curves for pure $C_{12}E_6$ ($\alpha_s = 1.0$) and for pure $C_{12}E_8$ ($\alpha_s = 0.0$).

sition of the surfactant. They are defined as follows. Let there be N_A molecules of $C_{12}E_6$, N_B molecules of $C_{12}E_8$, and N_W molecules of water in the solution. The total surfactant mole fraction is then defined

$$X = \frac{N_A + N_B}{N_A + N_B + N_W}, \tag{3.22}$$

while the relative composition is defined in terms of the relative proportion of $C_{12}E_6$

$$\alpha_s = \frac{N_A}{N_A + N_B}. \tag{3.23}$$

Thus, $\alpha_s = 0$ corresponds to pure $C_{12}E_8$ and water, and $\alpha_s = 1$ corresponds to pure $C_{12}E_6$ and water. The large rectangles indicate the regions where measurements were made. In addition to the pure $C_{12}E_6$ and water system (for which measurements were made over the range $10°C \leq T \leq 50°C$ with $5 \times 10^{-5} \leq X \leq 6 \times 10^{-4}$) and the pure $C_{12}E_8$ and water system, (for which measurements were made over the range $10°C \leq T \leq 55°C$ with $5 \times 10^{-5} \leq X \leq 5 \times 10^{-4}$), quasielastic light scattering measurements were also made for mixtures of $C_{12}E_6$ and $C_{12}E_8$ with three different relative compositions: $\alpha_s = 0.501$, $\alpha_s = 0.763$ and $\alpha_s = 0.848$. For $\alpha_s = 0.501$, measurements were carried out over the range $15°C \leq T \leq 56°C$ with $6.25 \times 10^{-5} \leq X \leq 2 \times 10^{-3}$. Data was obtained for $\alpha_s = 0.763$ over the range $10°C \leq T \leq 55°C$ and $5 \times 10^{-5} \leq X \leq 1 \times 10^{-3}$. Finally, for $\alpha_s = 0.848$, we measured in the region $10°C \leq T \leq 55°C$ and $6.25 \times 10^{-5} \leq X \leq 2 \times 10^{-3}$.

At the top of the Figure 3-6, the coexistence curves for liquid-liquid phase separation are indicated for pure $C_{12}E_6$ and pure $C_{12}E_8$. The phase boundary for the mixed $C_{12}E_6$, $C_{12}E_8$ and water system has been obtained by Puvvada and Blankschtein [17], and the two coexistence curves for pure $C_{12}E_6$ and water and pure $C_{12}E_8$ and water in Figure 3-6 are taken from that study. It should be noted here that in the mixed case there is also a phase separation into two coexisting liquid phases differing in total surfactant concentration, and that the coexistence curve for any fixed relative composition lies between the coexistence curves for pure $C_{12}E_6$ and pure $C_{12}E_8$. It was found experimentally by Puvvada and Blankschtein that the two

liquid phases of the phase separated solution contain the same relative composition of surfactant. In general, it is possible to have a three-phase equilibrium in such a system. Furthermore, it is not required in a two-phase equilibrium, such as the one observed, that the compositions of the two phases should be equal.

The data for the average diffusivity measured for the three mixtures studied are plotted in Figure 3-7(a-c). From left to right, the three plots represent an increasing relative proportion of $C_{12}E_6$. The leftmost plot contains all of the data obtained for various temperatures and total surfactant concentrations for solutions containing a roughly 50% mixture of $C_{12}E_6$ and $C_{12}E_8$ ($\alpha_s = 0.501$). The center plot shows the data for solutions containing about 75% $C_{12}E_6$ and 25% $C_{12}E_8$ ($\alpha_s = 0.763$), and the measurements presented in the rightmost plot are from solutions containing a relative mixture of about 85% $C_{12}E_6$ and 15% $C_{12}E_8$. In the region below $X = 1 \times 10^{-3}$, all three plots show behavior that is qualitatively similar to the behavior exhibited by pure $C_{12}E_6$ in Figure 3-2b. That is, at the lower temperatures (10°C-15°C) there is a weak dependence of the diffusivity, D, on concentration. Furthermore, comparing the data for $T = 10°C$ and $T = 15°C$ amongst the three plots and with the corresponding data for pure $C_{12}E_6$ and pure $C_{12}E_8$ from Figure 3-2, we see that the magnitude of D for each temperature varies only weakly with relative composition, α_s. As temperature is increased at fixed X, we again see that D increases with temperature and then begins to decrease. A strong concentration dependence also develops, the strength increasing with the relative proportion of $C_{12}E_6$ at any given temperature. Finally, we note that in general, in the regions exhibiting this concentration dependence that the magnitude of D decreases with increasing relative proportion of $C_{12}E_6$ at any given temperature and total concentration.

For the case of $\alpha_s = 0.501$ and $\alpha_s = 0.848$, measurements were extended beyond $X = 1 \times 10^{-3}$ (note that the critical concentration for phase separation for $C_{12}E_8$ is 1.1×10^{-3}). In these data, we clearly see the development, as the temperature is increased, of a minimum in D as a function of concentration similar to the minimum observed by Wilcoxon and Kaler [18] for pure $C_{12}E_6$, reproduced in Figure 3-3. At $T = 10°C$ and $T = 15°C$ we see from the extended concentration range that D

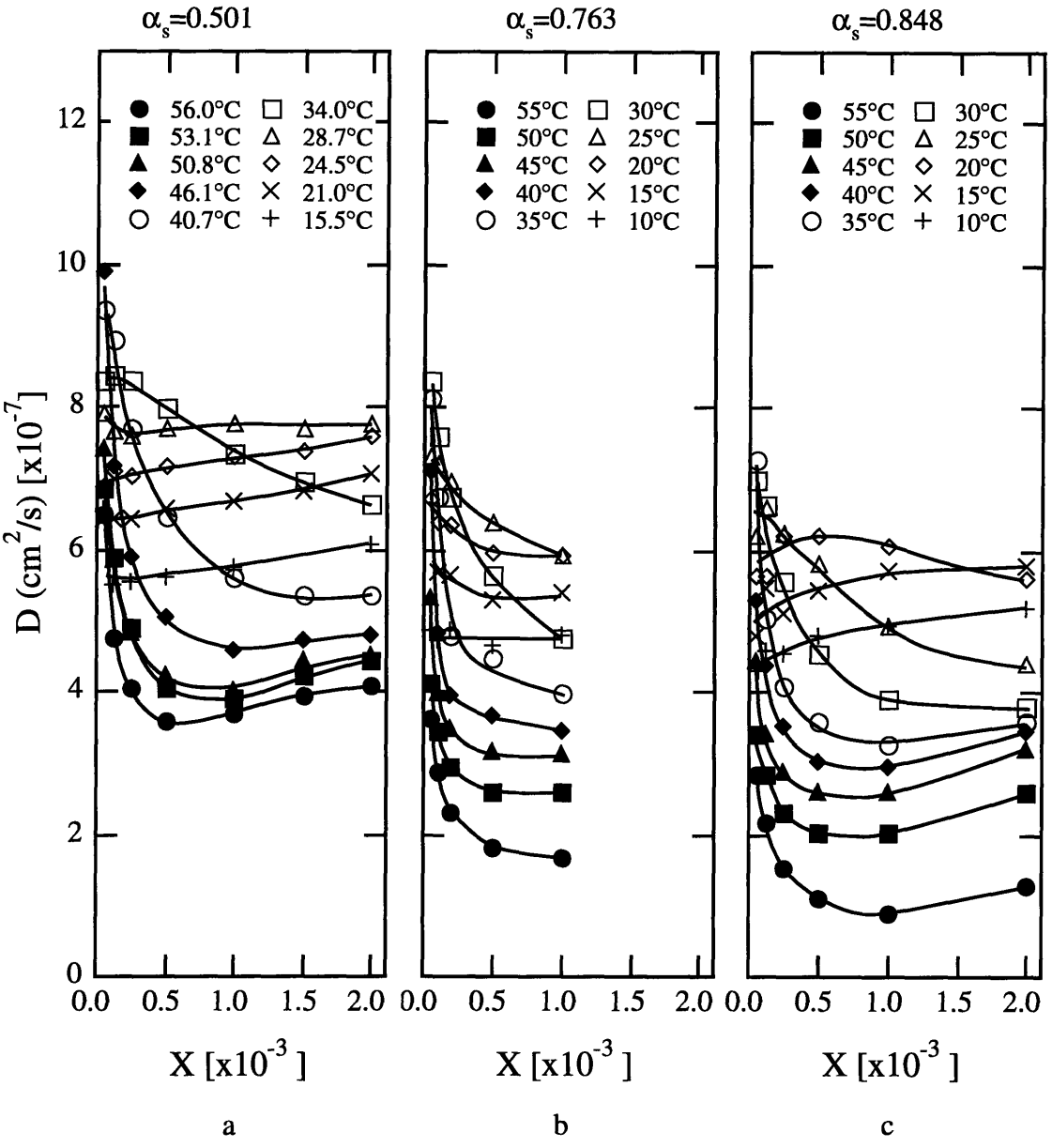

Figure 3-7: The average diffusivity, D, measured as a function of total surfactant mole fraction, X, for mixtures of $C_{12}E_6$ and $C_{12}E_8$. The different symbols represent measurements at different temperatures. The solid lines through the data points are intended as guides to the eye, to indicate the trends present in the data. Each plot corresponds to a different relative composition of $C_{12}E_6$. This relative composition is indicated at the top of each plot.

actually increases with concentration.

The temperature and concentration dependence of all of the data for the mixtures can be interpreted in exactly the same manner as the data for pure $C_{12}E_6$ and pure $C_{12}E_8$ were explained in the previous section. We now proceed, therefore, as we did in the previous section, and use Equation 3.21 to relate the measured diffusion coefficient to an average hydrodynamic radius, keeping in mind, of course, that the interpretation of the hydrodynamic radius as an actual particle size is not expected to be valid for concentrations in the vicinity of the observed minimum in D and higher. This interpretation is also questionable in regions of the phase diagram in the vicinity of the critical point of the mixed system at each fixed composition.

Figure 3-8(a-c) shows the same data that was presented in Figure 3-7(a-c) recast using Equation 3.21 as an apparent hydrodynamic radius. For concentrations below $X = 1 \times 10^{-3}$ (for which we have assumed that an interpretation of the hydrodynamic radius as an actual particle size is valid) we see that the particle size increases with concentration and temperature. As concentration is decreased, we see that the micellar size appears to approach a constant, minimum size. We can estimate this minimum size for each composition (including the two pure cases) by performing a linear extrapolation to zero total concentration of the data for each $T \leq 25°C$ in Figure 3-8 and in Figure 3-4. We chose $T \leq 25°C$ because for these temperatures, the dependence of micellar size on total concentration is weak at all compositions studied. The different estimates (for the different temperatures) at each composition were averaged, and the resulting minimum size is plotted as a function of relative solution composition in Figure 3-9. We see that there is a slight increase in the minimum radius with increasing relative proportion of $C_{12}E_6$. The curve, a fit of the points to a straight line, is described by the equation

$$R_{min}(\alpha_s)(\text{Å}) = 33.26 + 2.19\alpha_s. \tag{3.24}$$

We will need this estimate in order to compare our data with the models to be presented in the following chapters.

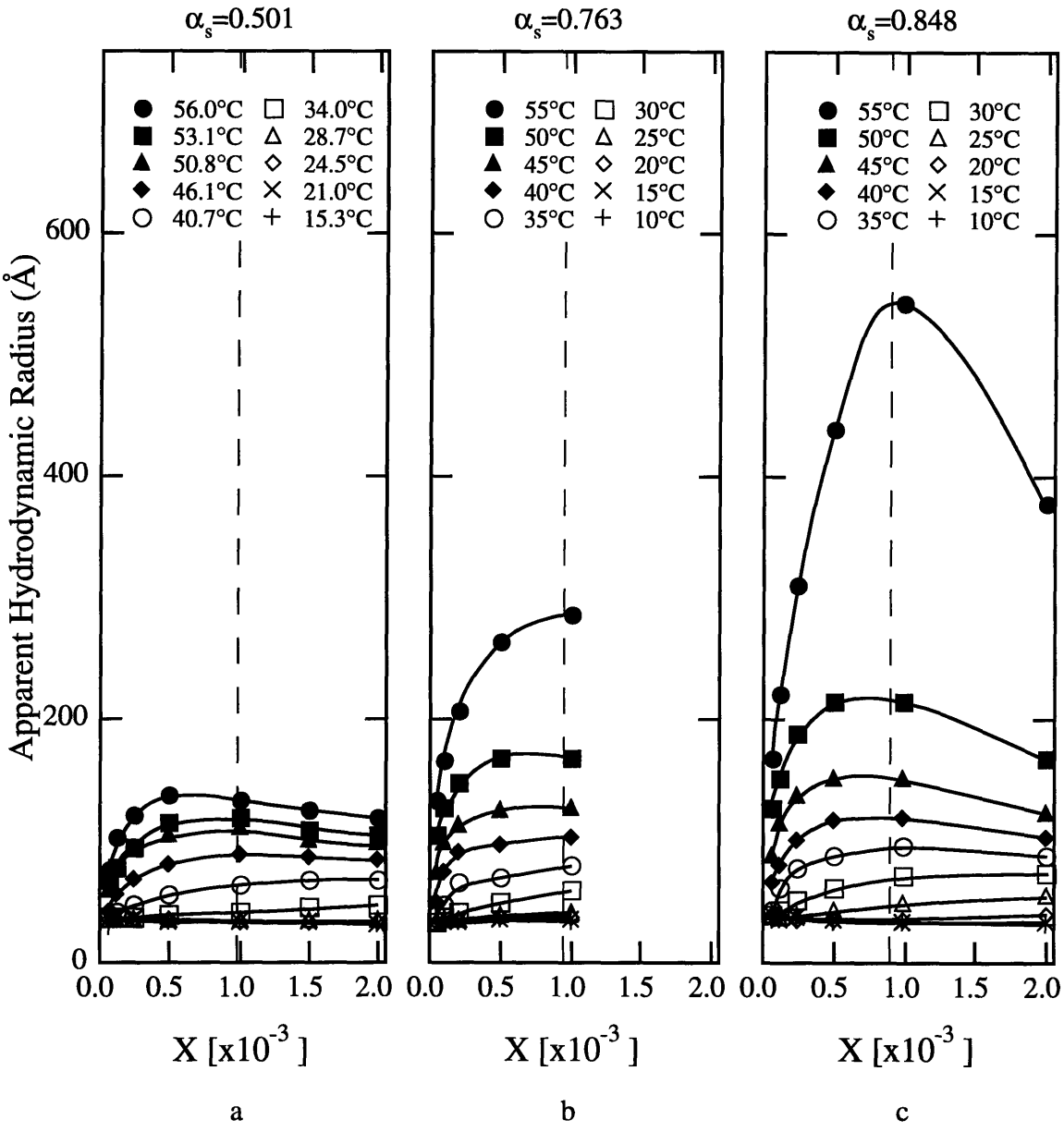

Figure 3-8: The apparent hydrodynamic radius computed from the data of Figure 3-7 for mixtures of $C_{12}E_6$ and $C_{12}E_8$ using Equation 3.21. The different symbols represent measurements at different temperatures. The solid lines through the data points are intended as guides to the eye, to indicate the trends present in the data. The relative composition of each mixture is noted at the top of the appropriate plot.

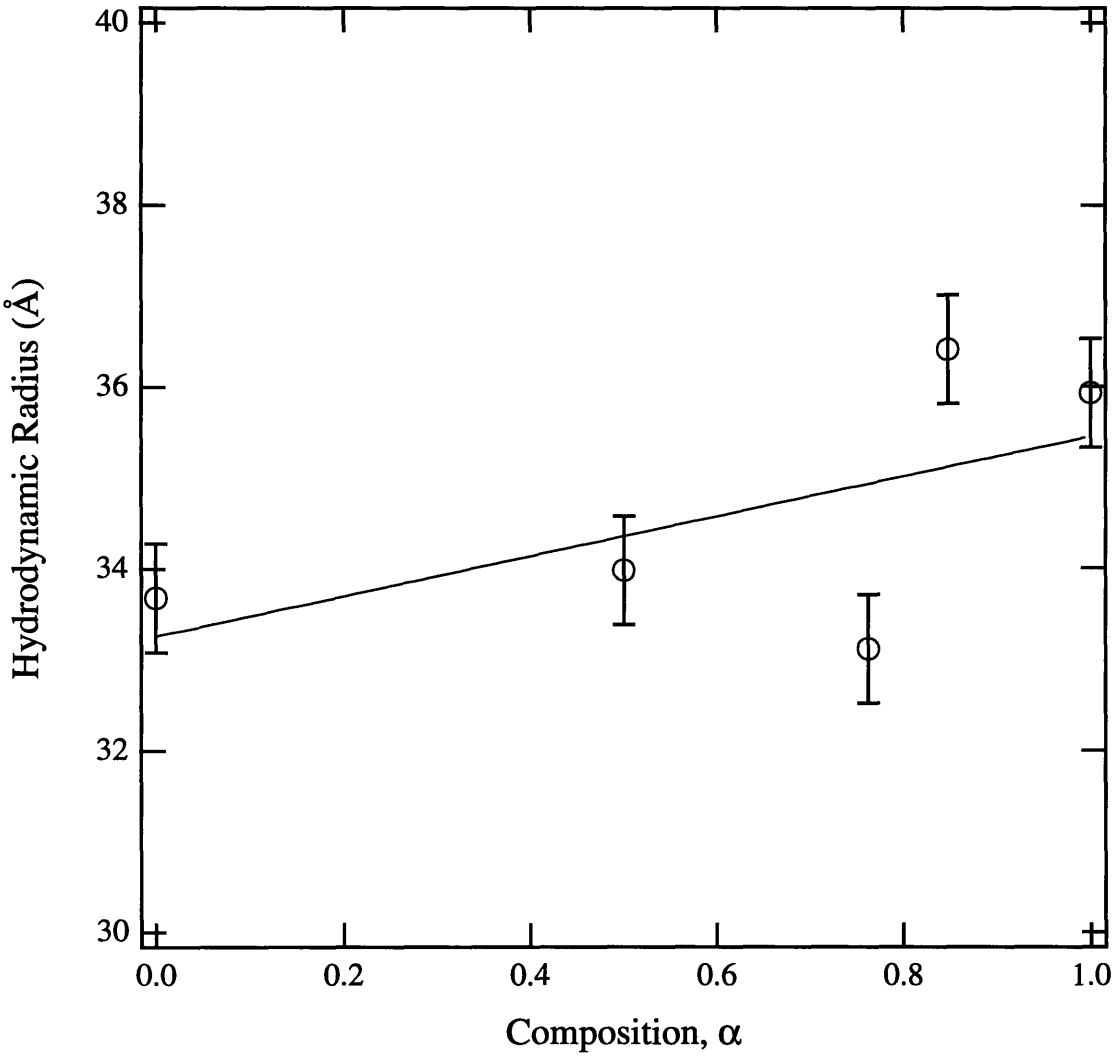

Figure 3-9: The minimum micellar radius as a function of solution relative composition. The curve is a fit to a straight line.

Returning to Figure 3-8, we note that the extent of micellar growth increases with the relative proportion of $C_{12}E_6$. Qualitatively, these results were expected: all of the features of the plots interpolate between the two limiting cases of $\alpha_s = 0$ (pure $C_{12}E_8$) and $\alpha_s = 1$ (pure $C_{12}E_6$), see Figure 3-4. Quantitatively, we will describe the changes in the apparent size of the micelles in terms of a generalization of the ladder model [10] which describes the linear growth of simple micelles. We will use these results to test the molecular-thermodynamic model of Puvvada and Blankschtein [16, 17]. These models will be discussed in the following chapters. We shall return later to the question of the interpretation of the observed minimum in D (reflected as a maximum in the apparent hydrodynamic radius). By including a crude treatment of intermicellar interactions, we shall suggest one possible explanation for this minimum. First, however, we must present some experimental evidence justifying our implied assumption in the above discussion that the mixed micelles composed of $C_{12}E_6$ and $C_{12}E_8$ grow in one dimension. This evidence will be presented in the following section.

3.2.3 Static and Dynamic Light Scattering from a Mixture of $C_{12}E_6$ and $C_{12}E_8$ and the Determination of Micellar Shape

As we have seen, dynamic light scattering measurements performed on a suspension of particles gives us information about the diffusion of those particles. In the absence of strong interactions, we can obtain an estimate of the size of the particles using the hydrodynamic radius. As was mentioned in Section 3.1.3, measurements of the total intensity of scattered light in the absence of strong interactions allows us to determine, among other properties, the apparent molecular weight of the suspended particles. By changing temperature and concentration, we can cause our micellar system to grow, and we can study how the average size (hydrodynamic radius) scales with the apparent particle mass. Since the measured hydrodynamic radius depends on the particle geometry while the mass does not, we can use the information of how

mass scales with size to distinguish among different hydrodynamic models for the micelles, provided that the geometries are sufficiently different (for example, we can hope to distinguish between rods and discs, but not between rods with flat ends and rods with spherical ends). There are many different approximate hydrodynamic models, connecting diffusion coefficient to particle geometry [55], but only three models for which exact solutions exist: the sphere, the prolate ellipsoid, and the oblate ellipsoid. For our purposes, it will be sufficient to compare the scaling of the mass with hydrodynamic radius to the predictions of these models. In fact, it will suffice to compare only with the prolate and oblate ellipsoid models since physically a spherical micelle with radius much larger than the extended molecular length is unfeasible.

A stock solution containing a mixture of $C_{12}E_6$ and $C_{12}E_8$ with relative composition $\alpha_s = 0.751$ and $X = 5.37 \times 10^{-4}$ was prepared by weight. From this stock solution, three samples were prepared with different total mole fractions: $X = 1.00 \times 10^{-4}$, $X = 2.00 \times 10^{-4}$ and $X = 3.32 \times 10^{-4}$. Static and dynamic light scattering measurements were performed at four different temperatures ($T = 25°C$, $T = 35°C$, $T = 40°C$ and $T = 45°C$) using the light scattering instrument built by Richard Chamberlin (described earlier).

The total intensity was measured at 12 angles with $11.5° \leq \theta \leq 162.6°$ and was found to be essentially angle independent. The transmitted intensity was monitored with a photodiode. Using toluene as a reference solvent, the procedure described in Section 3.1.3 was used to extract the Rayleigh ratio of the sample from the scattered intensity measurements. The resulting data for the Rayleigh ratio extrapolated to zero scattering angle for our measurements are plotted in Figure 3-10 From this data, we wish to extract the apparent molecular weight as described in Section 3.1.3.

In order to proceed, an estimate of the refractive index increment for our solution is needed (see Equation 3.18). In order to provide this estimate, a refractometer (Bauch and Lomb Abbe-3L) was used to measure the index of refraction of the stock solution, the three samples, and water at $T = 24°C$. These data are plotted in Figure 3-11. The refractive index increment,

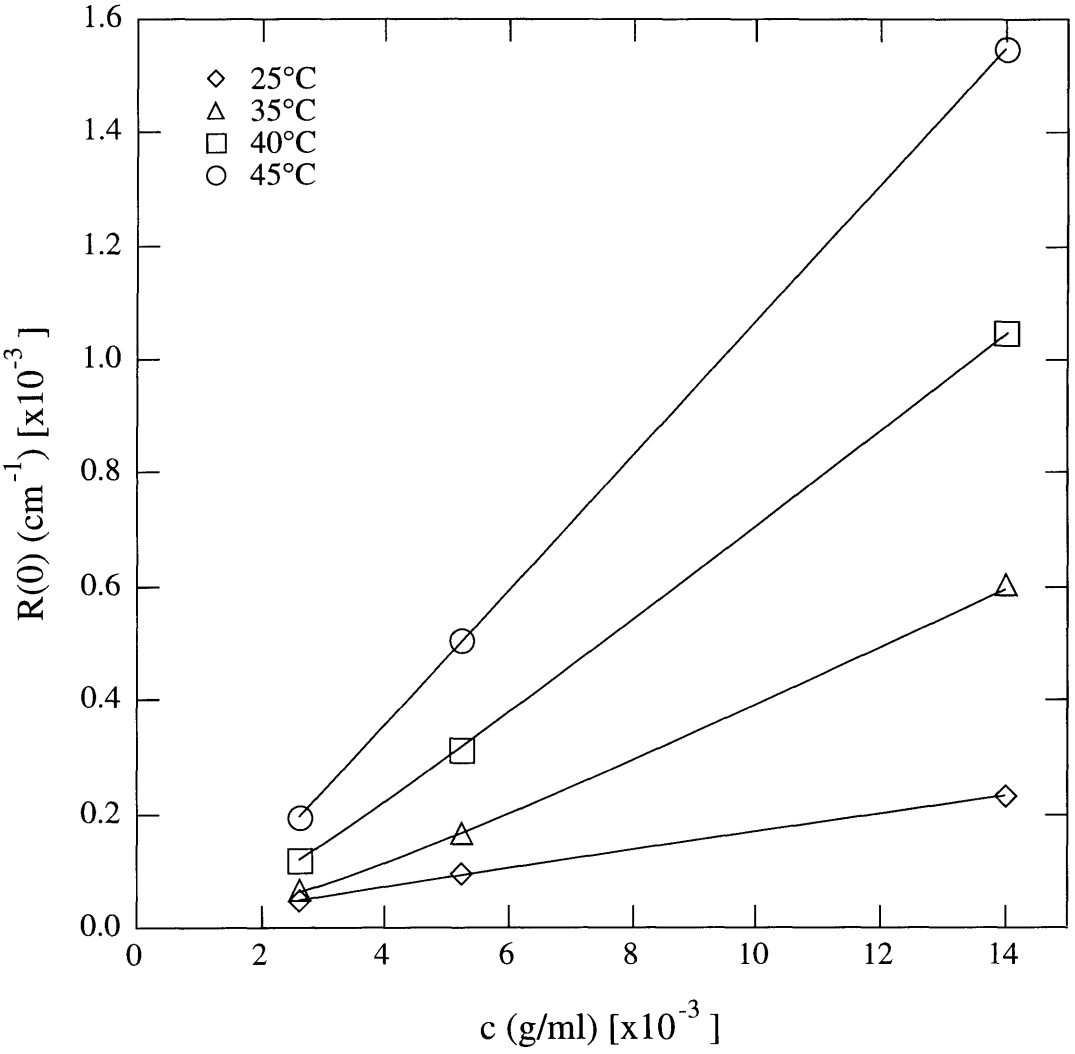

Figure 3-10: The Rayleigh ratio as a function of total surfactant mole fraction at various temperatures for an $\alpha_s = 0.751$ composition of $C_{12}E_6$ and $C_{12}E_8$. The lines are guides to the eye.

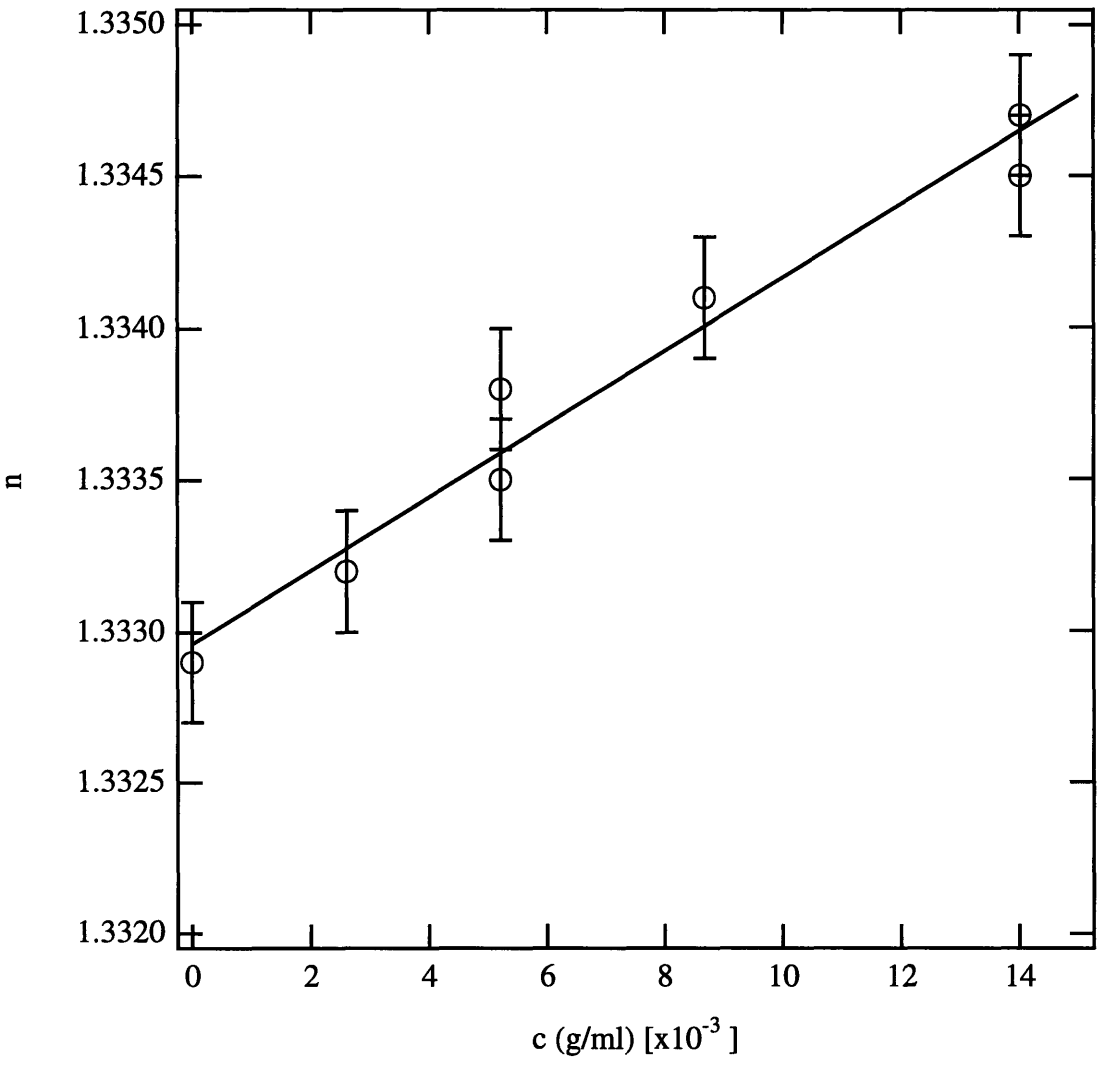

Figure 3-11: The measured refractive index as a function of total surfactant concentration at $T = 24°C$ for an $\alpha_s = 0.751$ mixture of $C_{12}E_6$ and $C_{12}E_8$. The curve is the best fit to a straight line, yielding a refractive index increment of 0.12

$$\frac{\partial n}{\partial c} = 0.12 \pm 0.01 \text{cm}^3/\text{g} \tag{3.25}$$

is obtained from the slope of the graph. In principle, $\partial n/\partial c$ could be a function of temperature. Degiorgio [54] reports values of the refractive index increment and its temperature dependence for selected amphiphiles in the C_iE_j series. In all cases, the temperature dependence is extremely weak. Thus, we are justified in using the value of the refractive index increment that we have determined for $T = 24°C$ at all of the temperatures corresponding to our intensity measurements. Using Equations 3.18 and 3.19, neglecting the effects of interactions, we obtain the apparent molecular weight. The results are plotted in Figure 3-12.

By extrapolating the data for $T = 25°C$ to zero concentration, we can eliminate the influence of both micellar growth and interactions, giving us an estimate of the molecular weight of a minimum sized micelle. Dividing by the effective molecular weight per monomer (assuming the micelle composition to be the same as the solution composition), we obtain an estimate of the minimum aggregation number, n_0. We find, in this way $n_0 = 135 \pm 20$. This value compares well with an estimate of n_0 for pure $C_{12}E_8$ micelles reported by Degiorgio [54] of $n_0 = 120$. We shall assume, therefore, that n_0 is not a strong function of composition in this system, and use $n_0 = 135$ for all compositions. This assumption is also supported by the weak dependence of the minimum radius on solution composition.

In addition to the total intensity measurements, dynamic light scattering measurements were also performed on the same samples under identical conditions, following the procedure outlined in Section 3.1.2. In Figure 3-13 we report the results of these measurements. Once again interpreting the change in diffusivity as arising from a change in particle size in a system of weakly interacting Brownian particles, we plot the hydrodynamic radius obtained from these data in Figure 3-14. An extrapolation of the $T = 25°C$ data to zero concentration yields a minimum radius of 3.4nm.

As we mentioned earlier, we want to compare the scaling of mass with radius to the predictions of the two physically reasonable hydrodynamic models for which

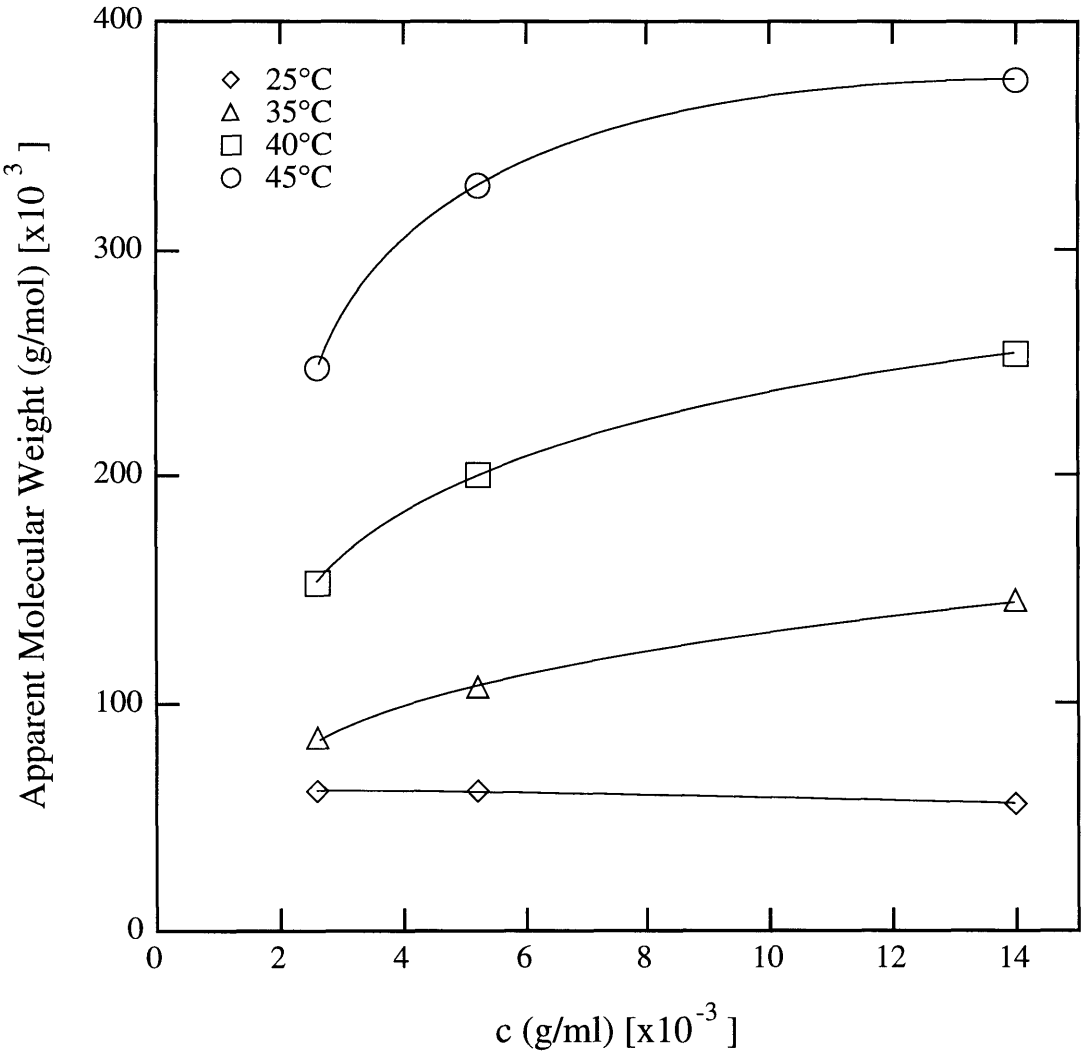

Figure 3-12: The apparent molecular weight as a function of total surfactant concentration at various temperatures for an $\alpha_s = 0.751$ mixture of $C_{12}E_6$ and $C_{12}E_8$. The curves are intended as guides to the eye.

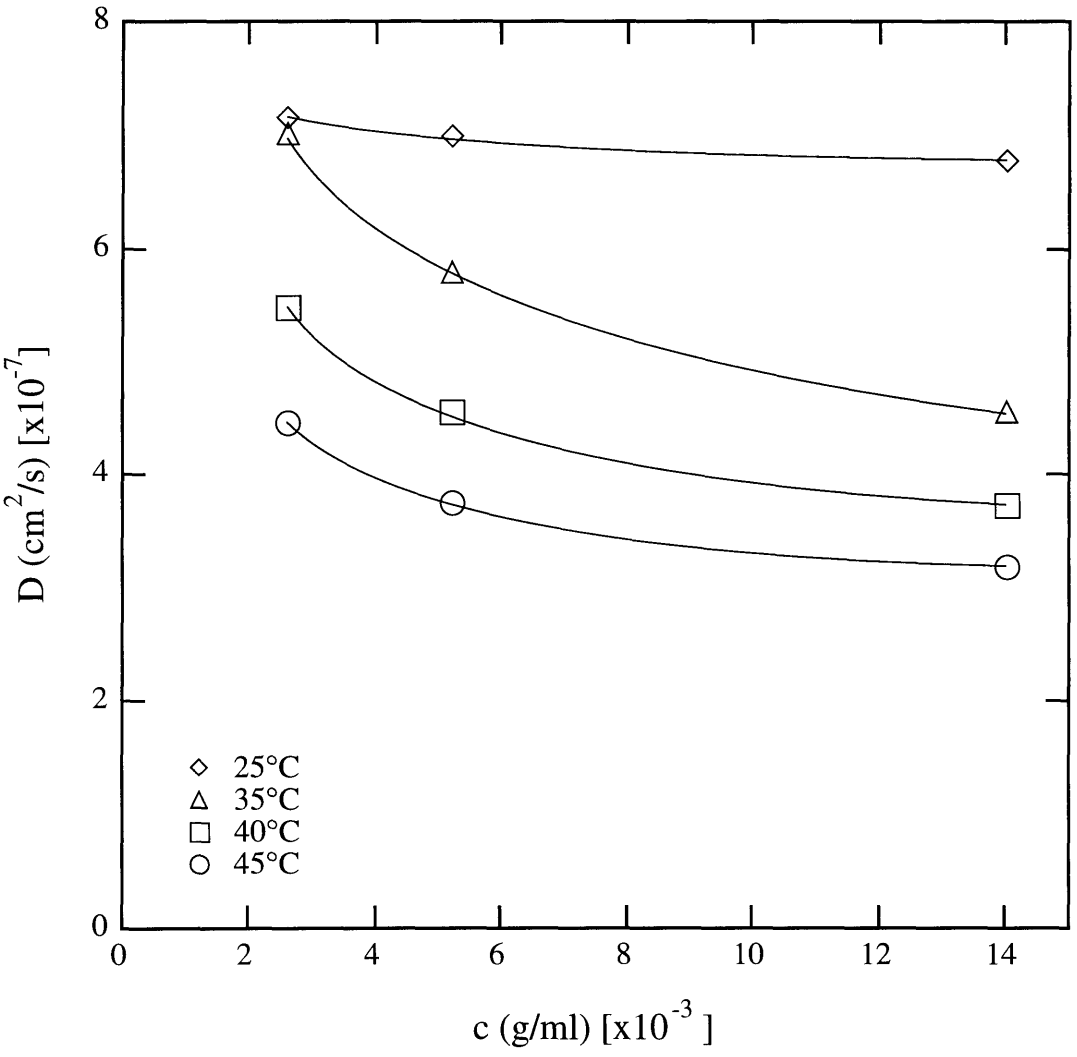

Figure 3-13: The average diffusivity as a function of total surfactant concentration at various temperatures for an $\alpha_s = 0.751$ mixture of $C_{12}E_6$ and $C_{12}E_8$. The curves are intended to serve as guides to the eye.

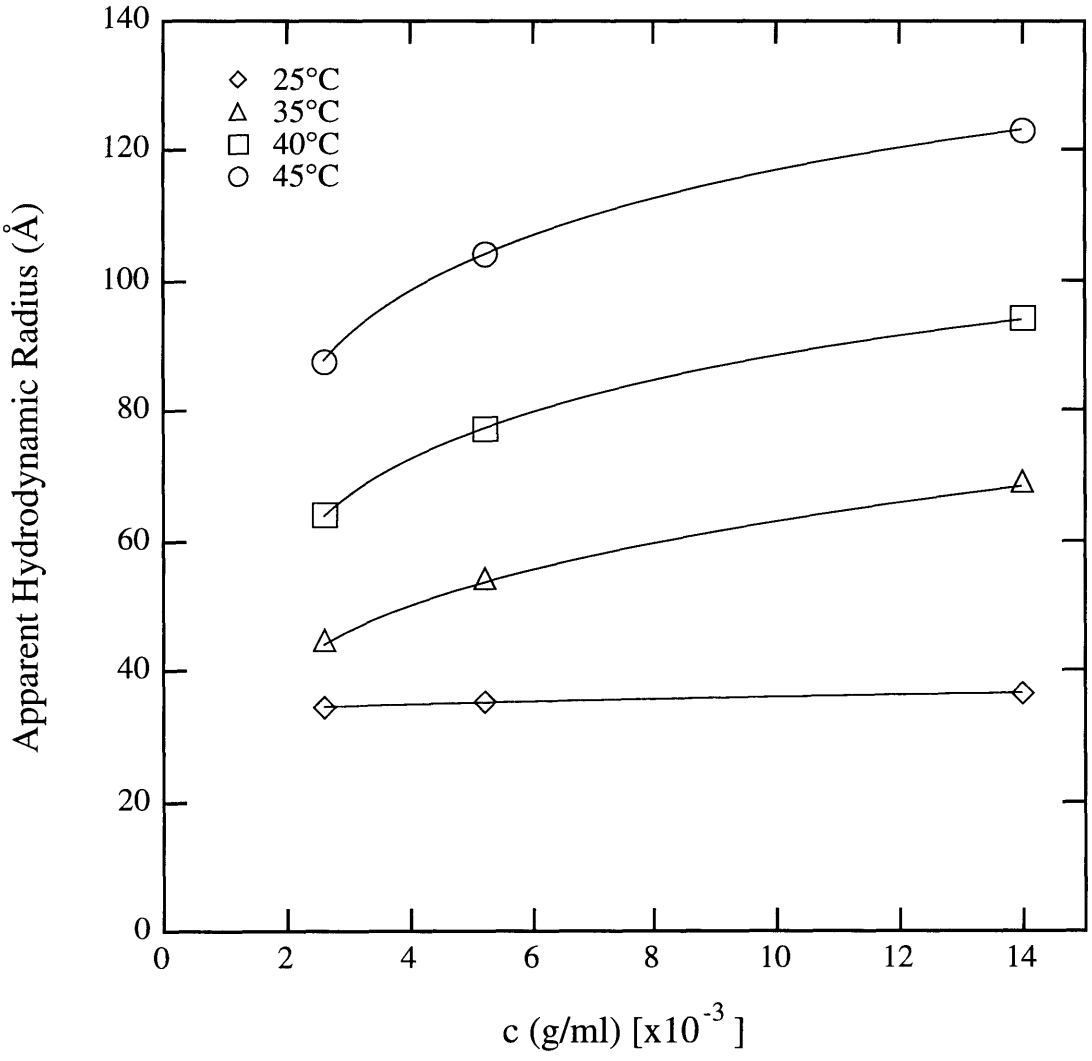

Figure 3-14: The average hydrodynamic radius as a function of total surfactant concentration at various temperatures for an $\alpha_s = 0.751$ mixture of $C_{12}E_6$ and $C_{12}E_8$. The curves are intended to serve as guides to the eye.

Table 3.2: Predictions for M and R_H for Prolate and Oblate Ellipsoids [56]

Shape	M	R_H	Notes
Oblate ellipsoid	$\frac{4}{3}\pi ab^2\rho$	$\frac{a\left(x^2-1\right)^{1/2}}{\arctan\left((x^2-1)^{1/2}\right)}$	$x = b/a$ a = semi-minor axis b = semi-major axis
Prolate ellipsoid	$\frac{4}{3}\pi a^2b\rho$	$\frac{b\left(1-x^2\right)^{1/2}}{\ln\left[\frac{1+(1-x^2)^{1/2}}{x}\right]}$	$x = a/b$ a = semi-minor axis b = semi-major axis

ρ=average mass density of micelles (depends on micelle hydration)

there exist exact solutions: the prolate ellipsoid (growth in one dimension) and the oblate ellipsoid (growth in two dimensions). Table 3.2 presents the formulae for the mass and hydrodynamic radius of these particles in terms of the various geometrical parameters associated with each shape.

The scaling of the apparent mass with the hydrodynamic radius is displayed in Figure 3-15. The data for all concentrations and temperatures is shown, all collapsing onto a single curve. The lines indicate the predictions of the two models in which we have set the semi-minor axis $a = 3.4$nm, the radius of a minimum sized micelle. Along the top axis are displayed values of the semi-major axis, b, that for each model give the corresponding hydrodynamic radius displayed along the bottom axis. For the purposes of this plot, ρ, the average mass density was left as an adjustable fitting parameter. Since in our total intensity measurement, we measure the scattering from the amphiphiles themselves, the molecular weight estimate that we obtain considers only the mass of the amphiphiles in the micelle. On the other hand, our estimate for the hydrodynamic radius is based on the diffusivity of the micelle in the solvent. The average size we obtain from the diffusivity must therefore include the effects of any water that is carried along with the micelle. We therefore estimate the average hydration of the micelles according to the formula

$$\rho = \frac{\alpha m_A + (1-\alpha)m_B}{\alpha\Omega_A + (1-\alpha)\Omega_B + n_W\Omega_W}, \tag{3.26}$$

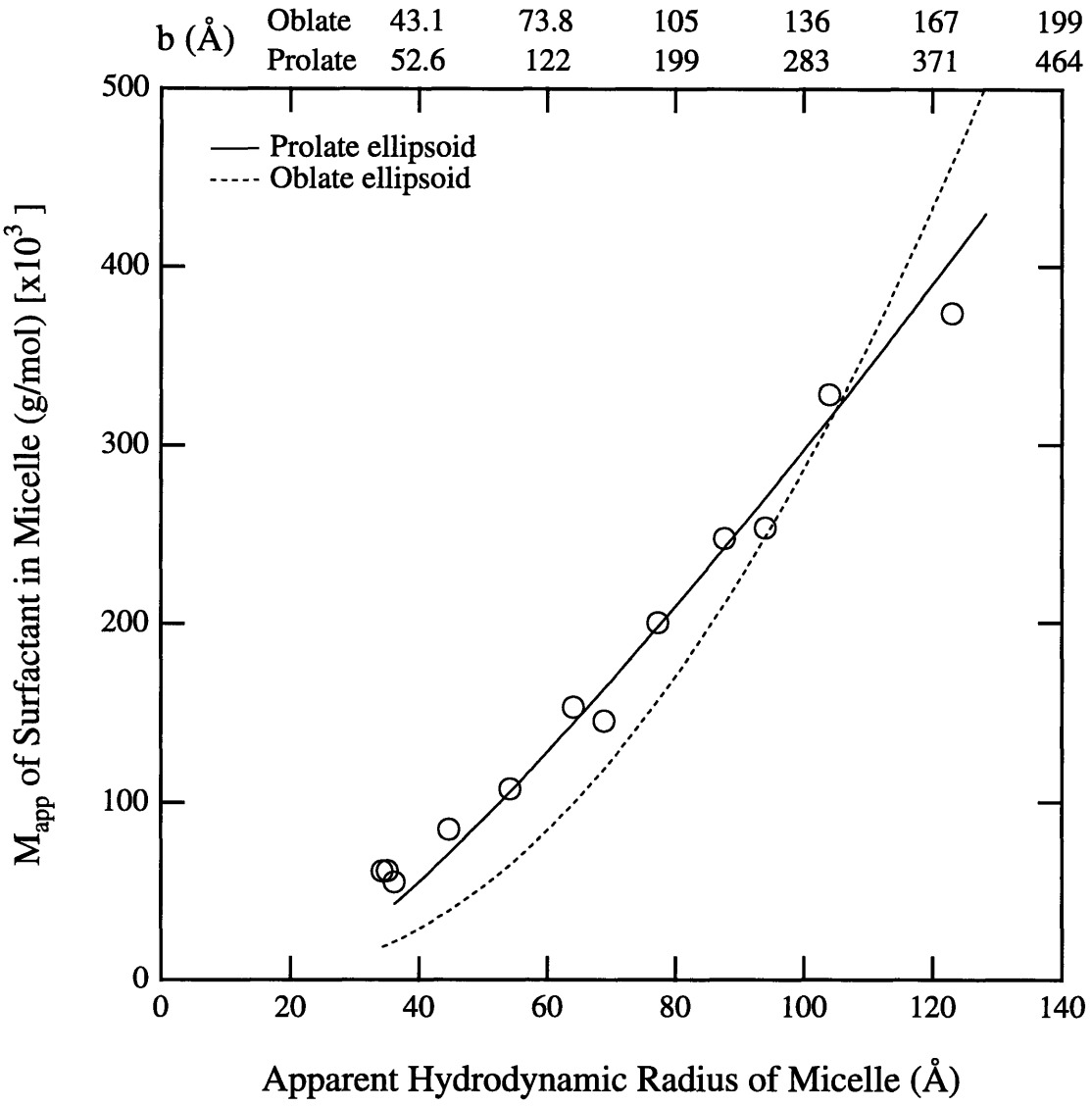

Figure 3-15: The scaling of the apparent molecular weight with the average hydrodynamic radius for an $\alpha_s = 0.751$ mixture of $C_{12}E_6$ and $C_{12}E_8$. The open circles represent all of the data for the various temperatures and concentrations presented in Figures 3-12 and 3-14. The solid line is the prediction of the prolate ellipsoid model assuming a semi-minor radius of $a = 3.4$nm and a micellar hydration of 12.8 water molecules per ethylene oxide group. The dashed line is the prediction of the oblate ellipsoid model assuming a semi-minor radius of $a = 3.4$nm and a micellar hydration of 18.4 water molecules per ethylene oxide group.

where n_W is the average number of water molecules per monomer in the micelles, m_A and m_B are the molecular weights of surfactant species A ($C_{12}E_6$) and B ($C_{12}E_8$), Ω_A, Ω_B and Ω_W are the molecular volumes of surfactant species A, surfactant species B and water, and α is the average micellar composition, which for these purposes we will assume is the same as the total solution composition. We will show in Chapter 4 that for a micellar solution with total concentration well above the critical micellar concentration, the optimum micellar composition must be very close to the total solution composition. To evaluate the molecular volumes Ω_A, Ω_B, and Ω_W, we make the further assumption that the mass density of both surfactant species and water is about 1.00g/cm^3. With this assumption, we obtain

$$n_W \left(\frac{1-\rho}{\rho}\right)\left(\frac{\alpha m_A + (1-\alpha)m_B}{m_W}\right). \tag{3.27}$$

Dividing by the average number of ethylene oxide groups per monomer, we can obtain an estimate of the average micellar hydration in terms of the number of water molecules per ethylene oxide group. Thus, for each curve in Figure 3-15, we have provided in the figure caption an estimate of the hydration of the micelle consistent with that curve.

Returning to our examination of Figure 3-15, we note first that the curvature of the data clearly favors the prolate ellipsoid model. We expect from this information alone that our data is consistent with micelles that grow in one dimension. In this connection, Jonströmer *et. al.* [24] have reported by means of NMR self-diffusion measurements that the hydration of micelles composed of pure $C_{12}E_8$ is about 8-9 water molecules per ethylene oxide group at both $T = 5°C$ and $T = 60°C$. From our light scattering measurements, we obtain a value of 12.8 water molecules per ethylene oxide group if we assume a prolate ellipsoidal geometry, and a value of 18.4 water molecules per ethylene oxide group if we assume an oblate ellipsoidal geometry. Comparison of our estimate of the micellar hydration with the estimate of Jonströmer *et. al.* [24] clearly favors the prolate ellipsoid model. This comparison is perhaps an additional piece of evidence supporting linear growth (rodlike micelles)

over growth in two dimensions (disclike micelles).

3.2.4 Light Scattering Determination of the Critical Micellar Concentration

In addition to the measurements already discussed, we have also used light scattering to provide an experimental determination of the critical micellar concentration for aqueous solutions containing pure $C_{12}E_6$ and for solutions containing pure $C_{12}E_8$. As was mentioned in Chapter 1, the critical micellar concentration is the concentration at which micelles first begin to appear in solution. Our physical picture of the situation may be explained as follows. Starting from zero total concentration, we imagine adding surfactant to the system slowly. Initially, the addition of surfactant to the system simply raises the concentration of free monomers in solution. When the concentration of free monomers reaches a sufficiently high level, it becomes advantageous to form micelles. At this point, additional surfactant added to the system creates the first micelles leaving the concentration of free monomers essentially constant. If the total surfactant concentration is increased further, the additional surfactant partitions itself between the formation of new micelles and the elongation of existing micelles, again leaving the concentration of free monomers in solution essentially unchanged. This physical picture will be investigated theoretically in Chapter 4.

We now recall that in Chapter 2, we showed that the intensity of light scattered from noninteracting particles suspended in solution should be proportional to the square of the particle mass and directly proportional to the number of such particles in the scattering volume. Therefore, below the critical micellar concentration, the scattering intensity should in principle increase linearly with concentration, since in this region we expect no micelles, and the number of free monomers in the scattering volume should increase linearly with concentration. Just above the critical micellar concentration before there is significant micellar growth, we also expect the scattering intensity to increase linearly with concentration, since in this region the free

monomer concentration is essentially fixed, and the number of micelles contained in the scattering volume should also increase linearly with concentration. The slope in this region, however, will be quite different from the intensity versus concentration slope from below the critical micellar concentration. If the micelles each contain n_0 monomers, then in the region above the critical micellar concentration, the concentration of micelles will increase at a rate which is n_0 times slower than the rate at which the free monomer concentration increased in the region below the critical micellar concentration. However, each micelle is n_0 times more massive than a free monomer and thus the intensity of the light scattered from each micelle is ${n_0}^2$ times more intense than the light scattered from a free monomer. As a result, the intensity versus concentration slope above the critical micellar concentration is expected to be n_0 times greater than the intensity versus concentration slope below the critical micellar concentration. Since n_0 is always much larger than unity for micelles (we found $n_0 \approx 135$ for our system in the previous section), we expect to see a sharp transition between these two slopes in the vicinity of the critical micellar concentration.

Unfortunately, in practice the transition of the intensity versus concentration curve that occurs at the critical micellar concentration is very difficult to observe due to experimental complications. The critical micellar concentration is extremely low (for $C_{12}E_6$ and $C_{12}E_8$ the critical micellar concentration is of the order of $10^{-5}M$). At such low concentrations, it is difficult to obtain a reliable measurement of the contribution to the total scattering intensity from the micelles since this contribution is small compared to the scattering intensity from the solvent. If we are to estimate the critical micellar concentration by total intensity measurements, we must rely on an extrapolation of measurements made at concentrations far enough above the critical micellar concentration so that the scattering intensity from the micelles is at least comparable to the scattering intensity from the solvent. For $C_{12}E_6$ and $C_{12}E_8$ such concentrations are if the order of $10^{-4}M$.

The accuracy of the determination of the critical micellar concentration can be improved dramatically if a reliable method of measuring the scattering intensity of

the micelles in the close vicinity of the critical micellar concentration can be found. The technique of dynamic light scattering offers a solution to this problem. Since the solvent particles and the free monomers are much smaller than the micelles, their motions are correlated over time scales much shorter than the characteristic decay time for the micelles. In other words, if we measure the intensity time autocorrelation function over time scales appropriate to see the characteristic time of the micelles, the correlations between free monomers and between solvent particles will have already decayed to zero. Hence, the time autocorrelation function can be written in the form

$$\langle I(0)I(t)\rangle = B + Ae^{-2\Gamma t}, \tag{3.28}$$

assuming that the micelles are monodisperse close to the critical micellar concentration. Since we are dealing with the Brownian motion of the micelles in the solvent, the decay rate, Γ, is related to the magnitude of the scattering vector, q, and the diffusivity, D, according to the relation $\Gamma = Dq^2$, as was shown in Chapter 2. The baseline, B, is proportional to the square of the average intensity, and the amplitude of the decay of the correlation function, A, is proportional to the square of the scattering intensity from the micelles only. By fitting the experimentally measured intensity time autocorrelation function to Equation 3.28, and taking the square root of A, we can obtain a quantity proportional to the intensity of light scattered from the micelles.

For concentrations in the close vicinity of the critical micellar concentration, the low signal makes the determination of Γ unreliable. However, in this region the value of A is relatively insensitive to Γ, due to the same noise that hinders the determination of Γ. We are justified then in fixing Γ to some reasonable value in this concentration region, so as to obtain a set of values for A which are consistently determined.

Dilute solutions of $C_{12}E_6$ and water and $C_{12}E_8$ and water were prepared by weight, filtered once and centrifuged as described in Section 3.1.1. The total mole fractions prepared for $C_{12}E_6$ were: $X = 5.00 \times 10^{-7}$, 1.01×10^{-6}, 2.01×10^{-6},

3.04×10^{-6}, 5.04×10^{-6}, 8.01×10^{-6} and 1.00×10^{-5}; and for $C_{12}E_8$ were: $X = 5.27 \times 10^{-7}$, 1.01×10^{-6}, 2.01×10^{-6}, 3.01×10^{-6}, 5.00×10^{-6}, 8.01×10^{-6} and 9.97×10^{-6}. Scattering cells containing pure water were also prepared and measured. Measurements of the time autocorrelation function were performed using the rotating arm instrument (described earlier) at $T = 25°C$ and $T = 59°C$ for the $C_{12}E_8$ solutions and at $T = 25°C$, $35°C$, $40°C$, $45°C$ and $49°C$ for the $C_{12}E_6$ solutions.

All measurements were made at a 90° scattering angle with a sample time of $1.0\mu s$. Because of the low signal associated with such dilute solutions, data was accumulated for 10 minutes for each measurement. At least two such measurements were made at each temperature and concentration. For the most dilute solutions, dust was sometimes a problem even after filtering and centrifugation because of the long accumulation time. For samples in which a 10 minute dust-free measurement could not be obtained, a series of measurements were performed, accumulating data for 2 minutes. Five such dust-free measurements were added together to provide the equivalent of a 10 minute measurement. Each set of measurements at a fixed temperature for all concentrations of either $C_{12}E_6$ or $C_{12}E_8$ was taken with the same laser intensity and with the same adjustment on the collection optics.

The resulting data were analyzed by fitting to Equation 3.28 above, having first normalized each correlation function measurement according to its total measurement time (the total number of sample times) so that all measurements in a set could be compared directly.

For the $C_{12}E_8$ solutions, for which very little micellar growth was observed from $T = 10°C - 55°C$, we obtained a reasonable estimate for Γ from the measurements on the sample with $X = 9.97 \times 10^{-6}$, and used that value of Γ to obtain A for all of the measurements in a set.

The data for the $C_{12}E_6$ solutions were analyzed in a similar way to extract A. However, due to the fact that at the higher of the concentrations studied here the apparent size changes at temperatures above room temperature, at these temperatures, Γ could not be fixed for all of the measurements in a set. At $T = 25°C$,

an estimate of Γ for ungrown micelles was found by fitting to the $X = 1.00 \times 10^{-5}$ data. For the $T = 25°C$ set, this value of Γ was used for all concentrations. For measurements from concentrations higher than $X = 3 \times 10^{-6}$ at $T = 35°C$ and $X = 2 \times 10^{-6}$ for $T > 35°C$, where the noise in the measurements were relatively low, Γ was allowed to vary as a fitting parameter. For the measurements where the noise was too great to accurately determine Γ, we fixed Γ to the value determined at $T = 25°C$ for the ungrown micelles.

In order to estimate the critical micelle concentration at a given temperature, we plot $I = \sqrt{A}$ against the surfactant concentration, as in, for example Figure 3-16. The location of the transition in the intensity versus concentration curve mentioned previously is determined by extrapolating the linear behavior from both above and below the transition and finding the intersection as shown in Figure 3-16. This procedure was carried out for the $C_{12}E_8$ and water solutions at $T = 25°C$ and $51°C$, and for the $C_{12}E_6$ and water solutions at $T = 25°C$, $35°C$, $40°C$, $45°C$ and $49°C$. The data and analysis are shown in Figure 3-17. No temperature dependence was seen for $C_{12}E_8$ between $T = 25°C$ and $51°C$, so additional measurements were not made. We estimate the critical micellar concentration (cmc) for $C_{12}E_8$ at $X_{CMC} = (1.95 \pm 0.1) \times 10^{-6}$. For the $C_{12}E_6$ and water solution, a weak dependence of the cmc with temperature was observed. The resulting values of the cmc are plotted as a function of temperature in Figure 3-18 along with other selected determinations of the cmc [57] using different techniques. The curve is a fit of all of the data to a straight line, which can be described by the equation

$$X_{CMC} = 1.9 \times 10^{-6} - 6.7 \times 10^{-9}(T - 25°C). \tag{3.29}$$

We see that the trend is for the critical micellar concentration to decrease slightly with increasing temperature.

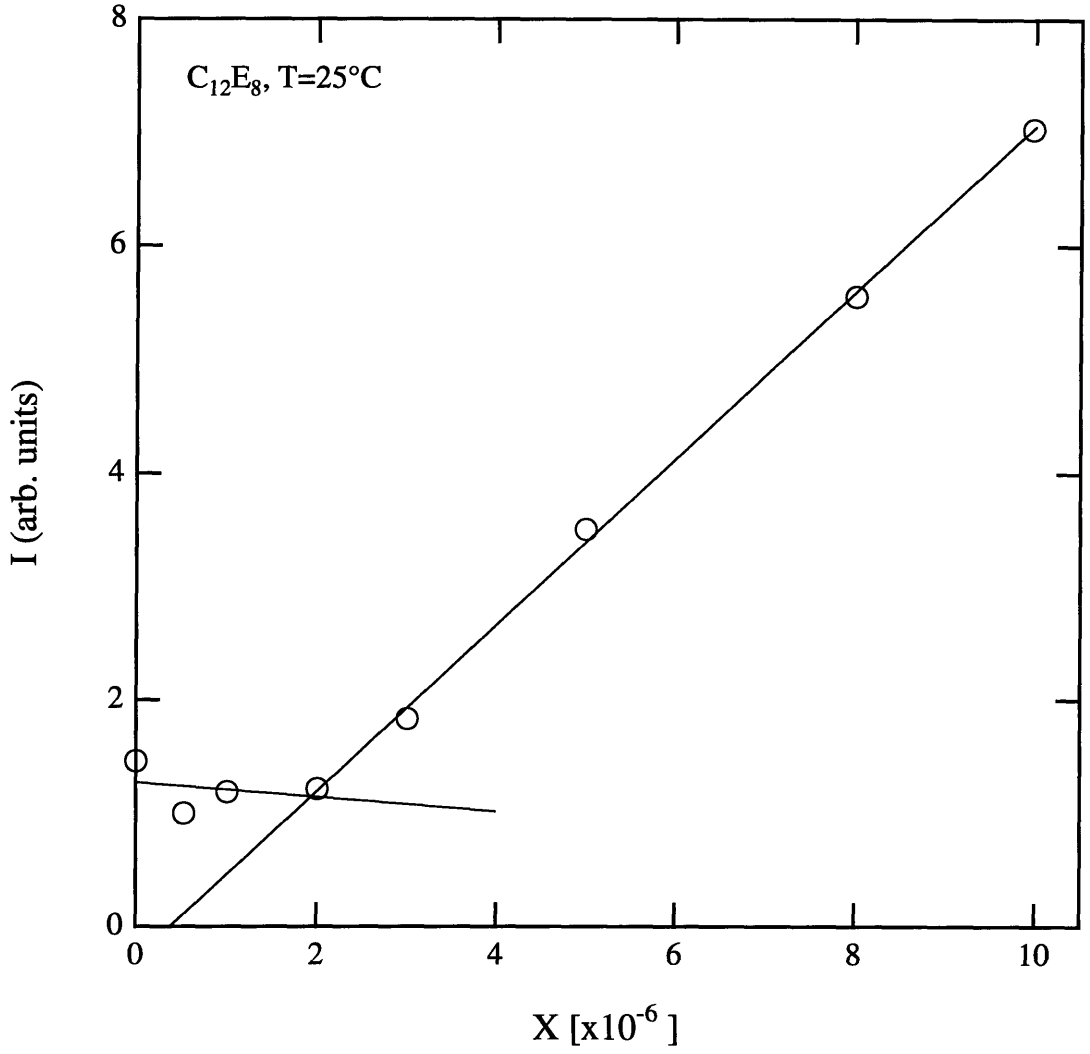

Figure 3-16: The intensity of scattering from micelles, I, as a function of total surfactant concentration in the vicinity of the critical micellar concentration at $T = 25°C$ for an aqueous solution containing pure $C_{12}E_8$. The curves are fits of the data to straight lines in the appropriate regions of the plot and are used to extract the critical micellar concentration as described in the text. Here, we find $X_{CMC} = 1.94 \times 10^{-6}$.

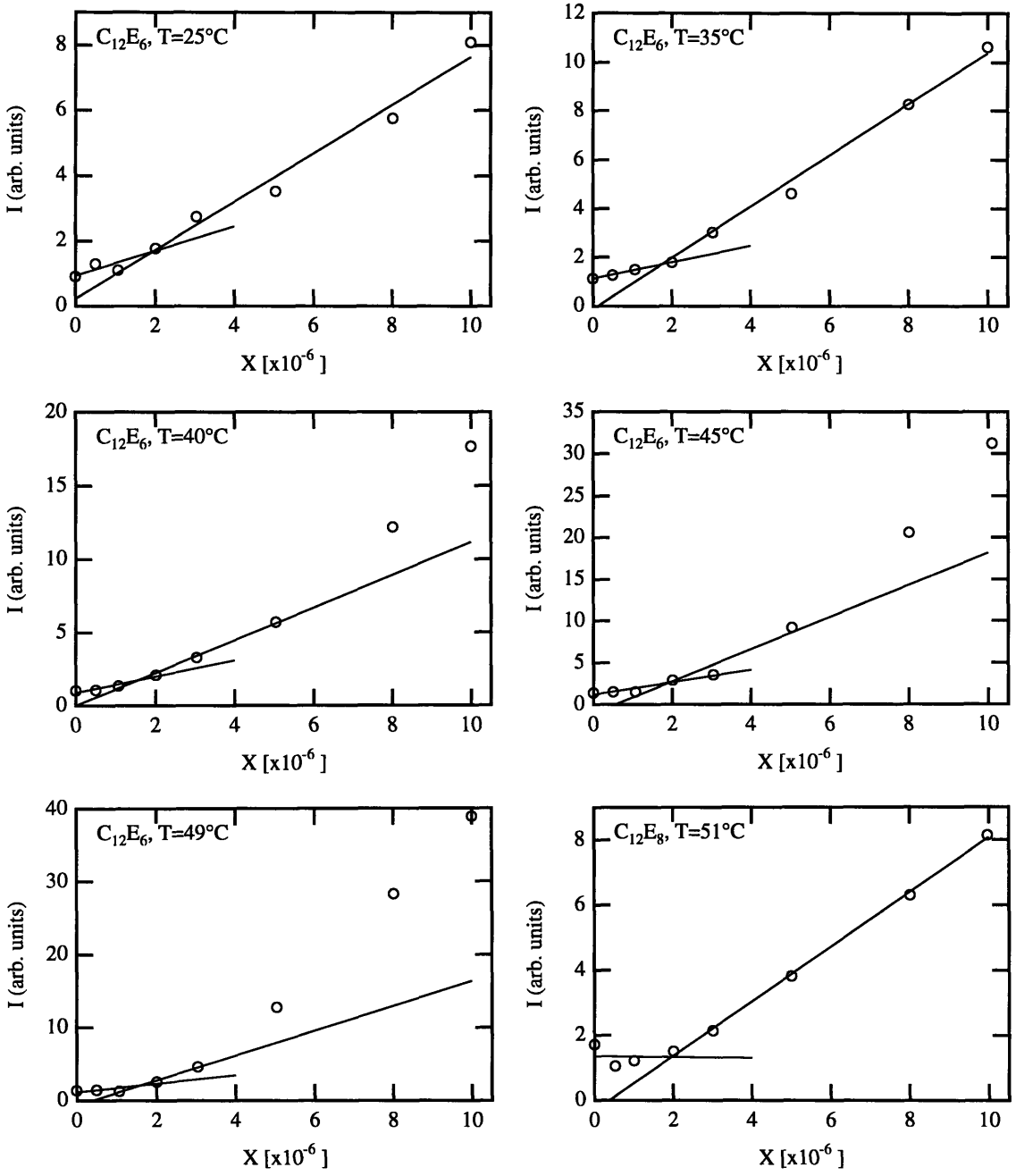

Figure 3-17: Plots of the intensity of scattering from micelles, I, as a function of total surfactant concentration in the vicinity of the critical micellar concentration at $T = 51°C$ for pure $C_{12}E_8$, and at $T = 25°C$, 35°C, 40°C, 45°C, and 49°C for pure $C_{12}E_6$. The curves are fits of the data to straight lines in the appropriate regions of the plot and are used to extract the critical micellar concentration as described in the text. We find for $C_{12}E_8$ at $T = 51°C$, $X_{CMC} = 1.96 \times 10^{-6}$. X_{CMC} values for $C_{12}E_6$ are presented in Figure 3-18

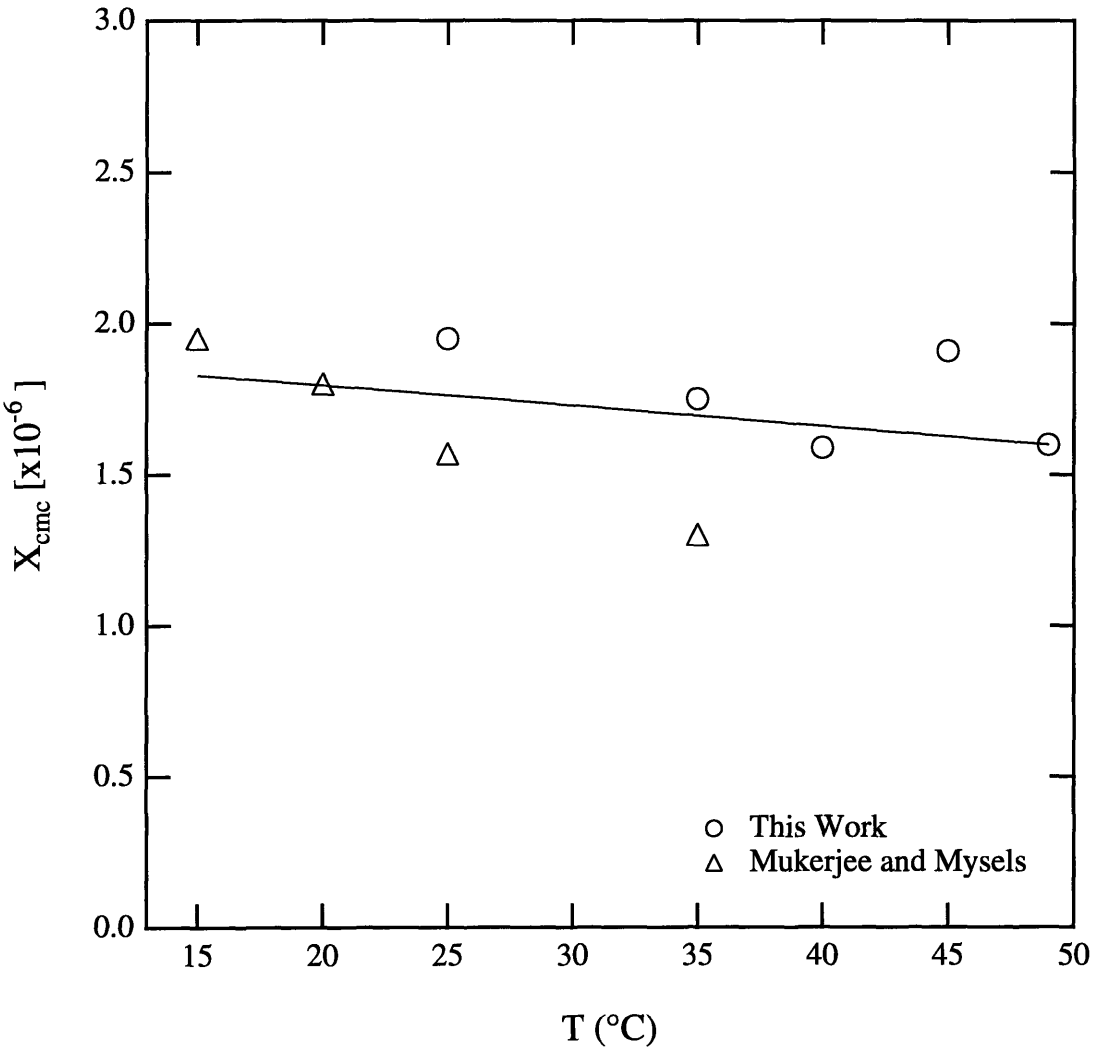

Figure 3-18: The critical micellar concentration of $C_{12}E_6$ as a function of temperature. The circles represent the values of the critical micellar concentration obtained from Figure 3-17. The triangles represent values measured using several different techniques and are taken from Reference [57].

Chapter 4

Extending the Ladder Model

In Chapter 3 we presented the results of an extensive light scattering study on the mixed $C_{12}E_6$, $C_{12}E_8$ and water system. It was found that, with increasing concentration, temperature, and relative proportion of $C_{12}E_6$ the mixed micelles exhibited a tendency to grow in one dimension. We shall examine the statistical mechanics of this one-dimensional growth in this chapter. Starting from first principles, in Section 4.1 we review the ladder model for micellar growth [10], which is suitable to explain the linear growth of micelles composed of a single surfactant species in the absence of interactions between the micelles. A geometric model of the micelles is proposed, and an expression is derived for the distribution of micellar sizes. Two limiting cases of particular interest are then discussed, the dilute limit, and the limit of strong micellar growth.

In Section 4.2, we propose the simplest possible generalization of the ladder model to the case of mixtures that is capable of explaining the data of Chapter 3 in the region where micellar interactions may be neglected. We begin with a general discussion in terms of a system containing k different kinds of amphiphiles present. Again, we begin from first principles, and our discussion parallels the discussion of Section 4.1. In Section 4.2.3, for simplicity, we restrict ourselves to a system containing two different kinds of surfactant and water. We further focus on a system in which the two kinds of surfactant are similar, and derive an expression for the distribution of micellar sizes and compositions. This expression is simplified in

Section 4.2.5 by the adoption of a random-mixing approximation within the micelle. This approximation is adopted because it greatly simplifies the sections that follow and because it will turn out that our data are consistent with the approximation. The approximation is not necessary, however, and so a full treatment of the problem is given in Appendix B. Proceeding with the simplified treatment, we show that the micellar distribution is narrow in the composition variable. This observation suggests that there is some "optimal" composition for the micelles, and that weighted sums over the micellar distribution can be greatly simplified. We conclude the chapter with a discussion of the micellar distribution in the dilute limit and the limit of strong micellar growth, and with a general discussion about the moments of the micellar distribution.

4.1 Review of Single-Component Ladder Model

In this section, we write a general expression for the partition function of our system of amphiphiles and water. We show that our general expression can be factored into two terms, the partition function of water in the absence of amphiphiles, and a partition function for the amphiphiles that includes the interactions between different amphiphiles and the interactions between amphiphiles and the surrounding water, but averaged over the different positions of the water molecules.

Because the amphiphiles are partly hydrophobic, the interaction energy between the water and amphiphiles can be reduced if the molecules group themselves into micelles in which the hydrophobic parts are shielded from the surrounding water. By considering the amphiphiles to be grouped into micelles, we can consider the interactions between different micelles separately from the interactions between amphiphiles and water and the interactions between different amphiphiles within a micelle.

In the dilute limit, when the distance between micelles is large, we can neglect the interactions between different micelles. In this case, the free energy of the system

resembles that of a mixture of ideal gases with each distinct micellar species as a separate chemical entity. Since the different micellar species can "react" with one another by the exchange of monomers with the solution, the chemical potentials of the different micellar species are all related to one another. The mole fraction of micelles of each distinct micellar species is found by equating the chemical potential of a monomer in solution to the chemical potential of a monomer in each distinct micellar species.

4.1.1 The Partition Function

Let us consider a system consisting of a single species of amphiphiles in water. Let there be N_W molecules of water and N_A amphiphiles in the system. In general, the partition function for this system may be written

$$Z = \frac{1}{h^{3N} N_W! N_A!} \int \prod_{i=1}^{N_W} d^3 y_i d^3 p_i \int \prod_{j=1}^{N_A} d^3 Y_j d^3 P_j e^{-\mathcal{H}(\{\boldsymbol{p}_i, \boldsymbol{y}_i, \boldsymbol{P}_j, \boldsymbol{Y}_j\})/k_B T} \tag{4.1}$$

where $\mathcal{H}$ is the Hamiltonian of the system that depends on the coordinates ($\boldsymbol{y}_i$) and momenta ($\boldsymbol{p}_i$) of all of the water particles in the system and on the coordinates ($\boldsymbol{Y}_j$) and momenta ($\boldsymbol{P}_j$) of all of the amphiphiles in the system. For our system, the Hamiltonian can be written

$$\mathcal{H}(\{\boldsymbol{p}_i, \boldsymbol{y}_i, \boldsymbol{P}_j, \boldsymbol{Y}_j\}) = \mathcal{H}_W(\{\boldsymbol{p}_i, \boldsymbol{y}_i\}) + \sum_{j=1}^{N_A} \frac{P_j^2}{2m_A} + U(\{\boldsymbol{y}_i, \boldsymbol{Y}_j\}), \tag{4.2}$$

where $\mathcal{H}_W(\{\boldsymbol{p}_i, \boldsymbol{y}_i\})$ is the Hamiltonian of water in the absence of solute, P_j is the magnitude of the momentum of the j^{th} amphiphile and m_A is the mass of an amphiphile. The term $U(\{\boldsymbol{y}_i, \boldsymbol{Y}_j\})$ is the potential energy of the interactions between water and amphiphiles, and of the interactions between different amphiphiles. This term therefore depends on the positions of all of the particles in the system.

The partition function for pure water can be written

$$Z_W = \frac{1}{h^{3N_W} N_W!} \int \prod_{i=1}^{N_W} d^3 p_i d^3 y_i e^{-\mathcal{H}_W(\{\boldsymbol{p}_i, \boldsymbol{y}_i\})/k_B T}. \tag{4.3}$$

We now wish to factor out of our total partition function Z, the partition function for pure water. That is, we write

$$Z = Z_W Z_A, \tag{4.4}$$

and we see that as a result of factoring out Z_W, the partition function for the amphiphiles Z_A could be written

$$Z_A = \frac{Z}{Z_W} = \frac{1}{h^{3N_A} N_A!} \int \prod_{j=1}^{N_A} d^3P_j d^3Y_j e^{-\left\{\sum_{j=1}^{N_A} \frac{P_j{}^2}{2m_A}\right\}/k_BT} e^{-\bar{U}(\{\mathbf{Y}_j\})/k_BT}, \tag{4.5}$$

where $\bar{U}$ is the interaction potential between water and amphiphiles averaged over the different positions of the water molecules:

$$\bar{U}(\{\mathbf{Y}_j\}) = -k_BT \ln\langle e^{-U(\{\mathbf{y}_i,\mathbf{Y}_j\})/k_BT}\rangle_W. \tag{4.6}$$

Until this point, the statements we have made are completely general. We now wish to consider specifically, the case of amphiphilic molecules in water. We have previously argued on physical grounds that a system of amphiphiles in water at sufficient concentration will self-assemble into a distribution of micelles in order to shield the hydrophobic regions of the amphiphiles from the surrounding water. In terms of our expression for the partition function, this means that the magnitude of the solvent-water interaction, $\bar{U}$, can be decreased dramatically if the N_A amphiphiles in the system are grouped into micelles. To describe the system in these terms, we will consider that the potential $\bar{U}$ can be modeled as a sum of terms indicating the interactions between the amphiphiles within each micelle and the interactions between each micelle and the surrounding solvent. In addition, there should also be a term that depends on the relative positions of all of the micelles to describe the interactions between different micelles. Mathematically, we can represent this

model for $\bar{U}$ by the equation:

$$\bar{U}(\{\boldsymbol{Y}_j\}) = \sum_{k=1}^{M} U_k^{int}(\{\boldsymbol{r}_{ik}\}') + U^{ext}(\{\boldsymbol{R}_k\}), \tag{4.7}$$

where the index k indicates the k^{th} micelle and M is the total number of micelles in the system. On the right hand side of the equation, we have changed notation for our position variables. Because we have grouped the amphiphiles into a distribution of micelles, it now makes sense to refer to the position of each micelle and the relative positions of the amphiphiles within that micelle rather than keeping track of the absolute positions of all of the amphiphiles separately. Here, $\boldsymbol{R}_k$ is the position of the center of mass of the k^{th} micelle, and $\boldsymbol{r}_{ik}$ is the position of the i^{th} independent amphiphile contained in the k^{th} micelle. Note that if the k^{th} micelle contains n_k monomers, that there are n_k independent position variables needed to describe the micelle. The definition of the center of mass of the micelle determines the position of one of the amphiphiles contained inside the micelle in terms of the relative positions of the other $n_k - 1$ amphiphiles. Therefore, there are $n_k - 1$ variables $\boldsymbol{r}_{ik}$ for the k^{th} micelle. The potential $U_k^{int}(\{\boldsymbol{r}_{ik}\}')$ measures the interactions between the amphiphiles within the k^{th} micelle and the interactions between the k^{th} micelle and the surrounding solvent. U_k^{int} depends, therefore on the relative positions of the amphiphiles within the k^{th} micelle, but not on the position of the micelle in the solution. The prime indicates that the set of $\boldsymbol{r}_{ik}$ should include only the $\boldsymbol{r}_{ik}$ for the k^{th} micelle. The potential $U^{ext}(\{\boldsymbol{R}_k\})$ measures the interactions between different micelles and depends on the positions of the center of mass of all of the micelles in the system. In principle, U^{ext} also depends on the relative orientations of the micelles with respect to one another if the micelles are not spherical.

Now that we have a physically reasonable model for $\bar{U}$, we have to incorporate it into our expression for the partition function. To do so, we must change the integration variables in Equation 4.5 over to the center of mass variables and relative position variables defined above. For each possible grouping of all of the amphiphiles into micelles, we must then integrate over the positions of all of the micelles and the

positions of all of the amphiphiles within each micelle. The total partition function $Z = Z_W Z_A$ should then be a sum over all of the different ways that the amphiphiles can be grouped into micelles. Symbolically, this can be written

$$\begin{aligned} Z &= Z_W \frac{1}{h^{3N_A} N_A!} \sum_{\text{different groupings}} \int \prod_{j=1}^{N_A} \left(d^3 P_j e^{-\frac{P_j^2}{2m_A k_B T}} \right) \times \\ &\quad \times \int e^{-\left\{\sum_{k=1}^{M} U_k^{int}(\{\boldsymbol{r}_{ik}\}') + U^{ext}(\{\boldsymbol{R}_k\})\right\}/k_B T} \prod_{k=1}^{M} \left(d^3 R_k \prod_{i=1}^{n_k - 1} d^3 r_{ik} \right), \quad (4.8) \end{aligned}$$

where we have exchanged our position variables $\{\boldsymbol{Y}_j\}$ (the positions of the N_A amphiphiles) for the center of mass and relative coordinates $\{\boldsymbol{R}_k\}$ and $\{\boldsymbol{r}_{ik}\}$.

In the case when our solution of micelles is dilute, such that the distance between micelles is large compared to the range of the interactions between them, we can neglect the effects of of $U^{ext}(\{\boldsymbol{R}_k\})$. Therefore, in the dilute limit, our expression for Z can be simplified:

$$Z = Z_W \frac{1}{{V_F}^{N_A} N_A!} \sum_{\text{different groupings}} \int \prod_{k=1}^{M} \left[d^3 R_k \prod_{i=1}^{n_k - 1} \left(e^{U_k^{int}(\{\boldsymbol{r}_{ik}\}')/k_B T} d^3 r_{ik} \right) \right]. \quad (4.9)$$

In addition to making the dilute approximation, we have additionally carried out the integrations over the momentum variables, resulting in the term ${V_F}^{N_A}$. Each factor of V_F comes from the integration over the momentum of an amphiphile:

$$\frac{1}{V_F} = \frac{1}{h^3} \int d^3 P_j e^{{P_j}^2/2m_A k_B T} = \left(\frac{2\pi m_A k_B T}{h^2} \right)^{3/2}. \quad (4.10)$$

The quantity V_F has units of volume, and is often called the Fermi volume.

In order to proceed, we must make clear the meaning of the summation over the different possible groupings of the amphiphiles into micelles. The indistinguishibility of the amphiphiles is already taken care of by the factor of $N_A!$ in Equation 4.9. Therefore, each term in the sum in Equation 4.9 results from considering a different association of the amphiphiles into micelles, as is indicated pictorially in Figure 4-1. Two different groupings of the amphiphiles are shown. Each distinct kind of

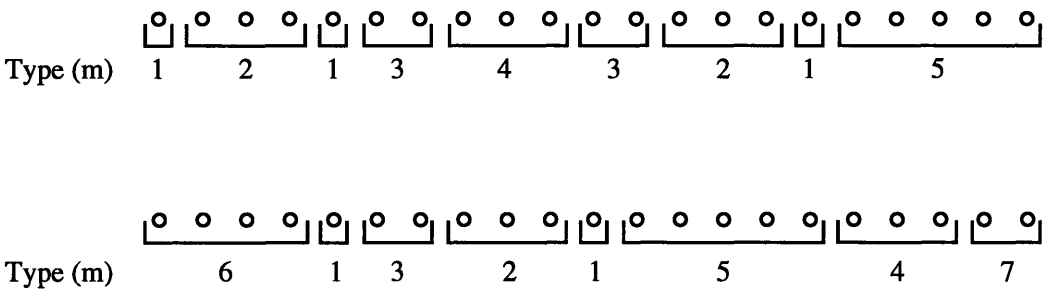

Figure 4-1: Two different possible groupings of amphiphiles into micelles. The circles represent amphiphiles, and the brackets identify the various micelles into which the amphiphiles are grouped. The numbers indicate the type of micelle. Note specifically that micelles with the same number of amphiphiles are not necessarily of the same type. In the first grouping, micelles of type 2 and micelles of type 4 both contain 3 amphiphiles, but presumably they differ in geometry. Likewise in the second grouping, micelles of type 3 and type 7 both contain 2 amphiphiles.

micelle in the figure has been labeled by a different value of the index m. We note specifically that micelles with the same number of monomers are distinct if they differ in geometry (in the figure both type 2 and type 4 micelles contain three monomers). As we shall see when we discuss mixed micelles in Section 4.2, micelles with the same number of monomers will also be distinct if they differ in relative composition. The index m, therefore, runs over all of the different possible micellar sizes and geometries.

Because two micelles of the same size and geometry (the same index m) will have the same interaction potential, the contribution from a term in the sum over the different possible groupings in Equation 4.9 depends only on the number of micelles of each type present in that term. We define the variable N_m as the number of micelles of each distinct size and geometry m and n_m as the number of monomers contained in a micelle of type m. The set of numbers $\{N_m\}$ then indicates the number of micelles of each distinct size and geometry present in a term in the sum in Equation 4.9. Each such term with the same set $\{N_m\}$ will make the same contribution to the total partition function. The number of such terms is equal to the number of ways that the N_A amphiphiles can be distributed amongst the distribution of micelles $\{N_m\}$. Since n_m is the number of amphiphiles contained in a micelle of type m, then the number of ways that the N_A amphiphiles can be distributed amongst a given distribution of micellar sizes and geometries $\{N_m\}$ is

$$\frac{N_A!}{\prod_m \left(N_m! \left(n_m!\right)^{N_m}\right)}. \tag{4.11}$$

This equation is understood as follows. In the numerator, we note that there are $N_A!$ ways to arrange the N_A amphiphiles. Of these possible arrangements, we must divide out the possible rearrangements of indistinguishable micelles ($\prod_m N_m!$) and the possible rearrangements of the indistinguishable amphiphiles within each micelle ($\prod_m (n_m!)^{N_m}$).

As a result of the above considerations, we may rewrite Z as the sum over all different possible micellar size and geometry distributions $\{N_m\}$ with the constraint

that the total number of amphiphiles is N_A:

$$Z = Z_W \sum_{\text{all } \{N_m\}}{}' \prod_m \left[\frac{1}{{V_F}^{N_m} N_m!} \left(\frac{\int d^3R_m}{{V_F}^{n_m-1} n_m!} \int \prod_{i=1}^{n_m-1} d^3r_{im} e^{-U_m^{int}(\{\boldsymbol{r}_{im}\})/k_BT} \right)^{N_m} \right], \tag{4.12}$$

where we have used the prime to indicate the presence of the constraint that for each allowed set of $\{N_m\}$, the total number of amphiphiles must be N_A. Since the interaction potential is identical for all of the micelles of a given size and geometry m, we have collected together the contributions from each of the N_m micelles of type m into a single term. In this sense, the interaction potential $U_m^{int}(\{\boldsymbol{r}_{im}\})$ considers the interactions between a single micelle of size and geometry m and the surrounding solvent and the interactions between the n_m amphiphiles within that micelle. The constraint that the total number of amphiphiles present in the solution is N_A may be written

$$N_A = \sum_m n_m N_m. \tag{4.13}$$

Equation 4.12, can be written the much more compact form

$$Z = Z_W \sum_{\text{all } \{N_m\}}{}' \prod_m \frac{1}{{V_F}^{N_m} N_m!} \left(\int d^3R_m Z_m \right)^{N_m}. \tag{4.14}$$

where the quantity Z_m collects together all of the factors internal to a single micelle of size and geometry indicated by the index m. Z_m is given by the expression

$$Z_m = \frac{1}{{V_F}^{n_m-1} n_m!} \int \prod_{i=1}^{n_m-1} d^3r_{im} e^{U_m^{int}(\{\boldsymbol{r}_{im}\})/k_BT}, \tag{4.15}$$

and represents the internal partition function for a single micelle of size and geometry m.

In the dilute limit, since the interaction energy between a single micelle of type m and the surrounding water, $U_m^{int}(\{\boldsymbol{r}_{im}\})$, does not depend on the position, $\boldsymbol{R}_m$, of the micelle, each explicit integration in Equation 4.14 yields a single factor of V,

the total volume of the system. Therefore,

$$Z = Z_W \sum_{\text{all } \{N_m\}} {}' \prod_m \frac{1}{N_m!} \left(\frac{V Z_m}{V_F}\right)^{N_m}. \tag{4.16}$$

4.1.2 The Free Energy and the Micellar Distribution in the Dilute Limit

The free energy of our system is given by

$$F = -k_B T \ln Z = F_0 - k_B T \ln Z_A \tag{4.17}$$

where $F_0 = -k_B T \ln Z_W$ is the free energy of water in the absence of amphiphiles. From Equation 4.16, we recall that $Z_A = Z/Z_W$ is a sum over all of the possible micellar size and geometry distributions (that is the sum over all possible sets $\{N_m\}$) subject to the condition that the total number of amphiphiles is fixed. When the system is very large (the total number of amphiphiles tends to infinity) the log of Z_A can be well approximated by the log of the maximum term in the sum over the different distributions of micellar sizes and geometries (that is, the term in which the particular set of micellar sizes and geometries $\{N_m\}$ gives the maximal contribution to Z). Therefore, the total free energy is approximately

$$F = F_0 - k_B T \sum_m N_m \ln \frac{V Z_m e}{V_F N_m}, \tag{4.18}$$

which resembles a mixture of ideal gasses where each micellar species m is a different "gas" with internal free energy $-k_B T \ln Z_m$. In Equation 4.18, $\{N_m\}$ is now the single micellar shape and size distribution that gives a maximal contribution to Z.

We must now find the form of the set $\{N_m\}$ that gives maximal contribution to Z, subject to the condition that the total number of amphiphiles is fixed. This is equivalent to finding the form of the set of micellar sizes and geometries $\{N_m\}$ that minimizes the free energy of the system subject to the condition that the total number of amphiphiles is fixed. To find the form of $\{N_m\}$, we will use the method

of Lagrange multipliers. We recall that the constraint that the total number of amphiphiles is constant may be written

$$N_A = \sum_m n_m N_m = \text{const.} \tag{4.19}$$

Minimizing $F(\{N_m\})$ subject to the constraint that N_A is constant is equivalent to minimizing a new function

$$\Omega = F(\{N_m\}) - \mu \sum_m n_m N_m. \tag{4.20}$$

without constraint, where F is the free energy. Performing a variation with respect to N_m and setting $\delta\Omega = 0$, we have

$$-k_B T \ln \frac{V Z_m}{V_F N_m} - n_m \mu = 0 \tag{4.21}$$

for each distinct micellar size and geometry m. To proceed in a purely mathematical way, we should now express each of the N_m as a function of the Lagrange multiplier μ and determine μ such that $\sum_m n_m N_m(\mu)$ is equal to the total (fixed) number of amphiphiles in the system. It will be more insightful, however, to examine the physical meaning of the Lagrange factor μ.

In principle, Equation 4.19 can be used to express one of the N_m (for example the concentration of free monomers) in terms of N_A and all of the other N_m. The free energy F is therefore implicitly a function of N_A. Minimizing Ω without constraint means that all of the partial derivatives of Ω should vanish. In particular, we must have that

$$\frac{\partial \Omega}{\partial N_A} = \frac{\partial F}{\partial N_A} - \mu = 0 \tag{4.22}$$

which implies that

$$\mu = \frac{\partial F}{\partial N_A}. \tag{4.23}$$

The chemical potential of a micelle of type m in solution is defined

$$\mu_m = \frac{\partial F}{\partial N_m} = \frac{\partial F}{\partial N_A}\frac{\partial N_A}{\partial N_m}. \tag{4.24}$$

Using the definition of the chemical potential μ (Equation 4.23) and our expression for the total number of amphiphiles in the system (Equation 4.19), we obtain for the chemical potential of a micelle of size and geometry m:

$$\mu_m = \mu n_m. \tag{4.25}$$

This condition holds for all of the different possible sizes and geometries, including the free monomers. Denoting the chemical potential of a free monomer in solution as μ_1, Equation 4.25 tells us that

$$\mu_1 = \mu, \tag{4.26}$$

and we see that the Lagrange multiplier, μ, is the chemical potential of a monomer. Equation 4.25 therefore tells us that the chemical potential of a micelle of type m is simply related to the chemical potential of a monomer. Since Equation 4.25 is true for all m, the chemical potentials of all of the different micellar species are related to one another. By substituting Equation 4.25 into Equation 4.21, we see that the variation of Ω with respect to N_m gives us an expression for the chemical potential of a micelle of size and geometry m in terms of the concentration of micelles of type m in the solution:

$$\mu_m = k_B T \ln N_m - k_B T \frac{V Z_m}{V_F}. \tag{4.27}$$

Denoting the mole fraction of micelles of type m

$$X_m = \frac{N_m}{N_W + N_A} = \frac{N_m}{N}, \tag{4.28}$$

where N is the total number of water molecules and amphiphiles in the system, we obtain

$$\mu_m = \mu_m^0 + k_B T \ln X_m \tag{4.29}$$

where the standard part of the chemical potential μ_m^0 is

$$\mu_m^0 = -k_B T \ln \frac{V Z_m}{V_F N}. \tag{4.30}$$

We are now in a position to obtain an expression for the equilibrium mole fraction of micelles of type m in solution in terms of the mole fraction of free monomers in solution at equilibrium. We proceed by noting that at equilibrium, the chemical potential of a monomer must be the same in solution and in a micelle of type m. Using Equation 4.25, the equilibrium condition between free monomers and micelles of type m can be written

$$\mu = \frac{\mu_m}{n_m}. \tag{4.31}$$

The chemical potential of a micelle of size and geometry m is given by Equation 4.29. Since Equation 4.29 is also true for the free monomers, we also have

$$\mu = \mu_1^0 + k_B T \ln X_1, \tag{4.32}$$

where we have denoted the mole fraction of free monomers as X_1, and the standard part of the chemical potential a free monomer as μ_1^0. Substituting Equations 4.32 and 4.29 into the equilibrium condition (Equation 4.31), we obtain the desired result

$$X_m = {X_1}^{n_m} e^{-(\mu_m^0 - n_m \mu_1^0)/k_B T}. \tag{4.33}$$

The mole fraction of micelles of type m in solution at equilibrium is determined by two physically significant factors. The first factor, $({X_1}^{n_m})$ represents the likelihood that the n_m monomers that make up the micelle of type m will be localized in the same region of space. The second term is a Boltzmann factor that expresses the free energy advantage associated with assembling a micelle of the appropriate geometry for a micelle of type m from the n_m localized monomers. The micellar distribution can be found in terms of the total mole fraction of surfactant, X, by determining X_1 in terms of X by enforcing the conservation of the total number of monomers in the solution. Performing this step requires that we first know the standard chemical

potential differences $\mu_m^0 - n_m\mu_1^0$ for the entire distribution.

4.1.3 One-Dimensional Growth and the Ladder Model

In Section 4.1.1 we defined m as an index that runs over the distinct sizes and geometries of micelles possible in the system. In principle, one should consider all possible different geometries and calculate Z_m for each geometry and total aggregation number, thus determining μ_m^0 for all m (including μ_1^0). In practice, this cannot be done, because it is not possible to consider all possible different geometries.

Many real systems exist at equilibrium in a well defined geometry or set of geometries, for example, a system that exists as small spheres in coexistence with rods of varying lengths. In such a system we can model the micelles with a small number of physically meaningful parameters, giving us a reasonable approximation to the actual distribution of micelles.

Far above the critical micellar concentration certain micellar systems have been shown to form a polydisperse solution of long, rodlike micelles. Near to the critical micellar concentration, these systems generally exist as a relatively monodisperse distribution of small spherical or ellipsoidal micelles with some minimum size, n_0. Micelles with total aggregation numbers significantly less than n_0 do not exist in equilibrium because the hydrophilic heads of the constituent amphiphiles cannot adequately screen the hydrophobic core of the micelle from the surrounding water. We shall be concerned with such a system. We model the long rodlike micelles as prolate spherocylinders as shown in Figure 4-2. A micelle of total aggregation number n consists of a cylindrical body of radius a containing $n - n_0$ monomers and two hemispherical end caps of radius a, each containing $n_0/2$ monomers. In general, we need not consider the ends of the micelle to be hemispherical, but for simplicity of the picture, we shall assume that they are. For $n \sim n_0$ this approximation will not be as accurate as, say, a prolate ellipsoidal model, but since we will be generally concerned with growth well above the critical micellar concentration, we may neglect the precise details of the distribution in the region near n_0. We shall furthermore assume that micelles with total aggregation numbers $n < n_0$ cannot exist.

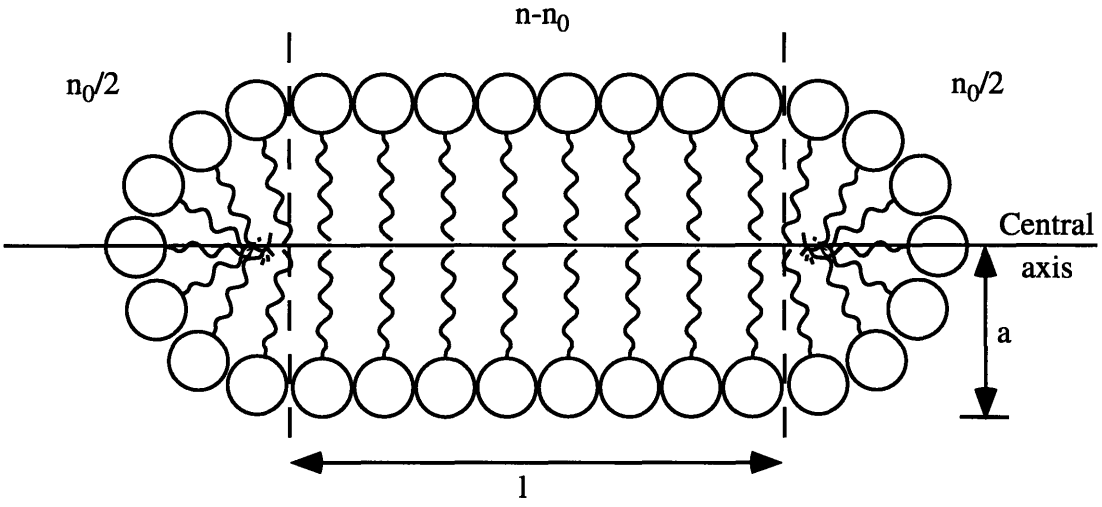

Figure 4-2: The geometry of a cross-section of a spherocylindrical micelle. A micelle of size n consists of a central cylinder of length l and radius a that contains $n - n_0$ monomers. At both ends of the cylinder are hemispherical end caps, each with radius a and containing $n_0/2$ monomers.

It is clear to see that in this model, distinguishable micelles differ in their total aggregation number only. Thus, the label m in the micellar distribution can be replaced by the total aggregation number n, and we can write the micellar distribution of sizes:

$$X_n = {X_1}^n e^{-(\mu_n^0 - n\mu_1^0)/k_B T}. \tag{4.34}$$

Here, μ_n^0 is the standard (internal) part of the chemical potential of an n-mer. That is, μ_n^0 is the change in the free energy associated with placing one n-mer into water apart from the entropy of mixing. Likewise, $\mu_n^0 - n\mu_1^0$ represents the change in free energy of the system associated with transferring n monomers from water into an n-mer. We shall call this quantity the free energy of micellization. Given our geometrical model, we should be able to make some statements about the free energy of micellization for increasing n.

As Tanford has suggested [58], the free energy of micellization per monomer in a micelle may be taken as a first approximation to be simply a function of the cross-sectional area of the surfactant molecule presented at the surface of the micelle. This area depends on the local geometry and packing in the micelle. For the spherocylindrical micelle pictured in Figure 4-2, there are two regions of distinct geometry, the hemispherical end caps and the cylindrical body. In the cylindrical body, each monomer sees the same local environment except, perhaps the monomers nearest the ends. Neglecting these effects, we will associate a standard part chemical potential per monomer in this region of μ_c^0. For each monomer in the spherical end caps, we will likewise associate a standard part chemical potential of μ_s^0. If we were to assume that the end caps were not hemispherical, then μ_s^0 would represent an average standard chemical potential per monomer in the end. Thus, we write

$$\mu_n^0 = n_0\mu_s^0 + (n - n_0)\mu_c^0 \tag{4.35}$$

and the free energy of micellization, $\mu_n^0 - n\mu_1^0$ may be written

$$\mu_n^0 - n\mu_1^0 = n_0\mu_s^0 + (n - n_0)\mu_c^0 - n_0\mu_1^0 - (n - n_0)\mu_1^0 \tag{4.36}$$

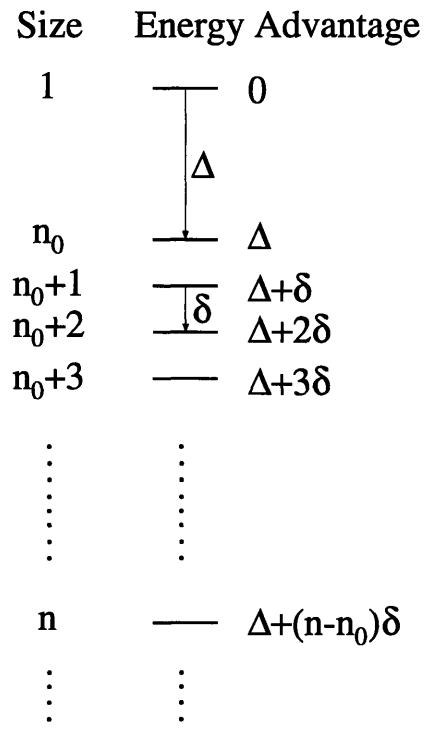

Figure 4-3: The sequence of free energy differences $\Delta + (n - n_0)\delta$ of the ladder model.

$$= n_0(\mu_s^0 - \mu_1^0) + (n - n_0)(\mu_c^0 - \mu_1^0) \tag{4.37}$$

The sequence of energy levels for increasing n is shown in Figure 4-3. This sequence may be described as and infinite ladder with a gap. The base of the ladder (the zero energy reference) refers to the free monomers in solution. This level is separated from the level corresponding to the minimum sized micelle by an energy gap of size

$$\Delta = n_0(\mu_s^0 - \mu_1^0). \tag{4.38}$$

Since we have said that the shielding of the hydrophobic regions of the amphiphiles inside a micelle from the surrounding solvent lowers the interaction energy of the amphiphiles with the solvent, we expect that $\mu_s^0 < \mu_1^0$ and so Δ will be a negative number.

For $n > n_0$, each level is separated from the previous energy level by a fixed

ladder rung spacing of

$$\delta = (\mu_c^0 - \mu_1^0). \tag{4.39}$$

For the same reason that we expect $\mu_s^0 < \mu_1^0$, we also expect that $\mu_c^0 < \mu_1^0$, indicating that δ is also a negative quantity. Thus, for our geometrical "ladder" model we express the micellar distribution in terms of two parameters, the gap spacing, Δ, and the rung spacing δ. Incorporating the ladder model (Equations 4.37-4.39) into our expression for the micellar distribution gives

$$X_n = {X_1}^n e^{-(\Delta+(n-n_0)\delta)/k_BT}. \tag{4.40}$$

It is useful to define the parameter K as follows:

$$K = e^{(\Delta-n_0\delta)/k_BT} = e^{\Delta\mu/k_BT}, \tag{4.41}$$

where $\Delta\mu$ measures the difference in energies to put n_0 monomers into the cylindrical portion of a micelle or to put the same n_0 monomers into the ends of a new micelle. If $\Delta\mu$ is positive (meaning that $K > 1$), then, since Δ and δ (on which K depends) are both negative numbers, $n_0\delta$ must have a larger magnitude than Δ, and we see that it is energetically favorable to put the monomers into the cylindrical region. This corresponds to micellar growth. With our definition of K (Equation 4.41), the micellar distribution is written

$$X_n = \frac{1}{K}{X_1}^n e^{-n\delta/k_BT}. \tag{4.42}$$

As was mentioned in Section 4.1.2, in order to determine the micellar distribution appropriate for a given total mole fraction of surfactant in solution, we must use the expression for the conservation of the total number of monomers in the system to obtain an expression for X_1 in terms of X. This conservation relation may be

written as a sum over the micellar distribution:

$$X = X_1 + \sum_{n=n_0}^{\infty} nX_n. \tag{4.43}$$

If we insert our expression for the micellar distribution (Equation 4.42) into the conservation relation, we can perform the sum, giving

$$X = X_1 + \frac{1}{K}\Lambda^{n_0}\left\{\frac{n_0}{(1-\Lambda)} + \frac{\Lambda}{(1-\Lambda)^2}\right\} \tag{4.44}$$

where we have made the definition

$$\Lambda = X_1 e^{-\delta/k_B T}. \tag{4.45}$$

In order for the sum to converge to a finite concentration, $\Lambda < 1$, indicating that X_1 is always less than the quantity $e^{\delta/k_B T}$. Equation 4.44 can be numerically solved for X_1 given any total concentration X if the values of Δ and δ have been determined.

At this point, the problem is in principle solved, since from the micellar distribution we can calculate, at least numerically, any experimentally observable quantity. Likewise, we can use experimental data to obtain information about the micellar distribution. It will, however, be interesting to examine the micellar distribution in the dilute regime, and also in the regime of strong micellar growth.

4.1.4 The Dilute Regime

As has been previously discussed, at low total surfactant concentrations there should exist a transition below which no micelles exist and above which essentially all additional surfactant added to the solution exists in micellar form. This transition is expected to occur over a narrow range of concentrations, and for this reason we can define a critical micellar concentration to identify the concentration at which the transition occurs. We wish to show here that Equation 4.44 implies such a transition.

Examining the form of Equation 4.44 and recalling the definition of Λ (Equation

4.45), we see that the value of X determined as a function of X_1 should show a sharp transition because of the factor Λ^{n_0} appearing in Equation 4.44. When Λ is not close to unity, the large power of n_0 effectively kills the contributions to the total concentration X from the second and third terms on the right hand side of Equation 4.44. In this region, $X = X_1$, and it is clear that no micelles are present in the solution.

As the total concentration, X, is increased, the value of X_1 (and thus Λ) increases. As Λ approaches unity, the value of Λ^{n_0} increases sharply and the second and third terms on the right hand side of Equation 4.44 can not be neglected. Remembering that these two terms come from the summation over the micellar distribution, we note that together, they should be proportional to the total number of monomers in the solution that exist in micellar form. The critical micellar concentration, therefore, lies in the vicinity of the concentration region where the second and third terms on the right hand side of Equation 4.44 first become comparable to the magnitude of X_1.

If $K > 1$, then when X approaches e^{δ/k_BT}, X_1 becomes comparable to e^{δ/k_BT}, meaning that the value of Λ approaches 1 and we can no longer neglect the second and third terms on the right hand side of Equation 4.44. In fact, as we increase the concentration further, X_1 can increase only very little, since its maximum value is e^{δ/k_BT}, as we saw in the previous section. If the value of X_1 exceeds e^{δ/k_BT}, then $\Lambda > 1$, and the summation over the micellar distribution resulting in Equation 4.44 does not converge. Therefore, most of the increase in X at the stage where X is about e^{δ/k_BT} is reflected as an increase in the second and third terms of Equation 4.44, and so we expect the critical micellar concentration to lie in the vicinity of $X = e^{\delta/k_BT}$.

On the other hand, if $K < 1$, then the second and the third terms on the right hand side of Equation 4.44 become significant before X reaches e^{δ/k_BT}. In this case, it is convenient to recall the definition of K (Equation 4.41) and the definition of Δ

(Equation 4.38) so that we may rewrite Equation 4.44

$$X = X_1 + \left(\frac{X_1}{e^{(\mu_s^0 - \mu_1^0)/k_BT}}\right)^{n_0} \left\{\frac{n_0}{(1-\Lambda)} + \frac{\Lambda}{(1-\Lambda)^2}\right\}. \tag{4.46}$$

We see that when X approaches the quantity $e^{(\mu_s^0 - \mu_1^0)/k_BT}$, X_1 becomes comparable to $e^{(\mu_s^0 - \mu_1^0)/k_BT}$, meaning that the second and third terms on the right hand side of Equation 4.46 begin to increase sharply and can no longer be neglected. We therefore expect the critical micellar concentration to lie in the vicinity of $X = e^{(\mu_s^0 - \mu_1^0)/k_BT}$. Furthermore, we note that the condition that $K < 1$ implies that $e^{(\mu_s^0 - \mu_1^0)/k_BT} < e^{\delta/k_BT}$. Therefore, from the definition of Λ (Equation 4.45), we see that when the second and third terms on the right hand side of Equation 4.46 become significant, that Λ is not necessarily very close to unity in the sense that Λ^{n_0} is still small compared to unity. We will see in the next section that this implies that for $K < 1$ we cannot physically realize the limit of strong micellar growth.

4.1.5 The Limit of Strong Micellar Growth

By strong micellar growth, it is meant that there are significant numbers of micelles with $n > n_0$, or equivalently, the levels in the micellar distribution X_n in Equation 4.42 for $n > n_0$ must be significantly occupied. This implies that Λ is close to unity. Let us then define

$$\Lambda = 1 - \frac{\epsilon}{n_0} \tag{4.47}$$

where $\epsilon \ll 1$. For almost all practical cases, the limit of strong micellar growth will also correspond to the limit $X \gg e^{\delta/k_BT}$, that is, the total concentration is far above the critical micellar concentration. We will first examine the limit of strong micellar growth when the total concentration is far above the critical micellar concentration. We shall then consider the conditions for which strong micellar growth can occur even close to the critical micellar concentration.

For total concentrations far above the critical micellar concentration, 4.44 gives,

to leading order in ϵ

$$X = e^{\delta/k_BT} + \frac{1}{K}\frac{{n_0}^2}{\epsilon^2}. \tag{4.48}$$

In the above equation, we could replace X_1 with e^{δ/k_BT} since $X \gg e^{\delta/k_BT}$ and the correction introduced by considering X_1 as different from e^{δ/k_BT} is of the next order in ϵ. Equation 4.48 implies that

$$K(X - e^{\delta/k_BT}) \gg {n_0}^2. \tag{4.49}$$

With Equation 4.48 as an estimate of ϵ/n_0, Equation 4.47 becomes

$$\Lambda \simeq 1 - \frac{1}{[K(X - e^{\delta/k_BT})]^{1/2}}, \tag{4.50}$$

and using Equation 4.50 in Equation 4.42 (also recalling the definition of Λ), the micellar distribution can be rewritten

$$X_n \simeq \frac{1}{K} e^{-n/[K(X-e^{\delta/k_BT})]^{1/2}}. \tag{4.51}$$

Thus, we see that in the limit of strong micellar growth, the micellar distribution is an exponential, whose width increases as $[K(X - e^{\delta/k_BT})]^{1/2}$.

As we mentioned in the previous section, in order to physically realize the limit of strong micellar growth as presented above, we must have that $K > 1$. This can be shown by examination of Equation 4.49. We note first that by definition, $X < 1$, since $X = 1$ corresponds to a solution containing only surfactant. In addition, the quantity e^{δ/k_BT} should be small compared to unity, since in general δ is a negative number indicating the stability of cylindrical micelles relative to free monomers. Therefore, on the left hand side of Equation 4.49 K multiplies a quantity $(X - e^{\delta/k_BT})$ that can be at most of the order of unity, and which in all practical cases is small compared to unity. However, we are told by Equation 4.49 that in order to realize the limit of strong micellar growth, the quantity $K(X - e^{\delta/k_BT})$ should be much greater than ${n_0}^2$. We know that for a micellar system, n_0 should be

large compared with unity. We therefore cannot realize the limit of strong micellar growth unless $K > 1$, since unless $K > 1$, we have no way to satisfy Equation 4.49.

We now wish to investigate the conditions for which strong micellar growth can occur for concentrations near to the critical micellar concentration. From Equation 4.51, we see that at a fixed total concentration that as K is increased, the micellar distribution becomes broader. Equivalently, if we consider a fixed width of the micellar distribution, increasing K will decrease the total concentration X for which that distribution occurs. We therefore wish to estimate the magnitude of K required to have large growth at low concentration. Let us consider the case when $X = e^{\delta/k_BT}$ and Λ is close to 1 as in Equation 4.47. As we have previously done, we expand the mass conservation relation (Equation 4.44) to leading order in ϵ. However, since X is no longer large compared to e^{δ/k_BT}, we cannot also replace X_1 with e^{δ/k_BT}. Instead of Equation 4.48, we have

$$X = X_1 + \frac{1}{K}\frac{{n_0}^2}{\epsilon^2}. \tag{4.52}$$

Using the definition of Λ and substituting $X = e^{\delta/k_BT}$, we get

$$e^{\delta/k_BT} = e^{\delta/k_BT}\left(1 + \frac{\epsilon}{n_0}\right) + \frac{1}{K}\frac{{n_0}^2}{\epsilon^2}, \tag{4.53}$$

which tells us that to leading order in ϵ,

$$Ke^{\delta/k_BT} = \frac{{n_0}^3}{\epsilon^3}. \tag{4.54}$$

Recalling that the quantity e^{δ/k_BT} is of the same order as the critical micellar concentration, Equation 4.54 implies that if $K \gg {n_0}^3/X_{CMC}$, where X_{CMC} is the critical micellar concentration, then even near the critical micellar concentration there is considerable micellar growth. If, on the other hand, it turns out that $K \ll {n_0}^3/X_{CMC}$, then near the critical micellar concentration the solution exists as a relatively monodisperse distribution of nearly minimum-sized micelles. We now investigate which limit applies to our experimental system.

For the case of pure $C_{12}E_6$ at 50°C, we will find that $n_0 \sim 135$, $K \sim 5 \times 10^{10}$, and $X_{CMC} \sim 1.7 \times 10^{-6}$. The value of K is much less than ${n_0}^3/X_{CMC} \sim 1.4 \times 10^{12}$. For lower temperatures, we will find that K is smaller than 5×10^{10}, and so for all temperatures studied we have for pure $C_{12}E_6$ that $K \ll {n_0}^3/X_{CMC}$. For pure $C_{12}E_8$ we will find that $n_0 \sim 135$, $X_{CMC} \sim 2.0 \times 10^{-6}$, and in the regions of temperature studied, $K < 6 \times 10^5$. Therefore, for pure $C_{12}E_8$ we also find that $K \ll {n_0}^3/X_{CMC}$, implying that near the critical micellar concentration both pure solutions exist as a relatively monodisperse distribution of nearly minimum-sized micelles. In the regions that show appreciable micellar growth, we can be sure that $X \gg e^{\delta/k_BT}$. As a result of this, we can simplify the expression for the micellar distribution even further, since we can neglect e^{δ/k_BT} as compared with X in Equations 4.49- 4.51. For the micellar distribution, we have

$$X_n \simeq \frac{1}{K} e^{-n/[KX]^{1/2}}. \tag{4.55}$$

Experimentally, we can measure certain averages over the micellar distribution. For example, with static light scattering, we can measure the weight-averaged aggregation number. In the limit of strong micellar growth, such measurements will allow us to experimentally determine K. Knowledge of the critical micellar concentration can then be used to determine the value of δ.

The weight-averaged aggregation number is defined by

$$\bar{n}_w = \sum_{n=n_0}^{\infty} n^2 X_n / \sum_{n=n_0}^{\infty} n X_n. \tag{4.56}$$

After inserting the micellar distribution and taking the limit of strong micellar growth, the weight-averaged aggregation number may be written

$$\bar{n}_w \simeq n_0 + 2\sqrt{KX}. \tag{4.57}$$

4.2 Extension to the Case of Mixtures

Now that we have discussed the statistical mechanics of single component micellar solutions and the ladder model for micelles that grow in one-dimension, we must generalize our discussion to the case of multicomponent mixtures. Let us consider a system consisting of z different kinds of amphiphiles in water. Let there be N_W molecules of water in the system, N_1 amphiphiles of type 1, N_2 amphiphiles of type 2, and so on up to N_z amphiphiles of type z. Let us denote the total number of amphiphiles in the system as

$$N_A = \sum_{a=1}^{z} N_a, \tag{4.58}$$

and the total number of particles in the system as

$$N = N_W + \sum_{a=1}^{z} N_a. \tag{4.59}$$

The total mole fraction of surfactant species a is then defined

$$X_a = \frac{N_a}{N}. \tag{4.60}$$

4.2.1 The Partition Function

Following the logic of Section 4.1.1, the partition function of our system may be written

$$Z = \frac{1}{h^{3N} N_W! \prod_{a=1}^{z} N_a!} \int \prod_{i=1}^{N_W} d^3y_i d^3p_i \int \prod_{j=1}^{N_A} d^3Y_j d^3P_j e^{-\mathcal{H}(\{\boldsymbol{p}_i, \boldsymbol{y}_i, \boldsymbol{P}_j, \boldsymbol{Y}_j\})/k_B T} \tag{4.61}$$

where $\mathcal{H}$ is the Hamiltonian of the system that depends on the coordinates ($\boldsymbol{y}_i$) and momenta ($\boldsymbol{p}_i$) of all of the water particles in the system and on the coordinates ($\boldsymbol{Y}_j$) and momenta ($\boldsymbol{P}_j$) of all of the amphiphiles in the system. For our system, we can write the Hamiltonian

$$\mathcal{H}(\{\boldsymbol{p}_i, \boldsymbol{y}_i, \boldsymbol{P}_j, \boldsymbol{Y}_j\}) = \mathcal{H}_W(\{\boldsymbol{p}_i, \boldsymbol{y}_i\}) + \sum_{j=1}^{N_A} \frac{P_j^2}{2m_j} + U(\{\boldsymbol{y}_i, \boldsymbol{Y}_j\}), \tag{4.62}$$

where $\mathcal{H}_W(\{\boldsymbol{p}_i, \boldsymbol{y}_i\})$ is the Hamiltonian of water in the absence of solute, P_j is the magnitude of the momentum of the j^{th} amphiphile and m_j is the mass of the j^{th} amphiphile. The term $U(\{\boldsymbol{y}_i, \boldsymbol{Y}_j\})$ is the potential energy of the interactions between water and amphiphiles, and of the interactions between different amphiphiles. This term therefore depends on the positions of all of the particles in the system.

As in Section 4.1.1, we write the total partition function as a product of the partition function for pure water in the absence of surfactant and a correction due to the presence of the amphiphiles. As before, the partition function of water, Z_W is given by Equation 4.3 and we write

$$Z = Z_W Z_A, \tag{4.63}$$

where Z_A is given by (analogously to Equation 4.5)

$$Z_A = \frac{Z}{Z_W} = \frac{1}{h^{3N_A} \prod_{a=1}^{z} N_a!} \int \prod_{j=1}^{N_A} d^3P_j d^3Y_j e^{-\left\{\sum_{j=1}^{N_A} \frac{P_j^2}{2m_j}\right\}/k_BT} e^{-\bar{U}(\{\boldsymbol{Y}_j\})/k_BT}, \tag{4.64}$$

and $\bar{U}$ is, as before, is the interaction potential between water and amphiphiles averaged over the different positions of the water molecules, given by Equation 4.6.

We proceed in exactly the same manner as in Section 4.1.1, modeling the interaction potential according to Equation 4.7, giving us for Z_A,

$$\begin{aligned} Z_A &= \frac{1}{h^{3N_A} \prod_{a=1}^{z} N_a!} \sum_{\text{differentgroupings}} \int \prod_{j=1}^{N_A} d^3P_j e^{-\frac{P_j^2}{2m_j k_BT}} \times \\ &\quad \times \int \prod_{k=1}^{M} \left(d^3R_k \prod_{i=1}^{n_k - 1} d^3r_{ik} \right) e^{-\{\sum_{k=1}^{M} U_k^{int}(\{\boldsymbol{r}_{ik}\}') + U^{ext}(\{\boldsymbol{R}_k\})\}/k_BT}, \end{aligned} \tag{4.65}$$

where, as before, the sum is over the different possible groupings of the amphiphiles into micelles and the position variables $\{\boldsymbol{Y}_j\}$ for the positions of the N_A amphiphiles have been exchanged in favor of the coordinates $\{\boldsymbol{R}_k\}$ (where $\boldsymbol{R}_k$ is the center of mass of the k^{th} micelle) and $\{\boldsymbol{r}_{ik}\}$ (where $\boldsymbol{r}_{ik}$ is the position of the i^{th} independent amphiphile contained in the k^{th} micelle relative to the center of mass). Recall that

the prime in $U_k^{int}(\{\boldsymbol{r}_{ik}\}', \boldsymbol{R}_k)$ indicates that the set of $\boldsymbol{r}_{ik}$ should include only the $\boldsymbol{r}_{ik}$ for the k^{th} micelle.

In the case when our solution of micelles is dilute, we can neglect the interactions between micelles, that is, we neglect the effects of $U^{ext}(\{\boldsymbol{R}_k\})$. Therefore, in the dilute limit, we can write Z

$$Z = Z_W \frac{1}{\prod_{a=1}^{z} {V_{Fa}}^{N_a} N_a!} \sum_{\text{differentgroupings}} \int \prod_{k=1}^{M} \left(d^3 R_k \prod_{i=1}^{n_k - 1} d^3 r_{ik} e^{U_k^{int}(\{\boldsymbol{r}_{ik}\}')/k_B T} \right), \tag{4.66}$$

where we have additionally carried out the integrations over the momentum variables, resulting in the term $\prod_{a=1}^{z} {V_{Fa}}^{N_a}$. Each factor of V_{Fa} comes from the integration over the momentum of a single amphiphile of species a:

$$\frac{1}{V_{Fa}} = \frac{1}{h^3} \int d^3 P_j e^{{P_j}^2/2m_a k_B T} = \left(\frac{2\pi m_a k_B T}{h^2} \right)^{3/2}. \tag{4.67}$$

The quantity V_{Fa} is the Fermi volume for a monomer of species a.

As in the single-component case, we must now make clear the meaning of the summation over the different possible groupings of the amphiphiles into micelles. We note that the indistinguishibility of the amphiphiles of a given species is already taken care of in Equation 4.66 by the factor $\prod_{a=1}^{z} N_a!$. Each term in the sum in Equation 4.66 therefore results from considering a different association of the amphiphiles into micelles, as before. We once again define the index m to run over all of the distinct kinds of micelles possible in solution. We note that now, a micelle is distinct if it differs in size, geometry, or relative composition.

Because two micelles with the same index m will have the same interaction potential, the contribution from a term in the sum over the different possible groupings in Equation 4.9 depends only on the number of micelles of each type present in that term. We define the variable N_m as the number of micelles of each distinct size, geometry and composition m, and we define n_{ma} as the number of monomers of species a contained in a micelle of type m. Furthermore, we denote the total number of monomers in a micelle of type m, regardless of their species, as n_m. The

quantity n_m is given by

$$n_m = \sum_{a=1}^{z} n_{ma}. \tag{4.68}$$

The set of numbers $\{N_m\}$ then indicates the number of micelles of each distinct size, geometry and composition present in a term in the sum in Equation 4.66. Each such term with the same set $\{N_m\}$ will make the same contribution to the total partition function. The number of such terms is equal to the number of ways that all of the amphiphiles can be distributed amongst the distribution of micelles $\{N_m\}$. Since n_{ma} is the number of amphiphiles of species a contained in a micelle of type m, the number of ways that the amphiphiles can be distributed amongst a given distribution of micellar sizes and geometries $\{N_m\}$ is

$$\frac{\prod_{a=1}^{z} N_a!}{\prod_m \left(N_m! \left(\prod_{a=1}^{z} n_{ma}!\right)^{N_m}\right)}. \tag{4.69}$$

This equation is understood as follows. In the numerator, we note that there are $N_a!$ ways to arrange the N_a amphiphiles of each species a. Of these possible arrangements, we must divide out the possible rearrangements of indistinguishable micelles ($\prod_m N_m!$) and the possible rearrangements the indistinguishable amphiphiles within each micelle ($\prod_m \prod_{a=1}^{z} (n_{ma}!)^{N_m}$)

As a result of the above considerations, we may rewrite Z as the sum over all different possible micellar size, geometry and composition distributions $\{N_m\}$ with the constraints that the total number of amphiphiles of each kind is N_a:

$$\begin{aligned} Z \;=\; & Z_W \sum_{\text{all } \{N_m\}}{}' \prod_m \frac{1}{{V_F}^{N_m} N_m!} \left(\int d^3 R_m \frac{1}{\prod_{a=1}^{z} {V_F}^{n_{ma}-1} n_{ma}!} \times \right. \\ & \left. \times \int \prod_{i=1}^{n_m - 1} d^3 r_{im} e^{-U_m^{int}(\{\boldsymbol{r}_{im}\})/k_B T} \right)^{N_m}, \end{aligned} \tag{4.70}$$

where we have defined an average Fermi volume, V_F, such that

$${V_F}^{N_A} = \prod_{a=1}^{z} {V_{Fa}}^{N_a}. \tag{4.71}$$

The prime in Equation 4.70 indicates the presence of the constraints that for each allowed set of $\{N_m\}$, the total number of amphiphiles of each species a must be N_a. Since the interaction potential is identical for all of the micelles with a given index m, we have collected together the contributions from each of the N_m micelles of type m into a single term as we did in the single component case. In this sense, the interaction potential $U_m^{int}(\{\boldsymbol{r}_{im}\})$o considers the interactions between a single micelle of size, geometry and composition indicated by m and the surrounding solvent and the interactions between the amphiphiles within that micelle. The constraints that the total number of amphiphiles of each species a present in the solution is N_a may be written

$$N_a = \sum_m n_{ma} N_m \tag{4.72}$$

for each species a, running from species 1 to species z.

Equation 4.70, can be written in the much more compact form

$$Z = Z_W \sum_{\text{all}\{N_m\}}{}' \prod_m \frac{1}{{V_F}^{N_m} N_m!} \left(\int d^3 R_m Z_m \right)^{N_m}. \tag{4.73}$$

where the quantity Z_m collects together all of the factors internal to a single micelle of type m. Z_m is given by the expression

$$Z_m = \frac{1}{\prod_{a=1}^{z} {V_f}^{n_{ma}-1} n_{ma}!} \int \prod_{i=1}^{n_m - 1} d^3 r_{im} e^{U_m^{int}(\{\boldsymbol{r}_{im}\})/k_B T}, \tag{4.74}$$

and represents the internal partition function for a single micelle of size, geometry and composition m. We note specifically that with this choice of Z_m, Equation 4.73 has exactly the same form as Equation 4.14 for the single component case.

In the dilute limit, since the interaction energy between a single micelle of type m and the surrounding water, $U_m^{int}(\{\boldsymbol{r}_{im}\})$, does not depend on the position, $\boldsymbol{R}_m$, of the micelle, each explicit integration in Equation 4.73 yields a single factor of V, the total volume of the system. Therefore,

$$Z = Z_W \sum_{\text{all}\{N_m\}}{}' \prod_m \frac{1}{N_m!} \left(\frac{V Z_m}{V_F} \right)^{N_m}. \tag{4.75}$$

4.2.2 The Free Energy and the Mixed Micellar Distribution in the Dilute Limit

The free energy of our mixed system has the same form as in Section 4.1.2:

$$F = -k_B T \ln Z = F_0 - k_B T \ln Z_A \tag{4.76}$$

where $F_0 = -k_B T \ln Z_W$ is the free energy of water in the absence of amphiphiles. We recall that from Equation 4.75, $Z_A = Z/Z_W$ is a sum over all of the possible micellar size, geometry and composition distributions (that is the sum over all possible sets $\{N_m\}$) subject to the condition that the total number of amphiphiles of each species is fixed. When the system is very large (the total number of amphiphiles tends to infinity) the log of Z_A can be well approximated by the log of the maximum term in the sum over the different distributions of micellar sizes, geometries and compositions (that is, the term in which the particular set of micellar sizes and geometries $\{N_m\}$ gives the maximal contribution to Z). Therefore, the total free energy is approximately

$$F = F_0 - k_B T \sum_m N_m \ln \frac{V Z_m e}{V_F N_m}, \tag{4.77}$$

which is of course the same form as we had in the single component case. We note that in Equation 4.77, $\{N_m\}$ is now the single micellar shape, size and composition distribution that gives a maximal contribution to Z.

Here, our treatment begins to differ slightly from the single component case. We must now find, as before, the form of the set of $\{N_m\}$ that gives maximal contribution to Z, but we now have z constraints to fulfill, namely that the total number of amphiphiles of each species is fixed. Solving this problem is equivalent to finding the form of the set of micellar sizes, geometries and compositions $\{N_m\}$ that minimizes the total free energy of the system subject to the z constraints that the total number of amphiphiles of each species is fixed. To find the form of $\{N_m\}$, we will again use the method of Lagrange multipliers. We recall that the z constraints

fixing the total number of monomers of each species may be written

$$N_a = \sum_m n_{ma} N_m = \text{const} \tag{4.78}$$

for each species a. Minimizing $F(\{N_m\})$ subject to the z constraints that each N_a is fixed is equivalent to minimizing the new function

$$\Omega = F(\{N_m\}) - \sum_{a=1}^{z} \mu_a \sum_m n_{ma} N_m. \tag{4.79}$$

without constraint, where F is the free energy. Here, there are z different Lagrange multipliers $\{\mu_a\}$, that enforce the z constraints mentioned above. Performing a variation with respect to N_m and setting $\delta\Omega = 0$, we have

$$-k_B T \ln \frac{V Z_m}{V_F N_m} - \sum_{a=1}^{z} n_{ma} \mu_a = 0 \tag{4.80}$$

for each distinct micellar size, geometry and composition m. As before, we could proceed in a purely mathematical way, expressing each N_m as a function of the z different μ_a and then determine the values of the $\{\mu_a\}$ such that $\sum_m n_{ma} N_m(\{\mu_a\})$ is equal to the total (fixed) number of amphiphiles of species a in the system, for each a. Instead, however, we will continue as in Section 4.1.2 by examining the physical meaning of the z Lagrange factors $\{\mu_a\}$. In principle, we can use the z equations implied by Equation 4.78 to express z of the N_m (for example the free monomer concentrations for each of the z different species of amphiphile) in terms of the z quantities $\{N_a\}$ and all of the other N_m. The free energy F is therefore implicitly a function of the $\{N_a\}$. Minimizing Ω without constraint means that all of the partial derivatives of Ω should vanish. In particular, we must have that

$$\frac{\partial \Omega}{\partial N_a} = \frac{\partial F}{\partial N_a} - \mu_a = 0 \tag{4.81}$$

for each of the z values of a. This implies that

$$\mu_a = \frac{\partial F}{\partial N_a}. \tag{4.82}$$

The chemical potential of a micelle of type m in solution is defined

$$\mu_m = \frac{\partial F}{\partial N_m}. \tag{4.83}$$

We note that

$$dF = \sum_{a=1}^{z} \frac{\partial F}{\partial N_a} dN_a, \tag{4.84}$$

and so

$$\mu_m = \frac{\partial F}{\partial N_m} = \sum_{a=1}^{z} \frac{\partial F}{\partial N_a} \frac{\partial N_a}{\partial N_m}. \tag{4.85}$$

Using the definition of the chemical potentials $\{\mu_a\}$ (Equation 4.82) and our expression for the total number of amphiphiles of species a in the system (Equation 4.78), we get

$$\mu_m = \sum_{a=1}^{z} \mu_a n_{ma}. \tag{4.86}$$

This equation holds for all of the different possible sizes, geometries and relative compositions, including the free monomers of each species. Denoting the chemical potential of a free monomer of type a in solution as μ_{1a}, Equation 4.86 tells us that

$$\mu_{1a} = \mu_a \tag{4.87}$$

and we see that the z Lagrange multipliers, $\{\mu_a\}$, are the chemical potentials of the different species of free monomers. Equation 4.86 therefore tells us that the chemical potential of a micelle of type m is simply related to the z chemical potentials of the different species of free monomers. Since Equation 4.86 is true for all m, the chemical potentials of all of the different micellar species are related to one another at equilibrium. By substituting Equation 4.86 into Equation 4.80, we see that the variation of Ω with respect to N_m gives us an expression for the chemical potential of a micelle of size and geometry m in terms of the concentration of micelles of type

m in the solution:

$$\mu_m = k_B T \ln N_m - k_B T \frac{V Z_m}{V_F}. \tag{4.88}$$

Denoting the mole fraction of micelles of type m

$$X_m = \frac{N_m}{N_W + N_A} = \frac{N_m}{N}, \tag{4.89}$$

where N is the total number of water molecules and amphiphiles in the system, we obtain

$$\mu_m = \mu_m^0 + k_B T \ln X_m \tag{4.90}$$

where the standard part of the chemical potential μ_m^0 is

$$\mu_m^0 = -k_B T \ln \frac{V Z_m}{V_F N}. \tag{4.91}$$

We are now in a position to obtain an expression for the equilibrium mole fraction of micelles of type m in solution in terms of the mole fraction of free monomers in solution at equilibrium. The chemical potential of a micelle of size and geometry m is given by Equation 4.90. Since Equation 4.90 is also true for the free monomers of each species, we also have

$$\mu_a = \mu_{1a}^0 + k_B T \ln X_{1a}, \tag{4.92}$$

where we have denoted the mole fraction of free monomers of species a as X_{1a}, and the standard part of the chemical potential a free monomer of species a as μ_{1a}^0. Substituting Equations 4.32 and 4.29 into the equilibrium condition (Equation 4.86), we obtain the desired result

$$X_m = \left(\prod_{a=1}^{z} {X_{1a}}^{n_{ma}} \right) e^{-(\mu_m^0 - \sum_{a=1}^{z} n_{ma} \mu_{1a}^0)/k_B T}. \tag{4.93}$$

The mole fraction of micelles of type m in solution at equilibrium is determined by two physically significant factors. The first factor, $(\prod_{a=1}^{z} {X_{1a}}^{n_{ma}})$ represents the

likelihood that the n_{ma} monomers of each species a that make up the micelle of type m will be localized in the same region of space. The second term is a Boltzmann factor that expresses the free energy advantage associated with assembling a micelle of the appropriate geometry for a micelle of type m from the localized monomers. The micellar distribution can be found in terms of the total mole fraction of each surfactant, X_a, by determining the $\{X_{1a}\}$ in terms of the X_a by enforcing the conservation of the total number of amphiphiles of each kind in the solution. Performing this step requires that we first know the standard chemical potential differences $\mu_m^0 - \sum_{a=1}^{z} n_{ma}\mu_{1a}^0$ for the entire distribution.

4.2.3 The Extended Ladder Model for a Two-Component System

For the purposes of what follows, we shall restrict ourselves to the consideration of two surfactant species and water to keep the expressions simpler. In this case, the form of the mixed micellar distribution is

$$X_m = (X_{1A}^{n_{mA}} X_{1B}^{n_{mB}})\, e^{-(\mu_m^0 - n_{mA}\mu_{1A}^0 - n_{mB}\mu_{1B}^0)/k_B T} \tag{4.94}$$

where we have replaced the index a in Equation 4.93 with either A or B corresponding to surfactant species 1 or 2.

As in Section 4.1.3, we proceed by introducing a physically reasonable model for the sequence of levels $\mu_m^0 - n_{mA}\mu_{1A}^0 - n_{mB}\mu_{1B}^0$. With two kinds of surfactant molecules and water present in the system, distinguishable micelles can, in principle, differ in total aggregation number, geometry, and relative composition. As in Section 4.1.3, we should consider all possible different geometries and compositions and calculate Z_m for each geometry, composition and total aggregation number, thus determining μ_m^0 for all m (including μ_{1A} and μ_{1B}). We cannot do this in practice, however, since it is impossible to consider all possible geometries, as was mentioned in the single-component case. We shall proceed as we did in Section 4.1.3, by assuming that our system exists at equilibrium in a well defined set of geometries.

We shall use the same geometrical model as was used for the single-component ladder model. That is, we shall consider micelles that exhibit one-dimensional growth, and model the long, rodlike micelles as prolate spherocylinders. Consider a micelle containing i monomers of type A and j monomers of type B. The total aggregation number is $n = i + j$. The hemispherical end caps will each contain $i_0/2$ monomers of type A and $j_0/2$ monomers of type B. As in the single-component ladder model, we will assume that the total number of monomers in the end caps, $n_0 = i_0 + j_0$, is the size of a "minimum micelle" which may depend on the relative composition of the micelle, but is independent of n.

If the two different kinds of amphiphiles have sufficiently different interactions with each other and with the water, then each arrangement of amphiphiles in a micelle with a given number of amphiphiles of each kind could have a different "micellization free energy" $\mu^0_m - n_{mA}\mu^0_{1A} - n_{mB}\mu^0_{1B}$. In this case, each arrangement of the monomers in the micelle would have to be counted as a different micelle. We wish to focus our attention on the case where the different amphiphiles are similar to each other. In this case, we can assume that for a region of a given geometry, the effective micellization free energy contributed from that region is mainly determined from the number and type of amphiphiles present there, but not on their specific arrangement. When we make this random mixing approximation, we are counting as different species of micelle, only those micelles which differ in any of the quantities i, j, i_0, or j_0. We define $X_{iji_0j_0}$ as the total mole fraction of micelles containing i monomers of type A and j monomers of type B, with the end caps containing a total of i_0 monomers of type A, and j_0 monomers of type B. $X_{iji_0j_0}$ is then given as the sum of the X_m over all of the m with the same i, j, i_0 and j_0 (differing in the distinguishable arrangement of the amphiphiles) within the micelle)

$$X_{iji_0j_0} = \sum_m{}' X_m = C(i,j,i_0,j_0)\left({X_{1A}}^i {X_{1B}}^j\right) e^{-(\mu^0_{iji_0j_0} - i\mu^0_{1A} - j\mu^0_{1B})/k_BT}. \qquad (4.95)$$

The prime indicates that the sum over m is to be carried out only over the micelles with the same i, j, i_0, and j_0 as described above. We assume, as we mentioned

above, that for similar surfactants, μ_m^0 depends only weakly on the arrangement of the amphiphiles in each region of the micelle. We have denoted the standard part of the chemical potential of any one micelle with the same i, j, i_0 and j_0 as $\mu_{ijij_0j_0}^0$. We have also made the substitutions $n_{mA} = i$, and $n_{mB} = j$. Therefore, C counts the number of ways to distinguishably arrange the monomers within a micelle. We have

$$C(i,j,i_0,j_0) = \frac{n_0!}{i_0!j_0!}\frac{(n-n_0)!}{(i-i_0)!(j-j_0)!}. \tag{4.96}$$

The first factorial term counts the number of ways to arrange the i_0 monomers of type A and the j_0 monomers of type B in the ends of the micelle. The second factorial term counts the number of ways to arrange the remaining $i - i_0$ monomers of type A and $j - j_0$ monomers of type B in the cylindrical region of the micelle. We will see later that these factorial terms can be absorbed into the standard part of the chemical potential for this species of micelle as a "mixing entropy" contribution to the "free energy of micellization".

From considerations similar to those made in Section 4.1.3 we will consider the standard part of the chemical potential per monomer in a region of a micelle to be simply a function of the cross-sectional area of the surfactant molecule presented at the surface of the micelle. As before, we have two regions of distinct geometry. In addition, however, we also have two different surfactant species in each region. We generalize Equation 4.35 by associating a standard part chemical potential per monomer $\mu_{sA}^0(i_0,j_0)$ to each monomer of type A in the ends of the micelle and a standard part chemical potential per monomer $\mu_{sB}^0(i_0,j_0)$ to each monomer of type B in the ends of the micelle. If the two surfactant species interact with each other, then μ_{sA}^0 and μ_{sB}^0 will depend on the relative composition in the ends of the micelle. Furthermore, we associate a standard part chemical potential per monomer $\mu_{cA}^0(i,j)$ to each monomer of type A in the cylindrical region of the micelle and a standard part chemical potential per monomer $\mu_{cB}^0(i,j)$ to each monomer of type B in the cylindrical region of the micelle. Again, if the two surfactant species interact with each other, μ_{cA}^0 and μ_{cB}^0 will be functions of the relative composition in the

cylindrical region of the micelle. Thus, we write

$$\mu^0_{ijio\,jo} = i_0\mu^0_{sA}(i_0,j_0) + (i-i_0)\mu^0_{cA}(i,j) + j_0\mu^0_{sB}(i_0,j_0) + (j-j_0)\mu^0_{cB}(i,j), \quad (4.97)$$

and the micellization free energy (without the mixing terms from C) becomes

$$\begin{aligned}\mu_{ijio\,jo} - i\mu^0_{1A} - j\mu^0_{1B} = i_0\Delta\mu^0_{sA}(i_0,j_0) + (i-i_0)\Delta\mu^0_{cA}(i,j) + \\ j_0\Delta\mu^0_{sB}(i_0,j_0) + (j-j_0)\Delta\mu^0_{cB}(i,j) \quad (4.98)\end{aligned}$$

where $\Delta\mu^0_{sA}(i_0,j_0) = \mu^0_{sA}(i_0,j_0) - \mu^0_{1A}$, $\Delta\mu^0_{cA}(i,j) = \mu^0_{cA}(i,j) - \mu^0_{1A}$, $\Delta\mu^0_{sB}(i_0,j_0) = \mu^0_{sB}(i_0,j_0) - \mu^0_{1B}$, and $\Delta\mu^0_{cB}(i,j) = \mu^0_{cB}(i,j) - \mu^0_{1B}$.

Returning now to the idea that the two surfactants we are considering are very similar, we shall make the simplest possible extension to the ladder model possible. That is, we shall consider that $\Delta\mu^0_{sA}$, $\Delta\mu^0_{sB}$, $\Delta\mu^0_{cA}$, and $\Delta\mu^0_{cB}$ are independent of i, j, i_0, and j_0. In addition, we assume that $n_0 = i_0 + j_0$ is a constant, independent of relative composition.

4.2.4 Size and Composition

Inserting Equation 4.98 into Equation 4.95 gives the micellar distribution in terms of i_0, j_0, i, j, and the four extended ladder model parameters $\Delta\mu^0_{sA}$, $\Delta\mu^0_{sB}$, $\Delta\mu^0_{cA}$ and $\Delta\mu^0_{cB}$. It will be more convenient, however to express the micellar distribution in terms size and composition variables instead of i_0, j_0, i, and j, since in the new variables it will become clear that the distribution is narrow in the composition variables. Thus, the problem of finding the equilibrium micellar distribution for a given total solution concentration and relative composition will be greatly simplified. It will also become clear how to reduce the expressions that will be obtained back to the single-component case in the limit that the two surfactant species become identical.

The total aggregation number of a micelle and the total number of monomers in

the end caps have been previously defined. We had

$$n = i + j \tag{4.99}$$

$$n_0 = i_0 + j_0. \tag{4.100}$$

The relative composition of the micelle is defined as the ratio of the total number of monomers of type A in the micelle to the total aggregation number of the micelle

$$\alpha = \frac{i}{i+j}. \tag{4.101}$$

We also define the relative composition in the end caps as the ratio of the total number of monomers of type A in the end caps to the total number of monomers of either kind in the end caps

$$\alpha_0 = \frac{i_0}{i_0 + j_0}. \tag{4.102}$$

Making these substitutions into the micellar distribution yields

$$X_{n\alpha\alpha_0} = C(n, \alpha, n_0, \alpha_0) \left({X_{1A}}^{n\alpha} {X_{1B}}^{n(1-\alpha)} \right) e^{-(\Delta(\alpha_0)+(n-n_0)\delta(\alpha))/k_BT}, \tag{4.103}$$

where we have defined

$$\Delta(\alpha_0) = n_0 \left(\alpha_0 \Delta\mu^0_{sA} + (1-\alpha_0)\Delta\mu^0_{sB} \right) \tag{4.104}$$

and

$$\delta(\alpha) = \alpha\Delta\mu^0_{cA} + (1-\alpha)\Delta\mu^0_{cB}. \tag{4.105}$$

We have written the micellar distribution with the three indices n, α and α_0. We have dropped n_0, because we consider n_0 as a parameter of the model rather than as a variable of the distribution, as we did for the single-component case. The

transformation of C into the new variables yields the unappealing expression

$$C(n,\alpha,n_0,\alpha_0) = \frac{n_0!}{(n_0\alpha_0)!(n_0(1-\alpha_0))!}\frac{(n-n_0)!}{(n\alpha-n_0\alpha_0)!(n(1-\alpha)-n_0(1-\alpha_0))!}. \tag{4.106}$$

4.2.5 Simplified Treatment of the Two-Dimensional Ladder Model

As a special case, let us consider the limit that $(\Delta\mu^0_{sA}-\Delta\mu^0_{cA})-(\Delta\mu^0_{sB}-\Delta\mu^0_{cB}) \ll k_BT$, that is, that the difference in micellization free energy to put an amphiphile of type A in the end-cap as opposed to the cylindrical region is about the same (as compared to k_BT) as the difference in micellization free energy to put an amphiphile of type B in the end-cap as opposed to the cylindrical region. In this case, the preference for amphiphiles to exist in the cylindrical region is the same for amphiphiles of type A and for amphiphiles of type B. We expect, as a result, that for such micelles, the composition in the micellar ends should be the same as the composition in the micellar body. We prove this statement in Appendix B.

We shall proceed here in the limit that $(\Delta\mu^0_{sA}-\Delta\mu^0_{cA})-(\Delta\mu^0_{sB}-\Delta\mu^0_{cB}) \ll k_BT$ for two reasons. First, since the treatment is much simpler, it will be easier to follow the essence of the calculations. Second, it will turn out that in the system that we have studied, this approximation will hold reasonably well. The full treatment (without making this approximation) is presented in Appendix B.

In the limit that $(\Delta\mu^0_{sA}-\Delta\mu^0_{cA})-(\Delta\mu^0_{sB}-\Delta\mu^0_{cB}) \ll k_BT$, we have said that we expect the composition in the micellar ends to be the same as the composition in the micellar body. In this case, $C(i,i,i_0,j_0)$ reduces to

$$C(i,j) = \frac{(i+j)!}{i!j!}, \tag{4.107}$$

or, equivalently $C(n,\alpha,n_0,\alpha_0)$ reduces to

$$C(n,\alpha) = \frac{n!}{(n\alpha)!(n(1-\alpha))!}, \tag{4.108}$$

and the micellar distribution can be written

$$X_{n\alpha} = C(n,\alpha)\left({X_{1A}}^{n\alpha}{X_{1B}}^{n(1-\alpha)}\right)e^{-\{\Delta(\alpha)+(n-n_0)\delta(\alpha)\}/k_BT} \tag{4.109}$$

with $\Delta(\alpha)$ and $\delta(\alpha)$ defined above in Equations 4.104 and 4.105. Since α and α_0 are equal, we have written the micellar distribution with only two indices: n, the total number of amphiphiles in the micelle, and α the relative composition of the micelle. From the form of $\Delta(\alpha)$ and $\delta(\alpha)$ we can see that our simplest possible extension of the single-component ladder model for the energy advantage to form a micelle is just a linear interpolation in relative composition between the ladder and gap spacings for the two pure surfactants, as shown in Figure 4-4. We emphasize, once again, that the sequence of energy differences presented in Figure 4-4 is appropriate to the case when the amphiphiles within the micelle are similar. Clearly, as the relative composition, α, approaches 0 or 1, we must recover the ladder and gap spacings for pure surfactant B and pure surfactant A, respectively. If the interactions between amphiphiles of type A and amphiphiles of type B within the micelle are sufficiently different however, then the interpolation between $\alpha = 0$ and $\alpha = 1$ need not be linear.

We return now to Equation 4.109 for the micellar distribution. This equation can be greatly simplified if we express everything in terms of size and composition variables and move the combinatorial terms to the exponent. We begin by dealing with the combinatorial terms. Applying Stirling's formula to $C(n,\alpha)$ (given by Equation 4.108), the micellar distribution becomes

$$\frac{{X_{1A}}^{n\alpha}{X_{1B}}^{n(1-\alpha)}}{\sqrt{2\pi\alpha(1-\alpha)}}e^{-\{\Delta(\alpha)+(n-n_0)\delta(\alpha)+nk_BT(\alpha\ln\alpha+(1-\alpha)\ln(1-\alpha))\}/k_BT}. \tag{4.110}$$

This equation consists of three important factors. In analogy with the single-component problem, the first factor, ${X_{1A}}^{n\alpha}{X_{1B}}^{n(1-\alpha)}$ represents the likelihood to find $n\alpha$ amphiphiles of type A and $n(1-\alpha)$ amphiphiles of type B localized in a region of space. The second factor is a Boltzmann factor that expresses the free

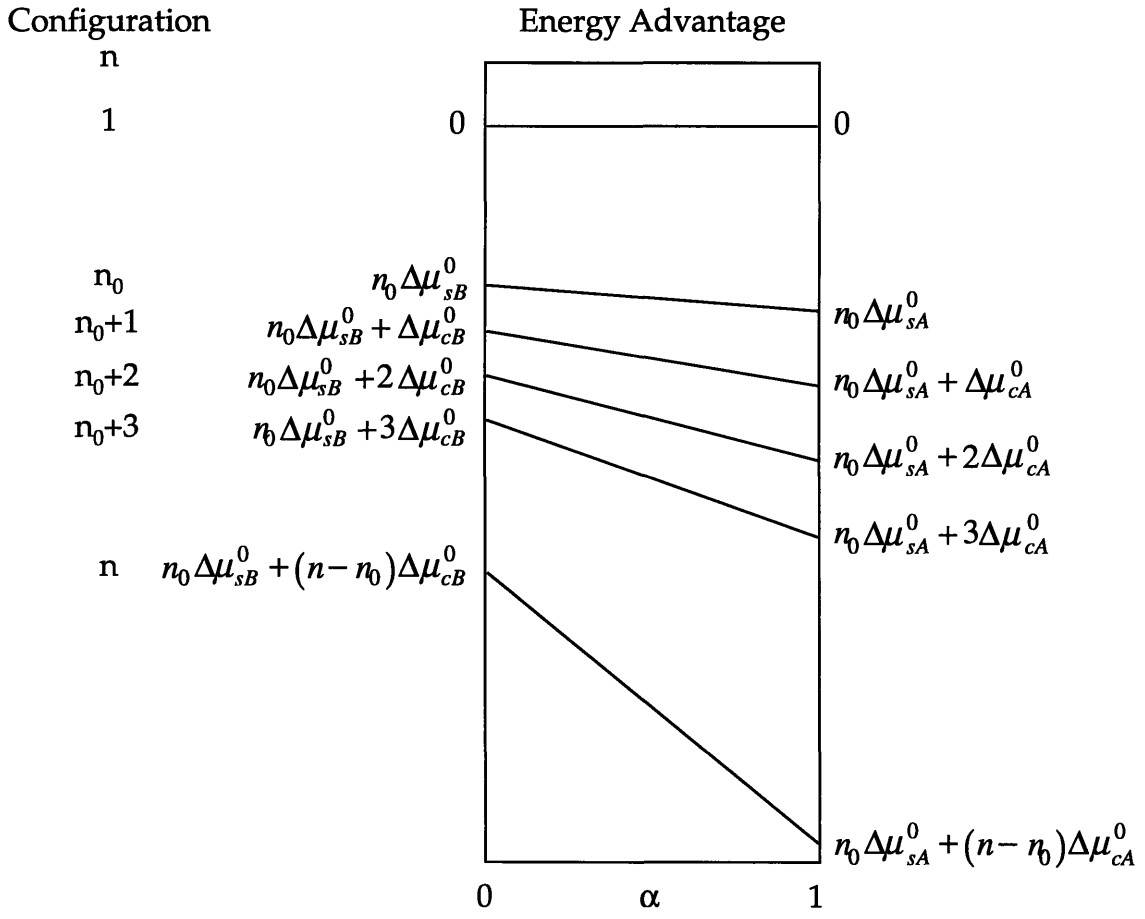

Figure 4-4: The sequence of free energy differences $\Delta(\alpha)+(n-n_0)\delta(\alpha)$ of the two-dimensional ladder model. The α dependence of the free energy advantage to form a micelle is a linear interpolation between the ladder and gap spacings for the two pure surfactants.

energy advantage to form a micelle of size n and total composition α from the localized monomers. As such, we can define the quantity in the exponent in Equation 4.110 as the "free energy of micellization". Denoting the free energy of micellization ΔG_{mic}, a notation we will use in Chapter 5, we have

$$\Delta G_{mic} = \Delta(\alpha) + (n - n_0)\delta(\alpha) + n\left(\alpha \ln \alpha + (1-\alpha)\ln(1-\alpha)\right). \tag{4.111}$$

We note that the term $\alpha \ln \alpha + (1-\alpha)\ln(1-\alpha)$, arising from the combinatorial term $C(n,\alpha)$, is just the ideal mixing entropy for a binary mixture, as we might have anticipated. Finally, returning to Equation 4.110, the third factor of interest, the terms under the square root, give the proper normalization of the distribution.

To continue towards the eventual simplification of Equation 4.109, we now wish to express everything in Equation 4.110 in terms of size and composition variables. Thus we define the total mole fraction of free monomers in solution at equilibrium

$$X_1 = X_{1A} + X_{1B}. \tag{4.112}$$

We also define the relative composition of free monomers in solution at equilibrium as the ratio of the number of free monomers of type A in solution at equilibrium to the total number of free monomers in solution at equilibrium

$$\alpha_1 = \frac{X_{1A}}{X_{1A} + X_{1B}}. \tag{4.113}$$

We may now eliminate X_{1A} and X_{1B} in terms of X_1 and α_1 in Equation 4.110. Substituting Equations 4.112 and 4.113 into Equation 4.110, we obtain

$$X_{n\alpha} = \frac{{X_1}^n}{\sqrt{2\pi n\alpha(1-\alpha)}} e^{-\left\{\Delta(\alpha)+(n-n_0)\delta(\alpha)+nk_BT\left(\alpha \ln \frac{\alpha}{\alpha_1}+(1-\alpha)\ln\frac{1-\alpha}{1-\alpha_1}\right)\right\}/k_BT}. \tag{4.114}$$

If we had been interested only in the free energy of the system, then when we used Stirling's approximation for the combinatorial term $C(n,\alpha)$, we could have dropped the terms that give the square root prefactor to the exponent in Equation 4.114. We

are, however, interested in the micellar distribution function. These terms must be therefore kept, since they will provide the proper normalization of the distribution.

Following the analysis of the ladder model for single-component systems presented in Section 4.1.3, it is useful to define the parameter K for the mixed system as follows

$$K(\alpha) = e^{\{\Delta(\alpha) - n_0\delta(\alpha)\}/k_BT} = e^{\Delta\mu(\alpha)/k_BT} \tag{4.115}$$

because, analogously to the definition for the single-component case, $\Delta\mu(\alpha)/k_BT$ measures the difference in energies to put n_0 monomers into the cylindrical part of an existing micelle or to create a new minimum micelle of size n_0. If $K > 1$ then it is energetically favorable upon increasing concentration to elongate existing micelles.

We also collect together the remaining terms in the exponent of the micellar distribution, those which are proportional to n. We define

$$B(\alpha) = \frac{\delta(\alpha)}{k_BT} + \alpha \ln \frac{\alpha}{\alpha_1} + (1-\alpha) \ln \frac{1-\alpha}{1-\alpha_1} \tag{4.116}$$

which is the free energy per monomer in an infinitely long cylindrical mixed micelle. In fact, the definition of B includes not just the mixing entropy of the n monomers in the micelle, but rather the difference between the mixing entropy for the n monomers in the micelle and the mixing entropy of the n monomers as free monomers in solution. With these definitions, the micellar distribution can we written in the much simplified form

$$X_{n\alpha} = \frac{{X_1}^n}{\sqrt{2\pi\alpha(1-\alpha)}} \frac{1}{K(\alpha)} e^{-nB(\alpha)} \tag{4.117}$$

Clearly if $B(\alpha)$ has a minimum between $0 \leq \alpha \leq 1$, then Equation 4.117 will be sharply peaked in α when $n \gg 1$. Let us examine whether or not $B(\alpha)$ has a minimum. As a specific example, Figure 4-5 shows the value of $B(\alpha)$ as a function of α for the case when $\alpha_1 = 0.399$ and $X_1 = 1.96 \times 10^{-6}$, using $\delta(\alpha)/k_BT = -12.94 - 0.42\alpha$. This particular form for $\delta(\alpha)$ is appropriate to the $C_{12}E_6$, $C_{12}E_8$ and water system at $T = 40°C$. The particular values will be extracted from our

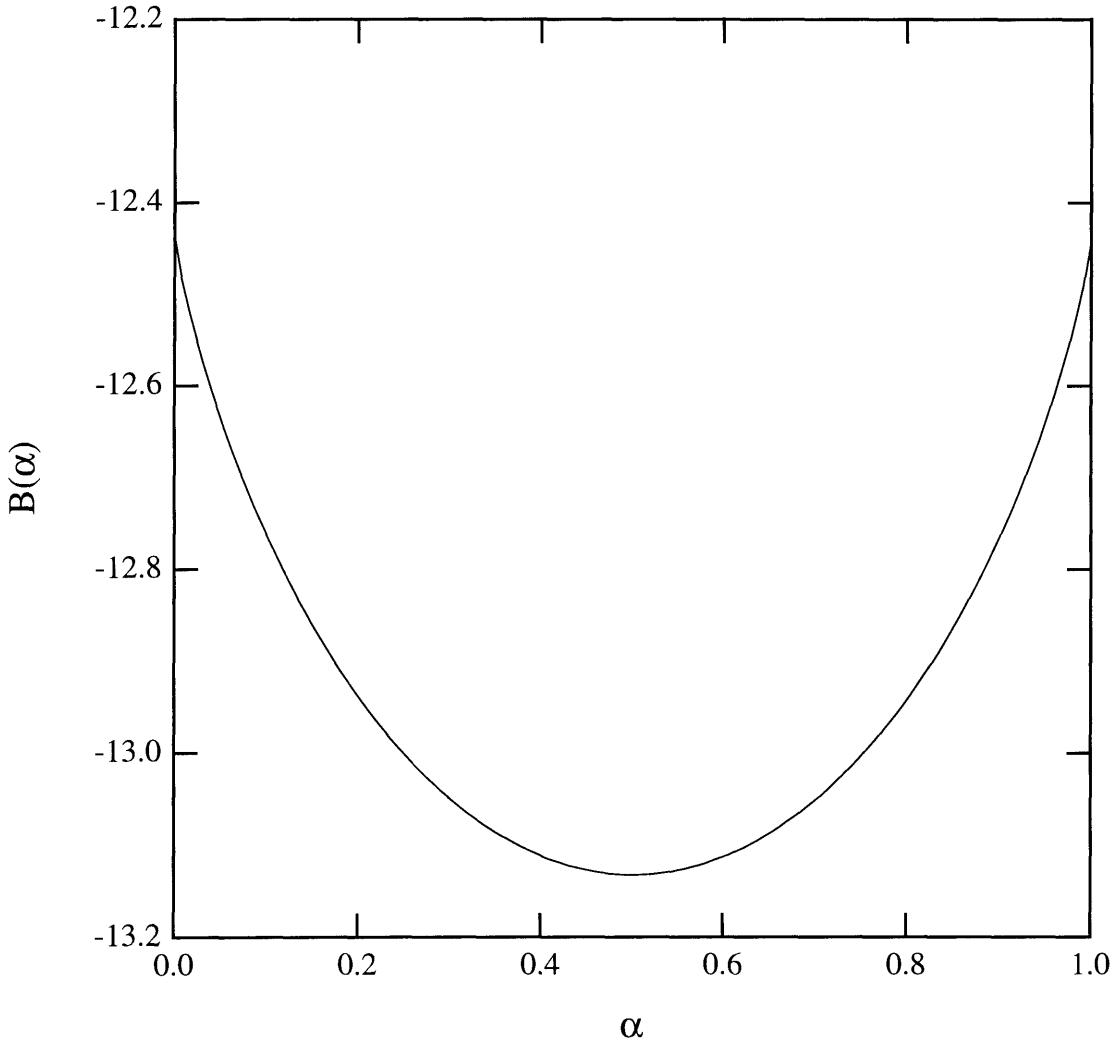

Figure 4-5: The α dependence of the quantity $B(\alpha)$ for the mixed $C_{12}E_6$, $C_{12}E_8$ and water system with $\alpha_1 = 0.399$ and $X_1 = 1.96 \times 10^{-6}$, using $\delta(\alpha)/k_BT = -12.94 - 0.42\alpha$ for $T = 40°C$ (extracted in Chapter 6 for the $C_{12}E_6$, $C_{12}E_8$ and water system).

experimental data in Chapter 6. In any case, it is obvious from the figure that for this particular choice of X_1, α_1 and $\delta(\alpha)$, $B(\alpha)$ has a well defined minimum near $\alpha = 0.5$. Since $n \geq n_0 \gg 1$, the micellar distribution will be narrow in α. Figure 4-6 shows the shape of the micellar distribution under the same conditions as Figure 4-5. The form of $\Delta\mu(\alpha)$ corresponding to the $\delta(\alpha)$ given above (extracted form our experimental data in Chapter 6) is $\Delta\mu(\alpha)/k_BT = 13.29 + 8.49\alpha$. As is indicated by Equation 4.117 we see that for a constant value of α the micellar distribution in n is a decaying exponential. Also, as we expected, since $B(\alpha)$ has a minimum near $\alpha = 0.5$ for our particular choice of α_1 and X_1, the micellar distribution is peaked in α about $\alpha = 0.5$. The width of the distribution in α is relatively narrow.

To find the location of the peak of the micellar distribution in composition, let us examine the first derivative of B,

$$B'(\alpha) = \frac{\delta'(\alpha)}{k_BT} + \ln\frac{\alpha}{1-\alpha} - \ln\frac{\alpha_1}{1-\alpha_1}. \tag{4.118}$$

Because $\delta'(\alpha)$ is a smoothly varying function over the range $0 \leq \alpha \leq 1$ that is finite at both of its endpoints, the behavior of $B'(\alpha)$ as α approaches either zero or one is controlled entirely by the logarithmic terms. When α approaches zero, $B'(\alpha)$ tends toward $-\infty$, while as α approaches one, $B'(\alpha)$ tends toward $+\infty$. Note, however, that at both endpoints, the value of $B(\alpha)$ is both finite, and well defined. Since its slope starts out at $\alpha = 0$ infinitely negative, and ends up at $\alpha = 1$ infinitely positive, B must have a minimum. This minimum naturally occurs at some optimal composition α^*, such that $B'(\alpha^*) = 0$. Setting $B'(\alpha^*) = 0$ in Equation 4.118, we obtain

$$\ln\frac{\alpha_1}{1-\alpha_1} - \ln\frac{\alpha^*}{1-\alpha^*} = \frac{1}{k_BT}\frac{\partial}{\partial\alpha}\delta(\alpha)\bigg|_{\alpha=\alpha^*} \tag{4.119}$$

Using the definition of $\delta(\alpha)$ (Equation 4.105), we obtain

$$\alpha^* = \frac{\alpha_1}{\alpha_1 + (1-\alpha_1)e^{(\Delta\mu^0_{cA} - \Delta\mu^0_{cB})/k_BT}}. \tag{4.120}$$

Note that when $\Delta\mu^0_{cA} - \Delta\mu^0_{cB}$ tends to zero, the denominator in Equation 4.120

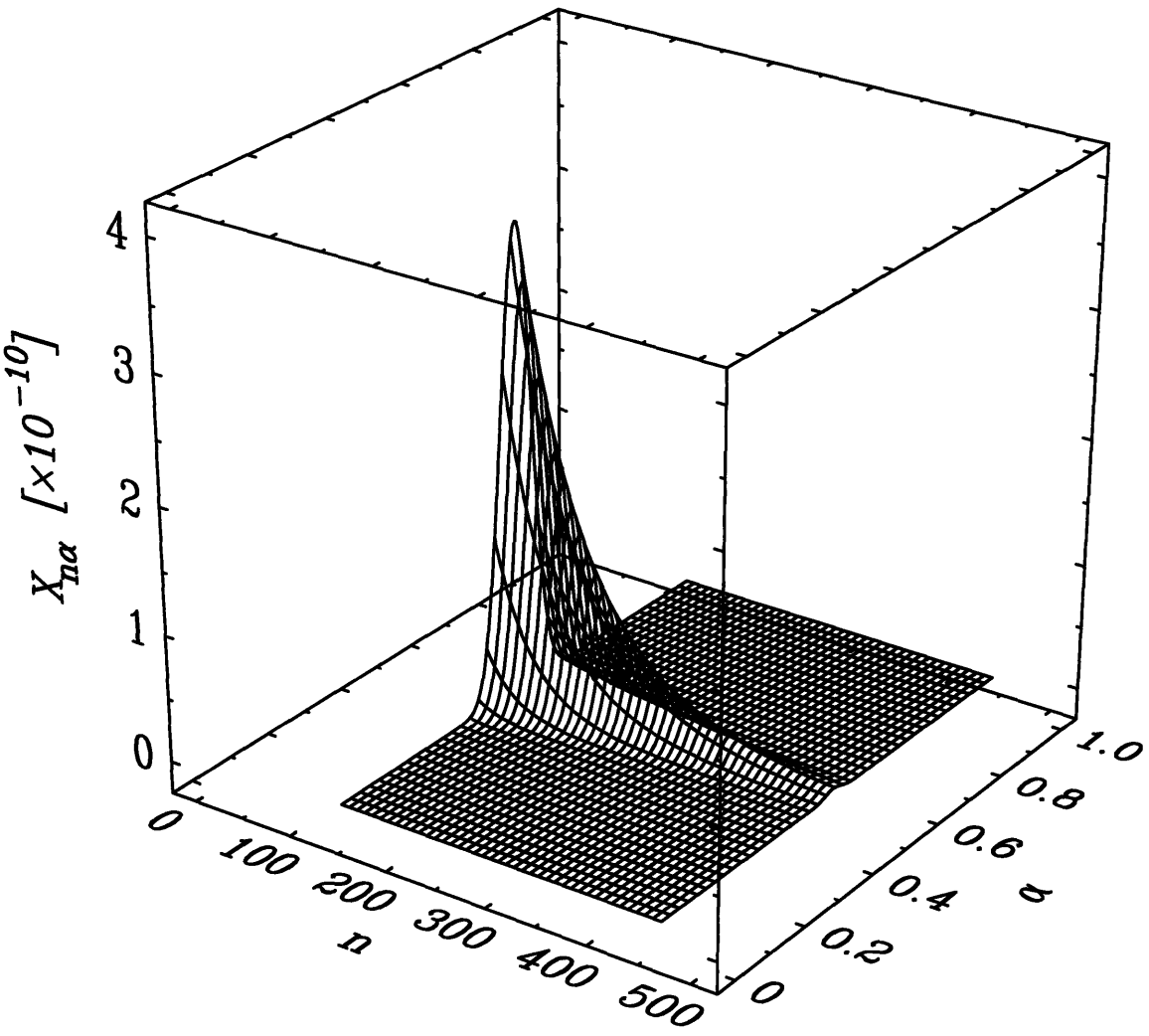

Figure 4-6: The micellar size and composition distribution for the mixed $C_{12}E_6$, $C_{12}E_8$ and water system with $\alpha_1 = 0.399$, and $X_1 = 1.96 \times 10^{-6}$ using $\delta(\alpha)/k_BT = -12.94 - 0.42\alpha$ and $\Delta\mu(\alpha)/k_BT = 13.29 + 8.49\alpha$ for $T = 40°C$ (extracted in Chapter 6). $X_{n\alpha}$is the concentration in mole fraction units of micelles with a total of n monomers and relative composition α. The minimum micellar size is $n_0 = 135$.

tends to unity, and Equation 4.120 indicates that $\alpha^* \approx \alpha_1$. For the particular example shown in Figures 4-5 and 4-6, we had $\alpha_1 = 0.399$, $X_1 = 1.96 \times 10^{-6}$, $\Delta\mu^0_{cB} = -12.94$ and $\Delta\mu^0_{cA} = -13.36$. Putting these values into Equation 4.120, we obtain $\alpha^* = 0.503$.

At this stage, we have the micellar size and composition distribution written in terms of the total concentration of free monomers in solution at equilibrium and relative composition of free monomers in solution at equilibrium. We have also shown that the micellar distribution should be peaked in composition. As was mentioned in Section 4.2.2, to determine the micellar distribution appropriate for a given total mole fraction and relative composition of surfactant in solution, we must use the two expressions that express the conservation of the total number of monomers of each kind in the solution. These expressions will determine the equilibrium values of X_1 and α_1 in terms of the total mole fraction of surfactant of type A, X_A, and the total mole fraction of surfactant of type B, X_B. We write

$$X_A = \alpha_1 X_1 + \sum_{n=n_0}^{\infty} \sum_{\alpha=0}^{1} n\alpha X_{n\alpha} \tag{4.121}$$

$$X_B = (1-\alpha_1) X_1 + \sum_{n=n_0}^{\infty} \sum_{\alpha=0}^{1} n(1-\alpha) X_{n\alpha}, \tag{4.122}$$

where the sum over α is to be taken over all of the allowed vales of α for a given n ($\alpha = i/n$ with i an integer running from 0 to n). It will be more convenient, however, to deal with the equation expressing the conservation of the total number of monomers in place of Equation 4.122. First, however, we will define total concentration and composition variables. Let the total mole fraction of both kinds of surfactant added to the solution be denoted X, and the relative composition of surfactant in the solution be denoted α_s. In terms of X_A and X_B, we have

$$X = X_A + X_B \tag{4.123}$$

$$\alpha_s = \frac{X_A}{X_A + X_B}. \tag{4.124}$$

The expression for the conservation of the total number of monomers in solution is

just the sum of Equations 4.121 and 4.122

$$X = X_1 + \sum_{n=n_0}^{\infty} \sum_{\alpha=0}^{1} nX_{n\alpha}. \tag{4.125}$$

We also rewrite Equation 4.121 in terms of X and α_s defined above

$$X_A = \alpha_s X = \alpha_1 X_1 + \sum_{n=n_0}^{\infty} \sum_{\alpha=0}^{1} n\alpha X_{n\alpha}. \tag{4.126}$$

Since $X_{n\alpha}$ has been expressed solely as a function of X_1 and α_1, Equations 4.125 and 4.126 represent two equations in the two unknowns X_1 and α_1 that can be solved numerically. The fact that the micellar distribution is narrow in α strongly suggests that in finding X_1 and α_1, we first carry out the summations over α by expanding the distribution about the optimal composition α^* and turning the sum into an integral.

4.2.6 Expanding About the Optimal Composition

All of the experimentally observed properties of the micellar system can be expressed as weighted averages of some variable over the micellar distribution. Thus, it is useful to consider a sum over the micellar distribution of the form

$$I = \sum_{n=n_0}^{\infty} \sum_{\alpha=0}^{1} f(n,\alpha) X_{n\alpha} = \sum_{n=n_0}^{\infty} \sum_{\alpha=0}^{1} \frac{f(n,\alpha)}{\sqrt{2\pi n\alpha(1-\alpha)}} \frac{{X_1}^n}{K(\alpha)} e^{-nB(\alpha)} \tag{4.127}$$

where $f(n,\alpha)$ is a smoothly varying function of n and α. We will show in the next few pages that since the micellar distribution is narrow in α, that the summation over α can be carried out, giving

$$I = \sum_{n=n_0}^{\infty} f(n,\alpha^*)\tilde{X}_n, \tag{4.128}$$

with

$$\tilde{X}_n = \frac{{X_1}^n}{K(\alpha^*)} e^{-nB(\alpha^*)}, \tag{4.129}$$

where α^* is the optimal composition, as defined in the previous section. After showing this, we shall use these results to express the mass conservation equations (Equations 4.125 and 4.126 in forms analogous to the single mass conservation relation for the single-component case. We will, in the following sections examine the micellar distribution in the dilute regime and in the limit of strong micellar growth. In particular, we shall investigate how the optimal micellar composition, α^*, is related to the initial solution composition, α_s.

We return now to the task at hand, which is to obtain Equation 4.128 from Equation 4.127. Let us examine Equation 4.127. To fully understand the meaning of the sum over α, we recall that the total size and composition variables were defined in Section 4.2.4 in terms of i, and j, the total number of monomers of type A in the micelle and the total number of monomers of type B in the micelle. The sum over the distribution should really be written

$$\sum_{i=0}^{\infty}\sum_{j=k}^{\infty}\frac{f(n,\alpha)}{\sqrt{2\pi n\alpha(1-\alpha)}}\frac{{X_1}^n}{K(\alpha)}e^{-nB(\alpha)}. \tag{4.130}$$

with

$$k=\begin{cases} n_0-i & \text{for } i\le n_0 \\ 0 & \text{for } i>n_0 \end{cases} \tag{4.131}$$

and recalling that $n=i+j$ and $\alpha=i/(i+j)$. Because the minimum micellar size $n_0 \gg 1$, the allowed values of α and n are closely spaced. In terms of i and j, we say that one of the two will always be large, meaning that the micellar distribution can be considered reasonably smooth with respect to a unit change in either i or j. That is, it is a reasonable approximation to replace the sums over i and j by integrals

$$\int_0^{\infty} di\int_k^{\infty} dj\frac{f(n,\alpha)}{\sqrt{2\pi n\alpha(1-\alpha)}}\frac{{X_1}^n}{K(\alpha)}e^{-nB(\alpha)} \tag{4.132}$$

with k defined as above. Now we wish to change variables back to n and α. Our

expression for the sum over the distribution becomes

$$\int_{n_0}^{\infty} dn \int_0^1 d\alpha J(n,\alpha) \frac{f(n,\alpha)}{\sqrt{2\pi n\alpha(1-\alpha)}} \frac{{X_1}^n}{K(\alpha)} e^{-nB(\alpha)}, \tag{4.133}$$

where $J(n,\alpha)$ is the Jacobian of the transformation

$$J(n,\alpha) = \begin{vmatrix} \frac{\partial i}{\partial \alpha} & \frac{\partial i}{\partial n} \\ \frac{\partial j}{\partial \alpha} & \frac{\partial j}{\partial n} \end{vmatrix} = \begin{vmatrix} n & \alpha \\ -n & 1-\alpha \end{vmatrix} = n. \tag{4.134}$$

Since n is large, we can expand the exponent in Equation 4.133 about the minimum value of B, which we have previously shown to be $B(\alpha^*)$. We obtain

$$\int_{n_0}^{\infty} dnn \frac{f(n,\alpha^*)}{\sqrt{2\pi n\alpha^*(1-\alpha^*)}} \frac{{X_1}^n}{K(\alpha^*)} e^{-nB(\alpha^*)} \int_{-\infty}^{\infty} d\xi e^{-n\frac{1}{2}\xi^2 B''(\alpha^*)}, \tag{4.135}$$

where $\xi = \alpha - \alpha^*$, and, because of the prefactor n appearing in the exponent, the limits of the integration over ξ can be safely extended to infinity. This Gaussian integral is easily evaluated. giving the result

$$\int_{n_0}^{\infty} dnn \frac{f(n,\alpha^*)}{\sqrt{2\pi n\alpha^*(1-\alpha^*)}} \sqrt{\frac{2\pi}{nB''(\alpha^*)}} \frac{{X_1}^n}{K(\alpha^*)} e^{-nB(\alpha^*)}. \tag{4.136}$$

Simplifying this slightly yields

$$\int_{n_0}^{\infty} dn \frac{f(n,\alpha^*)}{\sqrt{B''(\alpha^*)\alpha^*(1-\alpha^*)}} \frac{{X_1}^n}{K(\alpha^*)} e^{-nB(\alpha^*)}, \tag{4.137}$$

which can be expressed once more as a sum over n if desired

$$\sum_{n\alpha} f(n,\alpha) X_{n\alpha} = \sum_{n=n_0}^{\infty} \frac{f(n,\alpha^*)}{\sqrt{B''(\alpha^*)\alpha^*(1-\alpha^*)}} \frac{{X_1}^n}{K(\alpha^*)} e^{-nB(\alpha^*)}. \tag{4.138}$$

Using Equation 4.116 for B, it is easy to show that

$$B''(\alpha^*) = \frac{\delta''(\alpha^*)}{k_B T} + \frac{1}{\alpha^*(1-\alpha^*)}. \tag{4.139}$$

Equation 4.105 for $\delta(\alpha)$ implies that for our simple two-dimensional ladder model that $\delta''(\alpha^*) = 0$. Thus, our integration over α yields the extremely simple result that

$$\sum_{n\alpha} f(n,\alpha) X_{n\alpha} = \sum_{n_0=0}^{\infty} f(n,\alpha^*) \frac{{X_1}^n}{K(\alpha^*)} e^{-nB(\alpha^*)} = \sum_{n=n_0}^{\infty} f(n,\alpha^*) \tilde{X}_n \tag{4.140}$$

with

$$\tilde{X}_n = \frac{{X_1}^n}{K(\alpha^*)} e^{-nB(\alpha^*)}. \tag{4.141}$$

By performing the sum over α, we have obtained a renormalized micellar size distribution $\tilde{X}_n$ that depends only on the optimal micellar composition. If we compare the form of $\tilde{X}_n$ to the single-component micellar size distribution (Equation 4.42), we find that the two are identical. The single-component parameter δ is replaced in the renormalized mixed distribution by $B(\alpha^*)$, which is the generalized parameter $\delta(\alpha^*)$ corrected by accounting for the ideal mixing entropy of the two-component system. By this procedure, we have reduced the two-component problem to an equivalent single-component problem.

Returning now to the problem of solving for the concentration and composition of free monomers in solution at equilibrium, it is clear how to proceed. Performing the summations over α in Equations 4.125 and 4.126 gives us

$$X = X_1 + \sum_{n=n_0}^{\infty} n\tilde{X}_n \tag{4.142}$$

and

$$\alpha_s X = \alpha_1 X_1 + \alpha^* \sum_{n=n_0}^{\infty} n\tilde{X}_n \tag{4.143}$$

with

$$\tilde{X}_n = \frac{1}{K(\alpha^*)} \Lambda^n, \tag{4.144}$$

where we have defined Λ similarly to the definition for single- component systems in Section 4.1.3:

$$\Lambda = X_1 e^{-B(\alpha^*)}. \tag{4.145}$$

Now we see that the sums over n that we are left to calculate are exactly the same as in Section 4.1.3. Performing them gives

$$X = X_1 + \frac{1}{K(\alpha^*)}\Lambda^{n_0}\left\{\frac{n_0}{(1-\Lambda)} + \frac{\Lambda}{(1-\Lambda)^2}\right\} \tag{4.146}$$

and

$$\alpha_s X = \alpha_1 X_1 + \alpha^* \frac{1}{K(\alpha^*)}\Lambda^{n_0}\left\{\frac{n_0}{(1-\Lambda)} + \frac{\Lambda}{(1-\Lambda)^2}\right\}. \tag{4.147}$$

Equation 4.146 is identical with Equation 4.44 for the single- component case. This is the reason we chose Equation 4.125 for the conservation of the total number of surfactant monomers in the system as opposed to Equation 4.122 for the conservation of the total number of surfactant monomers of type B in the system. Remember, however, that since B and α^* depend on α_1, therefore Λ is a function of both X_1 and α_1. As in the single component case, however, in order for the sums over n to converge, $\Lambda < 1$, indicating here that X_1 is always less than $e^{B(\alpha^*)}$

Equations 4.146 and 4.147 can be solved numerically for X_1 and α_1 given X and α_s. Thus, the problem is in principle solved. Furthermore, we can use the micellar distribution to calculate any experimentally observable quantity, as before. We now proceed as we did in the single-component case by considering the micellar distribution in the dilute regime and in the regime of strong micellar growth. We expect similar results.

4.2.7 The Dilute Regime

As in Section 4.1.4, we wish to show that Equations 4.146 and 4.147 together imply a transition in concentration during which the number of micelles increases sharply. We note that Equation 4.146 has exactly the same form as Equation 4.44, and so the analysis presented there should also be applicable here.

Because of the factor Λ^{n_0} appearing in Equation 4.146, we see that when Λ is not close to unity, the second and third terms on the right hand side of Equation 4.146 and Equation 4.147 are very small. In this case, Equation 4.146 tells us that $X = X_1$, Equation 4.147 tells us that $\alpha_1 = \alpha_s$, and it is clear that no micelles are

present in the solution.

As the total concentration, X, is increased, the value of X_1 (and thus Λ) increases. As Λ approaches unity, the value of Λ^{n_0} increases sharply and the second and third terms on the right hand side of Equations 4.146 and 4.147 can not be neglected. Remembering that these two terms come from the summation over the micellar distribution, we note that together, in Equation 4.146, the second and third terms on the right hand side should be proportional to the total number of monomers in the solution that exist in micellar form. The critical micellar concentration, therefore, lies in the vicinity of the concentration region where the second and third terms on the right hand side of Equation 4.146 first become comparable to the magnitude of X_1.

If $K(\alpha^*) > 1$, then when X approaches $e^{B(\alpha^*)}$, X_1 becomes comparable to $e^{B(\alpha^*)}$, meaning that the value of Λ approaches 1 and we can no longer neglect the second and third terms on the right hand side of Equation 4.146. In fact, as we increase the concentration further, X_1 can increase only very little, since its maximum value is $e^{B(\alpha^*)}$, as we saw in the previous section. If the value of X_1 exceeds $e^{B(\alpha^*)}$, then $\Lambda > 1$, and the summation over the micellar distribution resulting in Equations 4.146 and 4.147 do not converge. Therefore, most of the increase in X at the stage where X is about $e^{B(\alpha^*)}$ is reflected as an increase in the second and third terms of Equation 4.146, and so we expect the critical micellar concentration to lie in the vicinity of $X = e^{B(\alpha^*)}$.

On the other hand, if $K(\alpha^*) < 1$, then the second and the third terms on the right hand side of Equation 4.146 become significant before X reaches $e^{B(\alpha^*)}$. In this case, it is convenient to recall the definition of $K(\alpha)$ (Equation 4.115) and the definition of $B(\alpha)$ (Equation 4.116) If we define a quantity $D(\alpha)$, such that

$$D(\alpha) = \frac{\Delta(\alpha)}{n_0 k_B T} + \alpha \ln \frac{\alpha}{\alpha_1} + (1-\alpha) \ln \frac{1-\alpha}{1-\alpha_1} \tag{4.148}$$

then we may rewrite Equation 4.146

$$X = X_1 + \left(\frac{X_1}{e^{D(\alpha^*)}}\right)^{n_0} \left\{\frac{n_0}{(1-\Lambda)} + \frac{\Lambda}{(1-\Lambda)^2}\right\}. \tag{4.149}$$

We see that when X approaches the quantity $e^{D(\alpha^*)}$, X_1 becomes comparable to $e^{D(\alpha^*)}$, meaning that the second and third terms on the right hand side of Equation 4.149 begin to increase sharply and can no longer be neglected. We therefore expect the critical micellar concentration to lie in the vicinity of $X = e^{D(\alpha^*)}$. Furthermore, we note that the condition that $K(\alpha^*) < 1$ implies that $e^{D(\alpha^*)} < e^{B(\alpha^*)}$. Therefore, from the definition of Λ (Equation 4.145), we see that when the second and third terms on the right hand side of Equation 4.149 become significant, that Λ is not necessarily very close to unity in the sense that Λ^{n_0} is still small compared to unity. We will see in the next section that this implies that for $K(\alpha^*) < 1$ we cannot physically realize the limit of strong micellar growth.

4.2.8 The Limit of Strong Micellar Growth

As in the single component case, by strong micellar growth, it is meant that there are significant numbers of micelles with $n > n_0$, or equivalently, the levels in the micellar distribution $\tilde{X}_n$ in Equation 4.141 for $n > n_0$ must be significantly occupied. This implies that Λ is close to unity. Let us then define

$$\Lambda = 1 - \frac{\epsilon}{n_0} \tag{4.150}$$

where $\epsilon \ll 1$. For almost all practical cases, the limit of strong micellar growth will also correspond to the limit $X \gg e^{B(\alpha^*)}$, that is, the total concentration is far above the critical micellar concentration. We will first examine the limit of strong micellar growth when the total concentration is far above the critical micellar concentration. We shall then consider the conditions for which strong micellar growth can occur even close to the critical micellar concentration.

For total concentrations far above the critical micellar concentration, 4.146 gives,

to leading order in ϵ

$$X = e^{B(\alpha^*)} + \frac{1}{K(\alpha^*)}\frac{{n_0}^2}{\epsilon^2}. \tag{4.151}$$

In the above equation, we could replace X_1 with $e^{B(\alpha^*)}$ since $X \gg e^{B(\alpha^*)}$ and the correction introduced by considering X_1 as different from $e^{B(\alpha^*)}$ is of the next order in ϵ. Equation 4.151 implies that

$$K(\alpha^*)[X - e^{B(\alpha^*)}] \gg {n_0}^2. \tag{4.152}$$

With Equation 4.151 as an estimate of ϵ/n_0, Equation 4.150 becomes

$$\Lambda \simeq 1 - \frac{1}{\{K(\alpha^*)[X - e^{B(\alpha^*)}]\}^{1/2}}, \tag{4.153}$$

and using Equation 4.153 in Equation 4.141 (also recalling the definition of Λ), the micellar distribution can be rewritten

$$\tilde{X}_n \simeq \frac{1}{K(\alpha^*)} e^{-n/\{K(\alpha^*)[X - e^{B(\alpha^*)}]\}^{1/2}}. \tag{4.154}$$

Thus, we see that in the limit of strong micellar growth, the micellar distribution is an exponential, whose width increases as $\{K(\alpha^*)[X - e^{B(\alpha^*)}]\}^{1/2}$.

As we mentioned in the previous section, in order to physically realize the limit of strong micellar growth as presented above, we must have that $K(\alpha^*) > 1$. This can be shown by examination of Equation 4.152. We note first that by definition, $X < 1$, since $X = 1$ corresponds to the case of pure surfactant. In addition, the quantity $e^{B(\alpha^*)}$ should be small compared to unity, since in general $B(\alpha^*)$ is a negative number indicating the stability of cylindrical micelles relative to free monomers. Therefore, on the left hand side of Equation 4.152 $K(\alpha^*)$ multiplies a quantity that can be at most of the order of unity, and which is in all practical cases is small compared to unity. However, we are told by Equation 4.152 that in order to realize the limit of strong micellar growth, the quantity $K(\alpha^*)[X - e^{B(\alpha^*)}]$ should be much greater than ${n_0}^2$. We know that for a micellar system, n_0 should be large compared with unity. We therefore cannot realize the limit of strong micellar growth unless $K(\alpha^*) > 1$,

since unless $K(\alpha^*) > 1$, we have no way to satisfy Equation 4.152.

We now wish to investigate the conditions for which strong micellar growth can occur for concentrations near to the critical micellar concentration. From Equation 4.154, we see that at a fixed total concentration that as $K(\alpha^*)$ is increased, the micellar distribution becomes broader. Equivalently, if we consider a fixed width of the micellar distribution, increasing $K(\alpha^*)$ will decrease the total concentration X for which that distribution occurs. We therefore wish to estimate the magnitude of $K(\alpha^*)$ required to have large growth at low concentration. Let us consider the case when $X = e^{B(\alpha^*)}$ and Λ is close to 1 as in Equation 4.150. As we have previously done, we expand the first mass conservation relation (Equation 4.146) to leading order in ϵ. However, since X is no longer large compared to $e^{B(\alpha^*)}$, we cannot also replace X_1 with $e^{B(\alpha^*)}$. Instead of Equation 4.151, we have

$$X = X_1 + \frac{1}{K(\alpha^*)} \frac{{n_0}^2}{\epsilon^2}. \tag{4.155}$$

Using the definition of Λ and substituting $X = e^{B(\alpha^*)}$, we get

$$e^{B(\alpha^*)} = e^{B(\alpha^*)} \left(1 + \frac{\epsilon}{n_0}\right) + \frac{1}{K(\alpha^*)} \frac{{n_0}^2}{\epsilon^2}, \tag{4.156}$$

which tells us that to leading order in ϵ,

$$K(\alpha^*) e^{B(\alpha^*)} = \frac{{n_0}^3}{\epsilon^3}. \tag{4.157}$$

Recalling that the quantity $e^{B(\alpha^*)/k_BT}$ is of the same order as the critical micellar concentration, Equation 4.157 implies that if $K(\alpha^*) \gg {n_0}^3/X_{CMC}$, where X_{CMC} is the critical micellar concentration, then even near the critical micellar concentration there is considerable micellar growth. If, on the other hand, it turns out that $K(\alpha^*) \ll {n_0}^3/X_{CMC}$, then near the critical micellar concentration the solution exists as a relatively monodisperse (in n) distribution of nearly minimum-sized micelles. We now investigate which limit applies to our experimental system.

Recalling the results of Section 4.1.5, we had for pure $C_{12}E_6$ at 50°C, that $K \sim$

5×10^{10} and ${n_0}^3/X_{CMC} \sim 1.4 \times 10^{12}$. For pure $C_{12}E_8$, whose critical micellar concentration is of the same order as that of $C_{12}E_6$, the corresponding value of K is several orders of magnitude lower: $K \sim 6 \times 10^5$. Thus, for any mixture of $C_{12}E_6$ and $C_{12}E_8$, we can be confident that $K(\alpha^*) \ll {n_0}^3/X_{CMC}$, implying that near the critical micellar concentration the solution exists as a relatively monodisperse solution of nearly minimum-sized micelles. In the regions that show appreciable micellar growth, we can be sure that $X \gg e^{B(\alpha^*)}$. As a result of this, we can simplify the expression for the micellar distribution even further, since we can neglect $e^{B(\alpha^*)}$ as compared with X in Equations 4.152- 4.154. For the renormalized micellar distribution, we have

$$\tilde{X}_n \simeq \frac{1}{K(\alpha^*)} e^{-n/[K(\alpha^*)X]^{1/2}}. \tag{4.158}$$

We now know the form of the micellar distribution in the limit of strong micellar growth, but we have not yet said anything of the value of the optimal composition in the same limit. In order to do so, we must deal with the second conservation equation (Equation 4.147). We can remove most of the dependence on Λ from this equation by substituting in Equation 4.146. The result is

$$\alpha_s X = \alpha_1 X_1 + \alpha^*(X - X_1). \tag{4.159}$$

Rearranging, we write this

$$\alpha^* - \alpha_s = \frac{X_1}{X}(\alpha^* - \alpha_1). \tag{4.160}$$

In the limit of strong micellar growth, we can replace X_1 with $e^{B(\alpha^*)}$, giving

$$\alpha^* - \alpha_s = \frac{e^{B(\alpha^*)}}{X}(\alpha^* - \alpha_1). \tag{4.161}$$

In the limit $K(\alpha^*) \gg {n_0}^3/X_{CMC}$, corresponding to the case of micellar growth at low concentration, there is no further simplification that can be made. In this case, $e^{B(\alpha^*)}$ is of the same order as X, and it is possible that α^* can be quite different from α_s, as long as α_1 is likewise shifted from α^* so as to satisfy Equation 4.161. In

fact, in order for α^* to be close to α_s in the limit that $K(\alpha^*) \gg {n_0}^3/X_{CMC}$, we must have that α_1 is close to α^*, which implies that $\Delta\mu_{cA}^0 - \Delta\mu_{cB}^0$ is small (see Equation 4.120).

On the other hand, consider the limit $K(\alpha^*) \ll {n_0}^3/X_{CMC}$, corresponding to the case where strong micellar growth begins at mole fractions well above $e^{B(\alpha^*)}$. As explained above, this limit corresponds to the experiments performed in this thesis. In this case, it is clear that the right hand side of Equation 4.161 is a small quantity. This implies that α^* should be very close to α_s, which we expect physically. Since $X_1 \ll X$, most of the material in the system exists as micelles. Any difference in α^* from α_s must be compensated by a shift in the free monomer composition. Since the free monomer concentration is so low, as compared to the concentration of monomers in the micelles, the allowable change in α^* from α_s must be very small. We define the small parameter

$$\gamma = \alpha^* - \alpha_s \tag{4.162}$$

and note that as a first approximation

$$\gamma \simeq \frac{e^{B(\alpha_s)}}{X}[\alpha_s - \alpha_1(\alpha_s)] \tag{4.163}$$

where, since γ is small, we have replaced α^* with α_s in Equation 4.161 and furthermore we have indicated that Equation 4.120 should be used to calculate $\alpha_1(\alpha_s)$. Performing this step gives

$$\gamma \simeq \frac{e^{B(\alpha_s)}}{X}\frac{\alpha_s(1-\alpha_s)}{\alpha_s + (1-\alpha_s)e^{-(\Delta\mu_{cA}^0 - \Delta\mu_{cB}^0)/k_BT}}(1 - e^{-(\Delta\mu_{cA}^0 - \Delta\mu_{cB}^0)/k_BT}). \tag{4.164}$$

We see that if $\Delta\mu_{cA}^0 - \Delta\mu_{cB}^0$ tends to zero, then $1 - e^{-(\Delta\mu_{cA}^0 - \Delta\mu_{cB}^0)/k_BT}$ tends to zero, and likewise, γ also tends to zero, meaning that α^* tends to α_s. Physically, this is expected, since if $\Delta\mu_{cA}^0 - \Delta\mu_{cB}^0$ tends to zero, then there is no preference for surfactant A or surfactant B to exist in any particular environment and we expect that $\alpha_s = \alpha_1 = \alpha^*$. If $\Delta\mu_{cA}^0 - \Delta\mu_{cB}^0$ becomes large and positive, then γ tends to $(1-\alpha_s)e^{B(\alpha_s)}/X$, whereas if $\Delta\mu_{cA}^0 - \Delta\mu_{cB}^0$ becomes large and negative, then γ tends

to $-\alpha_s e^{B(\alpha_s)}/X$. In both cases, γ is small, since $e^{B(\alpha_s)}$ is much smaller than X in the limit of strong micellar growth.

In the mixed system, the weight-averaged aggregation number is defined by

$$\bar{n}_w = \sum_{n=n_0}^{\infty} \sum_{\alpha=0}^{1} n^2 X_{n\alpha} / \sum_{n=n_0}^{\infty} \sum_{\alpha=0}^{1} n X_{n\alpha}. \tag{4.165}$$

After performing the summations over α according to the procedure described in Section 4.2.6, we obtain

$$\bar{n}_w = \sum_{n=n_0}^{\infty} n^2 \tilde{X}_n / \sum_{n=n_0}^{\infty} n \tilde{X}_n. \tag{4.166}$$

Since the form of Equation 4.166 is the same as that of Equation 4.56 for the single-component case, and $\tilde{X}_n$ has the same form as the single- component micellar distribution, we expect the same results for the weight-averaged aggregation number. That is, after inserting the renormalized micellar distribution and taking the limit of strong micellar growth, the weight-averaged aggregation number may be written

$$\bar{n}_w \simeq n_0 + 2\sqrt{K(\alpha^*)X}. \tag{4.167}$$

It should be noted here that others [34] have stated that in the same limit (strong micellar growth), the weight averaged aggregation number for a mixture containing two surfactants and water should scale like $X^{0.4}$ rather than $X^{0.5}$. They argue (correctly) that in the case of mixed micelles, the width of the composition distribution (fluctuations about the optimal composition) should be properly considered, and that this width is (as we also found) proportional to $\sqrt{n}$, where n is the total aggregation number of the micelles. However, they begin their analysis by writing down a free energy of micellization and neglecting the terms there that depend logarithmically on n. As a result, their expression for the micellar distribution is not properly normalized, and when they integrate over the composition distribution, they have an extra factor of $\sqrt{n}$ which is responsible for the difference in the exponents. In fact, if we generalize their analysis to a system with k different surfactant species,

they predict that the weight-averaged aggregation number should scale like $X^{2/(3+k)}$. This is physically unreasonable when we consider that a "pure" surfactant solution in reality contains a mixture of surfactant molecules with a large number of different isotopic substitutions.

4.2.9 Moments of the Micellar Distribution

In this section, we show that our general form for the micellar distribution implies that all moments (in n) of the distribution can be written in terms of the first and second moments (in n). By the k^{th} moment of the distribution, we mean

$$M_k = \sum_{n,\alpha} n^k X_{n\alpha} = X_1 + \sum_{n=n_0}^{\infty} n^k \tilde{X}_n. \tag{4.168}$$

In particular, the first moment

$$M_1 = X_1 + \sum_{n=n_0}^{\infty} n\tilde{X}_n = X \tag{4.169}$$

is just the total mole fraction of surfactant in the system. The renormalized micellar distribution $\tilde{X}_n$ is given by Equation 4.144

$$\tilde{X}_n = \frac{1}{K(\alpha^*)}\Lambda^n \tag{4.170}$$

with $\Lambda = X_1 e^{-B(\alpha^*)}$. Therefore, we may rewrite the k^{th} moment of the distribution

$$M_k = \Lambda e^{B(\alpha^*)} + \frac{1}{K(\alpha^*)} \sum_{n=n_0}^{\infty} n^k \Lambda^n. \tag{4.171}$$

Differentiating with respect to Λ and multiplying the resulting expression by Λ, we obtain

$$\Lambda \frac{dM_k}{d\Lambda} = \Lambda e^{B(\alpha^*)} + \sum_{n=n_0}^{\infty} n^{k+1} \Lambda^n = M_{k+1}, \tag{4.172}$$

which relates the k^{th} moment to the $(k+1)^{th}$, through Λ. Thus, we can write

$$\frac{M_{k+1}}{M_{j+1}} = \frac{dM_k}{d\Lambda}\frac{d\Lambda}{dM_j} = \frac{dM_k}{dM_j} \tag{4.173}$$

by the chain rule. For the particular case of $j = 1$, we have

$$\frac{M_{k+1}}{M_2} = \frac{dM_k}{dX}, \tag{4.174}$$

which suggests that we define the operator

$$\Theta = M_2\frac{d}{dX} \tag{4.175}$$

so that

$$M_{k+1} = \Theta M_k. \tag{4.176}$$

Thus, all of the moments of the distribution with $k > 2$ can be found by repeated operation on M_2 with Θ:

$$M_k = \Theta^{k-2}M_2. \tag{4.177}$$

The zeroth moment we must treat separately. Using Equation 4.173, we see that

$$\frac{dM_0}{dX} = \frac{X}{M_2}, \tag{4.178}$$

and furthermore, we note that when $X = 0$, $M_0 = 0$. Therefore, we can integrate Equation 4.178, giving

$$M_0 = \int_0^X \frac{x'}{M_2}dx'. \tag{4.179}$$

Thus, all of the moments (in n) of the distribution may be expressed in terms of the first moment, X, and the second moment, M_2.

Chapter 5

A Model Gibbs Free Energy for Mixed Micellar Solutions

In the previous chapter, we discussed the self-assembly and the growth of mixed surfactant micelles as an extension of the well-known ladder model [10] in the limit that intermicellar interactions are weak. We know that in many systems, however, these interactions can become strong enough under the right conditions to induce a phase transition in which the solution spontaneously separates into two coexisting isotropic phases that differ in total amphiphile concentration (and/or composition). Previous work on single-component micellar systems [11, 14, 12] has investigated such a phase transition and its effect on the micellar size distribution in terms of a particular model for the Gibbs free energy of the micellar system. This model accounts for the interactions between micelles at the level of a mean-field approximation, by considering only pairwise interactions between the monomers in different micelles. Puvvada and Blankschtein [16] have extended this Gibbs free energy model to the case of mixtures with regards to their molecular-thermodynamic model of micellization. We are interested in incorporating our two-dimensional ladder model into the thermodynamic framework of the generalized Blankschtein, Thurston and Benedek Gibbs free energy model, because from the resulting form of the Gibbs free energy we may calculate the total osmotic compressibility of the mixed micellar solution, taking into account the interactions between micelles. Furthermore, we

may calculate the contribution to the total osmotic compressibility from micelles of total aggregation number n, which we will see in Chapter 6 can be taken as the thermodynamic driving force for the diffusion of n-mers. We will use the calculation of the osmotic compressibility of the n-mers to provide a correction to the calculation of the average diffusivity of our micellar system when the interactions between micelles become important.

We shall also be interested in examining the molecular-thermodynamic model of Puvvada and Blankschtein. Their model provides a numerical procedure for computing the magnitude of the free energy to form a micelle. We shall investigate how this procedure can be used to estimate the magnitudes of the four parameters of the two-dimensional ladder model, so that in Chapter 6 we may compare the predictions of the model of Puvvada and Blankschtein to the two-dimensional ladder model parameters that we shall extract from the experimental data that was presented in Chapter 3.

In Section 5.1, we present the essentials of the Blankschtein, Thurston and Benedek Gibbs free energy model and the generalization to the case of mixtures as worked out by Puvvada and Blankschtein. We then indicate how the two-dimensional ladder model presented in Chapter 4 is to be incorporated into the thermodynamic framework of the generalized Gibbs free energy model. We find that by considering a mean-field approximation, including only pairwise interactions between the monomers in different micelles, the equilibrium micellar distribution is identical to the equilibrium micellar distribution we found for the case of weak interactions in Chapter 4. In Section 5.2 we examine the the osmotic pressure and total osmotic compressibility of the micellar system predicted by the Gibbs free energy model. We then calculate the contribution to the total osmotic compressibility from micelles of total aggregation number n and show that our result is reasonable.

In Section 5.3, we briefly describe the model of Puvvada and Blankschtein. In this section, we also indicate the means by which the four physically meaningful parameters of the two-dimensional ladder model may be obtained from the numerical procedure of Puvvada and Blankschtein, for the reasons mentioned above.

5.1 The Gibbs Free Energy

For the single component case, we consider a solution of N_S amphiphiles and N_W water molecules in equilibrium at temperature T and pressure P. If the concentration of amphiphiles is greater than the critical micellar concentration, then the amphiphiles self assemble into a distribution $\{N_n\}$ of micellar sizes, where N_n is the number of micelles containing n amphiphiles.

As in Chapter 4, for the mixed case let us concentrate on the specific example of two surfactant species and water. We consider, then a solution containing N_W molecules of water, N_A molecules of surfactant species A, and N_B molecules of surfactant species B in equilibrium at temperature T and pressure P. Assuming that the total concentration of surfactant in the solution is greater than the critical micellar concentration for the mixture, then there will also be a distribution of micelles, which, for linear micelles like those treated in the previous chapter, we shall denote $\{N_{n\alpha}\}$. Here, $N_{n\alpha}$ is the number of micelles in the solution with a total of n monomers, and relative composition α.

In both the single component case and the mixed case, the Gibbs free energy of the system is modeled as the sum of three additive parts:

$$G = G_f + G_m + G_{int} \tag{5.1}$$

where G_f is called the free energy of formation, G_m is called the free energy of mixing, and G_{int} is called the free energy of interaction. In this way we separate conceptually the factors responsible for micelle formation and growth, and the factors responsible for phase behavior and phase equilibria.

In the single component case, the free energy of formation, G_f, was modeled by Blankschtein, Thurston and Benedek [11, 14, 12] as

$$G_f = N_W \mu_W^0 + \sum_n N_n \mu_n^0 \tag{5.2}$$

where $\mu_W^0(T, P)$ is the change in the free energy of the solution when a water

molecule is added to pure water, and $\mu_n^0(T,P)$ is the free energy change of the solution when a single micelle of size n is added to pure water. G_f summarizes the many physical factors responsible for micelle formation and growth, including the hydrophobic effect, hydrogen bonding, electrostatic, steric and van der Waals interactions, as well as contributions to the free energy arising from the packing of the hydrophobic tails in the micellar core. The contributions to the formation free energy from these factors are considered for a dilute solution in the absence of intermicellar interactions, as is evident from the definitions of μ_W^0 and μ_n^0.

The generalization of Equation 5.2 appropriate to the case of our two-component mixture is

$$G_f = N_W \mu_W^0 + \sum_{n,\alpha} N_{n\alpha} \mu_{n\alpha}^0, \tag{5.3}$$

where $\mu_W^0(T,P)$ represents the change in the free energy of the solution when a water molecule is added to pure water, and $\mu_{n\alpha}^0$ represents the free energy change of the solution when a single micelle of total aggregation number n and relative composition α is added to pure water. Since the micelle is already formed when it is added to the pure water, $\mu_{n\alpha}^0$ includes implicitly inside of it the mixing entropy of the $n\alpha$ amphiphiles of type A and the $n(1-\alpha)$ amphiphiles of type B contained in the micelle.

Puvvada and Blankschtein [16] model G_f as

$$G_f = N_W \mu_W^0 + N_A \mu_{1A}^0 + N_B \mu_{1B}^0 + \sum_{n,\alpha} N_{n\alpha} \Delta G_{mic}(n,\alpha), \tag{5.4}$$

where $\mu_W^0(T,P)$, $\mu_{1A}^0(T,P)$, and $\mu_{1B}^0(T,P)$ are the standard-state chemical potentials of water, monomers of type A, and monomers of type B referred to infinite dilution in water. That is, $\mu_W^0(T,P)$ is the free energy change of the solution when a water molecule is added to pure water, μ_{1A}^0 is the free energy change of the solution when a single monomer of type A is added to pure water, and μ_{1B}^0 is the free energy change when a single monomer of type B is added to pure water. Comparing Equation 5.4 to Equation 5.3 and recalling that $N_A = \sum_{n,\alpha} n\alpha N_{n\alpha}$ and

$N_B = \sum_{n,\alpha} n(1-\alpha)N_{n\alpha}$, we identify

$$\Delta G_{mic} = \mu^0_{n\alpha} - n\alpha\mu^0_{1A} - n(1-\alpha)\mu^0_{1B}. \tag{5.5}$$

That is, the quantity $\Delta G_{mic}(n, \alpha, T, P)$ is the free energy of micellization for a micelle of total size n, and relative composition α. It represents the change in the free energy of the system when $n\alpha$ monomers of type A and $n(1-\alpha)$ monomers of type B are transferred from pure water into the micelle. We remember that the definition of $\mu^0_{n\alpha}$ implicitly contains the mixing entropy of the amphiphiles inside the micelle. In Chapter 4, we recall that we also defined the quantity ΔG_{mic} in a conceptually identical manner with the above definition. We had (see Equation 4.111)

$$\Delta G_{mic} = \Delta(\alpha) + (n - n_0)\delta(\alpha) + n\left(\alpha \ln \alpha + (1-\alpha)\ln(1-\alpha)\right), \tag{5.6}$$

where the definitions of the quantities $\Delta(\alpha)$ and $\delta(\alpha)$ are to be found in Chapter 4. The third term in Equation 5.6 is the mixing entropy of the amphiphiles within the micelle. It arises from the combinatoric factor that counts the number of distinct ways in which the $n\alpha$ amphiphiles of type A and the $n(1-\alpha)$ amphiphiles of type B can be arranged within the micelle, and is discussed in detail in Chapter 4. In addition, this combinatoric factor makes contributions to ΔG_{mic} that are logarithmic in n. These terms are small compared to terms linear in n and are therefore unimportant as far as the Gibbs free energy is concerned. These terms have been dropped here; however, they provide the proper normalization of the micellar distribution, as discussed in Chapter 4.

The free energy of mixing, G_m, refers to the mixing of the water molecules, formed micelles, and free monomers in solution with each other. As seen above, the mixing entropy of the monomers within the micelles is considered as part of the free energy of formation, G_f. In the single component case, Blankschtein, Thurston and

Benedek [11, 14, 12] model G_m as

$$G_m = k_B T \left[N_W \ln X_W + \sum_n N_n \ln \frac{X_n}{e} \right], \tag{5.7}$$

where $X_W = N_W/(N_W + N_S)$, $X_n = N_n/(N_W + N_S)$, and k_B is the Boltzmann constant. The quantity $-G_m/T$ is the mixing entropy of the water molecules, formed micelles, and free monomers in solution. $-G_m/T$ is physically reasonable since it is an entropic contribution to the total Gibbs free energy of the solution that reflects the number of ways that the water molecules, free monomers, and micelles can be positioned in the solution as a function of the relative proportions of each of these entities. The relative proportions are represented by the mole fractions X_W and $\{X_n\}$. We should note that Equation 5.7 differs slightly from the expression given in the treatment of Blankschtein, Thurston and Benedek [11, 14, 12] in that we have included in the model for G_m a factor of e under the logarithm of X_n (the physical reasons for this are explained in Appendix C). We have included the factor of e in order that we may avoid a redefinition of the standard part of the chemical potential, μ_n^0, as was made in reference [12].

The proper generalization of Equation 5.7 to the case of a two component mixture is [16]

$$G_m = k_B T \left[N_W \ln X_W + \sum_{n,\alpha} N_{n\alpha} \ln \frac{X_{n\alpha}}{e} \right] \tag{5.8}$$

where $X_W = N_W/(N_W + N_A + N_B)$ is the mole fraction of water in the solution, and $X_{n\alpha} = N_{n\alpha}/(N_W + N_A + N_B)$ is the mole fraction of micelles with n monomers and relative composition α, as defined in Chapter 4. The expression above again differs slightly from the form given in the work of Puvvada and Blankschtein [16], because of the factor of e. The reasons for including e here are the same as in the single component case. It should be noted that the sum in Equation 5.8 includes implicitly the cases of $n = 1$ with $\alpha = 0$ or $\alpha = 1$, corresponding to the free monomers in solution. Once these terms have been separated out, the remainder of the sum should be treated in the same manner as the sums over n and α of the micellar distribution that appeared in Chapter 4.

The free energy of interaction, G_{int}, is responsible for driving the phase separation of the solution. The form of G_{int} must therefore reflect the interactions between mixed micelles, free monomers in solution, and water. Because these interactions are too complicated to consider exactly in most physical systems, a simplified, mean-field model will be used to describe them. In the single component case, Blankschtein, Thurston and Benedek write [11, 14, 12]

$$G_{int} = -\frac{1}{2} C N_S \phi, \tag{5.9}$$

where ϕ is the total volume fraction of amphiphiles in the solution. Physically, Equation 5.9 may be interpreted as follows. Each amphiphile in the solution (of which there are N_S) interacts with an average effective potential that is caused by effective intermicellar amphiphile-amphiphile interactions. The magnitude of this potential is proportional to the total volume fraction ϕ of all of the other amphiphiles, indicating that the pairwise interaction between amphiphiles has been averaged over all possible positions of the amphiphiles. The parameter $C(T, P)$ measures the strength of the average effective potential.

The generalization of G_{int} appropriate to the case of a two-component mixture of surfactants is given by Puvvada and Blankschtein [16]. They write

$$G_{int} = -\frac{1}{2} C_{eff}(\alpha_s)(N_A + N_B)\phi \tag{5.10}$$

where ϕ is the total volume fraction of surfactant, α_s is the relative composition of the solution, and C_{eff} is an effective mean field interaction parameter measuring the strength of the interaction in the mixture that depends on three phenomenological parameters, C_{AW}, C_{BW}, and C_{AB} [16]:

$$C_{eff}(\alpha_s) = C_{AW}\alpha_s + C_{BW}(1-\alpha_s) - \left(\frac{\sqrt{\gamma_A \gamma_B}}{\gamma_{eff}}\right) C_{AB}\alpha_s(1-\alpha_s). \tag{5.11}$$

In Equation 5.11, $\gamma_A = \Omega_A/\Omega_W$ is the ratio of the molecular volumes of surfactant A and water, $\gamma_B = \Omega_B/\Omega_W$ is the ratio of the molecular volumes of surfactant B and

water, while $\gamma_{eff} = \alpha_s\gamma_A + (1-\alpha_s)\gamma_B$. The two parameters C_{AW} and C_{BW} represent the mean-field interaction potentials (as defined in the single component case) for pure surfactant A and pure surfactant B. As explained in reference [16], the parameter C_{AW} measures the difference between the mean-field interaction potential between water and surfactant A and the water-water and A-A interaction potentials. Likewise, the parameter C_{BW} measures the difference between the mean-field interaction potential between water and surfactant B and the water-water and B-B interaction potentials. The parameter C_{AB} measures specific interactions between amphiphiles of type A and type B that are not present between two amphiphiles of type A or two amphiphiles of type B. As explained in reference [16], for a mixture of nonionic surfactants, which interact with each other primarily by van der Waals forces, $C_{AB} \approx 0$, indicating that the mixture is nearly ideal.

The equilibrium micellar distribution can be calculated using the Gibbs free energy model we have described above. In the single component case, the chemical potential for each micellar species, μ_n, can be found by differentiating the Gibbs free energy with respect to N_n. The equilibrium micellar distribution is found by enforcing the condition that the chemical potential of an amphiphile should be the same everywhere in the solution. In Chapter 4, we saw that this condition implies that $\mu_n = n\mu_1$ where μ_1 is the chemical potential of a free amphiphile in solution. The result of performing these steps on the Gibbs free energy model of Blankschtein, Thurston and Benedek is that the equilibrium micellar distribution can be written [12]

$$X_n = {X_1}^n e^{-(\mu_n^0 - n\mu_1^0)/k_BT} \tag{5.12}$$

where X_1 is the mole fraction of free monomers in solution at equilibrium, μ_n^0 is the standard part of the chemical potential of a micelle of total aggregation number n, and μ_1^0 is the standard part of the chemical potential of a free monomer. This expression is identical to Equation 4.34 from Chapter 4, which gives the equilibrium micellar distribution in the limit that interactions between micelles can be neglected. That is, the particular form of the mean field interaction that has been included in

the Gibbs free energy model of Blankschtein, Thurston and Benedek leaves the micellar distribution unchanged from the case of no interactions. This occurrence is no accident. It follows directly from the fact that the model for the interaction free energy, G_{int}, contains no dependence on the micellar distribution.

The same method that was used to calculate the equilibrium micellar distribution in the single component case can be applied to the Gibbs free energy model for the mixed case [16]. We find [16]

$$X_{n\alpha} = X_{1A}^{n\alpha} X_{1B}^{n(1-\alpha)} e^{-\Delta G_{mic}(n,\alpha)/kT}, \tag{5.13}$$

where X_{1A} and X_{1B} are the mole fractions of free monomers of type A and type B in solution at equilibrium. Also, we have that $\Delta G_{mic}(n,\alpha)$ is given by Equation 5.6 for the generalized ladder model. The proper normalization of the micellar distribution above is contained in terms logarithmic in n included in ΔG_{mic} which were neglected in Equation 5.6. These terms originate from the combinatoric term that expresses the number of distinct ways that the $n\alpha$ amphiphiles of type A and the $n(1-\alpha)$ amphiphiles of type B can be assembled into a mixed micelle, as explained in Section 4.2.5. Putting in the proper normalization, the micellar distribution becomes

$$X_{n\alpha} = \frac{X_{1A}^{n\alpha} X_{1B}^{n(1-\alpha)}}{\sqrt{2\pi n\alpha(1-\alpha)}} e^{-\Delta G_{mic}(n,\alpha)/kT}. \tag{5.14}$$

Defining X_1 and α_1 as in Chapter 4 (see Equations 4.112 and 4.113) and explicitly writing $\Delta G_{mic}(n,\alpha)$, we see that the micellar distribution,

$$X_{n\alpha} = \frac{{X_1}^n}{\sqrt{2\pi n\alpha(1-\alpha)}} e^{-\left\{\Delta(\alpha)+(n-n_0)\delta(\alpha)+nkT\left(\alpha \ln \frac{\alpha}{\alpha_1}+(1-\alpha)\ln\frac{1-\alpha}{1-\alpha_1}\right)\right\}/kT}, \tag{5.15}$$

is identical to Equation 4.114 for the micellar distribution in the case of weakly interacting micelles. Since the interaction free energy, G_{int}, in the mixed case contains no dependence on the micellar distribution just as in the single component case, we expected that these interactions would leave the micellar distribution unchanged

from the noninteracting case.

5.2 The Osmotic Pressure and Osmotic Compressibility

In addition to computing the properties of the micellar distribution, we may also use the Gibbs free energy model to obtain useful expressions for the osmotic pressure and the osmotic compressibility of the mixed system. The osmotic pressure, π, is related to the chemical potential of water, μ_W, by the simple relation [12]

$$\Omega_W \pi = \mu_W^0 - \mu_W. \tag{5.16}$$

In the single component case, the Blankschtein, Thurston and Benedek Gibbs free energy model gives

$$\Omega_W \pi = -k_B T \left[\ln(1-X) + X - \sum_n X_n \right] - C\frac{\phi^2}{2\gamma}. \tag{5.17}$$

The generalization appropriate to the case of two component mixtures has been calculated by Puvvada and Blankschtein [16]

$$\Omega_W \pi = -k_B T \left[\ln(1-X) + X - \sum_{n,\alpha} X_{n\alpha} \right] - C_{eff}(\alpha_s)\frac{\phi^2}{2\gamma_{eff}}. \tag{5.18}$$

We note that the only difference between the single component case and the mixed case is that in the mixed case, the sum is over both the micellar sizes and compositions, and that C and γ are replaced by the quantities C_{eff} and γ_{eff}.

The osmotic compressibility can be found in either the single component case or the mixed case by differentiating with respect to X (recalling that ϕ can be expressed as a function of X as we noted above) and inverting. In the single component case,

Blankschtein, Thurston and Benedek [12] obtain

$$\left(\frac{\partial \pi}{\partial X}\right)^{-1} = \frac{\Omega_W}{k_B T}\left[\frac{X}{1-X} + \frac{\partial}{\partial X}\sum_n X_n - \frac{C}{k_B T}\frac{\gamma X}{(1+(\gamma-1)X)^3}\right]^{-1}. \tag{5.19}$$

In the mixed case, Puvvada and Blankschtein obtain [16]

$$\left(\frac{\partial \pi}{\partial X}\right)^{-1} = \frac{\Omega_W}{k_B T}\left[\frac{X}{1-X} + \frac{\partial}{\partial X}\sum_{n,\alpha} X_{n\alpha} - \frac{C_{eff}}{k_B T}\frac{\gamma_{eff} X}{(1+(\gamma_{eff}-1)X)^3}\right]^{-1}. \tag{5.20}$$

We can simplify these expressions slightly by recalling that the moments (in n) of the micellar distribution are related to each other. For the mixed case, we showed in Section 4.2.9, that

$$\frac{\partial M_0}{\partial X} = \frac{X}{M_2}, \tag{5.21}$$

where, of course, the zeroth moment of the distribution is $M_0 = \sum_{n,\alpha} X_{n\alpha}$. Making this substitution, the osmotic compressibility becomes

$$\left(\frac{\partial \pi}{\partial X}\right)^{-1} = \frac{\Omega_W}{k_B T}\left[\frac{X}{1-X} + \frac{X}{M_2} - \frac{C_{eff}}{k_B T}\frac{\gamma_{eff} X}{(1+(\gamma_{eff}-1)X)^3}\right]^{-1}. \tag{5.22}$$

Blankschtein, Thurston and Benedek obtain a similar result in the single component case, namely that

$$\left(\frac{\partial \pi}{\partial X}\right)^{-1} = \frac{\Omega_W}{k_B T}\left[\frac{X}{1-X} + \frac{X}{M_2} - \frac{C}{k_B T}\frac{\gamma X}{(1+(\gamma-1)X)^3}\right]^{-1}. \tag{5.23}$$

Again, we note that the only difference between the single component expression and the two component expression is that C and γ have been replaced with C_{eff} and γ_{eff}.

In Chapter 6, we will be interested in the contributions to the total osmotic compressibility arising from micelles of different total aggregation numbers, n, because, as we mentioned previously, these contributions can be taken as the thermodynamic driving force for the diffusion of n-mers. We will use the calculation of the osmotic compressibility of the n-mers to provide a correction to the calculation of the aver-

age diffusivity of our micellar system when the interactions between micelles become important. In the single component case, what we are interested in is $(\partial\pi/\partial X_n)^{-1}$. Recalling that

$$X = X_1 + \sum_{n=n_0}^{\infty} nX_n, \tag{5.24}$$

then differentiating Equation 5.17 by X_n gives us

$$\left(\frac{\partial\pi}{\partial X_n}\right)^{-1} = \frac{\Omega_W}{k_BT}\left\{1 + n\left[\frac{X}{1-X} - \frac{C}{k_BT}\frac{\gamma X}{(1+(\gamma-1)X)^3}\right]\right\}^{-1}. \tag{5.25}$$

In the simple case of extremely dilute solute, we may neglect G_{int} and G_m. In this case, we have

$$\left(\frac{\partial\pi}{\partial X_n}\right)^{-1} = \frac{\Omega_W}{k_BT} \tag{5.26}$$

or,

$$\pi_n = \frac{X_n}{\Omega_W}k_BT \tag{5.27}$$

which is the Van't Hoff law for the partial osmotic pressure of n-mers. We see that our expression for $(\partial\pi/\partial X_n)^{-1}$ is physically reasonable, since in the limit of no interactions it reduces to a sensible result.

In the mixed case, we are also interested in the contribution to the total osmotic compressibility arising from all of the micelles with total aggregation number n. That is, we are interested in $(\partial\pi/\partial\tilde{X}_n)^{-1}$. We recall that $\tilde{X}_n$, defined in Chapter 4 is the mixed micellar distribution integrated over the composition variable. We now recall that

$$X = X_1 + \sum_{n=n_0}^{\infty} n\tilde{X}_n, \tag{5.28}$$

in the mixed case. Differentiating Equation 5.18 by $\tilde{X}_n$ gives us an equation similar to Equation 5.25 for the single component case

$$\left(\frac{\partial\pi}{\partial\tilde{X}_n}\right)^{-1} = \frac{\Omega_W}{k_BT}\left\{1 + n\left[\frac{X}{1-X} - \frac{C_{eff}(\alpha_s)}{k_BT}\frac{\gamma_{eff}X}{(1+(\gamma_{eff}-1)X)^3}\right]\right\}^{-1}. \tag{5.29}$$

In the absence of interactions, we have

$$\left(\frac{\partial \pi}{\partial \tilde{X}_n}\right)^{-1} = \frac{\Omega_W}{k_B T} \tag{5.30}$$

or,

$$\pi_n = \frac{\tilde{X}_n}{\Omega_W} k_B T \tag{5.31}$$

which is again the Van't Hoff law for the partial osmotic pressure of n-mers.

5.3 The Model of Puvvada and Blankschtein

The model of Puvvada and Blankschtein provides a means to calculate the magnitude of ΔG_{mic}, the micellization free energy for a single micelle, from considerations at the molecular level. Since the process of micellization is reversible, ΔG_{mic} should be independent of the series of steps leading from the initial condition of free monomers in solution to the final state of the fully assembled micelle. Puvvada and Blankschtein provide us with a series of seven reversible steps leading from monomers in solution to the mixed micelle, chosen in such a way as to be able to clearly identify the various physicochemical factors important to the process of micellization. In this section, we shall summarize this thought process and identify the various contributions to ΔG_{mic}. We shall then identify the four phenomenological parameters of our extended ladder model in terms of the molecular model.

Before proceeding with an explanation of the steps of the thought process, it will be helpful to fully describe our assumptions about the initial and final states. Initially, we have $n\alpha$ molecules of surfactant A and $n(1-\alpha)$ molecules of surfactant B suspended in the solvent. For the moment, we will consider the possibility that one or both surfactant species might be charged. In this case, the hydrophilic regions of the amphiphiles will be surrounded by a cloud of counterions in the solvent. From these monomers, we wish to construct a mixed micelle suspended in solvent with total aggregation number n, relative composition α, and with some geometrical shape which we shall denote, as do Puvvada and Blankschtein, sh. The calculation

of $\Delta G_{mic}(n, \alpha, sh)$ depends on the following model for a micelle.

A micelle can be described as consisting of three distinct regions. The innermost region consists of a hydrophobic core containing no water. The density of the core region is assumed to be uniform and it is further assumed that the density is the same as of bulk hydrocarbon of chain length n'_C, where n'_C is taken to be one less than the hydrocarbon tail length of the amphiphiles in the micelle. The outermost CH_2 group of each hydrophobic tail is assumed to be hydrated, and these groups are considered to be in the next region of the micelle, not in the core. For a mixed micelle, we assume that the density will be the same as the density of a mixture of bulk liquid hydrocarbons of length n'_{CA} and n'_{CB}, with relative composition α, where n'_{CA} and n'_{CB} are taken to be one less than the hydrocarbon tail lengths of surfactant species A and surfactant species B, respectively. The outer layer contains the hydrophilic head groups, water, and any counterions present in the solvent. Between these two layers in the model micelle is a layer of hydrated CH_2 groups. This picture is supported by NMR measurements in both nonionic [59] and ionic [60] micellar solutions in which the micelle-water interface is studied in detail. Furthermore, density measurements in lecithin bilayers [61] and measurements of partial molal volumes and compressibilities of n-Alkanes dissolved in SDS micelles [62] support the assumption that the micellar core is indeed liquid-like, with a density close to that of the bulk liquid hydrocarbon. Note that since the hydrophobic core of the micelle does not contain any water, and cannot have a hole, one dimension of the core is limited to be less than or equal to the fully extended length of a hydrocarbon of chain length n'_C. For mixtures with different chain lengths, it is clear that this dimension must be less than the fully extended length of the longer chain. We denote this core-minor radius as l_c.

Let us now consider the steps leading from our initial to final states. In the first step, we imagine that we remove any charge from the hydrophilic regions of the amphiphiles and also discharge any counterions present. We proceed by breaking the chemical bond between the hydrophobic tail and the head group, which should now also include the single CH_2 group that will be associated with the hydrated layer

described above. It is now possible to deal with the tails separately from the heads. We continue, in the third step, by transferring the $n\alpha$ tails of surfactant A and the $n(1-\alpha)$ tails of surfactant B into a bulk hydrocarbon environment consisting of n-Alkanes of chain length n'_{CA} and n'_{CB} with relative composition α (the same as the micelle). In the fourth step, we form a hydrocarbon droplet with the proper core-minor radius l_c from the $n\alpha$ tails of type A and the $n(1-\alpha)$ tails of type B. The formation of this droplet entails the creation of an oil-solvent interface when we transfer the droplet from an environment of pure hydrocarbon back to solvent. As of yet, however, we have said nothing regarding the orientations of the hydrocarbon chains within the droplet. We know that each chain must be bound at one end to a head group of the appropriate kind which will reside at the surface of the droplet. Therefore, in the fifth step, we restrict the tails such that the correct end lies in the vicinity of the oil-solvent interface. At this stage, the micellar core is fully formed.

In the sixth step, we re-attach the head groups (including the extra single CH_2 group) to the tails at the micellar core-water interface. This step consists of three parts: recreating the chemical bond between head and tail, accounting for the partial screening of the surface of the micellar core from the solvent provided by the head groups, and accounting for the steric repulsion between head groups (which are now close enough to interact). In the seventh and final step, the head groups and counterions are recharged if they were discharged in the first step. The total free energy of micellization is computed by summing the contributions arising from each step. Noting that the bond-breaking and bond-reformation contributions cancel, we can identify five distinct free energy contributions: (1) the free energy contribution per monomer, $g_{w/hc}$, associated with transferring the tails from water to bulk hydrocarbon in the third step (denoted the hydrophobic free energy), (2) the creation and partial screening of the micellar core-solvent interface from the fourth and sixth steps, g_σ (denoted the interfacial free energy per monomer), (3) the loss of entropy associated with the restrictions applied to the tails in the micellar core in the fifth step, which we will call the packing free energy per monomer and denote $g_{hc/mic}$, (4) the free energy per monomer associated with the steric repulsions between the head

groups, g_{st}, from the sixth step, and (5) the electrostatic free energy per monomer, g_{elec} associated with discharging and charging the head groups and counterions in the first and seventh steps. The total free energy of micellization is given by

$$\Delta G_{mic}(sh, n, \alpha, l_c) = n(g_{w/hc} + g_\sigma + g_{hc/mic} + g_{st} + g_{elec}) = n(g_{mic}). \tag{5.32}$$

The details of the modeling of each of these contributions is given in reference [17], but it should be noted here that $g_{hc/mic}$, the packing free energy can be calculated only for three shapes: spheres, infinite cylinders, and bilayers (infinite discs). The optimal core-minor radius, l_c^* and optimal composition α^* are computed by minimizing the total free energy with respect to l_c and α, respectively. By comparing the magnitude of ΔG_{mic} for different shapes, one can also hope to predict the preferred micellar geometry.

For the case of interest to us, finite, prolate spherocylindrical micelles, Puvvada and Blankschtein linearly interpolate the micellization free energy between the optimum free energy for spheres and the optimum free energy for infinite cylinders. If the optimum spherical micelles have relative composition α_{sph} and the optimum infinite cylindrical micelles have relative composition α_{cyl}, then

$$\Delta G_{mic}(n, \alpha) = n\left[g_{mic}^{cyl}(\alpha_{cyl}) + \frac{n_{sph}}{n}\left(g_{mic}^{sph}(\alpha_{sph}) - g_{mic}^{cyl}(\alpha_{cyl})\right)\right] \tag{5.33}$$

with the relative composition of the micelle given by

$$\alpha = \alpha_{cyl} + \frac{n_{sph}}{n}(\alpha_{sph} - \alpha_{cyl}). \tag{5.34}$$

The total aggregation number for the spherical micelle, n_{sph} is computed by Puvvada and Blankschtein by considering the density of the micellar core using Tanford's expression for the dependence of the volume of n-Alkanes on chain length in pure liquid hydrocarbon [63]

$$V(\text{Å}^3) = (27.4 + 26.9n_C')n_{sph}. \tag{5.35}$$

For a mixed, spherical micelle of relative composition α_{sph}, with tail chain lengths n'_{CA} and n'_{CB}, we have

$$\frac{4}{3}\pi(l_c^*)^3 = n_{sph}\left(\alpha_{sph}V_A + (1-\alpha_{sph}V_B\right) \tag{5.36}$$

with

$$V_A = 27.4 + 26.9n'_{CA} \tag{5.37}$$

$$V_B = 27.4 + 26.9n'_{CB} \tag{5.38}$$

If we compare Equation 5.33 to the corresponding expression for the micellization free energy for the extended ladder model (Equation 5.6), we can identify the four physically meaningful extended ladder model parameters in terms of the molecular model of Puvvada and Blankschtein. We have

$$\Delta\mu_A = n_{sph}\left(g_{mic}^{sph}(1.0) - g_{mic}^{cyl}(1.0)\right) \tag{5.39}$$

$$\Delta\mu_B = n_{sph}\left(g_{mic}^{sph}(0.0) - g_{mic}^{cyl}(0.0)\right) \tag{5.40}$$

$$\Delta\mu_{cA}^0 = g_{mic}^{cyl}(1.0) \tag{5.41}$$

$$\Delta\mu_{cB}^0 = g_{mic}^{cyl}(0.0). \tag{5.42}$$

The mixing entropy term, included explicitly in the generalized ladder model expression for ΔG_{mic}, is included in the molecular model in the hydrophobic free energy, $g_{w/hc}$, as the entropy of mixing of the hydrocarbon tails.

Recall now our assumption made in Chapter 4 that $\Delta\mu_{cA}^0$, $\Delta\mu_{cB}^0$, $\Delta\mu_{sA}^0$ and $\Delta\mu_{sB}^0$ (or equivalently $\Delta\mu_A$, $\Delta\mu_B$, $\Delta\mu_{cA}^0$ and $\Delta\mu_{cB}^0$) are independent of composition. If this assumption is valid, then it implies that any nonlinearity in $g_{mic}^{cyl}(\alpha)$ and $g_{mic}^{sph}(\alpha)$ after subtracting out the mixing entropy term $k_BT[\alpha\ln\alpha + (1-\alpha)\ln(1-\alpha)]$ should be small. We shall find in Chapter 6 that the predictions of the molecular model of Puvvada and Blankschtein bear this out.

Chapter 6

Comparison With Experiment

In Chapter 3 we presented the results of a light scattering study of the mixed surfactant system containing $C_{12}E_6$, $C_{12}E_8$ and water. In Chapters 4 and 5, we examined the extension to the case of mixtures of the well known ladder model for one-dimensional micellar growth, the generalization to mixtures of the phenomenological Gibbs free energy of Blankschtein, Thurston and Benedek, and the molecular-thermodynamic approach of Puvvada and Blankschtein. It is the task of this chapter to examine the applicability of these models to the system we have studied experimentally. The chapter is broken into three sections. In Section 6.1, we begin with the presentation of a hydrodynamic model for weakly interacting rodlike micelles that is necessary for the quantitative analysis of our quasielastic light scattering data. We then proceed by applying the generalized ladder model, discussed at length in Chapter 4, to our data. In Section 6.2, we discuss the meaning of the physical parameters extracted from our data in terms of the molecular model of Puvvada and Blankschtein, and in Section 6.3, we generalize our hydrodynamic model in a qualitative way to account for the effects of intermicellar interactions. We use the expression for the osmotic compressibility obtained from the phenomenological model of Blankschtein, Thurston and Benedek to explain the minimum with increasing concentration in the diffusion coefficient observed in our light scattering data.

6.1 Two-Dimensional Ladder Model

In Chapter 4 we saw that we could construct the entire distribution of micellar sizes and compositions in terms of four thermodynamic parameters. Furthermore, we made the observation that weighted sums over the micellar distribution yielded experimentally observable quantities such as the weight-averaged aggregation number. In order to make a connection between our quasielastic light scattering data presented in Chapter 3 and our generalization of the ladder model, we must find a suitable way to relate the average diffusion coefficient (or hydrodynamic radius) to an appropriate sum over the micellar distribution. Since we also know from Chapter 4 that the distribution in composition should be narrow, we will here consider the summation over composition to be already carried out and consider therefore only the remaining summation over total aggregation number. We will proceed in a manner parallel to that of Missel *et. al.* [10], since they have previously addressed a similar problem in interpreting their quasielastic light scattering measurements from SDS micelles.

6.1.1 Obtaining $\bar{D}$ from the Micellar Distribution

We recall from Chapter 3 that the first order correlation function $g(t)$ for a polydisperse system can be written as an integral (Equation 3.7), or as the sum

$$g(t) = \sum_{i=1}^{\infty} A_i e^{-\Gamma_i t} \tag{6.1}$$

with the decay rate $\Gamma_i = D_i q^2$ for Brownian particles. The quantity D_i is the translational diffusion coefficient of the i^{th} species of particle and, of course, q is the magnitude of the scattering vector. The factor A_i is the fraction of the total scattered intensity that comes from the i^{th} species of particles. The magnitude of A_i is proportional to M_i, the mass of a particle of the i^{th} species and c_i, the total mass of all of the particles of species i per unit volume. This can be seen from Equation 2.47 and Equation 3.19. If the particles are large enough (comparable in size to

the wavelength of light), then a scattering form factor, P_i should also be included. Thus,

$$A_i = \frac{M_i c_i P_i}{\sum_{i=1}^{\infty} M_i c_i P_i}. \tag{6.2}$$

Computing the first cumulant (see Section 3.1.2) gives us the proper weighting for calculating the average decay rate

$$\bar{\Gamma} = \sum_{i=1}^{\infty} \frac{M_i c_i P_i \Gamma_i}{\sum_{i=1}^{\infty} M_i c_i P_i} = \sum_{i=1}^{\infty} A_i \Gamma_i \equiv \bar{D} q^2. \tag{6.3}$$

Dividing by q^2, we see that the average diffusivity from light scattering should be

$$\bar{D} = \sum_{i=1}^{\infty} A_i D_i, \tag{6.4}$$

where $D_i = \Gamma_i / q^2$ is the diffusivity of the i^{th} species of particle. Let us examine the A_i in more detail for the specific case of the two-dimensional ladder model. In this case, the index i should be replaced by the micelle total aggregation number n (which will be allowed to run from n_0, the minimum micelle size, to infinity) and the micelle relative composition α (which runs from 0 to 1). That is,

$$\bar{D} = \sum_{n=n_0}^{\infty} \sum_{\alpha} A_{n\alpha} D_{n\alpha}. \tag{6.5}$$

$A_{n\alpha}$ is proportional to the concentration of micelles of total size n and relative composition α, and the above equation represents a weighted average over the micellar size and composition distribution. The method for evaluating such weighted averages over the micellar size and composition distribution was discussed thoroughly in Chapter 4. We saw in Chapter 4 that since the distribution of micellar compositions is very narrow, only terms with α very close to the optimal composition α^* should be retained in (6.5), and we can write

$$\bar{D} = \sum_{n=n_0}^{\infty} A_{n\alpha^*} D_{n\alpha^*}, \tag{6.6}$$

with

$$A_{n\alpha^*} = \frac{M_n(\alpha^*)c_n(\alpha^*)P_n(\alpha^*)}{\sum_{n=n_0}^{\infty} M_n(\alpha^*)c_n(\alpha^*)P_n(\alpha^*)}, \tag{6.7}$$

where we recall that (from Chapter 4) α^* is the composition for which the micellar distribution in α has its maximum. Now we note that $M_n(\alpha^*)$, the mass of an n-mer at the optimal composition, can be written

$$M_n(\alpha^*) = nm(\alpha^*) \tag{6.8}$$

with

$$m(\alpha^*) = m_A\alpha^* + m_B(1-\alpha^*) \tag{6.9}$$

where m_A is the mass of a molecule of $C_{12}E_6$, and m_B is the mass of a molecule of $C_{12}E_8$.

Also, we note that the concentration of micelles containing n monomers, $c_n(\alpha^*)$, should be proportional to the micellar size and composition distribution integrated over the composition variable, $\tilde{X}_n$. We recall that $\tilde{X}_n$, defined in Chapter 4 by Equation 4.144, represents the mole fraction of micelles of total size n, regardless of their composition. Since $c_n(\alpha^*)$ has units of mass per unit volume, we write

$$c_n(\alpha^*) = M_n(\alpha^*)\frac{\tilde{N}_n}{V}, \tag{6.10}$$

where $\tilde{N}_n$ is the total number of micelles in the solution with total size n regardless of composition and V is the total volume of the solution. We note that since the total mole fraction of micelles with total size n regardless of composition, $\tilde{X}_n = \tilde{N}_n/(N_A + N_B + N_W)$, we can rewrite $c_n(\alpha^*)$

$$c_n(\alpha^*) = \tilde{X}_n M_n(\alpha^*)\rho = \tilde{X}_n nm(\alpha^*)\rho, \tag{6.11}$$

where ρ is the number density of particles in the solution,

$$\rho = \frac{N_A + N_B + N_W}{N_A\Omega_A + N_B\Omega_B + N_W\Omega_W}. \tag{6.12}$$

Note that we are using the same definitions of N_A, N_B, N_W, Ω_A, Ω_B and Ω_W as were used in Chapters 4 and 5: N_A, N_B and N_W are the total number of amphiphiles of type A, the total number of amphiphiles of type B, and the total number of molecules of water in the solution, respectively, and Ω_A, Ω_B and Ω_W are the molecular volumes of an amphiphile of type A, an amphiphile of type B and a water molecule, respectively.

Equations 6.8 and 6.11 can be used to simplify our expression for $A_{n\alpha^*}$. We see that all factors of ρ and $m(\alpha^*)$ cancel upon substitution into Equation 6.7, giving us the simpler expression

$$A_{n\alpha^*} = \frac{n^2 \tilde{X}_n P_n}{\sum_{n=n_0}^{\infty} n^2 \tilde{X}_n P_n}. \tag{6.13}$$

In order to proceed, we need an appropriate hydrodynamic model for the diffusion coefficient of our rodlike micelles and an appropriate form factor. We shall use the following approximation for the form factor of rodlike particles [64]:

$$\begin{aligned} P(X) &= \left[1 + \tfrac{x^2}{9} + \tfrac{7X^4}{2025}\right]^{-1} \quad 0 < X < 2 \\ P(X) &= \tfrac{\pi}{2\left(X + \frac{1}{\pi}\right)} \qquad\qquad\quad 2 < X < \infty \end{aligned} \tag{6.14}$$

with

$$X = \frac{2\pi l}{\lambda'} \sin \frac{\theta}{2} \tag{6.15}$$

where l is the length of the rod, λ' is the wavelength of light in the medium, and θ is the scattering angle. In order to use Equation 6.14, we need an expression for the length, l of the rod in terms of the total micelle aggregation number n. Recalling our spherocylindrical model (see Figure 4-2), we will assume that the density of material is about the same in the cylindrical body and in the hemispherical end caps. Thus, equating the number of monomers per unit volume in the two regions, we obtain the expression we need, namely:

$$\frac{n_0}{\frac{4}{3}\pi a^3} = \frac{n - n_0}{\pi a^2 l}, \tag{6.16}$$

remembering that from the spherocylindrical model, in a micelle with total ag-

gregation number $n > n_0$, each hemispherical end cap of radius a contains $n_0/2$ monomers and the cylindrical body of length l and radius a contains the remaining $n - n_0$ monomers. Solving for l, we obtain

$$l = \frac{4a}{3n_0}(n - n_0). \tag{6.17}$$

Since the form factor only becomes important when the length becomes comparable to the wavelength of light ($X \approx 1$, Equation 6.15) we can neglect the effects of the small ($\sim$ 3nm) end caps. Thus, we shall use the above expression for l in Equation 6.14 for the form factor. For a given solution composition, we will use for a, the hydrodynamic radius of the minimum sized micelles given by Equation 3.24. We will also use $n_0 = 135$, as obtained in Chapter 3. Having discussed a reasonable expression for the micellar form factor, we return to the question of an appropriate hydrodynamic model.

As was mentioned in Section 3.2.3, there exist many approximate expressions for the diffusivity of rodlike and wormlike particles [55]. However, most of these expressions for the diffusivity are limited in their range of validity to rods whose contour length is much larger than their diameter. We prefer to use the exact expression for the diffusivity of a prolate ellipsoid [56] as was used in Section 3.2.3, since we will be considering both elongated micelles (our data for $C_{12}E_6$) and micelles that are close to their minimum size (our data for $C_{12}E_8$). That is, we will use the expression

$$D(a,b) = \frac{k_B T \ln\left[\frac{1+(1-a^2/b^2)^{1/2}}{a/b}\right]}{6\pi\eta b(1-a^2/b^2)^{1/2}} \tag{6.18}$$

or equivalently

$$R_H(a,b) = \frac{b(1-a^2/b^2)^{1/2}}{\ln\left[\frac{1+(1-a^2/b^2)^{1/2}}{a/b}\right]} \tag{6.19}$$

where a is the semi-minor axis of the ellipsoid and b is the semi-major axis. We choose the semi-minor axis, a, for a given solution composition to be the same as the hydrodynamic radius of the minimum sized micelles for that solution composition as given by Equation 3.24. For a given value of n, the semi-major axis, b, will be

chosen in such a way so as to equate the volume of the prolate ellipsoid with the volume of our model prolate spherocylinder (also of radius a):

$$\frac{4}{3}\pi a^2 b = \pi a^2 l + \frac{4}{3}\pi a^3. \tag{6.20}$$

Having already obtained an expression for the length of the cylindrical portion of the spherocylinder (Equation 6.17), we obtain for b

$$b = \frac{3}{4}l + a = \frac{an}{n_0}. \tag{6.21}$$

Thus, using Equations 6.18, 6.14 and 6.13 in Equation 6.6 we can estimate $\bar{D}$ given a model for $\tilde{X}_n$. Likewise, we can use our measurements of $\bar{D}$ to give us some information about the parameters in our generalized ladder model.

6.1.2 Extracting the Two-Dimensional Ladder Model Parameters

The two-dimensional ladder model describes the concentration and composition dependence of the micellar distribution in terms of the four parameters $\Delta\mu^0_{sA}$, $\Delta\mu^0_{sB}$, $\Delta\mu^0_{cA}$ and $\Delta\mu^0_{cB}$. The temperature dependence of the micellar distribution is then reflected in a dependence on temperature of the four parameters. By using all of the appropriate measurements of $\bar{D}$ and the measurements of the scattering intensity from the micelles in the vicinity of the critical micellar concentration, we will extract values for the four parameters and examine their temperature dependence.

We recall from Chapter 4 that $\Delta\mu^0_{sA}$ represents the change in free energy of the solution per particle when n_0 amphiphiles of type A are transferred from water into a minimum micelle, and $\Delta\mu^0_{sB}$ represents the change in free energy of the solution per particle when n_0 amphiphiles of type B are transferred from water into a minimum micelle. Also, we recall that $\Delta\mu^0_{cA}$ represents the change in free energy of the solution when an amphiphile of type A is transferred from water into the cylindrical region of an elongated micelle, and $\Delta\mu^0_{cB}$ represents the change in free energy of the solution

when an amphiphile of type B is transferred from water into the cylindrical region of an elongated micelle. Recalling the single component ladder model, for a solution of pure surfactant A ($C_{12}E_6$), the ladder rung spacing is $\Delta\mu^0_{cA}$ and the ladder gap is $n_0\Delta\mu^0_{sA}$. Likewise, for a solution of pure surfactant B ($C_{12}E_8$), the ladder rung spacing is $\Delta\mu^0_{cB}$ and the ladder gap is $n_0\Delta\mu^0_{sB}$.

It will turn out that for total surfactant concentrations well above the critical micellar concentration, the average diffusivity, $\bar{D}$, is sensitive primarily to the two-dimensional ladder model parameter $K(\alpha^*)$, which from Chapter 4 we remember is determined by the differences $\Delta\mu_A/k_BT = (\Delta\mu^0_{sA} - \Delta\mu^0_{cA})/k_BT$ and $\Delta\mu_B/k_BT = (\Delta\mu^0_{sB} - \Delta\mu^0_{cB})/k_BT$. All of the measurements of $\bar{D}$ presented in Chapter 3, Figures 3-2 and 3-7 correspond to total concentrations well above the critical micellar concentration. In the vicinity of the critical micellar concentration, the micellar distribution becomes sensitive to the parameters $\Delta\mu^0_{cA}/k_BT$ and $\Delta\mu^0_{cB}/k_BT$ directly. Thus, our measurements of the intensity of light scattered from the micelles in the vicinity of the critical micellar concentration for pure $C_{12}E_6$ solutions and pure $C_{12}E_8$ solutions will allow us to determine $\Delta\mu^0_{cA}/k_BT$ and $\Delta\mu^0_{cB}/k_BT$. Using the values of $\Delta\mu_A/k_BT$ and $\Delta\mu_B/k_BT$ determined previously, we can find the values of $\Delta\mu^0_{sA}/k_BT$ and $\Delta\mu^0_{sB}/k_BT$.

Our method of extracting the two-dimensional ladder model parameters will proceed as follows. Using the theoretical considerations of Chapter 4, we will provide an estimate of the parameters $\Delta\mu^0_{cA}/k_BT$ and $\Delta\mu^0_{cB}/k_BT$ from the value of the critical micellar concentration for pure $C_{12}E_6$ solutions and pure $C_{12}E_8$ solutions. Fixing these parameters, we then fit our measurements of $\bar{D}$ well above the critical micellar concentration, but in the region where intermicellar interactions may still be neglected with the two-dimensional ladder model, precisely determining the values of $\Delta\mu_A/k_BT$ and $\Delta\mu_B/k_BT$. Having determined $\Delta\mu_A/k_BT$ and $\Delta\mu_B/k_BT$, we will fit the two-dimensional ladder model to our measurements of the intensity of light scattered from the micelles in the vicinity of the critical micellar concentration in order to more accurately redetermine the parameters $\Delta\mu^0_{cA}/k_BT$ and $\Delta\mu^0_{cB}/k_BT$. We then fix these new values of $\Delta\mu^0_{cA}/k_BT$ and $\Delta\mu^0_{cB}/k_BT$ and fit our measurements

of $\bar{D}$ once again, to verify that the dependence of the values of $\Delta\mu_A/k_BT$ and $\Delta\mu_B/k_BT$ extracted from our measurements of $\bar{D}$ depend only weakly on the values of $\Delta\mu^0_{cA}/k_BT$ and $\Delta\mu^0_{cB}/k_BT$. We now proceed through the fitting procedure in detail.

At a given temperature, the parameters $\Delta\mu^0_{sA}$, $\Delta\mu^0_{sB}$, $\Delta\mu^0_{cA}$ and $\Delta\mu^0_{cB}$ were obtained as follows. First, $\Delta\mu_A/k_BT = (\Delta\mu^0_{sA} - \Delta\mu^0_{cA})/k_BT$ and $\Delta\mu_B/k_BT = (\Delta\mu^0_{sB} - \Delta\mu^0_{cB})/k_BT$ were extracted from the dependence on concentration and composition of $\bar{D}$ well above the critical micellar concentration, but below $X = 1 \times 10^{-3}$, where (as was discussed in Chapter 3) the interpretation of our data in terms of an actual particle size is reasonable. We first justify that in the regions well above the critical micellar concentration, the micellar distribution should be sensitive primarily to $\Delta\mu_A/k_BT$ and $\Delta\mu_B/k_BT$. We then provide initial theoretical estimates of $\Delta\mu^0_{cA}/k_BT$ and $\Delta\mu^0_{cB}/k_BT$, and describe the fitting procedure used to extract $\Delta\mu_A/k_BT$ and $\Delta\mu_B/k_BT$. It should be noted here that since the data for $\alpha_s = 0.501$ (see Figure 3-7) was obtained using a different instrument from the remaining data, the temperatures at which the data was collected are slightly different. Values of $\bar{D}$ (and R_H) at the needed temperatures were inferred for $\alpha_s = 0.501$ from the raw data by interpolation.

That our measurements of $\bar{D}$ should be sensitive primarily to the differences $\Delta\mu_A/k_BT$ and $\Delta\mu_B/k_BT$ and not to any of the four parameters directly is understandable from the form of the mass conservation equations, Equation 4.146 and Equation 4.147. Since the lowest concentration measured (5×10^{-5}) is an order of magnitude above the critical micellar concentration for either surfactant, most of the surfactant exists as micelles, and X_1 will be small compared to the second and third terms in Equation 4.146. The value of $\Lambda = X_1 e^{-B(\alpha^*)}$ is determined quite precisely from the equation, due to the large power of n_0. Changing the value of the effective rung spacing $\delta(\alpha^*) = \alpha^*\Delta\mu^0_{cA} + (1-\alpha^*)\Delta\mu^0_{cB}$, (and thus $B(\alpha^*)$) will cause a shift in X_1 so as to keep Λ nearly fixed. Since X_1 is small compared to X, it can shift a large percentage of its initial value without strongly affecting the determination of Λ. Therefore, in this regime, the value of Λ, and thus the micellar

distribution is only weakly dependent on $\delta(\alpha^*)$, which depends directly on $\Delta\mu_{cA}^0$ and $\Delta\mu_{cB}^0$. The value of Λ is primarily determined from $K(\alpha^*)$, which is a function only of the differences $\Delta\mu_A/k_BT$ and $\Delta\mu_B/k_BT$. Although we have made our explanation in terms of the simplified treatment of the generalized ladder model presented in Chapter 4, examination of the corresponding equations in Appendix B will show that the same explanation is valid in the full treatment of the problem.

In Section 4.2.7, we concluded that the quantity $e^{B(\alpha^*)}$ must be of the same order as the critical micellar concentration. This suggests the following procedure. Using our determinations of the critical micellar concentration, we estimate $\Delta\mu_{cA}^0$ and $\Delta\mu_{cB}^0$ by equating $e^{B(1)}$ to the critical micellar concentration for pure $C_{12}E_6$, and $e^{B(0)}$ to the critical micellar concentration for pure $C_{12}E_8$. Thus, we have the simple relations

$$\Delta\mu_{cA}^0 = k_BT \ln X_{CMC}^{(C_{12}E_6)} \tag{6.22}$$

$$\Delta\mu_{cB}^0 = k_BT \ln X_{CMC}^{(C_{12}E_8)}. \tag{6.23}$$

Having fixed the values of $\Delta\mu_{cA}^0$ and $\Delta\mu_{cB}^0$, we extract the values of $\Delta\mu_A/k_BT$ and $\Delta\mu_B/k_BT$ from the measurements of $\bar{D}$. This is done as follows. At fixed values of $\Delta\mu_A/k_BT$ and $\Delta\mu_B/k_BT$, we numerically solve the mass conservation relations and obtain the micellar distribution for each concentration and composition measured. These distributions are used in the hydrodynamic model described above to give estimates of $\bar{D}$. A gradient descent minimization procedure is used to adjust $\Delta\mu_A/k_BT$ and $\Delta\mu_B/k_BT$ such that the mean square deviation of the calculated points from the measured points is minimal. We should also note here that the fitting procedure incorporates the full treatment of the generalized ladder model, discussed in Appendix B.

Having precisely determined the differences $\Delta\mu_A/k_BT$ and $\Delta\mu_B/k_BT$, we are in a position to more accurately determine $\Delta\mu_{cA}^0$ and $\Delta\mu_{cB}^0$. As was mentioned earlier, $\Delta\mu_{cA}^0$ and $\Delta\mu_{cB}^0$ are sensitive to measurements in the region near the critical micellar concentration. In Section 3.2.4, we presented measurements of the scattered inten-

sity from the micelles in the vicinity of the critical micellar concentration for pure $C_{12}E_6$ solutions and for pure $C_{12}E_8$ solutions. These data were used in Chapter 3 to estimate the critical micellar concentration. We shall also use these measurements here to extract values for $\Delta\mu^0_{cA}$ and $\Delta\mu^0_{cB}$. We proceed as follows.

The intensity of light scattered from the micelles is proportional to the second moment of the (renormalized) micellar distribution if we neglect the small effects of the form factor (see Equation 6.13). Using the generalized ladder model with fixed values of $\Delta\mu^0_{cA}$ and $\Delta\mu^0_{cB}$ and knowing $\Delta\mu_A/k_BT$ and $\Delta\mu_B/k_BT$ from our preliminary fitting described above, we can calculate the second moment of the distribution as a function of total surfactant concentration and fit to our measurements. We estimate $\Delta\mu^0_{cA}$ and $\Delta\mu^0_{cB}$ by varying $\Delta\mu^0_{cA}$ (for the $C_{12}E_6$ data) or $\Delta\mu^0_{cB}$ (for the $C_{12}E_8$ data) until the fit of the theoretical prediction of the concentration dependence of the second moment of the micellar distribution to the experimental data is optimal. It should be noted that for the $T = 49°C$ $C_{12}E_6$ data that the appropriate value of $\Delta\mu_A/k_BT$ was found by interpolating between 45°C and 50°C and for the $T = 51°C$ $C_{12}E_8$ data that the appropriate value of $\Delta\mu_B/k_BT$ was found by interpolating between 50°C and 55°C.

The fits of the generalized ladder model to the measurements of micelle scattering intensity in the vicinity of the critical micellar concentration are shown in Figures 6-1 and 6-2. The values of $\Delta\mu^0_{cA}$ and $\Delta\mu^0_{cB}$ obtained from each plot are also shown. The values of $\Delta\mu^0_{cA}$, when plotted as a function of temperature (see Figure 6-3) show no identifiable dependence on temperature. Therefore, we took $\Delta\mu^0_{cA}$ to be roughly temperature independent, with a value equal to the average of the measurements, that is, $\Delta\mu^0_{cA} = -13.36$. In the case of amphiphile B ($C_{12}E_8$), we had only two measurements of the scattered intensity versus concentration near the critical micellar concentration. One set of measurements was taken at $T = 25°C$ and is shown in Figure 6-1. The other set of measurements was taken at $T = 51°C$, and is shown in Figure 6-2(f). As we did for $C_{12}E_6$, we took $\Delta\mu^0_{cB}$ to be temperature independent, with a value equal to the average of our measurements, that is, $\Delta\mu^0_{cB} = -12.94$. The predictions of the two-dimensional ladder model in the

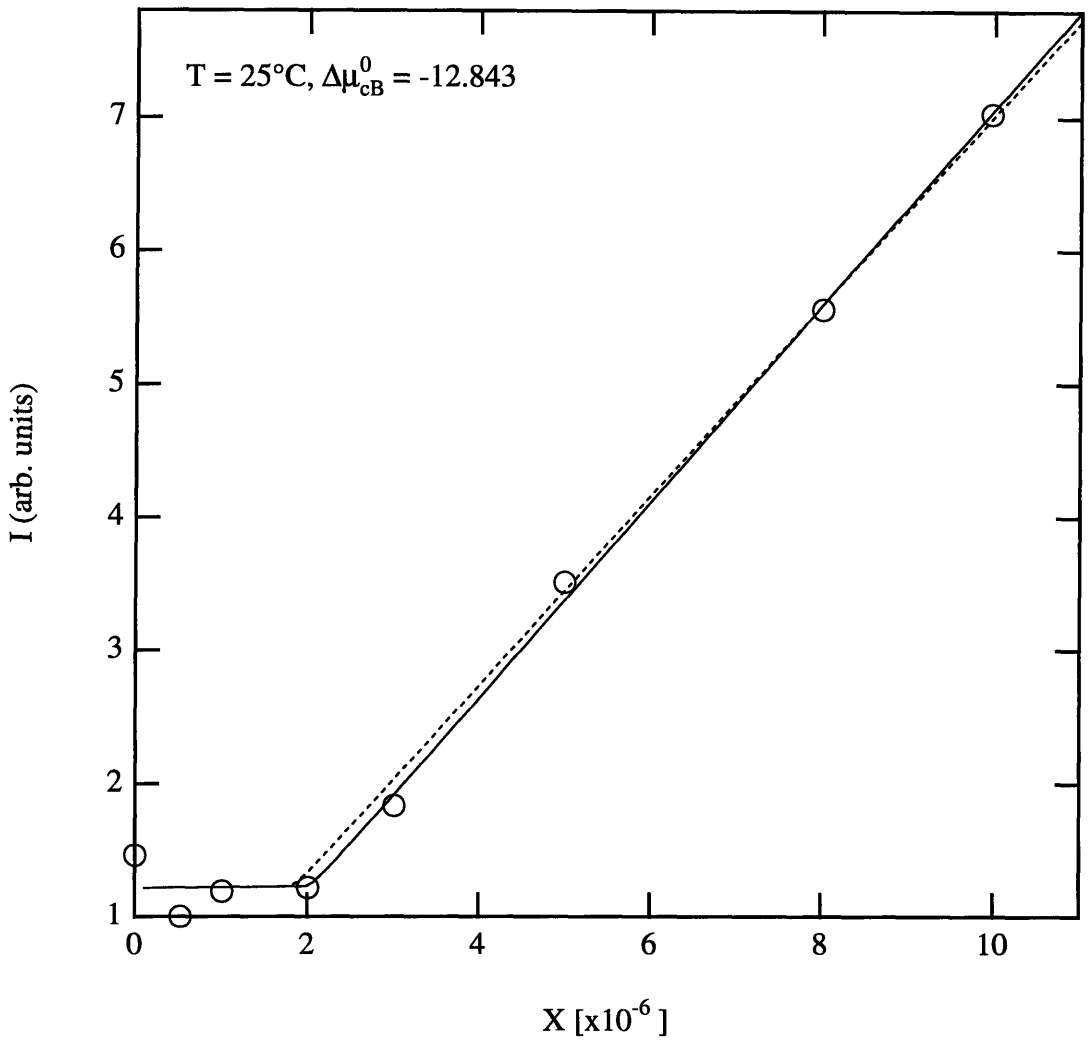

Figure 6-1: The Intensity of light scattered from micelles plotted as a function of total surfactant concentration in the vicinity of the critical micelle concentration for solutions of pure $C_{12}E_8$ at $T = 25°C$. The solid line is the optimal fit of the data to the two-dimensional ladder model. We find $\Delta\mu^0_{cB} = -12.843$. The dashed line is a fit of the data to the two-dimensional ladder model with $\Delta\mu^0_{cB}$ taken as the average of the optimal values of $\Delta\mu^0_{cB}$ found from the data for pure $C_{12}E_8$ at 25°C and 51°C ($\Delta\mu^0_{cB} = -12.94$).

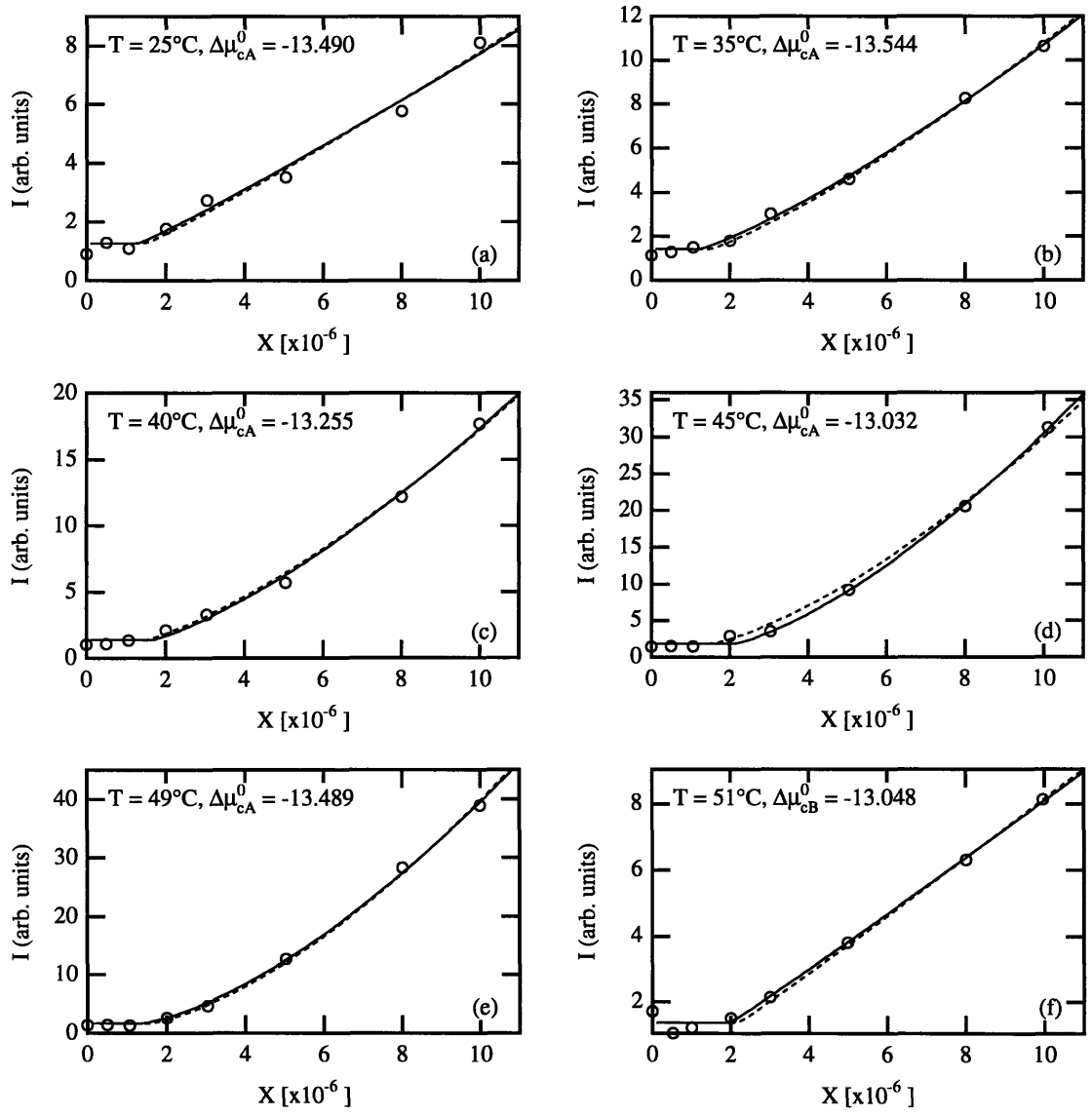

Figure 6-2: The Intensity of light scattered from micelles plotted as a function of total surfactant concentration in the vicinity of the critical micelle concentration for solutions of pure $C_{12}E_6$ and pure $C_{12}E_8$ at various temperatures. The solid lines indicate fits to the generalized ladder model with the parameters as indicated in the graphs. The dashed lines are fits to the generalized ladder model with $\Delta\mu^0_{cA}$ or $\Delta\mu^0_{cB}$ fixed to the average value of all of the measurements for either $C_{12}E_6$ or $C_{12}E_8$.

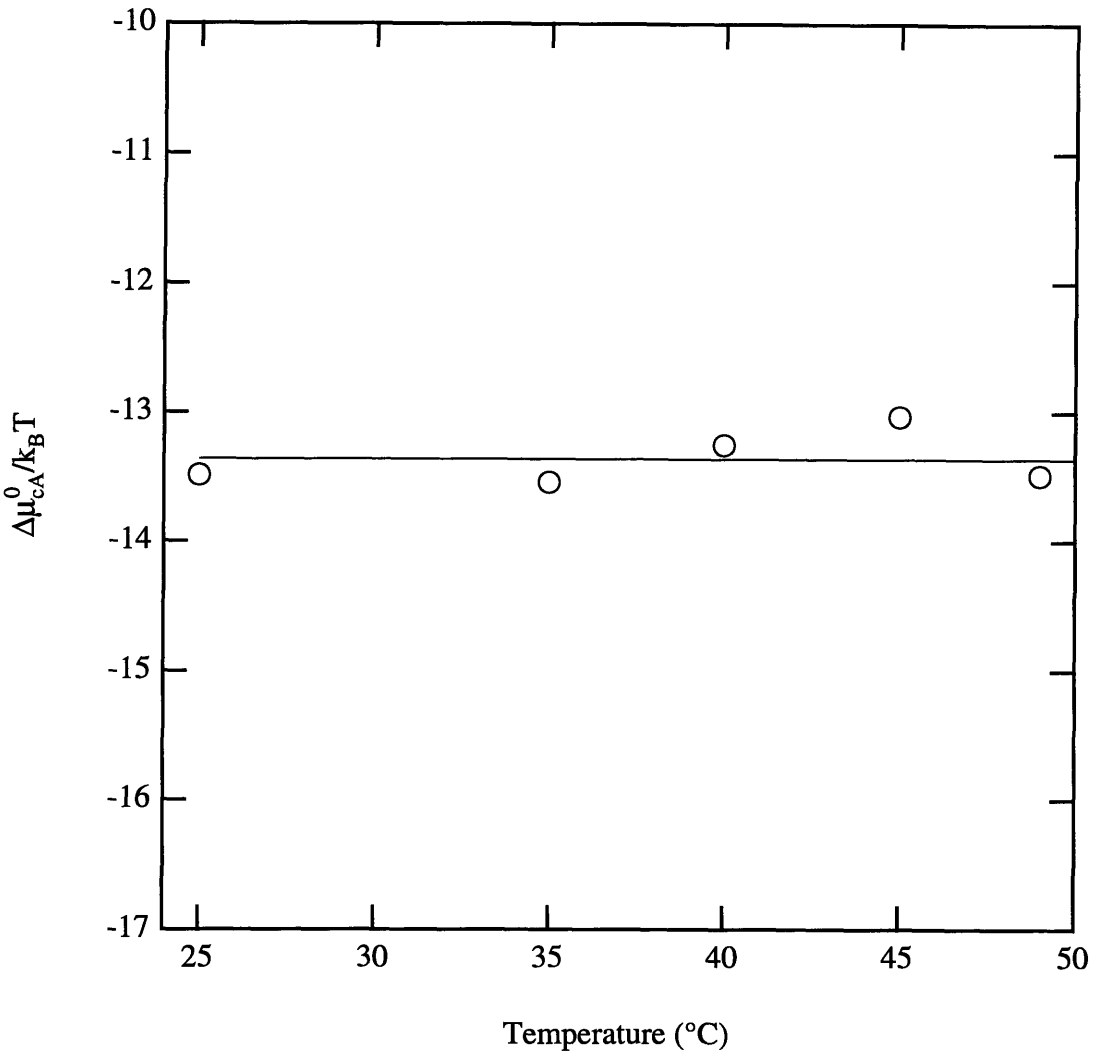

Figure 6-3: The values of $\Delta\mu^0_{cA}$ extracted from the data in the vicinity of the critical micellar concentration for pure $C_{12}E_6$ plotted as a function of temperature. The line represents the average value of the measurements.

vicinity of the critical micellar concentration with $\Delta\mu_{cA}^0$ and $\Delta\mu_{cB}^0$ fixed to these average values are also shown in Figures 6-1 and 6-2.

After obtaining the accurate estimates of $\Delta\mu_{cA}^0$ and $\Delta\mu_{cB}^0$, we repeat the procedure of fitting to our measurements of $\bar{D}$. It was found, as we expected, that the values of $\Delta\mu_A/k_BT$ and $\Delta\mu_B/k_BT$ did not differ significantly from their preliminary estimates.

Fits of the two-dimensional ladder model to our quasielastic light scattering measurements of $\bar{D}$ (shown as hydrodynamic radii) from $T = 30°C$ to $T = 55°C$ are presented in Figures 6-4 and 6-5. We recall that all of these measurements correspond to the region well above the critical micellar concentration for either surfactant and below $X = 1 \times 10^{-3}$, so that, as mentioned earlier, intermicellar interactions may be neglected. Note that the fit for $T = 55°C$ does not contain any data for pure $C_{12}E_6$, since the critical temperature for phase separation in the pure $C_{12}E_6$ and water system is $T_C = 51.1°C$. We have only attempted to fit our data for which $X < 1 \times 10^{-3}$ where we have assumed, as discussed in Chapter 3, that the measured diffusivity can be interpreted in terms of a particle size. We note that the theoretical curves fit the data reasonably well.

The final values of $\Delta\mu_A/k_BT = (\Delta\mu_{sA}^0 - \Delta\mu_{cA}^0)/k_BT$ and $\Delta\mu_B/k_BT = (\Delta\mu_{sB}^0 - \Delta\mu_{cB}^0)/k_BT$ extracted from the measurements in Figures 6-4 and 6-5 are presented in Figure 6-6. The open and closed circles represent the values of $\Delta\mu_A/k_BT$ and $\Delta\mu_B/k_BT$ obtained from the fitting procedure described above. The filled diamonds indicate values of $\Delta\mu_B/k_BT$ found from additional dynamic light scattering measurements made on pure $C_{12}E_8$ at the temperatures indicated. These data are tabulated in Appendix D. We recall that in the region of strong micellar growth, the weight-averaged aggregation number scales like $\langle n \rangle_W \sim \sqrt{KX}$ with $\ln K = n_0 \left(\Delta\mu_{sA}^0 - \Delta\mu_{cA}^0\right)/k_BT$ for pure $C_{12}E_6$ solutions and with $\ln K = n_0 \left(\Delta\mu_{sB}^0 - \Delta\mu_{cB}^0\right)/k_BT$ for pure $C_{12}E_8$ solutions. Therefore, the magnitude of these parameters indicate the tendency for micellar growth in the pure systems. From the figure, we see that the magnitude of $\Delta\mu_A/k_BT$ is always greater than the magnitude of $\Delta\mu_B/k_BT$, which is consistent with the observation that at a fixed temperature

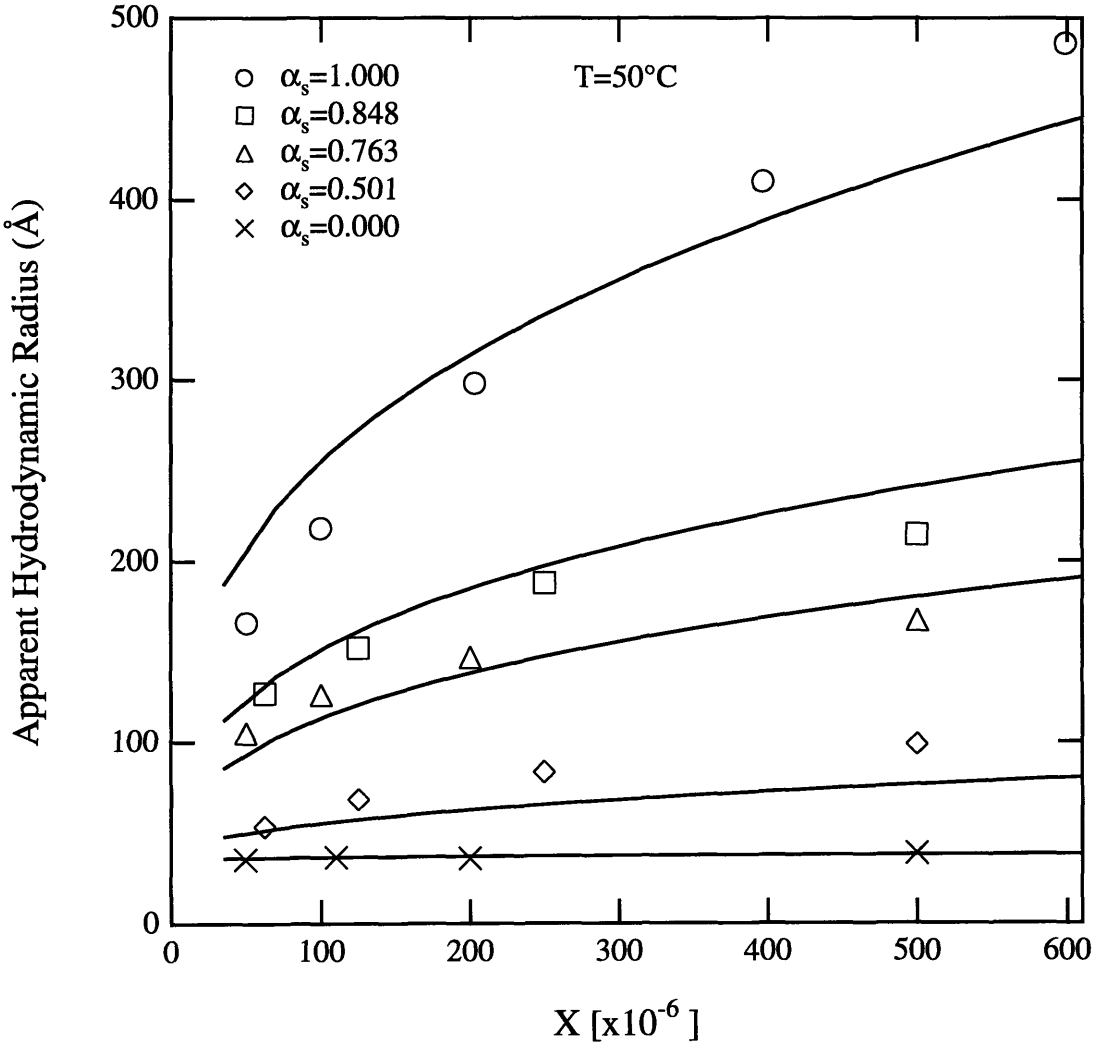

Figure 6-4: The apparent hydrodynamic radius is plotted against total surfactant concentration at $T = 50°C$ for the various relative compositions studied. The curves are fits to the two-dimensional ladder model. Note that only the data for which $X < 1 \times 10^{-3}$ was included in the fit.

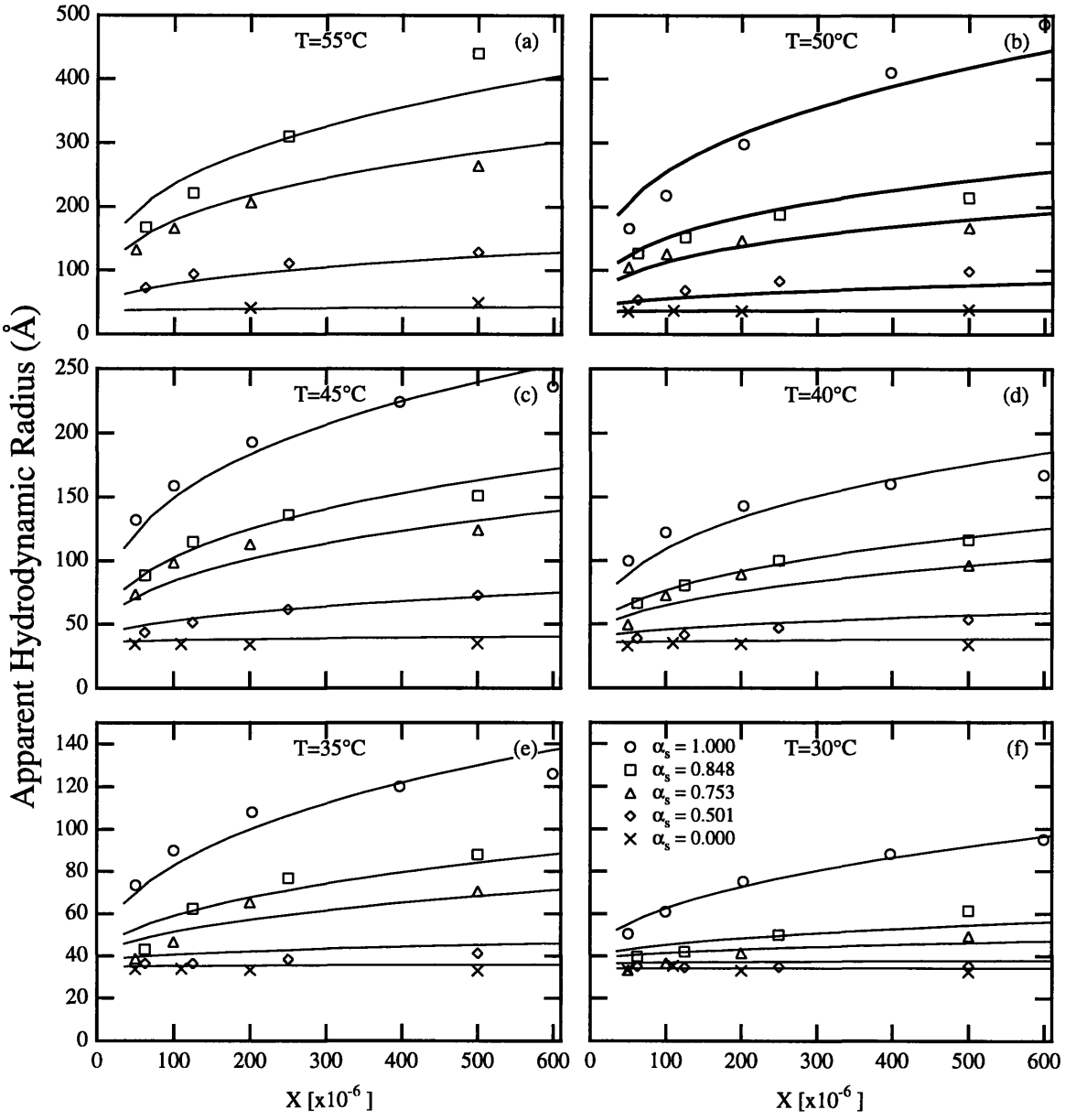

Figure 6-5: The apparent hydrodynamic radius is plotted against total surfactant concentration for various relative compositions studied at: $T = 55°C$ (a), $T = 50°C$ (b), $T = 45°C$ (c), $T = 40°C(d)$, $T = 35°C$ (e) and $T = 30°C$ (f). The symbols have the same meanings as in Figure 6-4. The curves are fits to the two-dimensional ladder model. Note that only the data for which $X < 1 \times 10^{-3}$ was included in the fit.

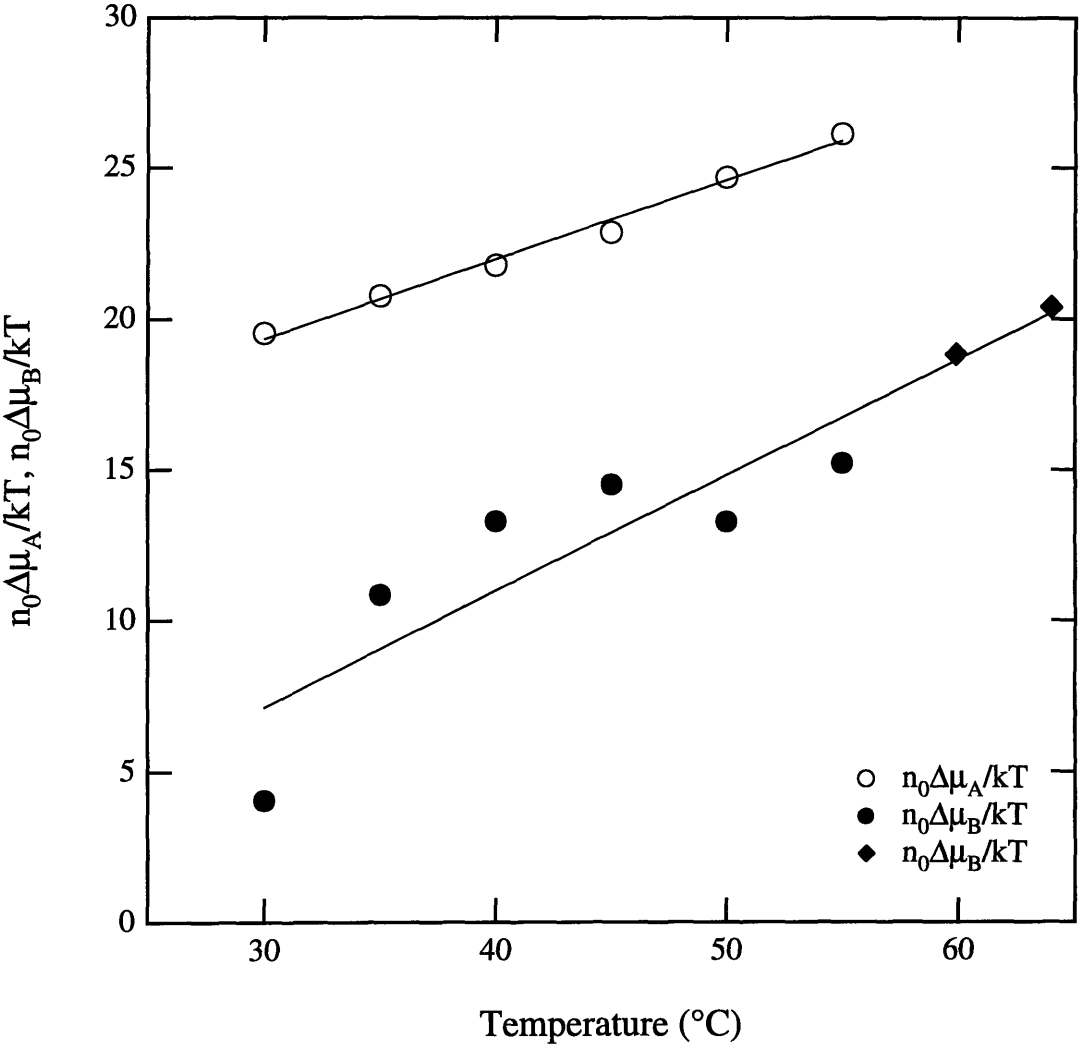

Figure 6-6: The two-dimensional ladder model growth parameters $n_0\Delta\mu_A/k_BT = n_0(\Delta\mu^0_{sA} - \Delta\mu^0_{cA})/k_BT$ and $n_0\Delta\mu_B/k_BT = n_0(\Delta\mu^0_{sB} - \Delta\mu^0_{cB})/k_BT$ for the $C_{12}E_6$, $C_{12}E_8$ and water system are plotted as a function of temperature. The open and closed circles represent the values of $n_0\Delta\mu_A/k_BT$ and $n_0\Delta\mu_B/k_BT$, respectively, extracted from the data presented in Figures 6-4 and 6-5. The closed diamonds represent values of $n_0\Delta\mu_B/k_BT$ found from additional dynamic light scattering measurements made on pure $C_{12}E_8$ at the temperatures indicated. These data are tabulated in Appendix D. We recall that, for our system, $n_0 = 135$.

$C_{12}E_6$ is observed to exhibit stronger growth than $C_{12}E_8$. We note further that the values for $\Delta\mu_A/k_BT$ all fall on a straight line with positive slope. This positive slope is physically reasonable, since it indicates the tendency of the micelles of $C_{12}E_6$ to grow with increasing temperature.

The temperature dependence of $\Delta\mu_B/k_BT = (\Delta\mu^0_{sB} - \Delta\mu^0_{cB})/k_BT$ is similar to the temperature dependence of $\Delta\mu_A/k_BT = (\Delta\mu^0_{sA} - \Delta\mu^0_{cA})/k_BT$, although it is clear from the figure that the values of $\Delta\mu_B/k_BT$ are much less well determined. The quantities $\Delta\mu_A/k_BT$ and $\Delta\mu_B/k_BT$ are accurately determined only in the limit of strong micellar growth. Since for $C_{12}E_8$ (amphiphile B) there is no strong micellar growth over the temperature range studied, the values of $\Delta\mu_B/k_BT$ are not well determined. It is clear, however, that a linear dependency of $\Delta\mu_B/k_BT$ with temperature is adequate to explain the data in this temperature region.

Using the values of $\Delta\mu^0_{cA}$ and $\Delta\mu^0_{cB}$ obtained from the measurements in the vicinity of the critical micellar concentration, we can now compute $\Delta\mu^0_{sA}$ and $\Delta\mu^0_{sB}$. All four of the two-dimensional ladder model parameters are plotted as functions of temperature in Figure 6-7. The structure of the two-dimensional ladder is identical with Figure 4-4 from Chapter 4. We note that in the figure, $n_0 = 135$ and for different temperatures, T, $\Delta\mu^0_{sA}$, $\Delta\mu^0_{sB}$, $\Delta\mu^0_{cA}$ and $\Delta\mu^0_{cB}$ take on the values as shown in Figure 6-7.

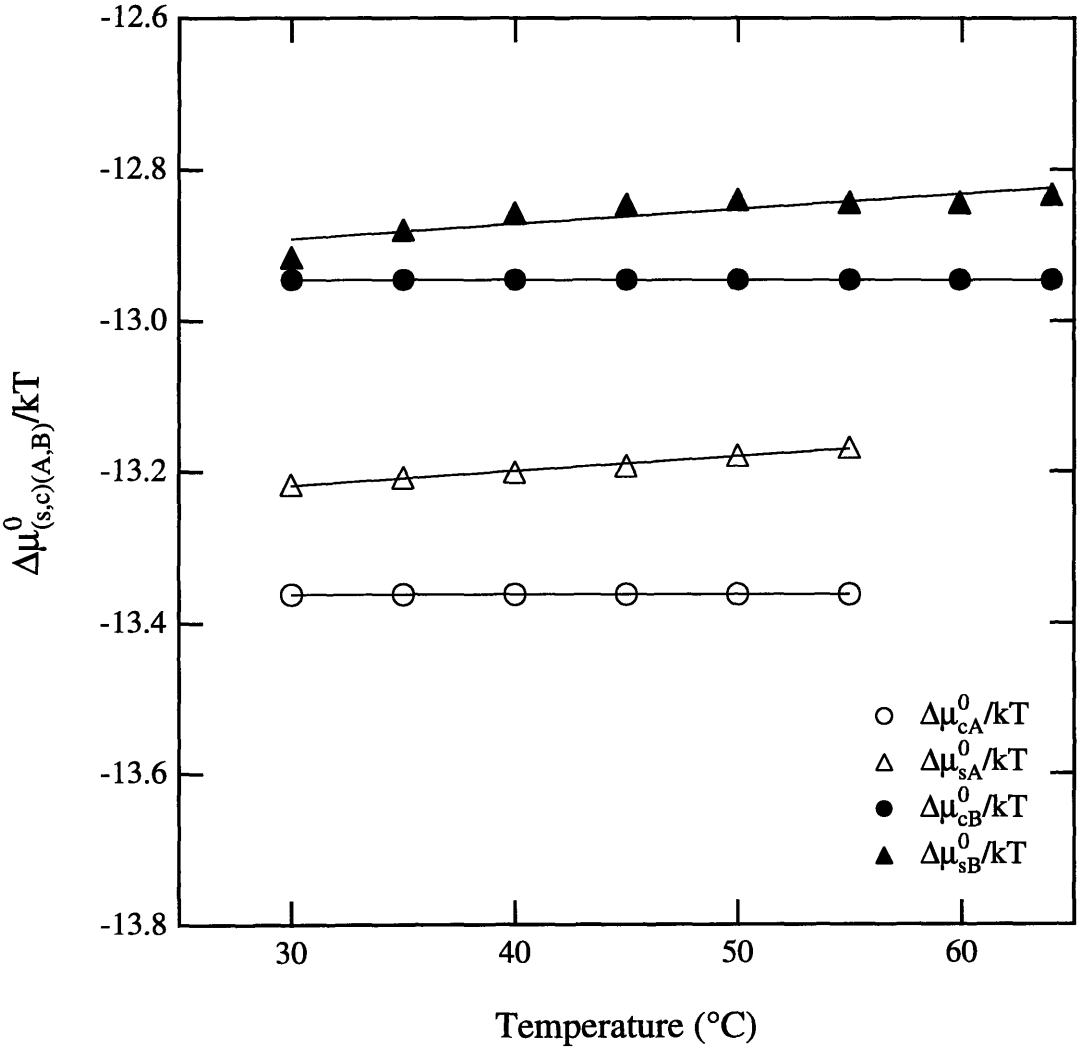

Figure 6-7: The four two-dimensional ladder model parameters $\Delta\mu^0_{sA}$, $\Delta\mu^0_{sB}$, $\Delta\mu^0_{cA}$ and $\Delta\mu^0_{cB}$ are plotted as functions of temperature.

6.2 The Molecular-Thermodynamic Model

In Section 5.3, we presented the basic ideas underlying the molecular model of Puvvada and Blankschtein [17], including a particular microscopic model of a micelle and the thought process they have used in order to identify the physical origin of the important contributions to the free energy of micellization. We then identified the relationships between their calculations and the physically significant parameters of the generalized ladder model.

The actual computations of the micellization free energy, ΔG_{mic} for the mixed $C_{12}E_6$, $C_{12}E_8$ and water system were carried out using a computer program supplied by S. Puvvada. This program evaluates numerically the magnitudes of the various contributions to the micellization free energy as described in Reference [17], sums these contributions and computes, based on the Gibbs free energy model discussed in Chapter 5 and Reference [16], such quantities as the critical micellar concentration, the weight-averaged micellar aggregation number and the location and shape of the coexistence curve for liquid-liquid phase separation.

Using this computational procedure and the relations 5.39-5.42, the predictions of the molecular-thermodynamic model were examined and compared with the physically meaningful parameters extracted from our generalized ladder model analysis. Most important are the predictions of the growth parameters $\Delta\mu_A$ and $\Delta\mu_B$. These are compared in Figure 6-8. We see that the predictions of the molecular model are in excellent agreement with the growth parameters obtained from our experimental data.

It should be noted here, however, that in order to obtain this excellent agreement, a slight modification to the molecular parameters in the computation of g_{st}, the steric free energy, was made. According to the model of Puvvada and Blankschtein [17], the steric free energy considers the contribution to the total free energy of micellization from the steric repulsions of the hydrophilic heads at the surface of the

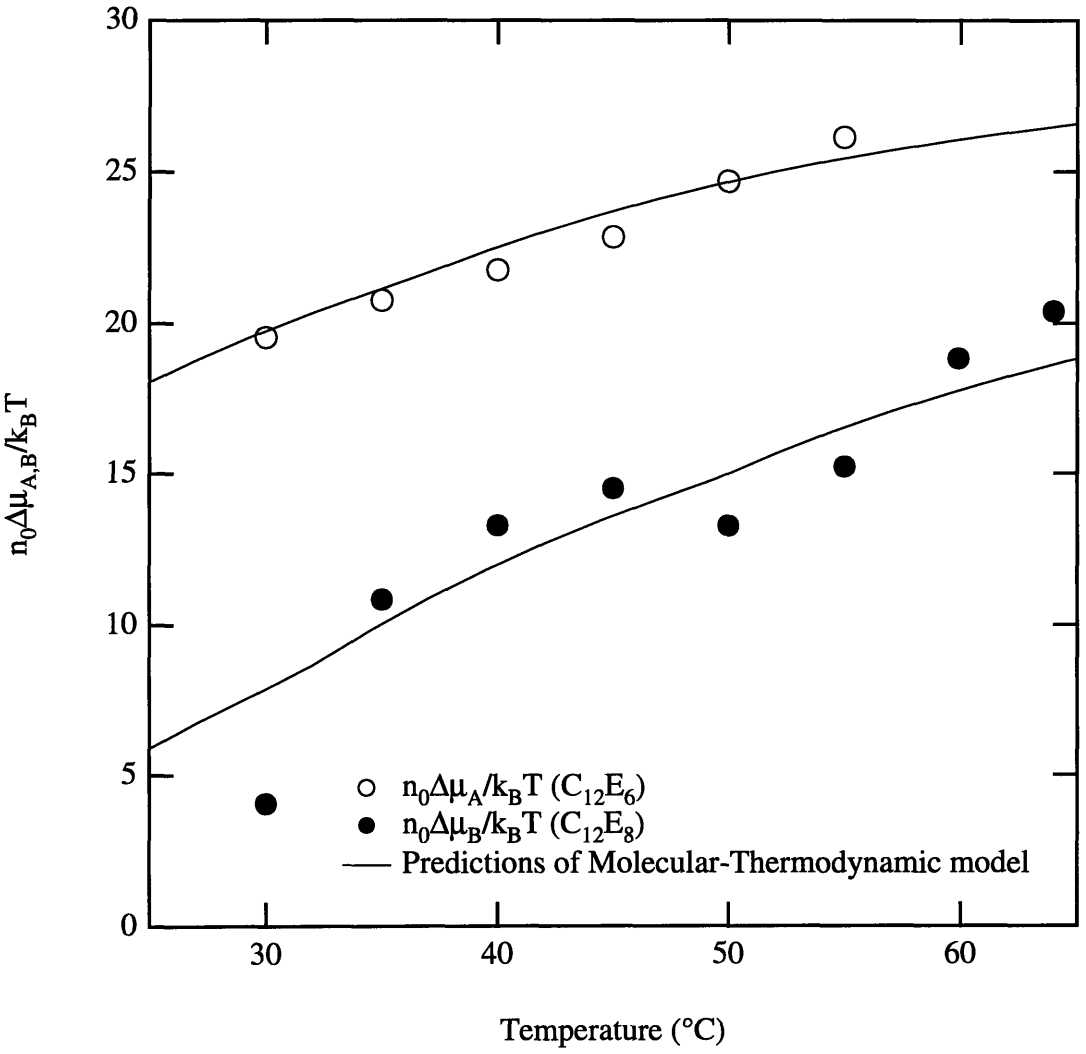

Figure 6-8: The predictions of the growth parameters $\Delta\mu_A$ and $\Delta\mu_B$ from the molecular model of Puvvada and Blankschtein

micelle. They model this contribution

$$g_{st} = -k_B T \ln \left[1 - \frac{\alpha a_{hA} + (1-\alpha) a_{hB}}{a} \right] \tag{6.24}$$

with a_{hA} as the average cross-sectional area of a surfactant A head, a_{hB} as the average cross-sectional area of a surfactant B head and a as the total area at the surface per surfactant monomer. We can see from the form of Equation 6.24 that the steric free energy has been modeled as an entropic contribution to the total free energy of micellization. The argument of the logarithm reflects the fractional reduction of available area at the micellar surface in which a new head group can be placed. As such, it represents the reduction in possible configurations available for an additional head due to the presence of existing heads at the micellar surface. Clearly, it has also been assumed that the concentration of head groups on the surface is small enough so that their excluded volumes may be considered in an additive fashion.

Puvvada and Blankschtein [17] propose a simple scaling argument to estimate the values of the parameters a_{hA} and a_{hB}. The area per head group should vary with temperature, reflecting the fact that the ethylene oxide groups of the C_iE_j surfactants are hydrated in aqueous solution, and that the extent of their hydration should decrease with temperature. They proposed that the area per head group for a surfactant species with j ethylene oxide groups, a_{hj} should vary linearly with temperature:

$$a_{hj} = a_{hj}^0 \left[1 - H(T - 298) \right], \tag{6.25}$$

where T is the absolute temperature and H reflects the decrease of the cross-sectional head group area with temperature. In a previous paper [15], Puvvada and Blankschtein applied a simplified version of the molecular model, considering only solutions containing a single surfactant species, to the $C_{12}E_6$ and water system. They found that for $C_{12}E_6$ $a_{h6}^0 = 38.1\text{Å}^2$ and $H = 0.0075K^{-1}$. Their value for H was determined by fitting the temperature dependence of the critical micellar concentration for $C_{12}E_6$. Considering the extremely weak dependence of the crit-

ical micellar concentration with temperature in the $C_{12}E_6$ and water system, the parameter H is not determined with great accuracy by this method. In order to compute the cross sectional area for other surfactants in the C_iE_j family, they suggested a scaling relation for how the area per head group at a given temperature should depend on the hydrophilic head group length: $a_{hj} \sim j^{0.8}$. Thus, for $C_{12}E_8$, $a^0_{h8} = 38.1 \times (8/6)^{0.8} = 48.0\text{Å}^2$ and $H = 0.0075K^{-1}$.

We found that using this simple scaling argument to relate the cross-sectional area per head group of $C_{12}E_8$ to $C_{12}E_6$ gave too high a value for the cross sectional area per head group for $C_{12}E_8$. We also found that the value of H was too high for the case of $C_{12}E_8$, resulting in an over-dehydration of the micellar heads with increasing temperature. We have assumed that our data provides a more sensitive estimation of these parameters. In order to obtain the predictions presented in Figure 6-8, we kept the linear temperature dependence, but estimated the cross sectional areas per head group for $C_{12}E_6$ and $C_{12}E_8$ according to:

$$a_{hA} = a^0_{h6}[1 - H_6(T - 298)] \tag{6.26}$$

$$a_{hB} = a^0_{h8}[1 - H_8(T - 298)] \tag{6.27}$$

with the parameters a^0_{hj} and H_j given in Table 6.1.

Table 6.1: Estimates of a^0_{hj} and H_j for $C_{12}E_6$ and $C_{12}E_8$

	$a^0_{hj}(\text{Å}^2)$	$H_j(K^{-1})$
$C_{12}E_6$	38.8	0.00725
$C_{12}E_8$	44.9	0.00559

In addition to predicting the growth parameters $\Delta\mu_A$ and $\Delta\mu_B$, we can use the molecular model of Puvvada and Blankschtein to compute the parameters $\Delta\mu^0_{cA}$ and $\Delta\mu^0_{cB}$ that are determined in the two-dimensional ladder model by fitting to our measurements in the vicinity of the critical micellar concentration. The predictions, as well as the experimental measurements are presented in Table 6.2.

Table 6.2: Predictions of $\Delta\mu^0_{cA}$ and $\Delta\mu^0_{cB}$ using the molecular model

$\Delta\mu^0_{cA}/k_BT$ ($C_{12}E_6$)		
T (°C)	Measured[a]	Prediction
25	-13.5	-13.57
35	-13.5	-13.65
40	-13.3	-13.69
45	-13.0	-13.72
49	-13.5	-13.74
$\Delta\mu^0_{cB}/k_BT$ ($C_{12}E_8$)		
T (°C)	Measured	Prediction
25	-12.8	-13.03
51	-13.0	-13.30

[a]Measurement accuracy about ±0.5

In Chapter 4, we assumed that in our two-dimensional ladder model, the parameters $\Delta\mu^0_{sA}$, $\Delta\mu^0_{sB}$, $\Delta\mu^0_{cA}$ and $\Delta\mu^0_{cB}$are independent of composition, α. This means that the quantities $\Delta(\alpha)/n_0 = \alpha\Delta\mu^0_{sA} + (1-\alpha)\Delta\mu^0_{sB}$ and $\delta(\alpha) = \alpha\Delta\mu^0_{cA} + (1-\alpha)\Delta\mu^0_{cB}$ should be linear functions of α. We now wish to check whether or not this assumption is consistent with the treatment of Puvvada and Blankschtein. The predictions of the molecular model for $\Delta(\alpha)/n_0$ and $\delta(\alpha)$ are plotted as a function of micelle relative composition at $T = 50$°C in Figure 6-9. The linear dependence of these quantities on composition is clearly evident. We conclude that the calculations of Puvvada and Blankschtein for the $C_{12}E_6$, $C_{12}E_8$ and water system are consistent with our assumption that $\Delta\mu^0_{sA}$, $\Delta\mu^0_{sB}$, $\Delta\mu^0_{cA}$ and $\Delta\mu^0_{cB}$are independent of composition.

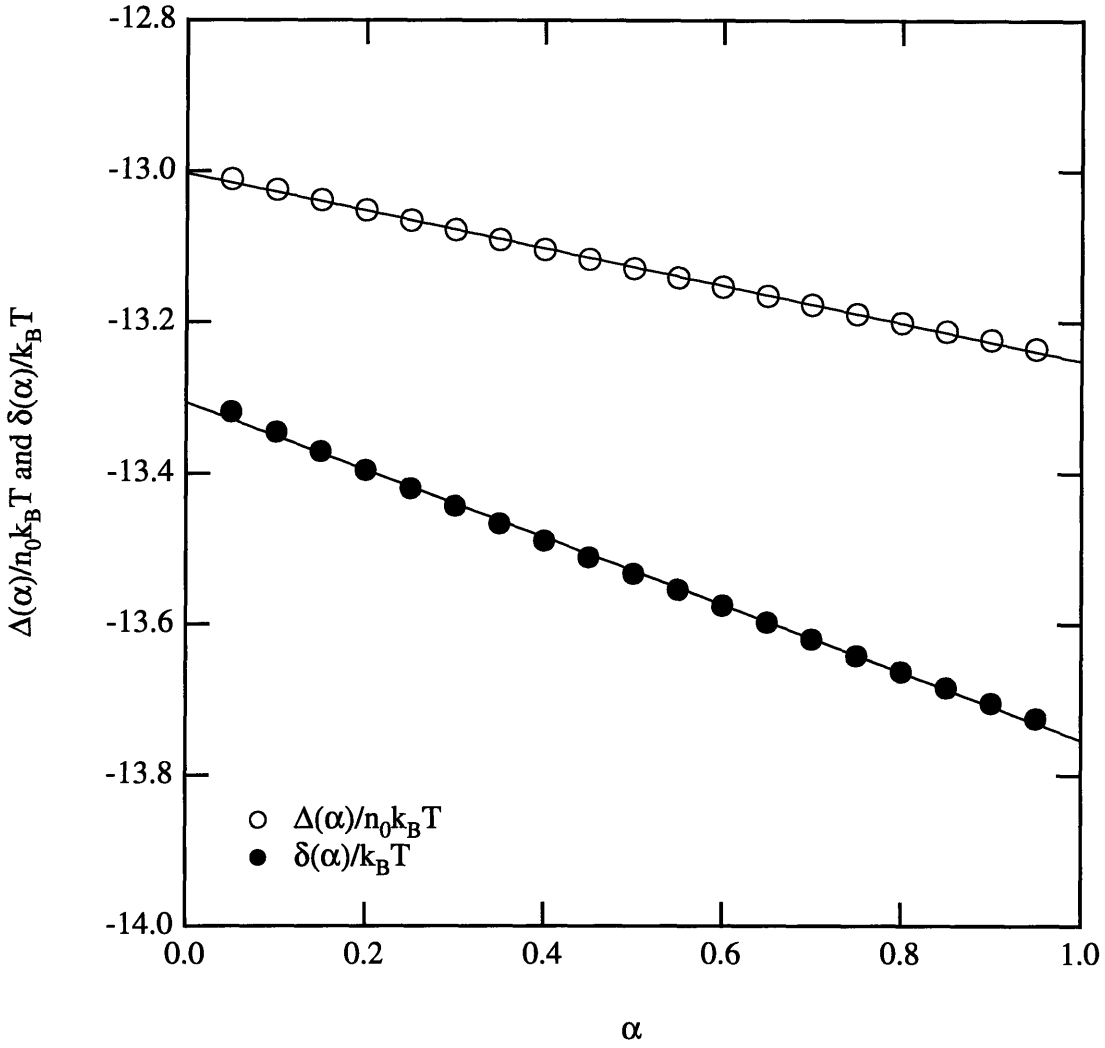

Figure 6-9: The quantities $\Delta(\alpha)/n_0 k_B T$ and $\delta(\alpha)/k_B T$ computed using the molecular-thermodynamic model of Puvvada and Blankschtein [16, 17] and plotted as a function of relative micelle composition α. The curves represent best fits to a straight line.

6.3 Intermicellar Interactions

To this stage we have analyzed and discussed only that subset of our experimental data for which a case can be made for neglecting the effects of intermicellar interactions. In Chapter 3, however, we saw clearly that at higher concentrations and temperatures these interactions become increasingly important, and may not be neglected. Unfortunately, aside from the possibility of complicated molecular dynamics simulations, there exists no quantitatively correct solution for the dynamics of polydisperse, non-spherical, interacting, colloidal particles. We shall, however, use the Gibbs free energy model presented in Chapter 5 in concert with our generalized ladder model to see to what extent we can describe qualitatively the interactions that are responsible for the concentration dependence of the mean diffusivity observed in our experiments. Furthermore, we shall examine briefly whether this model is consistent with the measurements of Wilcoxon and Kaler [18] of the osmotic compressibility of pure $C_{12}E_6$ solutions. Since the Gibbs free energy model permits us to obtain directly an analytic expression for the osmotic pressure, we shall begin with the second point.

6.3.1 The Osmotic Compressibility of Pure $C_{12}E_6$ Solutions

We recall from Chapter 5 that the generalized Blankschtein, Thurston and Benedek Gibbs free energy model gives Equation 5.22 for the osmotic compressibility. For $C_{12}E_6$, the ratio of molecular volumes (surfactant to water) is about $\gamma = 25$. M_2, also appearing in Equation 5.22, is the second moment (in n) of the micellar distribution, and can be calculated easily from the micellar distribution using the appropriate two-dimensional ladder model parameters from Section 6.1. We will assume that these parameters are concentration independent even in the region where interactions

become important. We have

$$M_2 = X_1 + \sum_{n=n_0}^{\infty} n^2 \tilde{X}_n = X_1 + \frac{\Lambda}{K}\left[\frac{{n_0}^2}{1-\Lambda} + \frac{\Lambda(2n_0+1)}{(1-\Lambda)^2} + \frac{2\Lambda^2}{(1-\Lambda)^3}\right]. \qquad (6.28)$$

Recall that Λ is determined by satisfying the conservation of mass equations (Equations 4.146 and 4.147). The parameter, C_{eff}, we shall treat for now as an adjustable parameter. We remember from Chapter 5 that C_{eff} is an effective mean field interaction parameter measuring the strength of intermicellar amphiphile-amphiphile interactions. Before we apply Equation 5.22 to the measurements of $(\partial\pi/\partial X)^{-1}$ by Wilcoxon and Kaler, we must correct the units. Wilcoxon and Kaler report the osmotic compressibility $(\partial\pi/\partial c)^{-1}$ with c in units of g/cm^3, while our expression is for $(\partial\pi/\partial X)^{-1}$ with X as the total surfactant mole fraction. The quantities c and X are related in general (for the mixed case) through the formula

$$c = \frac{X}{1+(\gamma_{eff}-1)X}\left(\frac{\alpha_s m_A + (1-\alpha_s)m_B}{\Omega_W}\right) \qquad (6.29)$$

where m_A and m_B are the molecular weights of $C_{12}E_6$ and $C_{12}E_8$, respectively. To obtain $(\partial\pi/\partial c)^{-1}$, we must multiply our expression for $(\partial\pi/\partial X)^{-1}$ (Equation 5.22) by

$$\frac{dc}{dX} = \frac{\alpha_s m_A + (1-\alpha_s)m_B}{\Omega_W}\left(\frac{1}{1+(\gamma_{eff}-1)X}\right)^2, \qquad (6.30)$$

which gives, as our final expression (simplified to the pure $C_{12}E_6$ case)

$$\left(\frac{\partial\pi}{\partial c}\right)^{-1} = \frac{m_A}{k_B T\,(1+(\gamma_{eff}-1)X)^2}\left(\frac{X}{1-X} + \frac{X}{M_2} - \frac{C_{eff}}{k_B T}\frac{\gamma X}{(1+(\gamma_{eff}-1)X)^3}\right)^{-1}. \qquad (6.31)$$

We have fit Equation 6.31 to the osmotic compressibility measurements of Wilcoxon and Kaler for pure $C_{12}E_6$ and water at $T = 45°C$ using M_2 computed from the generalized ladder model distribution for pure $C_{12}E_6$ and water at $T = 45°C$. The results are displayed in Figure 6-10. The solid line is the fit to the data of Wilcoxon and Kaler treating C_{eff} as an adjustable parameter. The dotted line is the fit to the data using the method of Puvvada and Blankschtein [17] to estimate C_{eff}, described

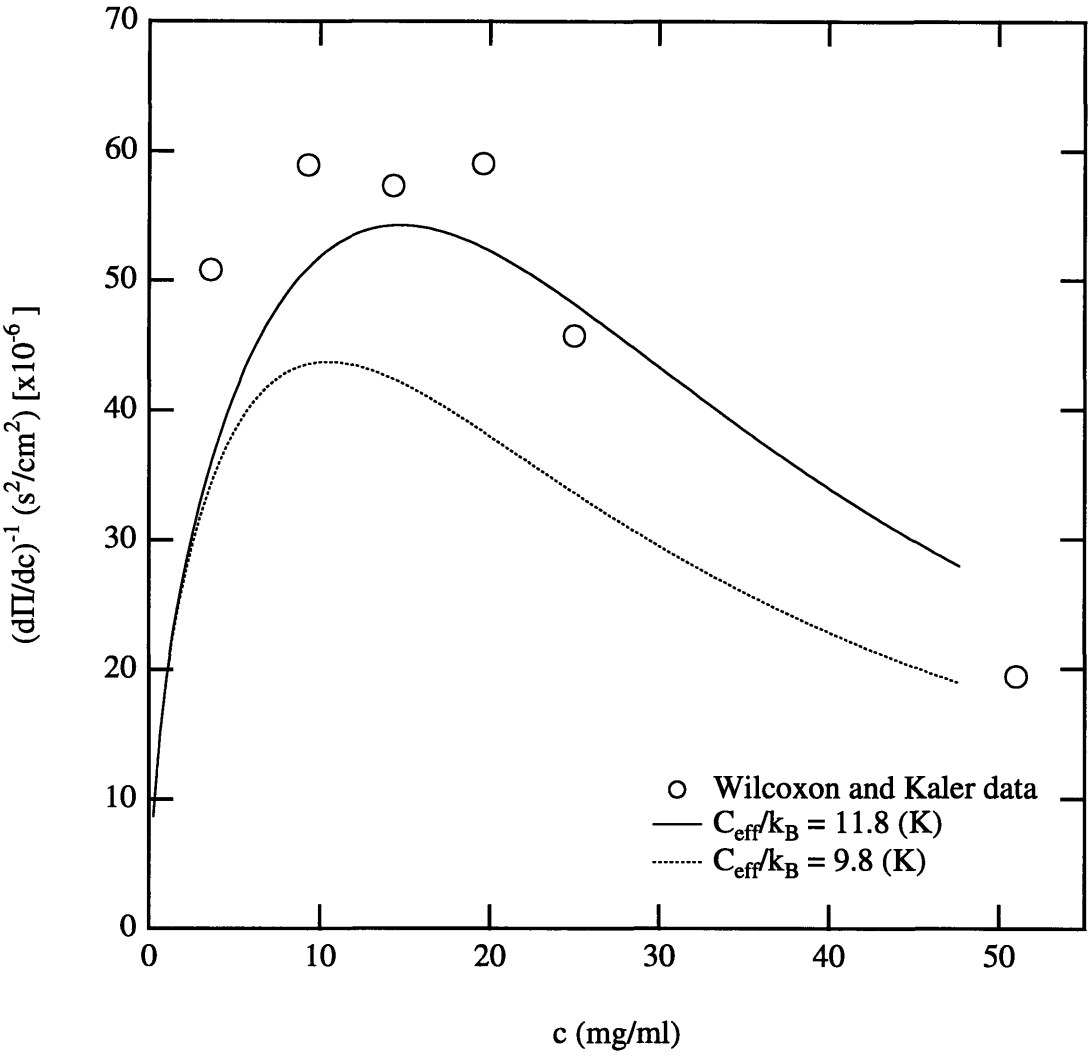

Figure 6-10: The osmotic compressibility for pure $C_{12}E_6$ and water at $T = 45°C$ is plotted as a function of concentration. The circles represent the data of Wilcoxon and Kaler [18]. The curves are fits to the model Gibbs free energy using the generalized ladder model distribution for pure $C_{12}E_6$ and water at $T = 45°C$. The solid line is the best fit considering C_{eff} as a free parameter. The dashed line is for C_{eff} computed using the method of Puvvada and Blankschtein

below.

Since the parameter C_{eff} controls the extent of the attractive (if $C_{eff} > 0$) interaction between monomers, the location and the shape of the phase boundary for liquid-liquid phase separation will depend on the magnitude, composition dependence, and temperature dependence of C_{eff}. Puvvada and Blankschtein have measured the coexistence curves for the pure $C_{12}E_6$ and water system, and the pure $C_{12}E_8$ and water system. They have also measured the cloud point of the mixed $C_{12}E_6$, $C_{12}E_8$ and water system as a function of total surfactant concentration at relative compositions $\alpha_s = 0.30$, 0.50, 0.70 and 0.85. It was found that choosing $C_{eff}(\alpha_s, T)$ as a linear function of both T and α_s was sufficient to explain the position and shape of the coexistence surface for the mixed system. Puvvada and Blankschtein used:

$$C_{eff}(\alpha_s, T) = C_{eff}(\alpha_s) + (T - T_{mix})C'_{eff}(\alpha_s) \tag{6.32}$$

with

$$C_{eff}(\alpha_s)/k_B = \alpha_s 14.48 + (1 - \alpha_s)14.45, \tag{6.33}$$

$$C'_{eff}(\alpha_s)/k_B = \alpha_s 0.776 + (1 - \alpha_s)1.121 \tag{6.34}$$

and

$$T_{mix} = \alpha_s 51.14 + (1 - \alpha_s)78.39. \tag{6.35}$$

We note that T_{mix} is a linear interpolation in composition between the critical temperature for phase separation for $C_{12}E_6$ ($T_C = 51.14°C$) and the critical temperature for phase separation for $C_{12}E_8$ ($T_C = 78.39°C$).

The range of temperature over which the fitting of the coexistence curves defines C_{eff} is about 2°C in the vicinity of T_{mix}. If we assume that the linear dependence of C_{eff} on temperature extends well into the single phase region, we obtain for pure $C_{12}E_6$ at 45°C, $C_{eff}/k_B = 9.8K$ which, when combined with the extended ladder model parameters for $C_{12}E_6$ at 45°C produces for the osmotic compressibility, the dotted line in Figure 6-10. Specifically, it should be noted that for pure $C_{12}E_6$,

C_{eff} was determined by Puvvada and Blankschtein over the temperature range of about $51°C - 53°C$, and we have extrapolated their linear dependence down to 45°C. Thus, the fact that the agreement of our expression for the osmotic compressibility to the data of Wilcoxon and Kaler using this estimate of C_{eff} is not very good is not surprising, since first we are extrapolating a large distance from the region where C_{eff} has been determined, and furthermore, we have no particular reason to expect a linear dependence on temperature of C_{eff} in the single phase region. The fact that we are able to reasonably fit (treating C_{eff} as an adjustable parameter) the osmotic compressibility data of Wilcoxon and Kaler using the same parameters extracted from our fit to our own dynamic data in the low concentration regime argues favorably for our interpretation of our dynamic data in Section 6.1. In addition, this good agreement indicates the success of the Gibbs free energy model of Thurston, Blankschtein and Benedek in capturing the essential features of the intermicellar interactions.

The contributions to the total osmotic compressibility of the solution from the three terms G_m, G_f and G_{int} of the model Gibbs free energy are examined in more detail in Figure 6-11. We note that the shape of the total osmotic incompressibility is determined at low concentrations almost entirely from the contribution from G_f, the free energy of formation. At higher concentrations, the contributions from G_m and G_{int}, which nearly cancel, begin to affect the total osmotic incompressibility causing it to diverge from the contribution due to G_f. We recall that G_f incorporates the Gibbs free energy calculated from our extended ladder model for micellization, but explicitly does not contain any terms representing the interactions between micelles. These interactions are treated jointly by G_m and G_{int}. G_m, we remember is a model mixing entropy among the different micellar species, the free monomers and water. G_m acts to increase the total osmotic incompressibility (decreasing the total osmotic compressibility) and is, as expected, a repulsive interaction between micelles. G_{int} acts in the opposite direction as G_m. It represents, therefore, the mean-field attraction between micelles, which is necessary in order for phase separation to occur.

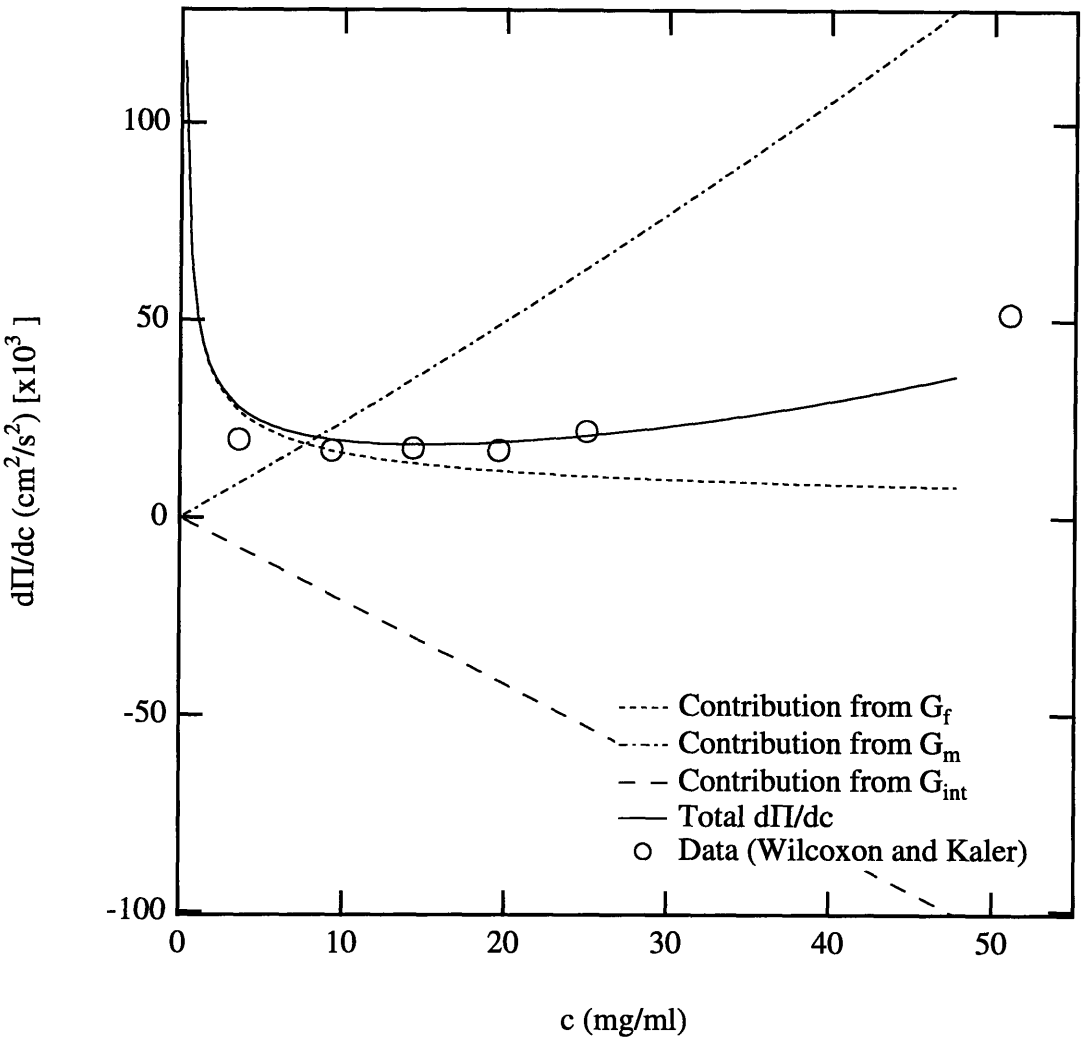

Figure 6-11: The osmotic incompressibility for pure $C_{12}E_6$ and water at $T = 45°C$ is plotted as a function of concentration. The circles represent the data of Wilcoxon and Kaler [18]. The solid line represents the best fit from Figure 6-10 considering C_{eff} as a free parameter. The dashed lines indicate the contributions to the total osmotic incompressibility arising from the three terms of the model Gibbs free energy: G_f, G_m and G_{int}.

6.3.2 The Minimum in the Observed Diffusivity

Having examined the osmotic compressibility predicted by the model Gibbs free energy presented in Chapter 5 and finding it consistent with the measurements of Wilcoxon and Kaler [18] for the pure $C_{12}E_6$ and water system, we turn now to the question of the minimum in the measured diffusivity as a function of solution concentration observed in this work for the mixed $C_{12}E_6$, $C_{12}E_8$ and water system. Let us first recall the analysis of our dynamic light scattering data in Section 6.1 and consider the analysis we performed from another perspective. Our two-dimensional ladder model allows us to predict the micellar distribution as a function of solution concentration (and relative composition). Using the hydrodynamic model presented in Section 6.1 we can compute from this distribution, the average hydrodynamic radius. We then computed the average diffusivity $\bar{D}$ from this average radius using the Stokes-Einstein relation, which is, of course, only valid in the limit of no interactions between micelles. The value of $\bar{D}$ thus obtained was then compared to the experimentally determined value.

When interparticle interactions become important, we can no longer use the Stokes-Einstein relation to relate the particle hydrodynamic radius to the diffusion coefficient. Instead, what is commonly used is a "generalized Stokes-Einstein" relation for the collective diffusion coefficient [65]

$$D = \frac{\left(\frac{\partial \pi}{\partial c}\right)_T}{\zeta}, \tag{6.36}$$

where the magnitude of D is determined by the competition between the osmotic incompressibility (acting as a thermodynamic driving force) and a friction factor ζ. In the limit of no interactions for a monodisperse system, the osmotic incompressibility, $\partial \pi / \partial c$ reduces to $k_B T/M$, and the friction factor becomes the usual expression for Stokes' friction: $\zeta = 6\pi\eta R_H/M$ with η as the solvent viscosity and M as the particle mass. Thus, in the limit of no interactions, we recover the Stokes-Einstein

relation

$$D = \frac{k_B T}{6\pi\eta R_H}. \tag{6.37}$$

We shall calculate the average diffusivity including particle interactions in the same way as was done in Section 6.1 by computing the proper weighted sum over the micellar distribution. If the interactions are not too strong, then we may substitute Equation 6.36 into Equation 6.6 for our calculation of the average diffusivity, giving

$$\bar{D} = \frac{\sum_{n=n_0}^{\infty} n^2 \tilde{X}_n P_n \frac{1}{\zeta_n} \frac{\partial \pi}{\partial c_n}}{\sum_{n=n_0}^{\infty} n^2 \tilde{X}_n P_n}, \tag{6.38}$$

where Equation 6.13, for $A_{n\alpha^*}$ was also used. In Equation 6.38, we will take $\zeta_n = 6\pi\eta R_H(n)/M_n$ with M_n as the mass of an n-mer at the optimal composition and where, since our measurements are at relatively low total concentrations it is reasonable to take the microscopic viscosity η to be the same as the solvent viscosity. We will also need $\partial\pi/\partial c_n$ in order to use Equation 6.38, which can be computed from Equation 5.29 for $\partial\pi/\partial\tilde{X}_n$ by changing concentration variables:

$$\frac{\partial \pi}{\partial c_n} = \frac{\partial \pi}{\partial \tilde{X}_n} \frac{\partial \tilde{X}_n}{\partial c_n}. \tag{6.39}$$

We note that the concentration of n-mers in mass per unit volume can be written

$$c_n = \frac{\tilde{X}_n M_n}{\Omega_W} \left(\frac{1}{1 + (\gamma_{eff} - 1)X} \right) \tag{6.40}$$

so that

$$\frac{\partial c_n}{\partial \tilde{X}_n} = \frac{M_n}{\Omega_W} \left(\frac{1 + (\gamma_{eff} - 1)(X - n\tilde{X}_n)}{(1 + (\gamma_{eff} - 1)X)^2} \right). \tag{6.41}$$

Putting all of this together in the limit of low concentration, we obtain

$$\bar{D} = \frac{\sum_{n=n_0}^{\infty} n^2 \tilde{X}_n P_n \frac{k_B T}{6\pi\eta R_H(n)} \left[1 + nX \left(1 - \frac{C_{eff}(\alpha_s)}{k_B T} \gamma_{eff} \right) \right]}{\sum_{n=n_0}^{\infty} n^2 \tilde{X}_n P_n} \tag{6.42}$$

Figure 6-12 shows the prediction of Equation 6.42 at $T = 45°\text{C}$ and $\alpha_s = 0.848$ treating C_{eff} as an adjustable parameter and using the micellar distribution calcu-

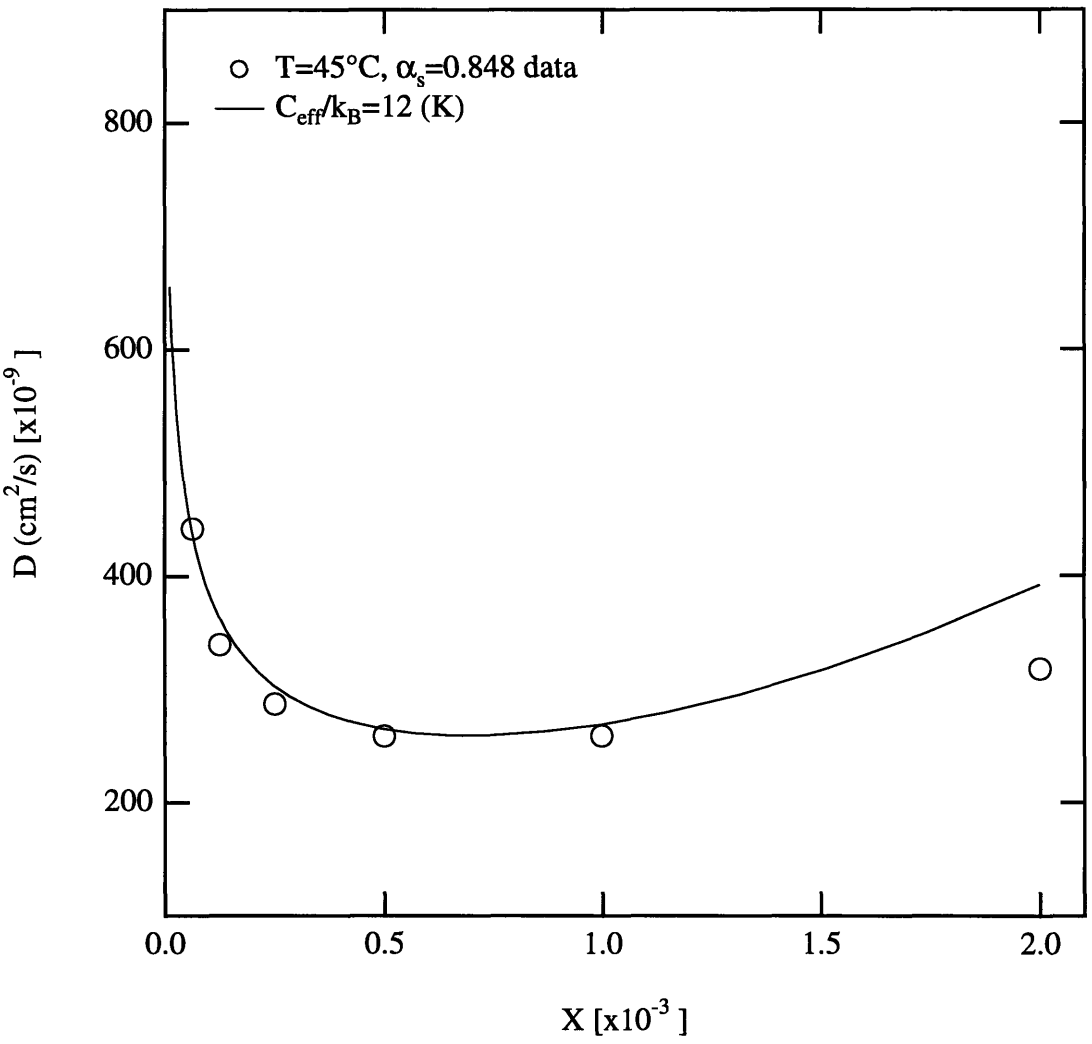

Figure 6-12: The mean diffusivity is plotted as a function of total surfactant concentration for the $\alpha_s = 0.848$ mixture of $C_{12}E_6$ and $C_{12}E_8$ at $T = 45°C$. The solid line represents the prediction of Equation 6.42 treating C_{eff} as an adjustable parameter and using the generalized ladder model parameters for $T = 45°C$ extracted in Section 6.1.

lated from the extended ladder model parameters extracted in Section 6.1 for 45°C. Although there is a systematic deviation from the observed data points at higher concentrations, the agreement is quite good, and the trends are qualitatively correct. In essence, our explanation for the observed minimum in $\bar{D}$ with concentration is then the same as the explanation of the maximum in the osmotic compressibility with concentration. That is, interactions affect the osmotic incompressibility which enters into the determination of $\bar{D}$ as a thermodynamic driving force for fluctuations. In the model Gibbs free energy, these interactions are modeled by a particular choice of the entropy of mixing in G_m, resulting in a repulsive interaction, and the mean-field model of the attraction between micelles contained in G_{int}. The correction that these effects apply to $\bar{D}$ is relatively minor since the two effects operate in opposite directions and tend to cancel. The value of $C_{eff}/k_B = 12K$ obtained in Figure 6-12 is reasonable since it is of the same order as the value of C_{eff}/k_B we found (in Figure 6-10) from the measurements of the osmotic compressibility for pure $C_{12}E_6$ made by Wilcoxon and Kaler. We stress that since the value of C_{eff} from Figure 6-12 is for an $\alpha = 0.848$ mixture of $C_{12}E_6$ and $C_{12}E_8$, while the value of C_{eff} from Figure 6-10 is for pure $C_{12}E_6$, and so we do not necessarily expect to obtain the two values to be the same. In principle, as the concentration increases, we must also take into account the increase in microscopic viscosity which acts to slow fluctuations and will cause a further decrease in $\bar{D}$. This could explain the small but systematic overestimation of $\bar{D}$ at the higher concentrations in Figure 6-12.

6.3.3 Summary

In this section, we have used the Gibbs free energy model presented in Chapter 5 to show that the minimum we observed in the measured diffusivity with increasing concentration in the mixed $C_{12}E_6$, $C_{12}E_8$ and water system is due to the effects of intermicellar interactions. We emphasize once again the physical explanation of this minimum in terms of the Gibbs free energy model we have used. We begin by discussing the bulk osmotic incompressibility.

By including the effects of intermicellar interactions into the model Gibbs free

energy for the micellar solution, we predict a minimum in the bulk osmotic incompressibility of the solution as a function of concentration. This minimum can be physically understood by examining the contributions to the total osmotic incompressibility from the three terms of the Gibbs free energy model as shown in Figure 6-11. At low concentrations, the osmotic incompressibility is dominated by the effects of G_f, the formation free energy. That is, the initial behavior of $\partial\pi/\partial c$ is determined by the effects of micellar growth. As we mentioned in Chapter 3, Debye [53] showed that for a dilute solution of particles suspended in a solvent, the osmotic incompressibility is inversely proportional to the weight-averaged molecular weight (*i. e.* $\sum n^2 X_n / \sum n X_n$) of the particles. Since the weight-averaged molecular weight of the micelles is expected to increase like the square root of the concentration, we expect this contribution to the osmotic incompressibility to initially decrease rapidly towards zero as is shown in Figure 6-11. As concentration is increased further, the contributions to the total osmotic incompressibility from the free energy of mixing, G_m, and the interaction free energy, G_{int}, become important. The free energy of mixing, G_m acts to oppose the increase in concentration of the micelles because of the reduction of entropy corresponding to this concentration increase. As shown in Figure 6-11 (the dash-dot line), the entropic effect of G_m causes the osmotic incompressibility to increase with concentration. The interaction free energy, G_{int}, represents an attractive interaction between micelles and therefore favors the increase of micelle concentration. We know that the interaction should be attractive because we know that the micellar system can phase separate. The energetic effect of G_{int} causes the osmotic incompressibility to decrease with increasing concentration. We see that the eventual rise of $\partial\pi/\partial c$ occurs because the effect of the entropic mixing term outweigh the effects of the attractive interaction energy term, G_{int}. Thus, our model is capable of explaining the maximum in the osmotic compressibility observed by Wilcoxon and Kaler [18] in pure $C_{12}E_6$ and water solutions with increasing concentration.

We can also use the Gibbs free energy model to calculate the partial osmotic compressibility arising from each distinct micellar species in the solution. Since a

generalized Stokes-Einstein relation relates the diffusion coefficient for each species of particle to its partial osmotic incompressibility and a friction factor, we can calculate the mean effective diffusion coefficient associated with the entire micellar distribution as a function of concentration. We find a minimum in the observed average diffusivity of the solution as a function of concentration in quantitative agreement with the experimental data. In this way, we showed that the initial decrease of the mean diffusivity with increasing concentration is due to the effects of micellar growth, just as was observed previously in the case of the osmotic incompressibility. The subsequent increase of the mean diffusivity at higher concentrations (above the critical concentration for liquid-liquid phase separation) results from the dominance of the entropic factor G_m as compared to the energetic factor, G_{int}, just as was discussed in the case of the total osmotic incompressibility.

An alternative possibility to explain the minimum in the diffusivity as a function of concentration is suggested by the treatment of semidilute surfactant systems proposed by Carale and Blankschtein [35]. As concentration is increased, the micelles in solution grow longer, and average diffusivity decreases. Simultaneously, the micelles fill up a greater portion of the available solution volume until, at some crossover concentration, X^*, the micelles begin to overlap. Above this crossover concentration, Carale and Blankschtein describe the solution as existing in a semidilute regime in which the micelles form a transient network of overlapping micelles. It is stated that, in this regime, the important length scale is an "average network size" that should be independent of the average micellar molecular weight. Kole, *et. al.* [27] argue that the diffusion coefficient should increase with concentration in this regime because of the decrease of the characteristic size of the cells of the network with increasing concentration. They argue further that the minimum in the diffusivity should occur in the vicinity of the crossover concentration, X^*, as defined by Carale and Blankschtein [35]. However, analysis of the diffusivity using this picture is currently only qualitative. Further work is needed if a quantitative analysis of the minimum in the diffusivity is to be possible using the entanglement picture.

Chapter 7

Conclusions

We have examined the micellization of aqueous solutions of mixed surfactant systems both experimentally and theoretically. Using the techniques of static and quasielastic light scattering we examined in detail the mixed system composed of water, $C_{12}E_6$ and $C_{12}E_8$ in Chapter 3. Quasielastic light scattering was used to characterize the average micellar size as a function of concentration, temperature and relative composition in the region well above the critical micellar concentration. It was found that as temperature, total concentration, or relative proportion of $C_{12}E_6$ was increased, that the micelles tended to grow.

For very dilute concentrations of pure $C_{12}E_6$ and $C_{12}E_8$, the intensity of light scattered from the micelles was used to estimate the critical micellar concentration. The critical micellar concentration for $C_{12}E_6$ solutions was found to decrease weakly with increasing temperature in the range $25°C < T < 50°C$ in agreement with a compilation of critical micellar concentration values for $C_{12}E_6$ taken from various sources by Mukerjee [57]. The critical micellar concentration of $C_{12}E_8$ solutions was found to be independent of temperature (to within the measurement accuracy) over the same range of temperature.

A combination of quasielastic and total intensity measurements were also performed on solutions containing a selected relative composition of the two surfactants. These data are consistent with a rigid prolate ellipsoid model for the micellar shape. Therefore, it was not necessary to consider the effect of micelle flexibility in the char-

acterization of the diffusion coefficient of each micelle, and a linear growth model of rigid micelles was adopted.

In Chapter 4, we examined the linear growth of mixed surfactant systems theoretically, in terms of a generalization of the ladder model [10] to the case of two surfactant species and water. Using this "two-dimensional" ladder model, we showed that the micellar size and composition distribution was highly peaked about some optimal composition, and for the case of similar surfactants, the problem could be reduced to an effective single-component ladder model problem with an effective gap and ladder spacing dependent on the optimal micellar composition. Thus, we were also able to show that in the limit of strong micellar growth that the weight averaged aggregation number for a two surfactant and water mixture should scale like $X^{0.5}$ as in the single-component case, not like $X^{0.4}$ as claimed by others [34].

In Chapter 6, the two-dimensional ladder model was successfully used to describe all of our experimental data in the regions below the critical concentration for liquid-liquid phase separation, where we argued that intermicellar interactions should be small. As a result, we obtained the temperature dependence of the four parameters $\Delta\mu_A$, $\Delta\mu_B$, $\Delta\mu^0_{cA}$ and $\Delta\mu^0_{cB}$ (or equivalently $\Delta\mu^0_{sA}$, $\Delta\mu^0_{sB}$, $\Delta\mu^0_{cA}$ and $\Delta\mu^0_{cB}$). We found that $\Delta\mu_A$ and $\Delta\mu_B$ varied roughly linearly with temperature, while $\Delta\mu^0_{cA}$ and $\Delta\mu^0_{cB}$ were found to be independent of temperature to within the measurement accuracy.

The molecular model of Puvvada and Blankschtein [16, 17] was used to compute the magnitudes of the physically meaningful parameters of the generalized ladder model, $\Delta\mu_A$, $\Delta\mu_B$, $\Delta\mu^0_{cA}$ and $\Delta\mu^0_{cB}$ for the $C_{12}E_6$, $C_{12}E_8$ and water system. Excellent agreement with the values extracted from our experimental data was obtained by allowing a slight modification to the cross-sectional areas per head group for the two surfactants. Thus we showed that the computational approach of Puvvada and Blankschtein is capable of describing the observed micellar size and composition distribution and that the approach can be used to provide a physical understanding of the various factors that are important in the process of micellization and micellar growth. Furthermore, we have demonstrated the utility of the two-dimensional lad-

der model in extracting useful thermodynamic information about our experimental system.

Also in Chapter 6, we used the two-dimensional ladder model and the generalized Blankschtein, Thurston and Benedek Gibbs free energy model [16] to examine the effects of intermicellar interactions. We found that the Gibbs free energy model was capable of explaining the maximum in the osmotic compressibility isotherms observed in pure $C_{12}E_6$ solutions by Wilcoxon and Kaler [18]. Furthermore, by simple considerations about the dynamics of the system, using the same Gibbs free energy we were also able to explain the minimum in the mean diffusivity isotherms observed in Chapter 3 for the mixed $C_{12}E_6$, $C_{12}E_8$ and water system. Physically, we understand the presence of this minimum as follows. The initial decrease of the mean diffusivity as concentration is increased is due to the effects of micellar growth. The subsequent increase of the mean diffusivity with concentration at higher concentrations is caused by the fact that the entropic term (which acts to increase the diffusivity) arising in the Gibbs free energy model from G_m dominates the attractive interactions included in G_{int} (which act to decrease the diffusivity). The treatment of intermicellar interactions we have used is therefore successful in explaining the concentration dependence of the average diffusivity, $\bar{D}$, of our data over the entire range of our measurements.

Our Gibbs free energy model, which includes the two-dimensional ladder model, a physically reasonable model for the entropy of mixing of the solution and a mean-field model for the interactions between micelles, has proven to be a very powerful tool for the analysis of the equilibrium and transport properties of our mixed micellar solution over a broad range of concentration. The model permits us to describe accurately micellar growth and the dependence of the mean diffusion coefficient on concentration both in the vicinity of the critical concentration for phase separation and in the dilute regime. In addition, this model Gibbs free energy predicts the phase separation of the mixed system [16, 17] and the equation of state, including the osmotic compressibility.

Our calculation of the diffusivity in the vicinity of the critical concentration for

phase separation assumes an effective viscosity equal to that of water and neglects the effects of hydrodynamic interactions. Our ability to explain the concentration dependence of the average diffusivity of the mixed micellar system over the entire range of our measurements indicates that hydrodynamic interactions and microscopic viscosity effects appear to be less important than the interactions that we have included in our treatment. Theoretically, however, one might be interested in improving our treatment by including such effects. In order to do so, however, the theoretical understanding of the dynamics of interacting colloidal suspensions needs to be improved. Current treatments [66, 67] are still limited to the exploration of the dynamics of interacting, monodisperse, spherical systems. To be applicable to our data, these theories need extension to the case of polydisperse solutions of nonspherical particles.

The great success of our approach in describing the properties of the $C_{12}E_6$, $C_{12}E_8$ and water system suggests that this approach might be applied to other pairs of interacting amphiphiles. As we saw in Chapter 3, $C_{12}E_6$ and $C_{12}E_8$ are surfactants which are structurally very similar and that share many similar properties. In Chapter 4, we used this similarity to justify the linear interpolation of gap and rung spacings with micelle composition between the gap and rung spacings for the two pure surfactants. It is expected that this linear interpolation will break down if the two surfactants become sufficiently different. By carrying out experiments on mixed systems containing amphiphiles with significantly different properties, it should be possible to investigate the different ways in which this interpolation scheme should be modified. An example of such a system would be a mixture containing both cationic and anionic surfactants. In addition, it would be interesting to examine the properties of a mixed system in which one pure component was known to form rodlike micelles while the other pure component was known to form disclike micelles. We hope that the work contained in this thesis will encourage others to explore these and other fascinating avenues of research.

Appendix A

The Thermodynamic Susceptibility χ

Here we discuss the thermodynamic susceptibility χ introduced in Chapter 2 and discuss the derivation of Equation 2.45 that relates χ formally to the osmotic compressibility. We recall first that our solution is to be considered in equilibrium at constant temperature and pressure with its surroundings. We will consider as our system, a small fixed volume of the solution, but containing enough particles to be considered thermodynamically. We will also limit ourselves to a solution that contains only water molecules and one kind of solute molecules, since our results are easily generalizable. Under these conditions, the Gibbs free energy of our system can be written

$$dG = \mu_W dN_W + \mu_S dN_S \tag{A.1}$$

where μ_W is the chemical potential of water, μ_S is the chemical potential of the solute molecules, N_W is the number of water molecules in the system, and N_S is the number of solute molecules. With time, the number of water molecules and solute molecules in our small fixed volume will fluctuate, but since we are at fixed pressure and temperature, these fluctuations will not be independent. The condition of fixed volume implies that

$$dV = \Omega_W dN_W + \Omega_S dN_S = 0 \tag{A.2}$$

where V is the small volume we are considering, and Ω_W and Ω_S are the molecular volumes of water and solute respectively. Thus, we assume that we are dealing with an incompressible fluid. We may use Equation A.2 to eliminate dN_W from Equation A.1, giving

$$dG = \left(\mu_S - \frac{\Omega_S}{\Omega_W}\mu_W\right) dN_S. \tag{A.3}$$

Thus we have,

$$\frac{\partial G}{\partial c} = \left(\mu_S - \frac{\Omega_S}{\Omega_W}\mu_W\right) \frac{V}{m_S} \tag{A.4}$$

where we have chosen concentration units of mass per unit volume, m_S is the mass of a solute particle, and therefore

$$dc = \frac{m_S}{V} dN_S. \tag{A.5}$$

We now recall that the thermodynamic susceptibility, χ, was defined as the second derivative of the Gibbs free energy with respect to the solute concentration in Equation 2.41. Therefore, we have that

$$\chi = \left(\frac{\partial \mu_S}{\partial c} - \frac{\Omega_S}{\Omega_W}\frac{\partial \mu_W}{\partial c}\right) \frac{V}{m_s}. \tag{A.6}$$

Next, we make use of the Gibbs-Duhem relation to eliminate the solute chemical potential. We recall that at constant pressure and temperature, the Gibbs-Duhem relation states that

$$N_W d\mu_W + N_S d\mu_S = 0, \tag{A.7}$$

and therefore, from Equation A.6, we obtain

$$\chi = -\left(\frac{N_W}{N_S} + \frac{\Omega_S}{\Omega_W}\right) \frac{V}{m_S}\frac{\partial \mu_W}{\partial c}. \tag{A.8}$$

The osmotic pressure is related to the chemical potential of water through the relation [12]

$$\Omega_W \pi = \mu_W^0 - \mu_W \tag{A.9}$$

where π is the osmotic pressure, and μ_W^0 is the standard state chemical potential of water, which is a function of pressure and temperature, but not a function of solute concentration. Differentiating with respect to solute concentration, we obtain the useful relation

$$\frac{\partial \pi}{\partial c} = -\frac{1}{\Omega_W}\frac{\partial \mu_W}{\partial c}. \tag{A.10}$$

Using Equation A.10 in our latest expression for χ, Equation A.8, and rearranging slightly, we obtain

$$\chi = V\left(\frac{N_W\Omega_W + N_S\Omega_S}{N_S m_S}\right)\frac{\partial \pi}{\partial c}. \tag{A.11}$$

Note that by definition

$$V = N_W\Omega_W + N_S\Omega_S, \tag{A.12}$$

so that the term in parenthesis is simply one over the solute concentration. Thus, we have that

$$\chi = \frac{V}{c}\frac{\partial \pi}{\partial c}, \tag{A.13}$$

which is exactly Equation 2.45. Note also that in terms of a light scattering experiment, the small fixed volume V can be considered as the fixed, illuminated scattering volume from which light is collected.

Appendix B

Full Treatment of the Extended Ladder Model

In Section 4.2.5, we applied a total random mixing approximation to the micellar size and composition distribution derived in Section 4.2.4. This total random mixing approximation is appropriate, as we will show, for the case that $(\Delta\mu^0_{sA} - \Delta\mu^0_{cA}) - (\Delta\mu^0_{sB} - \Delta\mu^0_{cB}) \ll k_BT$, and was used in Chapter 4 primarily for simplicity. It is possible to proceed with the analysis of the generalized ladder model without making this approximation.

B.1 The Micellar Distribution

We begin by repeating the primary result up through Section 4.2.4. That is, the distribution of micellar sizes and compositions can be written (Equations 4.103-4.106):

$$X_{n\alpha\alpha_0} = C(n,\alpha,n_0,\alpha_0)\left({X_{1A}}^{n\alpha}{X_{1B}}^{n(1-\alpha)}\right)e^{-(\Delta(\alpha_0)+(n-n_0)\delta(\alpha))/k_BT} \tag{B.1}$$

with

$$\Delta(\alpha_0) = n_0\left(\alpha_0\Delta\mu^0_{sA} + (1-\alpha_0)\Delta\mu^0_{sB}\right), \tag{B.2}$$

$$\delta(\alpha) = \alpha\Delta\mu^0_{cA} + (1-\alpha)\Delta\mu^0_{cB}. \tag{B.3}$$

and

$$C(n,\alpha,n_0,\alpha_0) = \frac{n_0!}{(n_0\alpha_0)!(n_0(1-\alpha_0))!}\frac{(n-n_0)!}{(n\alpha-n_0\alpha_0)!(n(1-\alpha)-n_0(1-\alpha_0))!}. \tag{B.4}$$

Once again, as in Section 4.2.5, it will be convenient to express everything in terms of total concentration and relative composition variables. We therefore define, as we did before, the total mole fraction of free monomers in solution at equilibrium

$$X_1 = X_{1A} + X_{1B} \tag{B.5}$$

and the relative composition of free monomers in solution at equilibrium

$$\alpha_1 = \frac{X_{1A}}{X_{1A}+X_{1B}}. \tag{B.6}$$

Using these definitions in Equation B.1 and using Stirling's formula to expand the factorials in $C(n,\alpha,n_0,\alpha_0)$, we can see will result in a rather ungainly expression. However, examining the form of Equations B.1-B.4, we can see that the form of our answer can be expressed as two factors, one factor containing α_0 and quantities proportional to n_0, and the other factor containing α and quantities proportional to $n-n_0$. That is

$$X_{n\alpha\alpha_0} = P(\alpha_0)Q(\alpha) \tag{B.7}$$

with

$$P(\alpha_0) = \frac{{X_1}^{n_0}}{\sqrt{2\pi n_0\alpha_0(1-\alpha_0)}} e^{-\left\{\Delta(\alpha_0)+n_0k_BT\left(\alpha_0\ln\frac{\alpha_0}{\alpha_1}+(1-\alpha_0)\ln\frac{1-\alpha_0}{1-\alpha_1}\right)\right\}/k_BT} \tag{B.8}$$

and

$$Q(\alpha) = \frac{{X_1}^{n-n_0}}{\sqrt{2\pi(n-n_0)\alpha(1-\alpha)}} e^{-(n-n_0)\left\{\delta(\alpha)+k_BT\left(\alpha\ln\frac{\alpha}{\alpha_1}+(1-\alpha)\ln\frac{1-\alpha}{1-\alpha_1}\right)\right\}/k_BT}. \tag{B.9}$$

Noting that the argument of the exponent in Equation B.8 is proportional to n_0 ($\Delta(\alpha_0)$ is proportional to n_0) and that the argument of the exponent in Equation

B.9 is proportional to $n - n_0$, it will be convenient to define the quantities

$$A(\alpha_0) = \alpha_0 \frac{\Delta\mu^0_{sA}}{k_B T} + (1-\alpha_0)\frac{\Delta\mu^0_{sB}}{k_B T} + \alpha_0 \ln\frac{\alpha_0}{\alpha_1} + (1-\alpha_0)\ln\frac{1-\alpha_0}{1-\alpha_1} \tag{B.10}$$

and

$$B(\alpha) = \alpha \frac{\Delta\mu^0_{cA}}{k_B T} + (1-\alpha)\frac{\Delta\mu^0_{cB}}{k_B T} + \alpha \ln\frac{\alpha}{\alpha_1} + (1-\alpha)\ln\frac{1-\alpha}{1-\alpha_1}. \tag{B.11}$$

Thus, we can write

$$X_{n\alpha\alpha_0} = \frac{{X_1}^{n_0}}{\sqrt{2\pi n_0 \alpha_0(1-\alpha_0)}} \frac{{X_1}^{n-n_0}}{\sqrt{2\pi(n-n_0)\alpha(1-\alpha)}} e^{-[n_0 A(\alpha_0) + (n-n_0)B(\alpha)]} \tag{B.12}$$

Following the conventions in Chapter 4, we define the parameter K as follows

$$K(\alpha, \alpha_0) = e^{n_0[A(\alpha_0) - B(\alpha)]}. \tag{B.13}$$

In the limit that $\alpha_0 = \alpha$, Equation B.13 clearly reduces to Equation 4.115. Thus, the micellar distribution can be written in the simple form

$$X_{n\alpha\alpha_0} = \frac{{X_1}^{n_0}}{\sqrt{2\pi n_0 \alpha_0(1-\alpha_0)}} \frac{{X_1}^{n-n_0}}{\sqrt{2\pi(n-n_0)\alpha(1-\alpha)}} \frac{1}{K(\alpha, \alpha_0)} e^{-nB(\alpha)}. \tag{B.14}$$

B.2 The Optimal Compositions

Recalling the discussion in Section 4.2.5, we note that if $A(\alpha_0)$ and $B(\alpha)$ each have a minimum, then Equations B.8 and B.9 will be sharply peaked around some optimal compositions α_0^* and α^*, meaning that the micellar distribution is also a peaked function. Furthermore, these optimal compositions will be related to one another through the quantity α_1. The functional form of $A(\alpha_0)$ and $B(\alpha)$ here are identical to the form of $B(\alpha)$ from Section 4.2.5. Thus, finding the minimum in A and B

yields

$$\ln\frac{\alpha_1}{1-\alpha_1} - \ln\frac{\alpha_0^*}{1-\alpha_0^*} = \frac{1}{k_BT}\frac{\partial}{\partial\alpha_0}\frac{\Delta(\alpha_0)}{n_0}\bigg|_{\alpha_0=\alpha_0^*} \tag{B.15}$$

$$\ln\frac{\alpha_1}{1-\alpha_1} - \ln\frac{\alpha^*}{1-\alpha^*} = \frac{1}{k_BT}\frac{\partial}{\partial\alpha}\delta(\alpha)\bigg|_{\alpha=\alpha^*}, \tag{B.16}$$

or

$$\alpha_0^* = \frac{\alpha_1}{\alpha_1 + (1-\alpha_1)e^{(\Delta\mu_{sA}^0 - \Delta\mu_{sB}^0)/k_BT}} \tag{B.17}$$

$$\alpha^* = \frac{\alpha_1}{\alpha_1 + (1-\alpha_1)e^{(\Delta\mu_{cA}^0 - \Delta\mu_{cB}^0)/k_BT}}. \tag{B.18}$$

Since the micellar ends contain n_0 monomers and the cylindrical body contains $n - n_0$ monomers, the overall optimal composition of a micelle of total aggregation number n is therefore

$$\alpha_{mic}^*(n) = \alpha^* + (\alpha_0^* - \alpha^*)\frac{n_0}{n}. \tag{B.19}$$

If we wish, we can compute α in terms of α_0 by eliminating α_1 in the above equations. We find that

$$\frac{\alpha^*}{1-\alpha^*} = \frac{\alpha_0^*}{1-\alpha_0^*} e^{\left[(\Delta\mu_{sA}^0 - \Delta\mu_{sB}^0) - (\Delta\mu_{cA}^0 - \Delta\mu_{cB}^0)\right]/k_BT}. \tag{B.20}$$

If the quantity $(\Delta\mu_{sA}^0 - \Delta\mu_{sB}^0) - (\Delta\mu_{cA}^0 - \Delta\mu_{cB}^0) \ll k_BT$, then Equation B.20 implies that the optimal composition in the micellar ends is the same as the optimal composition in the cylindrical body. That is, the total random mixing approximation made in Section 4.2.5 is appropriate.

Since the micellar distribution is peaked, sums over the micellar distribution should be treated in the same manner as in Section 4.2.6, except that here we must integrate over the relative composition of the micellar ends and the relative composition of the cylindrical body separately. Since the micellar distribution can be factored according to Equation B.7, the integrations act separately on the quantities $P(\alpha_0)$ and $Q(\alpha)$. The form of each of these terms is identical to the integrations

done in Section 4.2.6 with n replaced by n_0 in $P(\alpha_0)$ and $n - n_0$ in $Q(\alpha)$. We will therefore not repeat them here. The final result is

$$\sum_{n\alpha\alpha_0} f(n,\alpha,\alpha_0)X_{n\alpha\alpha_0} = \sum_{n=n_0}^{\infty} f(n,\alpha^*,\alpha_0^*)\tilde{X}_n \tag{B.21}$$

with the renormalized micellar distribution now given by

$$\tilde{X}_n = \frac{{X_1}^n}{K(\alpha^*,\alpha_0^*)} e^{-nB(\alpha^*)} \tag{B.22}$$

We now address the problem of solving for the quantities X_1 and α_1 in terms of the total mole fraction of surfactant added to the solution, X, and the relative composition of this surfactant, α_s. As in Chapter 4, this relationship is made through the two expressions conserving the number of surfactant monomers of each kind, or equivalently, the total number of surfactant monomers and the number of surfactant monomers of one kind (say type A). We have (having performed the integrations over composition)

$$X = X_1 + \sum_{n=n_0}^{\infty} n\tilde{X}_n \tag{B.23}$$

and

$$\alpha_s X = \alpha_1 X_1 + \sum_{n=n_0}^{\infty} \left(n_0\alpha_0^* + (n-n_0)\alpha^*\right)\tilde{X}_n. \tag{B.24}$$

Defining Λ as we did in Section 4.2.6,

$$\Lambda = X_1 e^{-B(\alpha^*)} \tag{B.25}$$

we can perform the summations over n in Equations B.23 and B.24, giving

$$X = X_1 + \frac{1}{K(\alpha^*,\alpha_0^*)}\Lambda^{n_0}\left\{\frac{n_0}{1-\Lambda} + \frac{\Lambda}{(1-\Lambda)^2}\right\} \tag{B.26}$$

and

$$\alpha_s X = \alpha_1 X_1 \frac{1}{K(\alpha^*,\alpha_0^*)}\Lambda^{n_0}\left\{\frac{n_0\alpha_0^*}{1-\Lambda} + \frac{\Lambda\alpha^*}{(1-\Lambda)^2}\right\}. \tag{B.27}$$

Equation B.26 is identical with Equation 4.146 from our simplified treatment, and

Equation 4.44 for the single- component case. In the limit mentioned above where $\alpha^* = \alpha_0^*$, Equation B.27 reduces exactly to Equation 4.147. In principle, the problem is solved, since we can numerically solve Equations B.26 and B.27 for X_1 and α_1 given the generalized ladder model parameters ($\Delta\mu_{sA}^0$, $\Delta\mu_{sB}^0$, $\Delta\mu_{cA}^0$ and $\Delta\mu_{cB}^0$) and the total concentration, X, and relative composition, α_s, of surfactant added to the solution. Using X_1 and α_1 thus determined, we know the entire distribution of micellar sizes and compositions, $X_{n\alpha\alpha_0}$. Furthermore, we can use this distribution to calculate any experimentally observable quantity, as mentioned in Chapter 4. We now examine, as before, the micellar distribution in the dilute regime and in the regime of strong micellar growth. Our results will be identical to those for the simplified treatment.

B.3 The Dilute Regime

As in Section 4.1.4 and in Section 4.2.7, we wish to show that Equations B.26 and B.27 together imply a transition in concentration during which the number of micelles increases sharply. We note that Equation B.26 has exactly the same form as Equation 4.146, and so the analysis presented there should also be applicable here.

Because of the factor Λ^{n_0} appearing in Equation B.26, we see that when Λ is not close to unity, the second and third terms on the right hand side of Equation B.26 and Equation B.27 are very small. In this case, Equation B.26 tells us that $X = X_1$, Equation B.27 tells us that $\alpha_1 = \alpha_s$, and it is clear that no micelles are present in the solution.

As the total concentration, X, is increased, the value of X_1 (and thus Λ) increases. As Λ approaches unity, the value of Λ^{n_0} increases sharply and the second and third terms on the right hand side of Equations B.26 and B.27 can not be neglected. Remembering that these two terms come from the summation over the micellar distribution, we note that together, in Equation B.26, the second and third terms on the right hand side should be proportional to the total number of monomers

in the solution that exist in micellar form. The critical micellar concentration, therefore, lies in the vicinity of the concentration region where the second and third terms on the right hand side of Equation B.26 first become comparable to the magnitude of X_1.

If $K(\alpha^*, \alpha_0^*) > 1$, then when X approaches $e^{B(\alpha^*)}$, X_1 becomes comparable to $e^{B(\alpha^*)}$, meaning that the value of Λ approaches 1 and we can no longer neglect the second and third terms on the right hand side of Equation B.26. In fact, as we increase the concentration further, X_1 can increase only very little, since its maximum value is $e^{B(\alpha^*)}$, as we saw in the previous section. If the value of X_1 exceeds $e^{B(\alpha^*)}$, then $\Lambda > 1$, and the summation over the micellar distribution resulting in Equations B.26 and B.27 do not converge. Therefore, most of the increase in X at the stage where X is about $e^{B(\alpha^*)}$ is reflected as an increase in the second and third terms of Equation B.26, and so we expect the critical micellar concentration to lie in the vicinity of $X = e^{B(\alpha^*)}$.

On the other hand, if $K(\alpha^*, \alpha_0^*) < 1$, then the second and the third terms on the right hand side of Equation B.26 become significant before X reaches $e^{B(\alpha^*)}$. In this case, it is convenient to recall the definition of $K(\alpha, \alpha_0)$ (Equation B.13) and the definition of Λ (Equation B.25), then we may rewrite Equation B.26

$$X = X_1 + \left(\frac{X_1}{e^{A(\alpha_0^*)}}\right)^{n_0} \left\{\frac{n_0}{(1-\Lambda)} + \frac{\Lambda}{(1-\Lambda)^2}\right\}. \tag{B.28}$$

We see that when X approaches the quantity $e^{A(\alpha_0^*)}$, X_1 becomes comparable to $e^{A(\alpha_0^*)}$, meaning that the second and third terms on the right hand side of Equation B.28 begin to increase sharply and can no longer be neglected. We therefore expect the critical micellar concentration to lie in the vicinity of $X = e^{A(\alpha_0^*)}$. Furthermore, we note that the condition that $K(\alpha^*, \alpha_0^*) < 1$ implies that $e^{A(\alpha_0^*)} < e^{B(\alpha^*)}$. Therefore, from the definition of Λ (Equation B.25), we see that when the second and third terms on the right hand side of Equation B.28 become significant, that Λ is not necessarily very close to unity in the sense that Λ^{n_0} is still small compared to unity. We will see in the next section that this implies that for $K(\alpha^*, \alpha_0^*) < 1$ we

cannot physically realize the limit of strong micellar growth.

B.4 The Limit of Strong Micellar Growth

As in the single component case, by strong micellar growth, it is meant that there are significant numbers of micelles with $n > n_0$, or equivalently, the levels in the micellar distribution $\tilde{X}_n$ in Equation B.22 for $n > n_0$ must be significantly occupied. This implies that Λ is close to unity. Let us then define

$$\Lambda = 1 - \frac{\epsilon}{n_0} \tag{B.29}$$

where $\epsilon \ll 1$. For almost all practical cases, the limit of strong micellar growth will also correspond to the limit $X \gg e^{B(\alpha^*)}$, that is, the total concentration is far above the critical micellar concentration. We will first examine the limit of strong micellar growth when the total concentration is far above the critical micellar concentration. We shall then consider the conditions for which strong micellar growth can occur even close to the critical micellar concentration.

For total concentrations far above the critical micellar concentration, B.26 gives, to leading order in ϵ

$$X = e^{B(\alpha^*)} + \frac{1}{K(\alpha^*, \alpha_0^*)} \frac{{n_0}^2}{\epsilon^2}. \tag{B.30}$$

In the above equation, we could replace X_1 with $e^{B(\alpha^*)}$ since $X \gg e^{B(\alpha^*)}$ and the correction introduced by considering X_1 as different from $e^{B(\alpha^*)}$ is of the next order in ϵ. Equation B.30 implies that

$$K(\alpha^*, \alpha_0^*)[X - e^{B(\alpha^*)}] \gg {n_0}^2. \tag{B.31}$$

With Equation B.30 as an estimate of ϵ/n_0, Equation B.29 becomes

$$\Lambda \simeq 1 - \frac{1}{\{K(\alpha^*, \alpha_0^*)[X - e^{B(\alpha^*)}]\}^{1/2}}, \tag{B.32}$$

and using Equation B.32 in Equation B.22 (also recalling the definition of Λ), the

micellar distribution can be rewritten

$$\tilde{X}_n \simeq \frac{1}{K(\alpha^*, \alpha_0^*)} e^{-n/\{K(\alpha^*,\alpha_0^*)[X - e^{B(\alpha^*)}]\}^{1/2}}. \tag{B.33}$$

Thus, we see that in the limit of strong micellar growth, the micellar distribution is an exponential, whose width increases as $\{K(\alpha^*, \alpha_0^*)[X - e^{B(\alpha^*)}]\}^{1/2}$.

As we mentioned in the previous section, in order to physically realize the limit of strong micellar growth as presented above, we must have that $K(\alpha^*, \alpha_0^*) > 1$. This can be shown by examination of Equation B.31. We note first that by definition, $X < 1$, since $X = 1$ corresponds to the case of pure surfactant. In addition, the quantity $e^{B(\alpha^*)}$ should be small compared to unity, since in general $B(\alpha^*)$ is a negative number indicating the stability of cylindrical micelles relative to free monomers. Therefore, on the left hand side of Equation B.31 $K(\alpha^*, \alpha_0^*)$ multiplies a quantity that can be at most of the order of unity, and which is in all practical cases is small compared to unity. However, we are told by Equation B.31 that in order to realize the limit of strong micellar growth, the quantity $K(\alpha^*, \alpha_0^*)[X - e^{B(\alpha^*)}]$ should be much greater than ${n_0}^2$. We know that for a micellar system, n_0 should be large compared with unity. We therefore cannot realize the limit of strong micellar growth unless $K(\alpha^*, \alpha_0^*) > 1$, since unless $K(\alpha^*, \alpha_0^*) > 1$, we have no way to satisfy Equation B.31.

We now wish to investigate the conditions for which strong micellar growth can occur for concentrations near to the critical micellar concentration. From Equation B.33, we see that at a fixed total concentration that as $K(\alpha^*, \alpha_0^*)$ is increased, the micellar distribution becomes broader. Equivalently, if we consider a fixed width of the micellar distribution, increasing $K(\alpha^*, \alpha_0^*)$ will decrease the total concentration X for which that distribution occurs. We therefore wish to estimate the magnitude of $K(\alpha^*, \alpha_0^*)$ required to have large growth at low concentration. Let us consider the case when $X = e^{B(\alpha^*)}$ and Λ is close to 1 as in Equation B.29. As we have previously done, we expand the first mass conservation relation (Equation B.26) to leading order in ϵ. However, since X is no longer large compared to $e^{B(\alpha^*)}$, we

cannot also replace X_1 with $e^{B(\alpha^*)}$. Instead of Equation B.30, we have

$$X = X_1 + \frac{1}{K(\alpha^*, \alpha_0^*)} \frac{{n_0}^2}{\epsilon^2}. \tag{B.34}$$

Using the definition of Λ and substituting $X = e^{B(\alpha^*)}$, we get

$$e^{B(\alpha^*)} = e^{B(\alpha^*)} \left(1 + \frac{\epsilon}{n_0}\right) + \frac{1}{K(\alpha^*, \alpha_0^*)} \frac{{n_0}^2}{\epsilon^2}, \tag{B.35}$$

which tells us that to leading order in ϵ,

$$K(\alpha^*, \alpha_0^*) e^{B(\alpha^*)} = \frac{{n_0}^3}{\epsilon^3}. \tag{B.36}$$

Recalling that the quantity $e^{B(\alpha^*)/k_BT}$ is of the same order as the critical micellar concentration, Equation B.36 implies that if $K(\alpha^*, \alpha_0^*) \gg {n_0}^3/X_{CMC}$, where X_{CMC} is the critical micellar concentration, then even near the critical micellar concentration there is considerable micellar growth. If, on the other hand, it turns out that $K(\alpha^*, \alpha_0^*) \ll {n_0}^3/X_{CMC}$, then near the critical micellar concentration the solution exists as a relatively monodisperse (in n) distribution of nearly minimum-sized micelles. We now investigate which limit applies to our experimental system.

Recalling the results of Section 4.2.8, we had for pure $C_{12}E_6$ at 50°C, that $K \sim 5 \times 10^{10}$ and ${n_0}^3/X_{CMC} \sim 1.4 \times 10^{12}$. For pure $C_{12}E_8$, whose cmc is of the same order as that of $C_{12}E_6$, the corresponding value of K is several orders of magnitude lower: $K \sim 6 \times 10^5$. Thus, for any mixture of $C_{12}E_6$ and $C_{12}E_8$, we can be confident that $K(\alpha^*, \alpha_0^*) \ll {n_0}^3/X_{CMC}$, implying that near the critical micellar concentration the solution exists as a relatively monodisperse solution of nearly minimum-sized micelles. In the regions that show appreciable micellar growth, we can be sure that $X \gg e^{B(\alpha^*)}$. As a result of this, we can simplify the expression for the micellar distribution even further, since we can neglect $e^{B(\alpha^*)}$ as compared with X in Equations B.31- B.33. For the renormalized micellar distribution, we have

$$\tilde{X}_n \simeq \frac{1}{K(\alpha^*, \alpha_0^*)} e^{-n/[K(\alpha^*, \alpha_0^*)X]^{1/2}}. \tag{B.37}$$

We now know the form of the micellar distribution in the limit of strong micellar growth, but we have not said anything of the value of the optimal compositions in the same limit. In order to do so, we must deal with the second conservation equation (Equation B.27). When Λ is close to unity as described by Equation B.29, it is the third term in Equation B.27 (and Equation B.26) that contributes the leading order term in ϵ. Since the third term is much greater than the second in Equation B.27, we do not make too great an error for our purposes if we replace α_0^* with α^*. Having done this, what follows is identical to the treatment of Section 4.2.8. We can now remove most of the dependence on Λ from Equation B.27 by substituting in Equation B.26. The result is

$$\alpha_s X \approx \alpha_1 X_1 + \alpha^*(X - X_1). \tag{B.38}$$

Rearranging, we write this

$$\alpha^* - \alpha_s = \frac{X_1}{X}(\alpha^* - \alpha_1). \tag{B.39}$$

In the limit of strong micellar growth, we can replace X_1 with $e^{B(\alpha^*)}$, giving

$$\alpha^* - \alpha_s = \frac{e^{B(\alpha^*)}}{X}(\alpha^* - \alpha_1). \tag{B.40}$$

In the limit $K(\alpha^*, \alpha_0^*) \gg {n_0}^3/X_{CMC}$, corresponding to the case of micellar growth at low concentration, there is no further simplification that can be made. In this case, $e^{B(\alpha^*)}$ is of the same order as X, so that if, say, α^* is very close to α_s, then α_1 will also be close to α^*, and this corresponds to the case when $\Delta\mu_{cA}^0 - \Delta\mu_{cB}^0$ becomes small (see Equation B.18).

On the other hand, consider the limit $K(\alpha^*, \alpha_0^*) \ll {n_0}^3/X_{CMC}$, corresponding to the case where strong micellar growth begins at mole fractions well above $e^{B(\alpha^*)}$. As explained above, this limit corresponds to the experiments performed in this thesis. In this case, it is clear that the right hand side of Equation B.40 is a small quantity. This implies that α^* should be very close to α_s, which we expect physically. Since

$X_1 \ll X$, most of the material in the system exists as micelles. Any difference in α^* from α_s must be compensated by a shift in the free monomer composition. Since the free monomer concentration is so low, as compared to the concentration of monomers in the micelles, the allowable change in α^* from α_s must be very small. We define the small parameter

$$\gamma = \alpha^* - \alpha_s \tag{B.41}$$

and note that as a first approximation

$$\gamma \simeq \frac{e^{B(\alpha_s)}}{X}[\alpha_s - \alpha_1(\alpha_s)] \tag{B.42}$$

where, since γ is small, we have replaced α^* with α_s in Equation 4.161 and furthermore we have indicated that Equation B.18 should be used to calculate $\alpha_1(\alpha_s)$. The important result of this discussion is that in the limit of strong micellar growth, the optimal composition in the *cylindrical* part of the micelles should be very close to α_s.

In the mixed system, the weight-averaged aggregation number is defined by

$$\bar{n}_w = \sum_{n=n_0}^{\infty} \sum_{\alpha=0}^{1} n^2 X_{n\alpha} / \sum_{n=n_0}^{\infty} \sum_{\alpha=0}^{1} n X_{n\alpha}. \tag{B.43}$$

After performing the summations over α according to the procedure described in Section 4.2.6, we obtain

$$\bar{n}_w = \sum_{n=n_0}^{\infty} n^2 \tilde{X}_n / \sum_{n=n_0}^{\infty} n \tilde{X}_n. \tag{B.44}$$

Since the form of Equation 4.166 is the same as that of Equation 4.56 for the single-component case, and $\tilde{X}_n$has the same form as the single- component micellar distribution, we expect the same results for the weight-averaged aggregation number. That is, after inserting the renormalized micellar distribution and taking the limit of strong micellar growth, the weight-averaged aggregation number may be written

$$\bar{n}_w \simeq n_0 + 2\sqrt{K(\alpha^*, \alpha_0^*)X}. \tag{B.45}$$

Appendix C

Examination of the Free Energy of Mixing

In Chapter 5, we made a slight modification to the Blankschtein, Thurston and Benedek expression for the free energy of mixing, G_m, for a single component micellar solution. In the second term of Equation 5.7 we wrote

$$k_B T \sum_n N_n \ln \frac{X_n}{e}, \tag{C.1}$$

while Blankschtein, Thurston and Benedek [12] did not include the factor of e in the logarithm. Here, N_n is the number of micelles of total size n and $X_n = N_n/N$ is the total mole fraction of micelles of total size n. N is the total number of water molecules and amphiphiles in the system. We wish to explain here the reasons why this factor of e should be included here and not absorbed into the standard part of the chemical potential for an n-mer (which is included in G_f, see Equation 5.2).

The origin of the second term in the Blankschtein, Thurston and Benedek expression for the free energy of mixing, G_m, can be understood from our general considerations of the partition function of the single component micellar system in Chapter 4. In Chapter 4, we showed that, from the partition function for our single component micellar system in the dilute limit, the free energy of the system in the

case of the ladder model could be written (see Equation 4.18)

$$F = F_0 - k_B T \sum_{n=n_0}^{\infty} N_n \ln \frac{V Z_n e}{V_F N_n}, \tag{C.2}$$

where F_0 is the free energy of water in the absence of amphiphiles, N_n is the number of micelles containing n amphiphiles, Z_n is the internal partition function for a micelle of size n, n_0 is the number of monomers in a minimum micelle, and V_F is the Fermi volume of an amphiphile.

The chemical potential of an n-mer is found by differentiating the free energy with respect to N_n. We find

$$\mu_n = \mu_n^0 + k_B T \ln X_n, \tag{C.3}$$

where $X_n = N_n/N$ is the mole fraction of micelles of size n, and the standard part of the chemical potential for a micelle of size n is

$$\mu_n^0 = -k_B T \ln \frac{V Z_n}{V_F N}, \tag{C.4}$$

in analogy with Equation 4.30 from Chapter 4. Here, N is the total number of water molecules and amphiphiles in the system. Using Equation C.4 to eliminate $k_B T \ln(V Z_n/V_F)$ from the free energy (Equation C.2), we get

$$F = F_0 + \sum_{n=n_0}^{\infty} \left(N_n \mu_n^0 + k_B T N_n \ln \frac{X_n}{e} \right). \tag{C.5}$$

We see that the factor of e comes naturally with $X_n = N_n/N$. In the above expression, μ_n^0 is defined as the change in the free energy of the system apart from the entropy of mixing when a single micelle of size n is added to water. If we allow the micelles to be in equilibrium with the monomers, then $\mu_n = n\mu_1$, and using Equation C.3 we have

$$\mu_n = \mu_n^0 + k_B T \ln X_n = n\mu_1^0 + n k_B T \ln X_1, \tag{C.6}$$

giving for the micellar distribution,

$$X_n = {X_1}^n e^{-(\mu_n^0 - n\mu_1^0)/k_BT}. \tag{C.7}$$

Let us now compare our approach above with the approach of Blankschtein, Thurston and Benedek [12] and Puvvada and Blankschtein [16]. The Blankschtein, Thurston and Benedek form for the free energy of mixing yields

$$F = F_0 + \sum_{n=n_0}^{\infty} \left(N_n \bar{\mu}_n^0 + k_BT N_n \ln X_n \right). \tag{C.8}$$

Thus, in Expression C.8, the factor of e under the logarithm from Equation C.5 is already included in the definition of the standard part of the chemical potential, $\bar{\mu}_n^0$. By comparing Equation C.8 for the free energy with Equation C.5 from our treatment, we can establish the physical meaning of the quantity $\bar{\mu}_n^0$: $\bar{\mu}_n^0 = \mu_n^0 - k_BT$. That is, $\bar{\mu}_n^0$ is the change of the free energy of the system apart from the entropy of mixing when a single micelle of size n is added to water less k_BT. This is clear to see from the expression for the chemical potential of an n-mer:

$$\mu_n = \frac{\partial F}{\partial N_n} = \bar{\mu}_n^0 + k_BT + k_BT \ln X_n \tag{C.9}$$

(*c. f.* Equation C.3). If we use Equation C.9 for further analysis, then in equilibrium, with $\mu_n = n\mu_1$, we get

$$\mu_n = \bar{\mu}_n^0 + k_BT \ln X_n + k_BT = n\bar{\mu}_1^0 + nk_BT \ln X_1 + nk_BT, \tag{C.10}$$

giving for the micellar distribution, the unappealing expression

$$X_n = e^{n-1} {X_1}^n e^{-(\bar{\mu}_n^0 - n\bar{\mu}_1^0)/k_BT}. \tag{C.11}$$

The analog of Equation C.11 for the micellar distribution in the mixed case was obtained by Puvvada and Blankschtein [16]. Blankschtein, Thurston and Benedek [12], when they obtain Equation C.9, prefer to redefine the standard part of the

chemical potential, denoting $\bar{\mu}_n^0 + k_B T$ as μ_n^0, without explanation. With this redefinition, Blankschtein, Thurston and Benedek obtain the same standard part of the chemical potential for an n-mer as we do. Thus, they obtain Equation C.7 for the micellar distribution. To avoid these complications, we consider it reasonable to include the factor of e in the expression for F as expressed in Equation C.5.

Appendix D

Additional Measurements on $C_{12}E_8$

Table D.1 lists the results of a few additional dynamic light scattering measurements performed on the pure $C_{12}E_8$ and water system at $T = 59.9°C$ and $T = 64.0°C$ using the swinging arm instrument described in Chapter 3. These data are used to extract additional values of the generalized ladder model growth parameter $\Delta\mu_B/k_BT$ in Section 6.1.2.

Table D.1: Additional Dynamic Light Scattering Measurements on $C_{12}E_8$

X	T (°C)	$\bar{D}$ (cm^2/s)	R_H (Å)
2.01×10^{-4}	59.9	8.85×10^{-7}	59.0
5.05×10^{-4}	59.9	9.10×10^{-7}	57.4
2.01×10^{-4}	64.0	9.22×10^{-7}	60.9
5.01×10^{-4}	64.0	7.93×10^{-7}	70.8

Bibliography

[1] J. N. Israelachivili. *Intermolecular and Surface Forces With Applications to Colloidal and Biological Systems.* Academic Press, New York, 1985.

[2] J. W. McBain. *Trans. Faraday Soc.*, 9:99–101, 1913.

[3] G. S. Hartley. *Aqueous Solutions of Paraffin Chain Salts.* Hermann, Paris, 1936.

[4] R. Pecora. Doppler shifts in light scattering from pure liquids and polymer solutions. *J. Chem. Phys.*, 40:1604, 1964.

[5] H. Z. Cummins, N. Knable, and Y. Yeh. Observation of diffusion broadening of rayleigh scattered light. *Phys. Rev. Lett.*, 12:150, 1964.

[6] N. C. Ford and G. B. Benedek. Observation of the spectrum of light scattered from a pure fluid near its critical point. *Phys. Rev. Lett.*, 15:649–653, 1965.

[7] Norman A. Mazer, George B. Benedek, and Martin C. Carey. An investigation of the micellar phase of sodium dodecyl sulfate in aqueous sodium chloride solutions using quasielastic light scattering spectroscopy. *J. Phys. Chem.*, 80:1075–1085, 1976.

[8] N.A. Mazer, M.C. Carey, and G.B. Benedek. The size, shape, and thermodynamics of sodium dodecyl sulfate (SDS) micelles using quasielastic light scattering spectroscopy. In K.L. Mittal, editor, *Micellization, Solubilization, and Microemulsions*, pages 359–381. Plenum, 1977.

[9] C. Y. Young, P. J. Missel, N. A. Mazer, G. B. Benedek, and M. C. Carey. Deduction of micellar shape from angular dissymmetry measurements of light scattered from aqueous sodium dodecyl sulfate solutions at high sodium chloride concentrations. *J. Phys. Chem.*, 82:1375–1378, 1978.

[10] P. J. Missel, N. A. Mazer, G. B. Benedek, C. Y. Young, and M. C. Carey. Thermodynamic analysis of the growth of sodium dodecyl sulfate micelles. *J. Phys. Chem.*, 84:1044–1057, 1980.

[11] Daniel Blankschtein, George M. Thurston, and George B. Benedek. Theory of phase separation in micellar solutions. *Phys. Rev. Lett.*, 54:955–958, 1985.

[12] Daniel Blankschtein, George M. Thurston, and George B. Benedek. Phenomenological theory of equilibrium thermodynamic properties and phase separation of micellar solutions. *J. Chem. Phys.*, 85:7268–7288, 1986.

[13] George M. Thurston, Daniel Blankschtein, Michael R. Fisch, and George B. Benedek. Theory of thermodynamic properties and phase separation of micellar solutions with lower consolute points. *J. Chem. Phys.*, 84:4558–4562, 1986.

[14] George M. Thurston. *Studies of Phase Separation in Micellar Solutions.* PhD thesis, Massachusetts Institute of Technology, 1986.

[15] Sudhakar Puvvada and Daniel Blankschtein. Molecular-thermodynamic approach to predict micellization, phase behavior and phase separation of micellar solutions. I. application to nonionic surfactants. *J. Chem. Phys.*, 92:3710–3724, 1990.

[16] Sudhakar Puvvada and Daniel Blankschtein. Thermodynamic description of micellization, phase behavior, and phase separation of aqueous solutions of surfactant mixtures. *J. Phys. Chem.*, 96:5567–5579, 1992.

[17] Sudhakar Puvvada and Daniel Blankschtein. Theoretical and experimental investigations of micellar properties of aqueous solutions containing binary mixtures of nonionic surfactants. *J. Phys. Chem.*, 96:5579–5592, 1992.

[18] J. P. Wilcoxon, D. W. Schaefer, and E. W. Kaler. Effects of isotopic substitution on the critical behavior of aqueous solutions of *n*-dodecylhexaoxyethylene glycol monoether ($C_{12}E_6$). *J. Chem. Phys.*, 90:1909–1917, 1989.

[19] L. D. Landau, E. M. Lifshitz, and L. P. Pitaevskiĭ. *Electrodynamics of Continuous Media.* Pergamon, New York, second edition, 1984.

[20] B. J. Berne and R. Pecora. *Dynamic Light Scattering.* Wiley, New York, 1976.

[21] J. D. Jackson. *Classical Electrodynamics.* Wiley, second edition, 1975.

[22] Wyn Brown, Robert Johnsen, Peter Stilbs, and Björn Lindman. Size and shape of nonionic amphiphile ($C_{12}E_6$) micelles in dilute aqueous solutions as derived from quasielastic and intensity light scattering, sedimentation, and pulsed-field-gradient nuclear magnetic resonance self-diffusion data. *J. Phys. Chem.*, 87:4548–4553, 1983.

[23] Tadashi Kato, Shin ichi Anzai, Sanae Takanoi, and Tsutomu Seimiya. Intermicellar interactions and micelle size distribution in aqueous solutions of polyoxyethylene surfactants. *J. Chem. Soc., Faraday Trans 1*, 85:2499–2506, 1989.

[24] Mikael Jonströmer, Bengt Jönsson, and Björn Lindman. Self-diffusion in nonionic surfactant-water systems. *J. Phys. Chem.*, 95:3293–3300, 1991.

[25] Nikko Chemicals Co., Ltd. *Homogeneous Polyoxyethylene Nonionic Surfactants NIKKOL BR-SY Series*, December 1985.

[26] Mario Corti and Vittoria Degiorgio. Micellar properties and critical fluctuations in aqueous solutions of nonionic amphiphiles. *J. Phys. Chem.*, 85:1442–1445, 1981.

[27] T. M. Kole, C. J. Richards, and M. R. Fisch. Evolution of the diffusion coefficient and correlation length of aqueous solutions of $C_{12}E_6$. *J. Phys. Chem.*, 98:4949–4954, 1994.

[28] J. P. Wilcoxon and E. W. Kaler. Statics and dynamics of concentration fluctuations in nonionic micellar solutions. *J. Chem. Phys.*, 86:4684–4691, 1987.

[29] Per-Gunnar Nilsson, Håkan Wennerström, and Björn Lindmann. Non-ionic micelles: Size, shape, hydration and intermicellar interactions from self-diffusion studies. *Chemica Scripta*, 25:67–72, 1985.

[30] Wyn Brown, Zhou Pu, and Roger Rymdén. Size and shape of nonionic amphiphile micelles: NMR self-diffusion and static and quasi-elastic light-scattering measurements on $C_{12}E_5$, $C_{12}E_7$, and $C_{12}E_8$ in aqueous solution. *J. Phys. Chem.*, 92:6086–6094, 1988.

[31] P. G. Cummins, E. Staples, J. Penfold, and R. K. Heenan. Geometry of micelles of the poly(oxyethylene) nonionic surfactants $C_{16}E_6$ and $C_{16}E_8$ in the presence of electrolyte. *Langmuir*, 5:1195–1199, 1989.

[32] D. J. Cebula and R. H. Ottewill. Neutron scattering studies on micelles of dodecylhexaoxyethylene glycol monoether. *Colloid and Polymer Science*, 260:1118–1120, 1982.

[33] Jean-Claude Ravey. Lower consolute curve related to micellar structure of nonionic surfactants. *Journal of Colloid and Interface Science*, 94:289–291, 1983.

[34] A. Ben-Shaul, D. H. Rorman, Hartland G. V., and W. M. Gelbart. Size distribution of mixed micelles: Rodlike surfactant-alcohol aggregates. *J. Phys. Chem.*, 90:5277–5286, 1986.

[35] Teresa R. Carale and Daniel Blankschtein. Theoretical and experimental determinations of the crossover from dilute to semidilute regimes of micellar solutions. *J. Phys. Chem.*, 96:459–467, 1992.

[36] R. Triolo, L. J. Magid, Jr. J. S. Johnson, and H. R. Child. Small-angle neutron scattering from aqueous micellar solutions of a nonionic surfactant as a function of temperature. *J. Phys. Chem.*, 86:3689–3695, 1982.

[37] Mario Corti, Claudio Minero, and Vittorio Degiorgio. Cloud point transition in nonionic micellar solutions. *J. Phys. Chem.*, 88:309–317, 1984.

[38] Laura Cantù, Mario Corti, Vittorio Degiorgio, Claudio Minero, and Roberto Piazza. Laser light-scattering study of nonionic micellar solutions. *Journal of Colloid and Interface Science*, 105:628–634, 1985.

[39] M. Zulauf, K. Weckström, J. B. Hayter, V. Degiorgio, and M. Corti. Neutron scattering study of micelle structure in isotropic aqueous solutions of poly(oxyethylene) amphiphiles. *J. Phys. Chem.*, 89:3411–3417, 1985.

[40] P. K. Vinson, J. R. Bellare, H. T. Davis, W. G. Miller, and L. E. Scriven. Direct imaging of surfactant micelles, vesicles, discs, and ripple phase structures by cryo-transmission electron microscopy. *Journal of Colloid and Interface Science*, 142:74–91, 1991.

[41] Katarina Edwards, Jonas Gustafsson, Mats Almgren, and Göran Karlsson. Solubilization of lecithin vesicles by a cationic surfactant: Intermediate structures in the vesicle-micelle transition observed by cryo-transmission electron microscopy. *Journal of Colloid and Interface Science*, 161:299–309, 1993.

[42] Richard A. Chamberlin. *Light Scattering Studies on Lecithin Micellar Solutions.* PhD thesis, Massachusetts Institute of Technology, 1991.

[43] Hans R. Haller, Christian Destor, and David S. Cannell. Photometer for quasielastic and classical light scattering. *Rev. Sci. Instrum.*, 54:973–983, 1983.

[44] Stephen W. Provencher. A constrained regularization method for inverting data represented by linear algebraic or integral equations. *Computer Physics Communications*, 27:213–227, 1982.

[45] Dennis E. Koppel. Analysis of macromolecular polydispersity in intensity correlation spectroscopy: The method of cumulants. *J. Chem. Phys.*, 57:4814–4820, 1972.

[46] George D. J. Phillies. Upon the application of cumulant analysis to the interpretation of quasielastic light scattering spectra. *J. Chem. Phys.*, 89:91–99, 1988.

[47] T. G. Braginskaya, P. D. Dobitchin, M. A. Ivanova, V. V. Klyubin, A. V. Lomakin, V. A. Noskin, G. E. Shmelev, and S. P. Tolpina. Analysis of the polydispersity by photon correlation spectroscopy. regularization procedure. *Physica Scripta*, 28:73–79, 1983.

[48] J. Skilling and R. K. Bryan. Maximum entropy image reconstruction: General algorithm. *Monthly Notices of the Royal Astronomical Society*, 211:111–124, 1984.

[49] Aleksey Lomakin. Personal communication.

[50] Stephen W. Provencher. Contin: A general purpose constrained regularization program for inverting noisy linear algebraic and integral equations. *Computer Physics Communications*, 27:229–242, 1982.

[51] J. Ehl, C. Loucheux, C. Reiss, and H. Benoit. Mesure de l'increment d'indice de refraction de differentes solutions de hauts polymeres, et du rapport de rayleigh de quelques liquides, en fonction de la temperature. *Makro. Chem.*, 75:35, 1964.

[52] T. M. Bender, R. J. Lewis, and R. Pecora. Absolute rayleigh ratios of four solvents at 488 nm. *Macromolecules*, 19:244–245, 1986.

[53] P. Debye. Molecular-weight determination by light scattering. *Journal of Physical Colloid Chemistry*, 51:18–32, 1947.

[54] V. Degiorgio. Nonionic micelles. In V. Degiorgio and M. Corti, editors, *Proceedings of the International School of Physics Enrico Fermi–Physics of Amphiphiles: Micelles, Vesicles and Microemulsions*, pages 303–335. North-Holland Physics Publishing, Amsterdam, 1985.

[55] José García de la Torre and Victor A. Bloomfield. Hydrodynamic properties of complex, rigid, biological macromolecules: Theory and applications. *Quarterly Reviews of Biophysics*, 14:81–139, 1981.

[56] F. Perrin. Mouvement brownien d'un ellipsoid (II). rotation libre et dépolarisation des fluorescences. translation et diffusion de molécules ellipsoidales. *Journal de Physique et le Radium*, 7:1–11, 1936.

[57] P. Mukerjee and K. J. Mysels. *Critical Micelle Concentrations of Aqueous Surfactant Systems.* U. S. Department of Commerce, National Bureau of Standards, Washington, D. C., February 1971.

[58] C. Tanford. Theory of micelle formation in aqueous solutions. *J. Phys. Chem.*, 78:2469–2479, 1974.

[59] Franca Podo, Ashoka Ray, and George Némethy. Structure and hydration of nonionic detergent micelles. a high resolution nuclear magnetic resonance study. *Journal of the American Chemical Society*, 95:6164–6171, 1973.

[60] B. Cabane. Structure of the water/surfactant interface in micelles: an NMR study of SDS micelles labelled with paramagnetic ions. *J. Physique*, 42:847–859, 1981.

[61] John F. Nagle and D. Allan Wilkinson. Lecithin bilayers: Density measurements and molecular interactions. *Biophysical Journal*, 23:159–175, 1978.

[62] Einar Vikingstad and Harald Høiland. Partial molal volumes and partial molal compressibilities of *n*-alkanes in sodium dodecanoate solutions. *Journal of Colloid and Interface Science*, 64:510–513, 1978.

[63] Charles Tanford. *The Hydrophobic Effect: Formation of Micelles and Biological Membranes.* Wiley, New York, 1973.

[64] B. H. Zimm. Apparatus and methods for measurement and interpretation of the angular variation of light scattering; preliminary results on polystyrene solutions. *J. Chem. Phys.*, 16:1099–1116, 1948.

[65] P. N. Pusey and R. J. A. Tough. Particle interactions. In Robert Pecora, editor, *Dynamic Light Scattering: Applications of Photon Correlation Spectroscopy*, pages 85–179. Plenum, 1985.

[66] B. Cichocki and B. U. Felderhof. Diffusion coefficients and effective viscosity of suspensions of sticky hard spheres with hydrodynamic interactions. *J. Chem. Phys.*, 93:4427–4432, 1990.

[67] B. Cichocki and B. U. Felderhof. Dynamic scattering function of a dense suspension of hard spheres. *Physica A*, 204:152–168, 1994.

Acknowledgements

I would like to express my gratitude to Prof. George Benedek for his supervision of my thesis work. His encouragement and advice were invaluable to me during this project. I am also grateful for his careful reading of this thesis and his insightful comments. These comments were responsible for a dramatic improvement in the clarity and readability of this work.

I am also deeply grateful to Alfred Gschwendtner and the members of the Opto-Radar Systems Group of MIT Lincoln Laboratory. Without their financial support during my graduate career, this project would not have been possible. In addition, I am indebted to them for their encouragement, which was mostly responsible for my decision to pursue a Ph.D. in the first place. The person I believe most responsible for my decision to begin this undertaking was Dr. David Biron at Lincoln Laboratory. It is with deep sadness that I recall his untimely death in the last year of my research project. I regret that I cannot now share my gratitude and sense of accomplishment with him.

I would also like to thank Doo Soo Chung and Sudhakar Puvvada for introducing me to the world of surfactants. They got me interested in this specific project, and my discussions with them were always educational. I am appreciative to Prof. T. Tanaka for serving as a reader of this thesis.

I am indebted to Prof. Daniel Blankschtein for supplying me with surfactants, encouragement and advice. His name appears many times in this thesis, and for good reason. His work provides much of the basis for the work contained herein. I am deeply appreciative of his willingness to meet with me repeatedly and discuss my measurements and results. These discussions always helped to keep me motivated when I became discouraged.

I owe a great deal of thanks to the other members of Prof. Benedek's research group. Carolyn Berland and Jayanti Pande were always willing to discuss politics, history and philosophy whenever thinking about my research became too much of a chore. The other members of the group, Canwen Liu, Olutayo Ogun, Bernard Fine and Neer Asherie were always helpful and willing to help me whenever I got into a bind. Most of all, however, I am grateful to Aleksey Lomakin. He was always willing to share with me his knowledge and expertise on light scattering and physics in general. His comments and assistance during this project kept me headed in the right direction. His dedication to Thursday lunches and willingness to argue with me about any subject at any time are deeply appreciated.

Shanna Sipple gave me much support during the final year of this researh project. Her willingness to listen and encourage me during this time means more to me than I can express here.

Most of all, I would like to thank my parents Jane and George, my sister Jenifer, and my brother Anthony. Without their support, I most certainly would not have been capable of finishing this project. I wish to especially thank my parents for their tolerance of my obsession with this thesis, their willingness to bear with me when I became discouraged, and their willingness to share their joy when I was encouraged by my progress.